10-20-2022 2:15 PM

Spatiotemporal Changes of Lagged Compound Dry and Wet Spells in the Northwest North America Under Climate Change

Reza Rezvani, *The University of Western Ontario*

Supervisor: Najafi, Mohammad Reza, *The University of Western Ontario*

A thesis submitted in partial fulfillment of the requirements for the Master of Engineering Science degree in Civil and Environmental Engineering

Abstract

Communities around the world are exposed to hydroclimatic extremes (i.e., floods and droughts), which affect a multitude of water-resources dependant sectors and bring about a variety of socioeconomic impacts. Recently, an upsurge in the occurrence of hydrometeorological extremes and their temporal swings is observed in several regions around the world. Such transitions to the contrasting extremes such as the drought to flood in California (2016 – 17) or the flood to drought in the upper Mississippi River basin (2011 – 12) has raised concerns about the increasing variability and rapid transitions between hydrological extremes and their associated compounding economic and environmental impacts. The intensification of the global hydrological cycle associated with climate change can further alter the drivers of such extremes and their interactions. Consecutive flood and drought events can undermine the safety and functionality of communities and infrastructure systems; therefore, it is important to understand their characteristics, including their spatiotemporal frequency, magnitude, and seasonality in a changing climate. In this study, flood-drought swings along with changes in the corresponding processes are investigated based on precipitation and streamflow data in the Northwest North America. To this end, meteorological wet and dry conditions, as drivers of hydrologic floods and droughts, are investigated using the Standardised Precipitation Index and Standardised Precipitation Evapotranspiration Index for multiple accumulation periods (1, 3, and 6-months), calculated based on the downscaled and statistically bias corrected simulations of six Global Climate Models from the 5th phase of the Coupled Model Intercomparison Project with two medium and high emission scenarios for 1.5°C-4 °C global warming levels. Further, we use the Variable Infiltration Capacity hydrologic model simulated streamflow to project the future hydrological response of the study area to the lagged compound floods and droughts under

global warming. Our findings indicate increasing risk of lagged compound hydroclimatic events under climate change inferred from the projected increases in the frequency of such events. Moreover, flood-drought swings occur more swiftly since the transition times between contrasting events for both climatic and hydrological extremes are projected to decrease in a warming world. While the study area is more prone to flood-to-drought transitions, such events are projected to also intensify under climate change. We identify future hotspots for the each of the characteristics of lagged compound hydroclimatic events. Our findings assert the necessity of integrating mitigation measures targeting the compound hydroclimatic events into Disaster Risk Reduction strategies at the identified hotspots.

Key words: Hydrology, Climate change, Extreme events, Flooding, Droughts, Compound extremes, Wet and dry spells, Drought index, Compound flood and drought, Multi-hazard, Multi-model ensemble, Dry-wet abrupt alternation, Drought-flood abrupt alteration, streamflow, precipitation

Lay Summary

Floods and droughts have profound impacts on a wide range of sectors such as water, agriculture, energy production, infrastructure, and ecosystem health. Although the characteristics, changing behaviour, and social impacts of floods and droughts have been previously investigated in many studies, traditionally floods and droughts have been treated separately. Therefore, the intersection between these two extremes has been overlooked, even though their rapid transitions can lead to greater economic and environmental impacts than the sum of each individual type of event. Historically, several catastrophic instances of transition between drought and flood have been recorded, such as the widespread floods in 2016 – 17 that occurred on the back of the multi-year drought of California. Such sudden swings can place substantial strain on emergency response teams and exacerbate tensions between stressed resources for flood relief or long-term water resource management. On top of all, scientists have shown that the global warming, a phenomenon occurring due to emission of greenhouse gasses that is warming up the atmosphere, can cause climate change, which could bring about changes to the weather patterns. Climate change has drastically contributed to intensification of weather and climate related extreme events (including floods and droughts) in some locations and is expected to continue this intensification in the future. Therefore, understanding the characteristics of flood-drought transitions as well as their projected future behaviour under climate change is of particular importance for a multitude of water-resources dependant sectors. In this study, we investigate how often floods and droughts swing, how long their transition takes, and how do their severity alter in a changing climate. Our results indicate that more frequent flood-drought alterations are expected in the future. Future flood-to-drought transitions are projected to occur more swiftly and between more intense floods and droughts if the global

warming is not limited. Our findings illustrate the future hotspots for flood-drought transitions and provide valuable insights for decision makers to develop policies and take actions to cope with such disastrous compound natural hazards and adapt to their changing behaviour under a changing climate.

Acknowledgment

It is with my great pleasure to thank my dear supervisor, Dr. Mohammad Reza Najafi for giving me this amazing research opportunity and supporting me all through my research, financially and scientifically. I find Dr. Najafi's support and courtesy second to none as he was always available to cater for my needs and welcomed any sorts of questions I had. His contributions to this work through supervision, project administration, and funding acquisition made my research path barrier-free to achieve my academic milestones. I cannot thank Dr. Najafi enough for how impactful he has been in my academic life and could not have asked for a better supervisor than him.

I truly appreciate my committee members and examiners, Dr. Isaac Luginaah, Dr. Chris Power, and Dr. Sabina Rakhimbekova for spending their precious time to review this thesis and give invaluable suggestions to improve my work. Without a doubt, their insights have made this research richer.

I would like to extend my gratitude to my research partners Dr. Wooyoung Na, and Melika Rahimi Movaghar for their wholehearted support. Their contribution through brainstorming was of great value in conceptualization and methodology. Dr. Na helped in reviewing this thesis as well. I also would like to thank the Hydrologic Impacts team at the Pacific Climate Impact Consortium (PCIC), especially Arelia (Werner) Schoeneberg, for providing the datasets used in this study.

Finally, I would like to thank my mother for giving me birth and raising me singlehandedly with all her sacrifices. She has taught me one of the most important lessons of my life, which is how to be responsible. I am also grateful to my aunt and grandmother, who supported me emotionally

and financially specially during the difficult times of the COVID-19 pandemic, when I was miles away from my home and mother. Last but not least, I would like to thank my father who encouraged me to thrive all through my life.

Table of Content

List of Figures

List of Tables

List of Acronyms

AbTr	Abrupt transition
AR	Atmospheric River
B.C.	British Columbia
BCCA	bias-corrected constructed analogs
BCCAQ	Bias Correction/Constructed Analogues with de-trended Quantile mapping
CCE	Compound climatic event
CHE	Compound hydrologic event
CHCE	Compound hydroclimatic event
CI	Confidence interval
DFAAI	Drought-flood abrupt alternation Index
DI	Drought intensity
DS	Drought severity
ECDF	empirical cumulative distribution function
ECSI	Empirical compound flood-drought severity index
ECWA	Empirical Compound Weighting Angle
ENSO	El Nino - Southern Oscillation
EPr	Exceedance probability
FDC	flow duration curve
FAbTr	Fraction of CHEs with AbTr
FTr3	Fraction of CHEs with Tr less than three months
FM	Flood magnitude

FRB	Fraser River Basin
FV	Flood volume
GCM	Global Climate Model
GMT	Global Mean Temperature
IPCC	the Inter Governmental Panel on Climate Change
KKZ	Katsavounidis-Kuo-Zhang
LCHCE	Lagged compound hydroclimatic event
NAO	North Atlantic Oscillation
NRCANmet	the Natural Resources Canada observational dataset
NWNA	northwest North American
PBCmet	the PCIC meteorology for BC
PCIC	the Pacific Climate Impact Consortium
PDS	partial duration series
PDSI	Palmer drought severity index
PNWNA	Pacific Northwest North America
PNWNAmet	PCIC meteorology for northwest North America
POT	peaks over threshold
PRB	Peace River Basin
QMAP	quantile mapping
RCP	Representative Concentration Pathway
ROS	Rain-on-snow
SEA	Seasonality of CHEs
SPEI	standardized precipitation evapotranspiration index

SPI	Standardised Precipitation Index
SREX	Special Report on Climate Extremes
SS	Strength of the seasonality
SWE	snow water equivalent
Tr	Transition time
U.S.	The United States of America
WMO	The World Meteorological Organization

Chapter 1: Motivation

1.1. Natural Hazards and Hydrological Extreme Events

Communities around the world are exposed to natural hazards, such as earthquakes, floods, tornadoes, volcanic eruptions, droughts, hurricanes, and storms (Kundzewicz and Kaczmare, 2000; Wang et al., 2021; Zhang and Najafi, 2020). Amongst all, hydrologic extremes (i.e., floods and droughts) occur globally and more frequently compared to others, as their occurrence is not confined to a specific geographical location (Van Loon, 2013), which makes societies more prone to these impactful events.

Flooding is natural and essential to a healthy environment, but severe events can cause human hardship and economic loss (Ribeiro et al., 2014). The vulnerability of properties and societies in flood-prone areas have increased in the last decades due to population growth and urbanization (Yazdi et al., 2013; Elshorbagy et al., 2017). Despite significant efforts at the local, national, and global levels to reduce the negative impacts from natural hazards, flood induced costs and losses have been increasing in recent decades globally, and floods remain the most destructive and frequent natural hazards in the world (Bubeck et al., 2016).

Although a unique definition of drought does not exist due to the existence of several drought types, droughts are generally defined as 'prolonged absence or marked deficiency of precipitation', a 'deficiency of precipitation that results in water shortage for some activity or for some group' or a 'period of abnormally dry weather sufficiently prolonged for the lack of precipitation to cause a serious hydrological imbalance' (Trenberth et al., 2013). Also referred to as ‘the creeping disaster’ (Mishra and Singh, 2010) due to larger spatial and temporal coverage, droughts can cover extensive areas and last for months to years, with devastating impacts on the

environment and society (Van Loon, 2013). Moreover, the 5th assessment report of the Intergovernmental Panel on Climate Change has reported an increase in the observed trends of droughts in many regions globally since the mid-20th century (2014).

1.2. Impacts of Climate Change on Hydrological Extremes

There is clear and growing evidence that climate change likely increases the frequency and intensity of hydrologic extremes (He, 2019; Hirabayashi et al., 2013; Herring et al., 2015). Changes in the spatial and temporal patterns of hydrological factors have been attributed to climate change in many regions including the Pacific Northwest (Najafi et al., 2017a&b). Higher temperatures have the potential to intensify and accelerate the hydrological cycle. Previous studies have shown that flood risk is projected to increase if the global warming continues. Warming results in increased concentrations of atmospheric moisture due to increasing evaporation and transpiration, which is expected to lead to an increase in extreme precipitation if other conditions, such as atmospheric circulation, do not change. Moreover, the Clausius-Clapeyron relation indicates that as the air warms, its water holding capacity increases by about 7% $°C^{-1}$ (Skliris et al., 2016). Therefore, failure to limit the global warming could lead to more extreme rainfall events due to the increased atmospheric moisture content and extended water holding capacity of the atmosphere (Garcia et al., 2022; He et al., 2020; Bush and Lemmen, 2019). At the same time, the rising global temperature could increased evapotranspiration, which in return could lead to more frequent drought occurrences if the moisture deficits from increased evapotranspiration are not offset by the precipitation increases (He et al., 2020; Bush and Lemmen, 2019).

1.3. Compound Weather and Climatic Extremes

Natural hazards can overwhelm the capacity of human and infrastructure systems to cope, which in turn create societal or ecological impacts. Weather- and climate-related extreme events arise from complex interactions between various physical processes across multiple spatial and temporal scales (Zscheischler et al., 2020). When multiple hazards and/or drivers (i.e., climatic processes) combine, their impacts are often amplified compared to individual hazard occurrences (Bevacqua et al., 2021). Such combinations/interactions are referred to as compound weather and climatic extremes and are defined as 'a combination of multiple drivers and/or hazards that contributes to societal or environmental risk' (Zscheischler et al., 2018). The research of compound extreme events has been evolved into an interdisciplinary matter at the interface of climate science, climate-impact research, engineering, and statistics.

In a recently proposed typology, Zscheischler et al. (2020) categorize compound extreme events as: a) preconditioned events, whereby one or more hazards can exacerbate the impact(s) of a pre-existing climate-driven hazard; b) multivariate event, which refers to the cooccurrence of multiple climate drivers and/or hazards in the same geographical region, causing an impact; c) temporally compounding events, that is a succession of hazards that affect a given geographical region, leading to an (amplified) impact; and d) spatially compounding events, that occur when multiple connected locations are affected by the same or different hazards within a limited time window. It should be noted that there are soft boundaries between the categories of this typology, since a compound extreme event might be classified into multiple of these categories due to the complexity of compound hazards.

1.4. Compound Hydroclimatic Events

Recently, an upsurge in the occurrence of hydrometeorological extremes and their temporal swings is observed in several regions around the world. Such transitions to the contrasting extremes such as the drought to flood in California (2016 – 17) (Swain et al., 2018; Wang et al., 2017), and the United Kingdom (2012) or the flood to drought in the upper Mississippi River basin (2011 – 12), and Kentucky, Ohio, Indiana, and Illinois in 2019 (Ford et al., 2021) has raised concerns about the increasing variability and rapid transitions between hydrological extremes and their associated compounding economic and environmental impacts. In this study, Compound Hydroclimatic Events (CHCH) are defined as the temporal transition between flood and drought or wet and dry spells, in a relatively short period (within 6 months). The compound hydroclimatic events can be identified as compound extreme events and be categized as preconditioned events (type a), temporally compounding (type b), or spatially compounding (type d) based on the aforementioned typology (Zscheischler et al., 2020). The CHCEs can undermine the safety and functionality of communities and infrastructure systems due to amplified impacts. For instance, flood to drought events can reduce the reliability of water resources (Ford et al., 2021), while drought to flood occurrence can make fragilities in reservoir operations with potential catastrophic outcome (Garcia et al., 2022). Therefore, it is important to understand the characteristics of such impactful compound extremes (the CHCEs), including their spatiotemporal frequency, transition time, magnitude, and seasonality in a changing climate.

1.5. Research Gaps

To date, most of the studies on floods and droughts have treated the two extremes separately. Therefore, the problematic transitions between the two extremes have been overlooked in the scientific literature. Moreover, no studies to date have proposed a systematic framework to investigate the CHCEs. Therefore, these compound events have been referred to using several terminologies such as rapid drought cessation (Maxwell et al., 2017), extreme precipitation reversals (Marston and Ellis, 2018), precipitation whiplash (Swain et al., 2018), drought to deluge (Hoover et al., 2022) amongst others. Most studies undertaken until now have focused on meteorological extremes using the precipitation data, whereas the impacts of floods and droughts are exerted through the streamflow. Thus, characterising CHCEs based on streamflow records have been overlooked. In addition, there has not been any attempts to quantify the severity and non-stationarity of the compound hydrological events (CHEs). Understanding the CHCEs require an understanding of the drivers and processes of both floods and droughts, in addition to how their likelihoods interact (Leonard et al., 2014). However, all studies to date have solely focused on one type of floods and droughts. Therefore, no study is available to date (to author's knowledge) that have considered both the compound climatic events (CCEs) (as potential drivers for hydrological floods and droughts) and compound hydrologic events (CHEs) by utilizing multiple climatic and hydrological variables to characterise such compound events.

Despite many instances of the CHCEs being reported globally (see Parry (2019) for an exhaustive list of the recorded events), most of the studies have investigated these events in the U.S. and China. Although several CHCEs with proximity to Canada have occurred through the U.S., the occurrence of such compound events in Canada has not been investigated. Given the expected intensification of the hydroclimatic extremes under global warming and the fact that

Canada is warming three times faster the average global warming rate (Bush and Lemmen, 2019), it is important to explore the changing behaviour of these compound events in Canada. In addition, conducting such investigation on a watershed scale can provide invaluable high-resolution insights about the regional impacts of CHCEs under climate change, valuable to a wide range of decision makers.

1.6. Research Objectives

In this study, we aim to characterise the CHCEs on a watershed scale and project their spatial and temporal changes in the future under climate change. Streamflow alterations can impact a wide range of sectors and activities such as water supply and engineering design. However, the extreme streamflow conditions (i.e., hydrologic floods and droughts) are propagation of extreme meteorological events. Thus, the first objective of this study is to better understand the climatic processes of CHCEs by characterising the compound climatic events (CCEs) under climate change. To do so, downscaled bias-corrected simulation of an ensemble of Global Climate Models (GCMs) consisting of 12 model-scenarios and the outputs of Variable Infiltration Capacity (VIC) hydrologic model forced with the downscaled and bias corrected ensemble of GCMs are used to project the current and future state of climate. Our second objective is to characterise the CHEs under global warming. To this end, high resolution streamflow simulations of VIC hydrologic model forced with the ensemble of climate models is used to assess how different characteristics of such compound hydrological extremes are projected to vary temporally and spatially if global warming is not limited.

1.7. Research Questions

To achieve our objectives of this study, we particularly will answer the following questions:

- How often do CHCEs occur at different global warming levels?
- How long does it take for the flood and drought of a CHCE to swing (transition time) at different global warming levels?
- Bearing in mind the projected intensification of the global hydrological cycle in a warming climate, would the study area experience successions of more severe hydroclimatic extremes? If so, to what extent are such CHCEs expected to intensify?
- How does the seasonality of CHCEs change in a warming world?

This thesis aims to answer to the raised research questions by showing the overall patterns of the future projections of the questioned characteristic of a given CHCE type (CCE and CHE). The future spatial hotspots for the given characteristic are also illustrated.

1.8. Thesis Outline

To accomplish the research objectives and address the research questions raised above, a thorough literature review on floods, droughts, and compound events including compound hydroclimatic events studies is presented in chapter 2. The study area and the datasets used are introduced in chapter 3 followed by a description of the applied methodology. The results are presented in the first section and discussed in the second section of chapter 4. The thesis conclusions as well as recommendation for future work are noted in chapter 5.

Chapter 2: Literature Review

2.1. Flooding

2.1.1. Flooding and Drivers

Floods are the most frequent natural hazard in Canada and worldwide, affecting many communities on a regular basis. Floods occur fast and could happen at any time of the year, often having clearly visible, and dramatic social, economic, and environmental consequences. Therefore, they have received more attention by the media and scientific literature compared to other natural hazards (Van Loon, 2013). Several processes generate flooding in Canada, many of which may be changed by variations in climate. Flooding in Canada is primarily caused by hydrometeorological conditions such as excess snowmelt runoff, rain on snow, rain, and ice-jams (Burn et al., 2016; Pietroniro et al., 2004) or more rarely, by the failure of man-made dams like the Mount Polley mine tailings spill in 2014 (Byrne et al., 2018). For instance, increased rainfall intensity is likely to cause increases in floods for pluvial regimes; however, investigating the flood generating processes can sometimes be quite challenging for more complex types of flooding such as rain-on-snow (Whitfield, 2012).

2.1.2 Examples of Historical Floods Events

Numerous instances of floods have occurred globally generated through different mechanism and exerting catastrophic costs. One of the deadliest floods in the history of human beings is the China's flood of 1937 that occurred on the back of a 2-years long drought and estimated to have had 1-4 million fatalities (Shukla, 2020).

Canadian communities have experienced 287 major flood events from 1900 to 2012 (Nastev and Todorov, 2013) countrywide. The frequency of floods has increased within this time window, with 80% of these events recorded after 1970 (Lebre, 2021). Moreover, the flood events have intensified in recent years as seen in the increases of flood insured costs in recent years reported by insurance/reinsurance companies (Munich RE, 2017). Historically, severe floods have hit Canada. For example, the costliest flood in Canada's history is the rain-on-snow induced flood that originated in the Canadian Rockies in 2013, which was associated with the onset of the rainy season coincided with persistent summer snowpack at alpine elevations (Teufel et al., 2016). As the event progressed, the precipitation regime switched to snow, leading to fresh snow accumulation on the warm mountains that subsequently contributed to snow melt and aggravated the flooding (Pomeroy et al., 2016).

Recently, an extreme two-day precipitation occurred in British Columbia (B.C.) on November 14th and 15th 2021, which was caused by an atmospheric river (AR) event and led to massive flooding in southwestern B.C. As the province's costliest recorded event, the flooding caused at least five fatalities, several landslides, wash-outs, and bridge collapses that closed all the highways, pipelines and rail lines, disconnecting Vancouver and southwestern B.C. with the rest of Canada for several days (Gillet et al., 2022). The estimated streamflow maxima exceeded one in a hundred-year events in several basins in the B.C. region since the antecedent wet condition preceding this AR event exacerbated the streamflow. Moreover, the rising temperatures during the event led to significant snowmelt and added to the runoff. Although the Insurance Bureau of Canada (2021) has estimated the damages to be as much as 450 million Canadian dollars, it is believed that the reported losses underestimate the actual costs as many households did not have insurance coverage. Details of the states of multiple hydrological processes (streamflow,

snowmelt, the antecedent conditions) during this flooding event and its costly impacts is well documented in Gillet et al. (2022).

2.1.3. Previous Research Related to Floods

Previously, the changing behaviour of future floods around the world have been assessed by several studies. The global scale assessment of Hirabayashi et al. (2013) shows growing risk of future floods due to increasing exposure. Considering flood risk and climate change, Kundzewicz et al. (2014) reported increasing economic losses from floods, while the authors were not able to attribute peak streamflow trends to increased rainfall intensity. Whitfield (2012) suggests that while warming of the atmosphere would intensify the hydrologic cycle, the variety and complexity of flood generating mechanisms make broad generalizations about future floods unwise.

Floods make up the largest social and economic losses of any climate-related phenomenon in Canada (Nastev & Todorov, 2013). Thus, changes in the observed floodings in Canada have been investigated in many studies. Using partial duration series (PDS), Caissie and El-Jabi (1993) analysed 237 stations from across Canada to provide a better description of floods. The study of trends in timing and magnitude of seasonal floods conducted by Cunderlik and Ouarda (2009) reveals statistically significant earlier occurrence of snowmelt floods, increased frequency of fall floods in some watersheds, and decreasing snowmelt peaks in some stations. Using a total of 280 gauging stations across Canada, Burn and Whitfield (2016) analyzed the changes in floods and flood regimes in the country. Although the nature and strength of changes vary for different flood-generating mechanisms, decreasing flood magnitude in nival catchments, increasing flood magnitude in pluvial catchments were reported by the authors. Furthermore,

pluvial flood-generation processes might have had increasing importance in mixed-regime catchments while snowmelt events have decreasing importance.

On the other hand, the future characteristics of flood events in Canada have been also investigated. Although countrywide studies are rare, there a several studies investigating the surface runoff changes on a regional scale. Future projections indicate an increase in annual flow in northwestern Canada including the Mackenzie and Yukon River basins, mainly due to the higher precipitation amounts projected at higher latitudes (Poitras et al., 2011; Thorne, 2011). Moreover, shifts in the timing of the maximum streamflow to winter, earlier freshet onset and higher runoff in spring, and reduced summer runoff in the Peace and Columbia basins in B.C. is projected for the 2050s (Schnorbus et al., 2014).

2.2. Droughts

2.2.1. Droughts and Drivers

Drought is a complex phenomenon; therefore, it is defined in many ways. Although a universal definition and single indicator for drought does not exist, mainly due to the existence of different drought types, drought is commonly defined as "a sustained period of below-normal water availability that is a recurring and worldwide phenomenon, with spatial and temporal characteristics that vary significantly from one region to another" (Tallasken and Van Lanen, 2004). Drought is a major natural disaster with severe and often long-lasting consequences, affecting all regions of the world (Fleig et al., 2006; Parry, 2019). Compared to floods, droughts have a much larger spatial and temporal scale (Van Loon, 2013).

Droughts begin with a period of rainfall deficit, which is a prolonged period of precipitation below the average expected conditions for the location and time of year, called a meteorological

drought. The duration and severity of the meteorological drought will have different implications for the propagation of drought through the hydrological cycle in different locations (Van Loon 2015). When a meteorological drought is coupled with high temperatures, soil moisture or agricultural drought may develop, which has implications for wildlife food web and crop yields. Under soil moisture drought conditions, groundwater recharge and hydrological response to rainfall may be limited, leading to hydrological droughts, as low river flows and groundwater levels loom. The abnormally low streamflow could impact freshwater ecosystems and their inhabitants (ecological drought), and limit hydropower generation, drinking water supply, crop production (irrigation), and waterborne transportation. The impacts of the different aforementioned drought types can collectively form socio-economic droughts, whereby a water resources system fails to meet water demands (Parry, 2019; Van Loon, 2013).

Droughts around the world have different characteristics, which are closely linked to the region's hydroclimate. Droughts usually occur naturally, but multiple climatic and anthropogenic drivers (such as changes in land and water management or human decisions and activities) could aggravate them (AghaKouchak et al., 2020). Often droughts are triggered by dynamic interactions between atmosphere and land surface, which alter the water fluxes such as precipitation, evaporation, and evapotranspiration over a longer duration (Haile et al., 2019). Since the global atmospheric circulation controls the average pattern of rainfall, temperature and associated evapotranspiration in different climate zones, an atmospheric circulation anomaly may cause drought (Tallaksen and Van Lanen, 2004). Therefore, droughts are often caused by the unusual timing, location, or persistence of regional weather patterns. Spatially large and temporally long droughts arise because of the large-scale atmospheric circulations coupled with the feedback mechanisms. However, the spatial and temporal variations of droughts are highly

heterogenous, which pose challenges for the estimation of the future risks brought about by this natural disaster. Besides climate variability, anthropogenic impacts (e.g., water diversions), climate change, and land-use changes, intensified by topographic complexities can accelerate intense and frequent drought events (Haile et al., 2019).

2.2.2. Examples of Historical Drought Events

Countless drought instances have been recorded in the world, such as the three-years-long drought of China during 1876-79 (with almost 3 million fatalities due to famine), or Bangladesh in 1943 (with almost 2 million fatalities) (World Economic Forum, 2019). Canada has also experienced devastating droughts. Generally, droughts in Canada affect one or two parts of the country and are relatively short, ranging from one or two seasons (Agriculture and Agri-Food Canada, 2016). Although droughts can occur in many Canadian communities across the country, the most susceptible areas to droughts are the Prairies, which is Canada's agricultural hub, and interior valley of B.C. (Bonsal et al., 2011). This is mainly due to their location being in the lee of major mountain ranges resulting in low precipitation with high variability (Moazami et al., 2022). Although the country has experienced several droughts, the drought in 2001 and 2002 almost spanned the entire southern half of the country stretching from B.C. to the Maritimes bringing conditions unseen for at least 100 years in some regions (The Canadian Encyclopedia, 2015). Recorded as the country's first coast-to-coast drought, this prolonged and extensive drought dropped agricultural production by almost $3.6 billion, caused employment losses of more than 41,000 jobs, and negatively affected water supplies that were previously reliable (Agriculture and Agri-Food Canada, 2016).

When considering droughts, B.C. is no exception. Although the province has been historically hit by several droughts, in 2014 and 2015, many watersheds in B.C. experienced streamflow drought, being likely the most severe since streamflow monitoring began in the mid-20th century (Coulthard et al., 2016). Despite wet winters of the B.C.'s watersheds, record-breaking low snowpacks as well as dry spring and summer, and high summer temperature exacerbated the drought conditions. Although near-normal to slightly below-normal snowpack were present near the end of the preceding winter, the abnormally warm temperatures in March and April led to record low snow water equivalent (SWE). Moreover, extraordinary warm and dry conditions due to a persistent upper ridge off the west coast of North America, was compounded with the low SWE that created one of the worst droughts in the region (Szeto et al., 2016). During this drought, the provincial government assigned the highest possible (Level-4) drought rating to large areas in southern B.C. and issued several extreme-low streamflow advisories, and extreme wildfire risk ratings (Szeto et al., 2016).

2.2.3. Droughts and their Changing Behavior

Global observations indicate that drought frequency has increased, with substantial variation (Dai, 2011). For example, the frequency and intensity of droughts in east Asia, Mediterranean, and West Africa has increased since 1950s. Furthermore, droughts have occurred more frequently in the tropics and subtropics since the 1970s. On the other hand, the global warming is projected to increase the drought occurrence and duration by a factor of two and six, respectively, by the end of the 21st century (Burke et al., 2006; Sivakumar et al., 2014). Moreover, the increasing global temperature could accelerate droughts onset and intensity, which would exacerbate drought condition when coupled with the increasing future water need of societies (Trenberth et al., 2014; Haile et al., 2019).

Since prolonged, large-area droughts in Canada are amongst the country's costliest natural disaster, with impacts on a wide range of sectors such as agriculture, forestry, industry, health, and society, drought research has scientifically received considerable attention. Previously, several Canada-wide trend analyses of temperature and precipitation (common inputs to meteorological drought indices) have been conducted. For instance, Vincent and Mekis (2006) investigated drought related temperatures (maximum temperature > 90^{th} percentile) and showed that the number of warm summer days (maximum temperature > 25 °C) increased over most of the country during 1950 – 2003. Moreover, the authors showed a decrease in the consecutive number of days with no measurable precipitation mainly over British Columbia and Atlantic Canada.

Results from trend investigations using drought indices substantially vary, both temporally and spatially. An analysis of agro-climatic conditions by Qian et al. (2010) showed several positive trends in growing season and annual SPI values in western and eastern Canada and decreasing trends in some regions in the Prairies (from 1895 – 2007). However, it has been noted that the general increases in precipitation are partially offset by increases in temperature, creating more evaporative demand (Bonsal et al., 2011). Girardin et al.'s analysis based on the Canadian Drought Code (an index based on daily maximum temperature and precipitation to assess forest fire potential) found that drought severity in central and eastern Canada essentially remained unchanged during the period of 1913 – 1998. Several drought indicators show large-area, multi-year dry episodes over the Canadian Prairies during the 1890s, 1910s, 1930s, 1980s, and 2000s (Klaassen, 2002). Overall, although instrumental records indicate significant increases in temperature over Canada, this has not subsequently led to increases in drought frequency,

whereas the observed trends and patterns tend to show decadal-scale variability coincident with that of precipitation.

Although no Canada-wide studies of future drought projections have been previously conducted since droughts have rarely occurred outside the Prairies, some have carried out regional-scale analyses (mostly over the Prairie region) using one or more drought indices (Bonsal et al., 2019). Future projections (2041-2070) of the annual and summer SPEI (using 6 CMIP5 models coupled with medium and high emission scenarios) over all the western Canadian river basins indicated that the southern watersheds showed a gradual increase in annual water deficit throughout the 21st century, while the opposite was true for northern basins (Dibike et al., 2017). Furthermore, the future frequency of severe-to-extreme drought conditions (measure by PDSI and soil moisture) is projected to increase (using medium emission scenario) by the late 21st century for much of southern Canada, including southeast British Columbia, the Prairies and Ontario (Dai, 2012; Zhao and Dai, 2015, 2016). Despite the overall consistency in the projected increased likelihood of future droughts over southern interior continental regions of Canada, the magnitude of these changes has large uncertainties. This is mainly due to the shortcomings of the drought indices that estimate the potential evapotranspiration, which may lead to an overestimation of drought intensity previously reported by other studies (Sheffield et al., 2012; Trenberth et al., 2014). The discrepancies in the estimated potential evapotranspiration arise since different methods that estimate the potential evapotranspiration use different variables (e.g., Thornthwaite method and Penman-Monteith method). Moreover, the different datasets used as well as the considered baseline period can cause discrepancies in the potential evapotranspiration estimates (Trenberth et al., 2014).

2.3. Compound Weather and Climate Extremes

2.3.1. Definition of Compound Extremes

Weather and climate-related extreme events (such as droughts, heatwaves, and storms) arise from complex interactions between various physical processes (Singh et al., 2020; Singh and Najafi 2020). These hazards often can overwhelm the capacity of natural and human systems to cope and create societal or ecological impacts (Zscheischler et al., 2020). When multiple drivers and/or hazards combine, their impacts can be amplified in different ways such as: a) multiple hazards occurring at the same time; b) previous climate conditions or weather events increasing the system's vulnerability to successive hazards; or c) spatially concurrent hazards leading to regionally or globally compounding effects (Bevacqua et al., 2021; Zscheischler et al., 2020).

Compound events (also referred to as correlated or complex extremes) were first introduced by the Inter Governmental Panel on Climate Change (IPCC) Special Report on Climate Extremes (SREX) in 2012 as "a combination of multiple drivers and/or hazards that contributes to societal or environmental risk." This initiative, however, has been evolved into an interdisciplinary matter at the interface of climate science, climate impact research, engineering, and statistics. The evolution of compound extremes science has led to the development of more thorough definitions of such climatic hazards. For instance, Leonard et al. (2014) introduced a systematic framework to study compound extreme events by defining a compound event to be "an extreme impact that depends on multiple statistically dependant variables or events." This definition has been evolved to define compound extreme events as "the combination of multiple drivers and/or hazards that contributes to societal or environmental risk" (Zscheischler et al., 2018).

Although the occurrence of such impactful compound extreme events might seem to have low probability, Zscheischler et al. (2018) have accounted for dependencies between all relevant drivers of multiple observed compound events and have described the processes by which many of such rare events may become foreseeable and to some extent predictable. Therefore, the traditional risk assessment methods, that only consider one driver/hazard at a time, could lead to underestimation of the potential risks of compound extreme events (Singh et al., 2021; 2022). Processes causing extreme events often interact and are spatially and/or temporally dependant (Zscheischler et al., 2018), which in return calls for the development of contemporary systematic approaches for risk reduction that considers the increasing risk of compound extremes.

2.3.2. Typology of Compound Extreme Events

Recently, Zscheischler et al. (2020) have proposed a typology of compound extreme events. In their framework, compound extreme events are consisted of modulators, drivers, hazards, and impacts. Hazard is the climate-related phenomena, which is the cause of impact. Hazards in turn are caused by one or several climatic drivers such as storm surge, wave, amongst others. Drivers are affected by modulators which could be low-frequency modes of climate variability such as the El Nino – Southern Oscillation (ENSO), weather systems such as severe storms, tropical cyclones, and stationary high-pressure systems, which could influence the frequency and location of a driver. On top of all, the anthropogenic factors (such as land use changes and anthropogenic climate change) could potentially alter all elements of compound extreme events.

According to Zscheischler et al.'s (2020) typology, compound extreme events can be categorized into 4 different groups namely: a) preconditioned events, whereby one or more hazards can cause or amplify an impact because of a pre-existing climate-driven precondition; b) multivariate

event, which refers to the cooccurrence of multiple climate drivers and/or hazards in the same geographical region, causing an impact; c) temporally compounding events, that is a succession of hazards that affect a given geographical region, leading to an (amplified) impact; and d) spatially compounding events, that occur when multiple connected locations are affected by the same or different hazards within a limited time window. It is noted that not all events can be easily assigned to a single type of aforementioned categories, but rather can be classified into multiple categories of compound extremes.

2.3.3. Compound Extremes Studies

Previously, a variety of compound weather and climate extremes have been investigated, regionally and globally. Singh et al. (2020) have reviewed the covariability of temperature and precipitation across Canada. The authors showed that the signs of accelerated warming and wetting conditions over northern while hot and dry conditions are reported for the Prairie provinces. Compound flooding in the coastal regions of Canada have been studied by Jalili Pirani and Najafi (2020, 2022), that provided evidence of changing interrelationships between drivers of flooding. Mukherjee and Mishra (2020) explored compound drought and heat waves and reported significant increases in the drought-related heatwaves and affected global land area in recent years. Such compound events have been shown to be on a rise in many regions in the northern hemisphere when considering the frequency, severity, and duration. Zhou et al. (2019) projected increases in the intensity and frequency of compound drought and aridity events. Using soil moisture deficit and high vapour pressure deficit, the authors showed that the projected increase in frequency and intensity of such compound events could exert increasingly negative effects on continental productivity. The cooccurrence and correlation of hot and dry summers are studied by Zscheischler and Seneviratne (2017). The authors showed that the dependent structure

of the variables affect the occurrence frequency of multivariate extremes, which calls for a multivariate perspective to appropriately assess changes in climate extremes and their impacts. Post wildfire extreme rainfall events over the western U.S. were explored by Touma et al. (2022). Considering the business-as-usual emission scenario, the authors showed that the frequency of such compound extreme events increases by 100% over California and 700% over PNWNA by the end of the 21st century.

2.4. Compound Hydroclimatic Events

2.4.1. Examples of Compound Hydroclimatic Events

Historically, there have been several compound hydroclimatic events (CHCEs) recorded globally. Successive floods and droughts are commonplace in many regions of the world such as Asia and North America with many recorded instances of such compound extremes. For example, the state of California experienced a prolonged drought during 2012 – 16, when surprisingly a succession of storm systems resulted in the most intense rainfall on any year on record (Wang et al., 2017). This record-breaking extreme precipitation abruptly caused groundwater recharge and rapidly re-filled reservoirs, causing severe and repeated flooding over large areas. Massive flooding rapidly refilled the Oroville reservoir in northern California, over-topped it, and resulted in damages to the spillway. Moreover, almost 500 residents were evacuated in Manteca after a levee was compromised. Hundreds of roads were disrupted, and many buildings were damaged, leading to declaration of two state of emergencies and serious economic losses (Vahedifard et al., 2017).

Such transitions from one extreme to the opposite extreme have also been experienced in the Europe. For instance, successive dry winter in 2010 – 11 and 2011 – 12 in England and Wales

led to substantially lower than normal river flows and groundwater levels in late March 2012. However, a swift succession of storms through the summer delivered persistent heavy rainfall, which eventually turned into the wettest nine months in the England and Wales. The persistence and magnitude of the rainfall rapidly increased the river flows and caused widespread, protracted, and repeated flooding (Parry et al., 2013).

The succession of the floods and droughts as compound events could occur in both directions. While in the case of California, and England and Wales, droughts were followed by floods, the opposite cases have also been reported. For instance, while the flood of 2011 along the Mississippi Rive brought about approximately $2 to $4 billion damages, a subsequent drought in 2012 over the same region caused almost $30 billion in economic losses (Ford et al., 2021). More recently, compound flood to drought events have been experienced in the Midwest region of the United States, affecting parts of Kentucky, Ohio, Indiana, and Illinois in 2019 (Ford et al., 2021). Although extreme hydrologic hazards (i.e., floods and droughts) are typically studied individually, many successive occurrences of such extremes suggest that studying hydrological hazards in isolation fails to consider their additional or magnified impacts due to swift transitions between the two.

2.4.2. Impacts of Compound Hydroclimatic Events

Abrupt alterations between droughts and flooding, featuring quick transitions from one extreme to the other are particularly problematic for water managers (Swain 2015; Swain et al. 2016; Maxwell et al. 2017). The challenging periods of successive drought and flooding place substantial strain on emergency and hazard response teams (Leonard et al. 2014), threaten the stability of water supply infrastructure (e.g., levees in California) (Vahedifard et al., 2017;

Vahedifard et al., 2015), and exacerbate existing tensions between the under-stress resources for flood relief or long-term water resource management. The compound nature of such transitions is highlighted by situations in which emergency declarations are enacted for both drought and flood in quick succession (e.g., in California during 2016-17) (Wang et al., 2017). Furthermore, intense rainfall events following droughts can rapidly erode sediment that is accumulated during the preceding dry period (the National Institute of Water and Atmospheric Research, 2005), the removal of which can hinder ecosystem recovery (Westwood et al. 2017). On larger scales, extreme rainfall can cause substantial mass movement events (Swain 2015), with the resulting sediment impacting water supply infrastructure (e.g., reservoirs and levees in California in 2016-17). In addition, prolonged periods of drought could change soil properties and inhibit the infiltration of rainfall, which in turn increases the responsiveness of river flows and exacerbates flooding (Mahaffey and Wentworth 2016). Moreover, Gimble et al. (2016) has shown that drought history can effectively reduce the soil infiltration through increased hydrophobicity in forest soils regardless of soil type and tree species, leading to increased risk of flash flooding after droughts.

2.4.3. Previous Studies on Compound Hydroclimatic Events

Recent devastating CHCEs across the world, such as in Australia (Mount et al. 2017), England (Parry et al., 2013), and California (Wang et al., 2017) has ignited the motivation of studying such disastrous events. Although using different terminologies and indicators to refer to CHCEs, all conducted studies have aimed for characterising the same phenomena. However, a thorough study considering different types of Compound Hydroclimatic Events (Compound Climatic Events and Compound Hydrologic Events) using multiple climatic and hydrologic variables has not been conducted. Moreover, regional assessments of the spatial and temporal patterns of the

characteristics of such compound events under climate change for Canada is not available to date.

Using the Palmer drought severity index (PDSI) to classify droughts on a monthly basis, Maxwell et al. (2013) suggested that tropical cyclones could bring about synoptic conditions favourable for drought to flood events. Moreover, the large-scale ocean-atmosphere influences on such tropical cyclones have been investigated. The results revealed that the negative phase of the North Atlantic Oscillation (NAO-) and the positive phase of the Atlantic Multi-decadal Oscillation (AMO+) are the most suitable conditions (produces the greatest likelihood) for the occurrence of drought busting tropical cyclones in the Gulf and southeastern coastal United States (Maxwell et al., 2013). In another study, Maxwell et al. (2017) explored the changes in the mechanisms causing rapid drought cessation in the southern United States. Considering three storm types of Frontal, Tropical, and Airmass, the authors used the PDSI to show the soil moisture deviations brought about by each storm type when experiencing warm season droughts. The results indicated that 73% of all warm-season droughts were ended rapidly with the three storm types ending droughts over similar spatial areas. Even though frontal storms were the most frequent mechanism for rapid drought cessation over the period of 1979 – 2013, their occurrences significantly decreased and were negatively correlated to the increases in the Northern Hemisphere temperatures. Similarly, the future projections suggested continued decreases in the frequency and relative contribution of frontal storms causing rapid drought cessations (Maxwell et al., 2017).

Motivated by the California's 2016 – 17 compound flood – drought event, Swain et al. (2018) showed the frequency of such compound events is projected to increase throughout the 21st century over California. Using the Community Earth System Model Large Ensemble of climate

model simulations, the authors projected increases in the frequency of wet and dry extremes, as well as increases in the compound extreme dry-to-wet events. These substantial increases were despite modest changes to the climatology of rainy season precipitation. Moreover, the future projections of precipitation showed shifts in the climatology of precipitation seasonality to earlier occurrences over the entire California. Composite analysis of the authors over California using simulations of large-scale atmospheric circulation patterns also confirmed that wet years were linked to strong low-pressure anomalies over the northeastern Pacific Ocean, while dry years coincided with seasonally persistent high-pressure patterns extending across the northeastern Pacific. Moreover, the authors showed that the spatial characteristics of large-scale atmospheric patterns driving California's precipitation extremes may remain stationary in the future under business-as-usual emission scenario (RCP8.5). However, Swain et al. (2018) suggested that more work is required to better understand the underlying changes in both remote (i.e., tropical and Arctic teleconnections) and regional-scale (atmospheric rivers and orographic precipitation) influences on compound hydrometeorological extremes.

The rapid transition of one hydrological extreme to the contrasting extreme is also investigated in Ford et al. (2021). The authors investigated the changes in the characteristics of flood to drought events similar to the incidents recorded for the Midwest United States. Using the Standardised Precipitation Index (SPI), the authors showed that the region has became wetter since the 1950s, with annual wet extremes increasing at much larger rates than annual dry extremes. Furthermore, hotspots (eastern Missouri to western Ohio) for rapid flood to drought transition events were identified considering the frequency of such compound extreme occurrences. Since the study used observed precipitation only, the authors suggested using future climate simulations to

investigate the projected changes in the characteristics of extreme precipitation events as well as transition between dry and wet conditions.

Ansari et al. (2022) studied the spatiotemporal evolution of the features of wet-dry events and their transitions across a watershed in south Asia. Considering the daily observed precipitation and temperature data of 15 climate stations, the authors used the standardized precipitation evapotranspiration index (SPEI) to characterize the wet and dry conditions for the period of 1981 – 2014. Temporally, the results indicated a strong change in the basin's climatic features associated with El Nino-Southern Oscillation (ENSO) at the end of 1997, as wet and dry conditions prevailed before and after 1997, respectively. Moreover, their spatial results showed higher susceptibility of this monsoon-dominated region towards wet events in the eastern part, whereas the western portions are more prone to dry events. Also, the surrounding region of the Himalaya divide line and monsoon-dominated part of the basin were found to be the hotspots for rapid dry-wet transitions.

In another work, the ecological impacts of the CHCEs (i.e., drought to deluge) have been investigated in a semi-arid grassland (Hoover et al., 2022). In this experimental study, the authors questioned how a deluge during a drought could impact the productivity and carbon cycling in a semi-arid grassland. Hoover et al.'s findings showed that the deluge imposed during extreme drought stimulates carbon fluxes and plant growth. However, the precipitation amount, event size, and timing were concluded to be important as well. Moreover, while the deluge's positive effects on carbon fluxes and plant growth persisted for a month, the negative effects of extreme drought on the end-of-season productivity were not completely offset by the deluge. Therefore, in the case of consecutive contrasting hydroclimatic extremes (i.e., drought to

deluge), the deluge can stimulate temporally dynamic ecosystem processes (e.g., net ecosystem exchange) while can only partially compensate for reductions in ecosystem.

Chapter 3. Study Area, Data, and Methods

3.1. Study Area

The northwest North America (NWNA) is our study area, which extends over the northwestern corner of the United States and the southwestern part of Canada. The NWNA is consisted of the states of Washington, Idaho, western Montana, and Oregon in the United States (U.S.) and the province of B.C. and some portions of Alberta in Canada. Three large river basins of Peace, Fraser, and Columbia extend over a large portion of the NWNA (Figure 1). NWNA is chosen in this study since compound hydroclimatic events within (2021 in British Columbia; Gillet et al., 2022) or in proximity (2016-17 in California; Swain et al., 2018) to the study area have been reported previously.

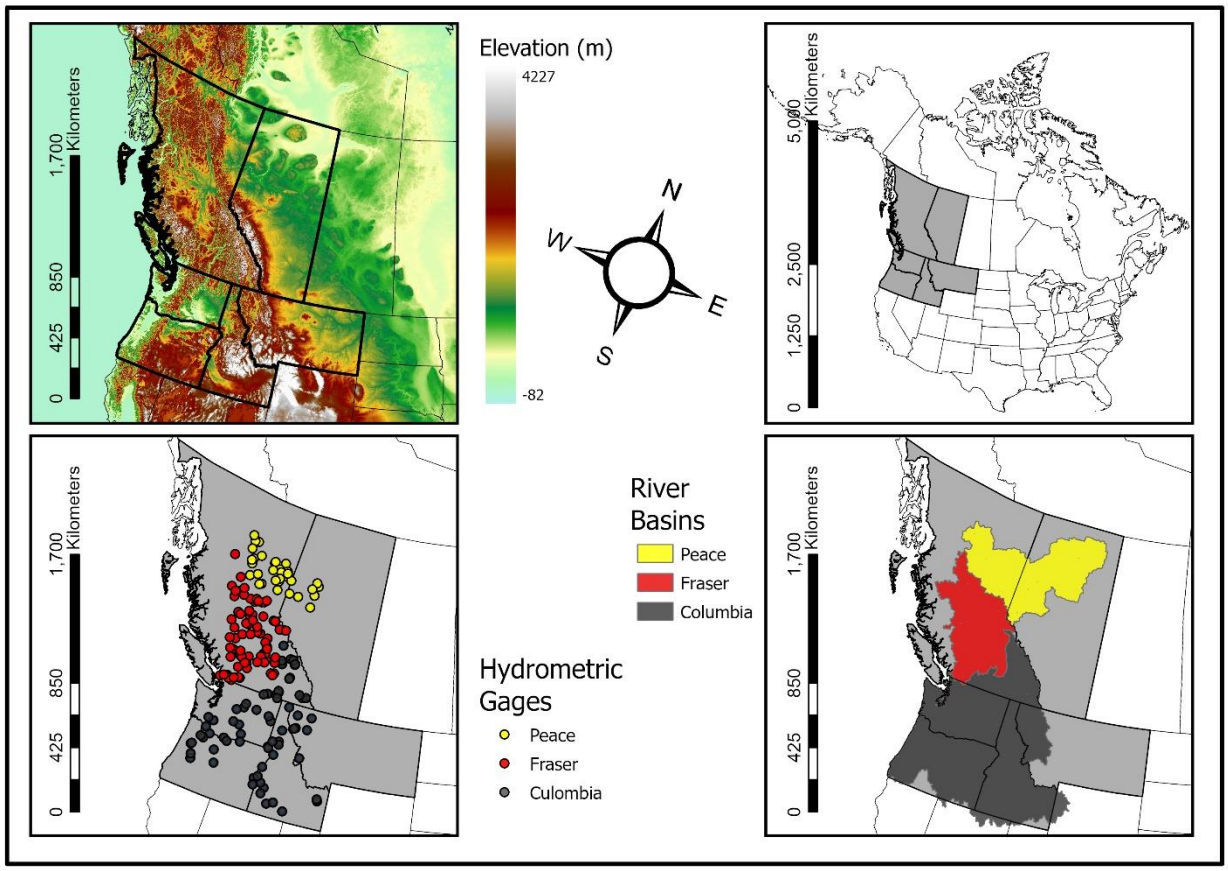

Figure 1 - Location map of the Northwest North America and the three large river basins of Peace, Fraser, and Columbia. The dots show the location of the Hydrometric Gauges used in this study.

3.1.1. Peace River Basin

Located in the western Canada, the Peace River Basin (PRB) headwaters is situated in the Rocky Mountains. With a total drainage area of approximately 101,000km^2, the PRB covers parts of north-central B.C. and northeastern Alberta (Vore et al., 2020; Romolo et al., 2006). The PRB is a heterogenous catchment with elevation ranging from 400 to over 2800m. The average temperature over basin ranges from -11.7°C in January and 12.4°C in July (Najafi et al., 2017). Precipitation in snow dominated over the PRB as almost half of its annual precipitation falls as

snow during October – April. The PRB is ecologically and economically important as it powers the Bennett Hydroelectric Dam, Peace Canyon Dam, and Site C Dam and Reservoir, and is the main contributor to the Peace-Athabasca Delta, the largest boreal inland delta in the world (Timoney, 2013).

3.1.2. Fraser River Basin

As the largest drainage basin in B.C., the Fraser River Basin (FRB) drains almost 230,000km^2 from its headwaters in the Rocky Mountains (near Jasper, Alberta) to the Pacific Ocean at Vancouver (Schnorbus et al., 2010). The FRB is a physiographically heterogenous catchment with elevations ranging from sea level to 4000m and can be divided into three regions: (i) eastern mountains (including the Rocky and Columbia Mountains); (ii) interior plateau in the central part of basin; and (iii) coastal mountains in the southwestern part (Shrestha et al., 2016). Therefore, the basin provides an unevenly drainage with high-elevation snow in the Rocky, northern Columbia, and southern Coast Mountains creating the most runoff. The FRB is snow dominated having the mean annual precipitation ranging between 200 and 5000mm. Average temperature of the basin ranges from -8.9°C in January to 13.1°C in July (Najafi et al., 2017). The basin is mostly forested (76% of the catchment), and it contains 12 ecoregions and 9 biogeoclimatic zones (Schnorbus et al., 2010). The FRB is economically invaluable for B.C. as the economic activity within the basin makes up 80% of provincial and 10% of federal gross domestic product. Moreover, the Fraser River is one of the most productive salmon rivers in the world with its lakes and tributaries providing spawning habitats for all five species of eastern Pacific salmon and more than 100 other species of fish (Canadian Heritage Rivers System, 2009). Streamflow over most of the FRB is nival (dominated by snowmelt during the spring freshet). Moreover, the

western portion of the FRB is affected by strong, seasonal incursions of moist air from the Pacific in fall and winter, often associated with cyclonic storms (Curry et al., 2019).

3.1.3. Columbia River Basin

The Columbia River Basin (CRB) drains an area of 560,000 km^2. Characterized by contrasting climatic regimes, the western slopes of the Cascade and Olympic Mountains in the Pacific coastal drainages experience moderate temperatures and receive some of the highest precipitation in North America. On the other hand, locations in the interior of the CRB receive considerably less precipitation. The average annual precipitation is variable across the region and ranges from less than 200mm in central Washington to 500-750mm near the mountain foothills across the basin and 1000 or more inches in some mountain areas. Precipitation primarily falls during the period from October through March, while summers are relatively dry. Throughout winter, when the majority of precipitation occurs, snow accumulates in upper elevations of the basin. This snow melts in the spring and early summer, resulting in peak flows for the year (State of Washington, 2011). The CRB is bounded to the east and north by the cold and moist Rocky Mountains. Therefore, precipitation within the mountainous regions has been winter dominant, causing the region's hydrology to be snowmelt driven (Chegwidden et al., 2019).

3.2. Data

3.2.1. Observations

In this study, we use the Pacific Climate Impacts Consortium (PCIC) meteorology for NWNA, or PNWNAmet data (Werner et al., 2019), which provides gridded daily observations by interpolating records of a high density network of hydrometric gages over northwest North

American (NWNA) domain (NWNA; 40°N to 72°N and -169°W to -101°W) and is publicly available. This gridded meteorological forcing dataset (PNWNAmet) is commonly used as a target dataset for statistical downscaling and hydrologic modelling since it includes observed daily station data that is interpolated to a suitable resolution for such applications. Temporally, the PNWNAmet covers 1945-2012 and provides maximum and minimum temperature as well as precipitation and wind speed with a spatial resolution of 1/16° (approximately 6km). The high resolution of this gridded dataset makes it a suitable candidate for hydrologic modeling since many distributed hydrologic models (e.g., Variable Infiltration Capacity model) have the same spatial resolution to this dataset. The PNWNAmet interpolates a set of long-term homogenized stations via the trivariate thin plate spline interpolation method using a high resolution, high station density climatology as a predictor. The dataset was generated by the minimum temperature, maximum temperature and precipitation interpolated separately using latitude, longitude and a 1971-2000 climatology from ClimateWNA (v5.10) as predictors. Werner et al. (2018) have shown the PNWNAmet is a robust daily gridded meteorological dataset for hydrologic modeling over the NWNA compared to other commonly used products such as the Natural Resources Canada observational dataset (NRCANmet) (Hopkinson et al., 201; McKenney et al., 2011) or the PCIC meteorology for BC (PBCmet) due to its high resolution and larger spatial and temporal extent. Therefore, the PNWNAmet have been utilized in several studies over the NWNA (Mahmoudi et al., 2021; Dibike et al., 2021; Shrestha et al., 2019).

3.2.2 Climate Simulations

Global Climate Models (GCMs) are large-scale physically-based numerical models of the atmosphere, which can simulate the climate under different scenarios and are used to study climate change on a global scale (EURO-CORDEX Guidelines, 2017; Tallaksen and Van Lanen,

2004). GCMs describe various components of the Earth system as well as their nonlinear interactions and feedbacks. GCMs can simulate the past climate using measured values as forcing data, whereas for future projections values, particular emission scenarios are employed. Generally, it is required to specify the boundary conditions, including time-dependent atmospheric greenhouse gas concentrations, when using the numerical climate model simulations (Cannon et al., 2020), since the nature of the climate simulations is determined by details of these boundary conditions. For instance, the future temporal evolution of atmospheric greenhouse gas concentrations could be determined by one of the four representative carbon pathways (RCP2.6, RCP4.5, RCP6, RCP8.5) (Moss et al., 2008) defined in the Fifth Assessment Report of the Intergovernmental Panel on Climate Change (IPCC). Given that the structure of the models, greenhouse gasses emission scenarios, and the boundary conditions of different models vary, the outputs of different GCMs would vary (Tallaksen and Van Lanen, 2004).

- 3.2.2.1 GCM Selection

In this study, a representative ensemble with 12 members consisting of 6 models participating in the 5th Phase of the Coupled Model Intercomparison Project (CMIP5) each paired with the two medium and high representative concentration pathway (RCP4.5 and 8.5) radiative forcing scenarios are used. Although using as many scenarios as possible from a large ensemble is ideal as it allows to better quantify the uncertainty range of a large ensemble simulations (members having different boundary conditions), this is not always feasible due to computational costs. Therefore, a subset of all scenarios, which presents the full range in simulated future changes across the large ensemble is used. Even though one can manually select GCM scenarios that capture most of the simulated range through visualizing climate variables, selecting representative climate scenarios is a challenging task when dealing with multivariate data,

particularly in a high-dimensional space. To overcome this challenge, Cannon (2015) has proposed an automated procedure called the Katsavounidis–Kuo–Zhang (KKZ) algorithm for GCM selection (using a cluster analysis). On average, the KKZ algorithm requires 40% fewer scenarios compared to other selection methods like k-means clustering to represent the 90% range of simulations across a large ensemble. Our GCMs were selected using the KKZ algorithm as this results in selecting a range of GCMs that extends across the overall range of the ensemble, specifically for climate extremes (Schoeneberg and Schnorbus, 2021). The GCMs used in this study are listed in Table 1.

Table 1 - List of GCMs used in this study, their modeling institute and atmospheric resolution (Jiang et al., 2016)

Model Name	Modeling Institute (Country)	Atmospheric Resolution
ACCESS1-0	Commonwealth Scientific and Industrial Research Organization and Bureau of Meteorology (Australia)	~1.9° × 1.25°, L38
CanESM2	Canadian Centre for Climate Modelling and Analysis (Canada)	~2.8° × ~2.8°, L35
CCSM4	National Centre for Atmospheric Research (United States)	1.25° × ~0.9°, L26
CNRM-CM5	Centre National de Recherches Météorologiques/Centre Européen de Recherche et Formation Avancées en Calcul Scientifique (France)	~1.4° × ~1.4°, L31
HadGEM2-ES	Met Office Hadley Centre (United Kingdom)	~1.9° × 1.25°, L38
MPI-ESM-LR	Max Planck Institute for Meteorology (Germany)	~1.9° × ~1.9°, L47

- 3.2.2.2. Downscaling and Bias Correction

Although GCMs provide invaluable hydroclimatic information, they cannot be used for regional climate change impact assessments and hydrologic modeling due to their coarse spatial resolution (Table 1). Moreover, the coarse resolution of GCMs fails to reflect the detailed spatial variations in climate that are introduced by local orography, various land surface properties, and proximity to water. Therefore, downscaling is used to translate the coarse resolution of GCM simulations into finer scales. Moreover, since the internal structure of GCMs vary, their climatic simulations often have discrepancies compared to the observed climatic variables, which is referred to as systematic biases. Therefore, bias correction techniques must be applied to match the climatic simulations of the GCMs to that of the observations. To this end, daily values of minimum temperature, maximum temperature and precipitation are regridded to match the resolution of our hydrologic model (1/16°) and statistically bias corrected using the Bias Correction/Constructed Analogues with de-trended Quantile mapping reordering downscaling technique (BCCAQv2) and the Pacific Climate Impact Consortium (PCIC) meteorology for northwest North America (PNWNAmet) (Werner et al., 2019) as the reference meteorology. As a hybrid method, BCCAQv2 combines results from bias-corrected constructed analogs (BCCA) (Maurer et al., 2010) and de-trended quantile mapping (QMAP) (Gudmundsson et al., 2012). The BCCAQv2 method better preserves changes in quantiles and extremes (Cannon et al., 2015) as compared to its original implementation. Moreover, the BCCAQv2 works well for hydrologic extremes because of its ability to resolve event-scale spatial gradients (Werner and Cannon, 2015).

- 3.2.2.3. Global Warming Levels

We assess the regional patterns of the compound hydroclimatic events (CHCEs) using the projections of relevant hydrological variables at the global warming levels of +1.5 to +4°C Global Mean Temperature (GMT) compared to the Pre-Industrial (PI) era of 1860-1900. This follows the 2015 Paris Agreement, which aims to limit the average global warming level well below the 2°C, and to pursue efforts to limit the warming to 1.5°C compared to the PI (UNFCC 2015) era, as well as the recent release of the IPCC's special report on global warming of 1.5°C (IPCC, 2018). Consequently, understanding the impacts of different global warming levels on the local-scale hydrology is a policy relevant issue. The present-day state of the climate is represented by the base period of 1970-2000. An important temporal dimension of each global warming level (i.e., 1.5 to 4°C) is the 30-year period over which a specific warming level is exceeded. Given the structure of the models, greenhouse gas emission scenarios, and the boundary conditions of different models vary, it is expected that the 30-year period over which the average global warming reaches a specific level (e.g., +1.5°C compared to PI era) would differ from model to model (Seneviratne et al., 2018). To consistently assess the regional climate change impacts, each of the global warming periods for every member of our multi-model ensemble is determined as the center of the 30-year moving window over which the global mean temperature (GMT) exceeded the PI's GMT by that given global warming level (i.e., 1.5-4°C). The global warming periods for every ensemble member is presented in Table 2.

On a global scale, the future projections vary over a smaller range compared to regional changes (Seneviratne et al., 2016). However, it has been shown (Seneviratne et al., 2016) that the projections of different hydrological variables based on multi-model means show a high degree of linearity in the regional changes in extreme event intensity when making comparisons at

different levels of global warming. The authors have also shown that the temperature and precipitation extremes in the CMIP5 multi-model ensemble are mostly independent of the considered emissions scenarios. Therefore, there is little impact on the timing of greenhouse gas emissions in the emissions scenarios (Seneviratne et al., 2018). Thus, the differences in land-use or aerosol forcing in the RCP scenarios used in the (CMIP5) simulations may not strongly affect the overall projected behavior of temperature and precipitation extremes. Therefore, the climatology of projections at each global warming level is model and scenario independent when taking the multi-model mean. Thus, integrating global temperature targets, such as +1.5°C and +2°C GMT levels compared to the PI, into regional- and impact-related climate targets could be more powerful because such targets are more directly aligned with individual national interests. However, the relationship between changes in regional climate and the global warming levels are expected to alter in the presence of time-varying local forcings such as land-use and land-cover change, urban development, or human water consumptions.

Table 2 - The 30-years period over which different global warming levels occur for each member of the multi-model ensemble of GCMs used in this study

Ensemble Member	Pre-Industrial (1860-1900) GMT (°C)	+1.5°C GMT	+2°C GMT	+3°C GMT	+4°C GMT
ACCESS1-0_rcp45	13. 6	[2014, 2043]	[2036, 2065]	-	-
ACCESS1-0_rcp85		[2012, 2041]	[2024, 2053]	[2045, 2074]	[2065, 2094]
CanESM2_rcp45	13.7	[2002, 2031]	[2017, 2046]	[2058, 2087]	NA
CanESM2_rcp85		[1999, 2028]	[2012, 2041]	[2034, 2063]	[2053, 2082]
CCSM4_rcp45	13.4	[2000, 2029]	[2025, 2054]	-	-
CCSM4_rcp85		[1999, 2028]	[2018, 2047]	[2043, 2072]	[2065, 2094]
CNRM-CM5_rcp45	13.5	[2023, 2052]	[2044, 2073]	-	-
CNRM-CM5_rcp85		[2016, 2045]	[2030, 2059]	[2052, 2081]	-
HadGEM2_rcp45	13.5	[2015, 2044]	[2030, 2059]	-	-
HadGEM2_rcp85		[2009, 2038]	[2021, 2050]	[2041, 2070]	[2057, 2086]
MPI-ESM-LR_rcp45	13.5	[2009, 2038]	[2031, 2060]	-	-
MPI-ESM-LR_rcp85		[2006, 2035]	[2020, 2049]	[2045, 2074]	[2066, 2095]

3.2.3. Hydrological Simulations

- 3.2.3.1 Hydrologic Modelling

To replicate climate state dependent hydrologic response of the three large river basins of the study area, outputs from the Variable Infiltration Capacity (VIC) hydrologic model set up by Pacific Climate Impact Consortium (PCIC) (Werner and Schnorbus, 2021) was used. VIC is a

spatially distributed macro-scale hydrologic model, which can be implemented over large areas and have been shown to robustly represent the key processes such as evapotranspiration, snow accumulation, snowmelt, soil moisture and surface and subsurface runoff in the NWNA (Curry et al., 2019; Chegwidden et al., 2019; Shrestha et al., 2019 & 2021; Werner et al., 2013; Schnorbus et al., 2010). As a research model, various forms of the VIC model have been applied to most of the major river basins around the world, as well as globally. VIC model calculates water and energy balance at each grid cell with sub-grid variability of the soil column, land surface vegetation classes and topography represented by a spatial probability distribution. The model uses computational grids with a spatial resolution of 1/16° to model the spatial variability. The sub-grid variability is described with hydrologic response units (HRUs), which are derived using vegetation classes and 200-m elevation bands (Werner and Schnorbus, 2021). The hydrologic model uses the Arno conceptual model (Todini, 1996) to represent the soil moisture processes by considering three-soil layers. The spatial heterogeneity of runoff is modeled with variable infiltration curves to generate subsurface flow. Surface runoff is then generated when the moisture exceeds the storage capacity of the soil (see Liang et al. 1994; Liang et al. 1996; and Hamman et al. 2018 for more details about VIC model). We use output water fluxes of an updated version of the VIC model (VIC-GL, capable of simulating glaciers) since glaciers provide water to streams in many catchments of British Columbia when seasonal snowpacks are depleted (during summer and early autumn; Schnorbus, 2018).

The model is calibrated and evaluated using daily maximum and minimum temperature, precipitation, and average wind speed from PNWNAmet gridded meteorological dataset (with a spatial resolution of 1/16°) to generate the Reference Simulation for the 1945 to 2012 historical record (see Schnorbus, 2017 for VIC-GL calibration). After parametrization and calibration, the

model was forced with the downscaled and bias corrected climate simulations of the multi-model ensemble of GCMs to generate an ensemble of future hydrologic projections.

3.3. Methods

3.3.1. Compound Hydroclimatic Events

Different flood and drought generation mechanisms result in different characteristics for the corresponding flood and drought events. The two extremes can be quantified using different climatic and hydrologic variables such as precipitation, evapotranspiration, streamflow, soil moisture amongst others. Therefore, different types of compound flood and drought events can be defined. For instance, in Swain et al. (2018), authors use precipitation to project the future meteorological drought to flood compounds, while streamflow data has been used in Li et al. (2017). Moreover, representation of floods and droughts could be done using indices that can represent the climatic conditions, which could potentially lead to these extreme events. For example, Ford et al. (2019) have investigated the compound flood and droughts by utilizing the Standardized Precipitation Index (SPI) to extract the two extremes, while Ansari and Grossi (2022) have applied the Standardised Precipitation Evapotranspiration Index (SPEI). In Maxwell et al. (2013; 2017), meteorological droughts have been measured with the Palmer Drought Severity Index (PDSI). Li et al. (2017) implemented the Drought-flood abrupt alternation Index (DFAAI) by using the streamflow to model the abrupt flood-drought swings. Although the studies using flood/drought indices provide invaluable insights for water resources managers, making conclusions based on monthly indices could be misleading. For instance, an extreme short duration flood that is followed by a drought might not be captured and one might conclude the analyzing period to be dry (Yang et al., 2021). Moreover, the impacts of floods and droughts

are felt on a local scale, which are affected by a variety of physical characteristics (e.g., topography) or pre-existing conditions (e.g., soil moisture) of the catchment. Therefore, a thorough understanding of the characteristic of flood and drought transition calls for investigating both climatic ignition of flood and drought events as well as catchment hydrologic responses to these climatic conditions.

In this study, we analyse both the compound climatic events (CCEs) and compound hydrologic events (CHEs), collectively referred to as compound hydroclimatic events (CHCEs), to better shed light on the future risk of such problematic transitions with compounding economic and environmental impacts. To this end, precipitation and potential evapotranspiration are used to calculate the SPI and SPEI drought indices. The two drought indices are then utilized to find and characterise the CCEs. The SPI and SPEI drought indices are based on the probability of the accumulated precipitation and climatic water balance (defined as precipitation minus potential evapotranspiration), respectively (on different timescales). These indices are flexible and powerful with a relatively simple calculation procedure. Moreover, the SPI and SPEI can analyze both wet and dry periods/cycles. Since meteorological droughts can propagate to other components of the hydrologic cycle (e.g., streamflow, soil moisture, groundwater), streamflow simulations are also utilized to show the CHEs. To better illustrate, the methodology applied in this study is summarised in Figure 2.

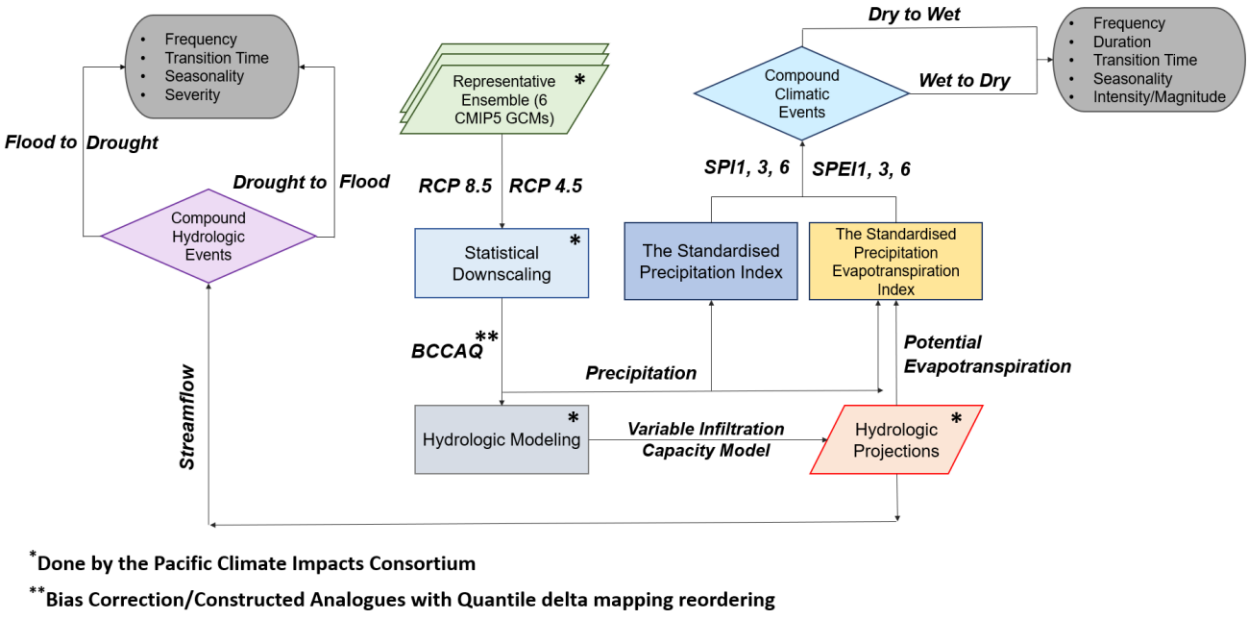

Figure 2 - The methodology applied in this study to characterise the compound hydroclimatic events (CHCEs).

3.3.2. Compound Climatic Events

- 3.3.2.1. The Standardised Precipitation Index

Drought is an insidious natural hazard that results from lower-than-expected levels of precipitation compared to what is considered normal and can affect all climatic regimes (Van Loon, 2015). Regional climate characteristics are heterogenous since the amount, seasonality, and form of precipitation differ widely between different location. Therefore, the extent of droughts is region dependant (Abbasian et al., 2020 & 2021). On the other hand, droughts have different meanings to various stakeholders such as water resources managers and engineers, agricultural producers, and hydroelectric power plant operators. The perspective distinction also exists within sectors as the drought impacts may differ markedly (Fleig et al., 2006). Many drought indices have been developed and used by meteorologists globally with different

complexities. But, just as a single definition of drought does not exist, there is no single drought index that meets the requirements of all (WMO, 2012). However, scientists have realized that a suitable index is one that is simple, easy to calculate, and statistically relevant and meaningful. Previously, McKee et al. (1993) developed the SPI, on account of the different impacts of precipitation deficits on groundwater, reservoir storage, soil moisture, snowpack, and streamflow. The SPI is a temporally and spatially invariant probability-based drought index (capable of analyzing both wet and dry periods/cycles), that is flexible, and powerful with a relatively simple calculation. Precipitation is the only parameter required for calculating the SPI. However, one needs at least 20 – 30 years of monthly precipitation values with maximum 15 – 25% missing data as suggested by the WMO (2012). The SPI can be calculated for different time scales (accumulation periods) such as 1, 3, 6, 9, 12, and 24 months, which could provide early warning of drought and assess meteorological, agricultural, and hydrological droughts and their severity (McKee et al., 1993). Drought planners, research institutes, researchers, and many National Meteorological and Hydrological Services around the world use the SPI for drought monitoring (WMO, 2012).

- 3.3.2.2. The Standardised Precipitation Evapotranspiration Index

The Standardised Precipitation Evapotranspiration Index (SPEI) is originally developed by Vicente-Serrano et al. (2010) and is calculated based on the monthly climatic water balance, which is defined as the difference between the precipitation and the potential evapotranspiration (PET) at a given accumulation period. Thus, unlike the SPI that only assesses precipitation variance, the SPEI also considers demand from evapotranspiration. Therefore, the SPEI captures the main impact of increased temperatures on water demand. SPEI is theoretically based on a

climatic water balance. Similar to SPI, a SPEI can capture both wetness and dryness at the surface.

- 3.3.2.3. Calculation of the SPI and SPEI

The SPI and SPEI are based on the probability of precipitation and climatic water balance accumulated on a given time scale. SPI quantifies the standardized deficit or surplus of precipitation over any period of interest (also known as accumulation period), whereas SPEI is interpreted as a relative measure of surface water surplus or deficit with respect to hydroclimate of the reference period. Computing the SPI and SPEI involves fitting a probability density function (PDF) to the precipitation totals and climatic water balance of the accumulated period and finding the cumulative probability. By applying a quantile-to-quantile normal score transformation (Equation 3.2), the SPI/SPEI is then generated by transforming the cumulative probability to the standardised normal random variable (Equation 3.1) with mean zero and standard deviation of one, which is the value of the SPI/SPEI (Figure 3).

$$f(x) = \frac{1}{\sqrt{2\pi\sigma^2}} \exp\left[-\frac{(x-\mu)^2}{2\sigma^2}\right] \quad \text{(Equation 3.1)}$$

Where f(x) is the PDF of normal distribution, and σ and μ are standard deviation and mean, respectively (in our case would be one and zero, respectively).

$$y = F_Y^{-1}(F_x(x)) \quad \text{(Equation 3.2)}$$

Where F_x (x) is the is the cumulative probability of the fitted distribution function to the precipitation, F_Y (y) is the standardised normal cumulative distribution function, and y is the transformed result (here leads to SPI/SPEI).

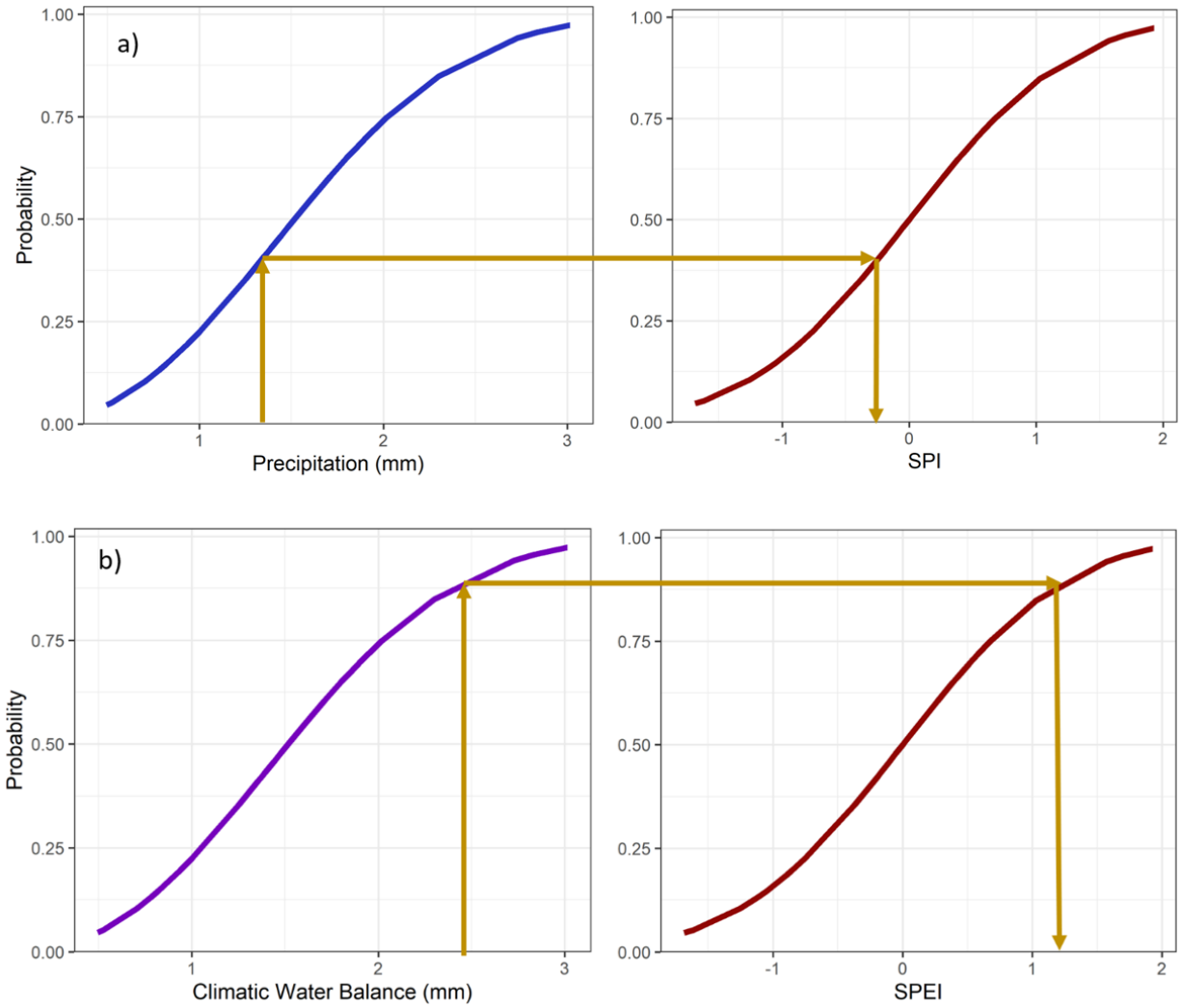

Figure 3 - SPI (a) and SPEI (b) calculation procedure (here for one month accumulation period). After fitting the proper density function (in this example we use the Gamma for SPI and Log-logistic for SPEI) to the monthly precipitation data (a) and climatic water balance (b), the cumulative probability is generated (blue and purple lines). Then, the SPI and SPEI is calculated by transforming (yellow line) the cumulative probability (blue and purple lines) to the standardised normal random variable with mean zero and standard deviation of one (red line).

The classification system shown in Figure 4 (proposed by McKee et al. (1993) and adopted by Vicente-Serrano et al. (2010)) is used to categorize wet and dry periods based on SPI and SPEI

values. A dry (wet) period occurs when the SPI/SPEI is continuously negative (positive) and reaches an intensity of -1 (+1) or less (more). Thus, every wet/dry event has a duration defined by its beginning and end, and an intensity for each month that the event continues.

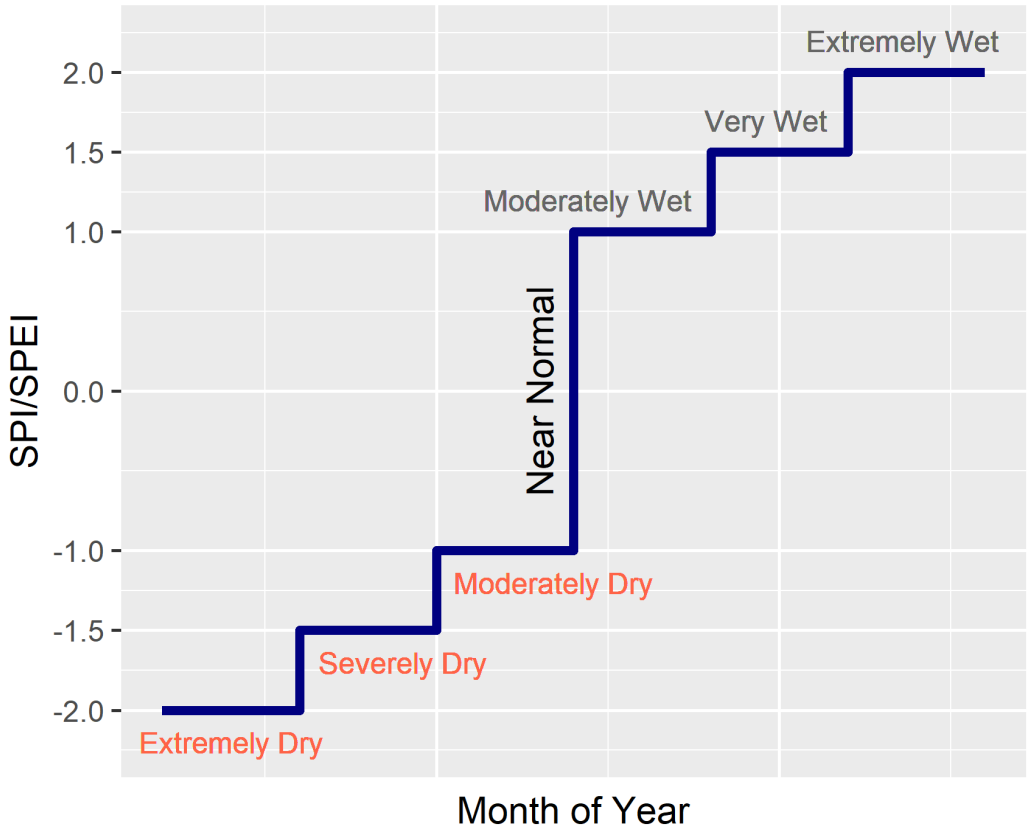

Figure 4 - Classification of wet and dry conditions based on the SPI/SPEI values (McKee et al., 1993; Vicente-Serrano et al., 2010)

The choice of the proper PDF fitted to the precipitation totals and climatic water balance is crucial since only a proper fit appropriately standardizes the index. Therefore, choosing a suitable theoretical distribution function to describe and normalize highly nonnormal precipitation or climatic water balance distributions is a key decision in the tow indices algorithm (Pieper et al., 2020). Originally, McKee et al. (1993) proposed using Gamma distribution to

calculate the SPI. On the other hand, Vicente-Serrano et al. (2010) have proposed fitting a Log-logistic distribution when they developed the SPEI index.

- 3.3.2.4. Algorithm for Calculating the SPI and SPEI

One of the strengths of the SPI and SPEI is their ability to be calculated over multiple accumulation periods (moving averaging windows), which can reflect the drought impacts on different water resources that are of interest to a variety of stakeholders. While drought indices (SPI and SPEI) calculated over short accumulation periods (1-3 months) reflect the short-term conditions with applications for meteorological droughts and short-term soil moisture conditions, anomalies over longer accumulation periods (e.g., 6 months) affect the streamflow, reservoirs, and groundwater response. Therefore, in this study, we investigate the compound climatic events (which could potentially lead to compound hydrologic events) using the SPI and SPEI calculated over 1-, 3-, and 6-months timescales to better understand the compounding impacts of such transitions on different water-resources dependant sectors. Since the two drought indices have been widely used globally as well as in Canada, we have chosen the Gamma and Log-logistic distributions amongst all candidate distributions to fit to precipitation and climatic water balance records, respectively, to find the SPI and SPEI values. The Gamma (Equation 3.3) and Log-logistic (Equation 3.4) distributions were selected following the recommendations of McKee et al (1993) and Vicente-Serrano et al., 2010), respectively. Moreover, previously several studies have calculated the SPI and SPEI indices in Canada and have shown these two distributions adequately estimate SPI and SPEI in Canada (Tam et al., 2019; Gurrapu et al., 2022). The selected distributions were fitted to the precipitation totals using an unbiased probability weighted moment (PWM), since this method does not result in biased standard deviation values (Tam et al., 2019).

$$f(x|\alpha,\beta) = \frac{x^{\alpha-1}e^{-\beta x}\beta^{\alpha}}{\Gamma(\alpha)}$$ (Equation 3.3)

Where $\Gamma(\alpha)$ is the Gamma function, α and β are shape and rate parameters, and $x, \alpha, \beta > 0$.

$$f(x|\alpha,\beta) = \frac{(\beta/\alpha)(x/\alpha)^{\beta-1}}{(1+(x/\alpha)^{\beta})^{2}}$$ (Equation 3.4)

Where α and β are scale and shape parameters, respectively.

- 3.3.2.5. Definition and Characteristics of Compound Climatic Events

To represent the dry and wet climatic conditions, we respectively use -1 and +1 thresholds based on the calculated SPI and SPEI values, and investigate the variability and characteristics of the compound climatic events (CCEs) with different accumulation periods. A wet-to-dry (or dry-to-wet) CCE occurs when a wet (dry) period of any duration (at least one month) is followed by a dry (wet) period of any duration (at least one month). The timespan between the end of the first period (dry or wet) to the start of the second contrasting period (wet or dry) is defined as the transition time (Figure 5). Moreover, abrupt transition is referred to the transition time that is less than 1 month. The positive sum of the SPI/SPEI for all the months within a wet or dry event can be termed the event's magnitude. Intensity is defined as the average SPI/SPEI value during the event and is calculated by dividing the event's magnitude to its duration. To make sure only impactful CCEs are presented, we limit the transition time to 6 months. The count of the transitions over each warming period of 30-years is reported as the frequency of CCEs at that given warming level. Furthermore, we investigate the changes in the area experiencing wet, dry, and concurrent wet-dry conditions annually at different global warming levels. The seasonality of the area undergoing wet, dry, and concurrent wet-dry conditions with different accumulation

periods are also investigated under climate change. In addition, we explore if the future CCEs are projected to intensify if the global warming is not limited.

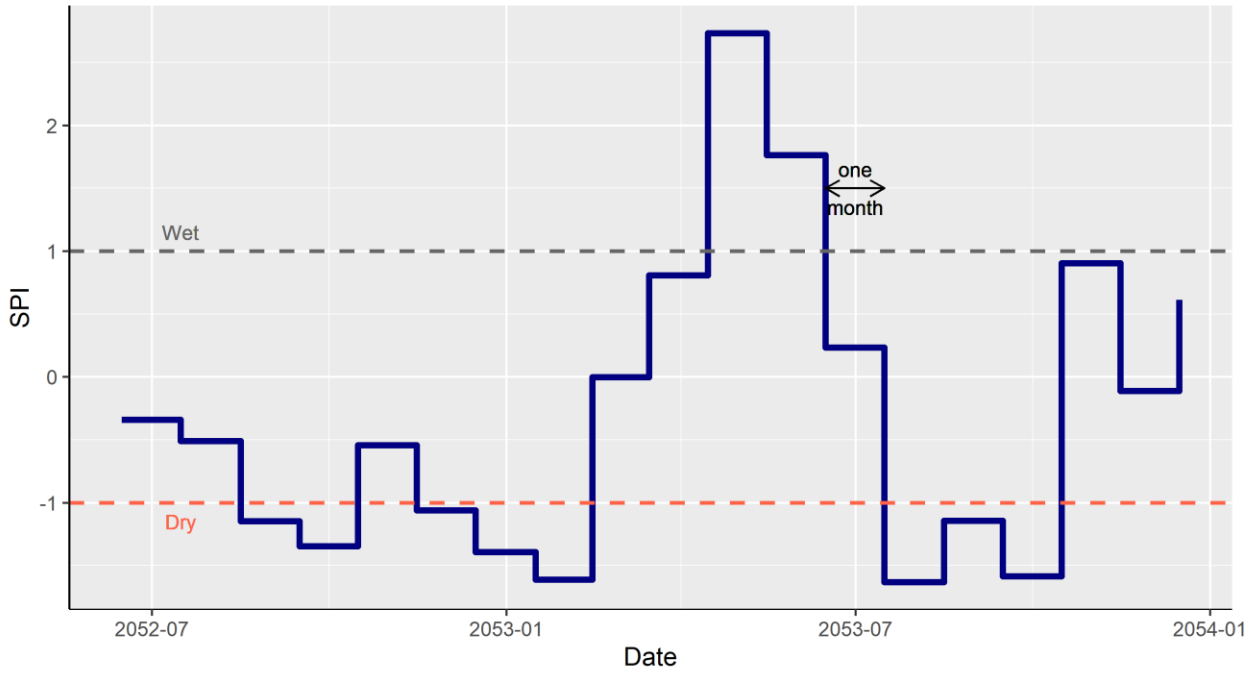

Figure 5 - Example of compound climatic event (CCE, wet-to-dry). The blue line shows the SPI3 timeseries, while the orange and gray dashed lines illustrate the thresholds used for dry and wet conditions. Here, the transition time of the wet-to-dry CCE is one month (time span between the end of the former and the start of the latter event).

3.3.3. Compound Hydrologic Events

- 3.3.3.1. Definition of Compound Hydrologic Events

In this study, we investigate the compound hydrologic events (CHEs) by using daily streamflow simulations as an indicator of the state of the water in the rivers of the study area. While ecosystems can be sensitive to streamflow alterations, understanding the state of streamflow is crucial for a wide range of stakeholders as water supply plans, legal settlements (water rights,

court decrees), engineering design (reservoirs, bridges), operations (power production, navigation), and disaster risk reduction strategies are centered around streamflow information (USGS, no date). Hydrologic droughts have been well documented by Van Loon (2015) and Fleig et al. (2006). To identify the complete drought event (from its first to last day), threshold level method (theory of runs) was applied on the timeseries of the streamflow. The total water deficit of hydrologic droughts derived by the theory of runs has been shown to be superior to the cumulative streamflow anomaly, the PDSI, and the Surface Water Supply Index (Keyantash and Dracup, 2002). This is because the theory of runs allows modeling the overall course of the flood and drought events compared to the drought indices that attribute wetness and dryness to a relatively large period (e.g., a month or year). It is worth mentioning that droughts should not be confused with low flows, as the latter refers to the timeseries of the annual minimum n-day discharge, the mean annual minimum n-day discharge, or a percentile of the flow duration curve (FDC), which does not consider the time of drought development (see Khaliq et al., 2008 for more details about the evolution of low-flow regimes in Canada).

To study and assess the spatial aspects of the drought events covering large regions such as the NWNA, events must be consistently defined and identified throughout the region. To this end, the monthly varying threshold of 15% quantile of daily discharge is used to develop the drought partial duration series (PDS). Using a monthly varying threshold allows extracting the events with flows being abnormally low in that given time of the year over the entire course of the records. This is important since the low discharge in cold and warm season have distinct characteristics and implications. In a similar fashion to droughts, the peaks over threshold (POT) method is used to extract the hydrologic floods. The floods are modelled with POT using the 95% quantile of daily simulated streamflow data. Since rivers can overflow when at the bankfull

state regardless of the time of year, a fixed threshold is used. Moreover, previously the 95th quantile of daily streamflow has been used in the study area to represent the floods (Pirani and Najafi, 2022). A CHE occurs when a one of the hydrologic extremes (i.e., flood and drought) is followed by the contrasting extreme within 6 months. Furthermore, an abrupt transition refers to transition times shorter than a month. An example of a CHE is illustrated in Figure 6.

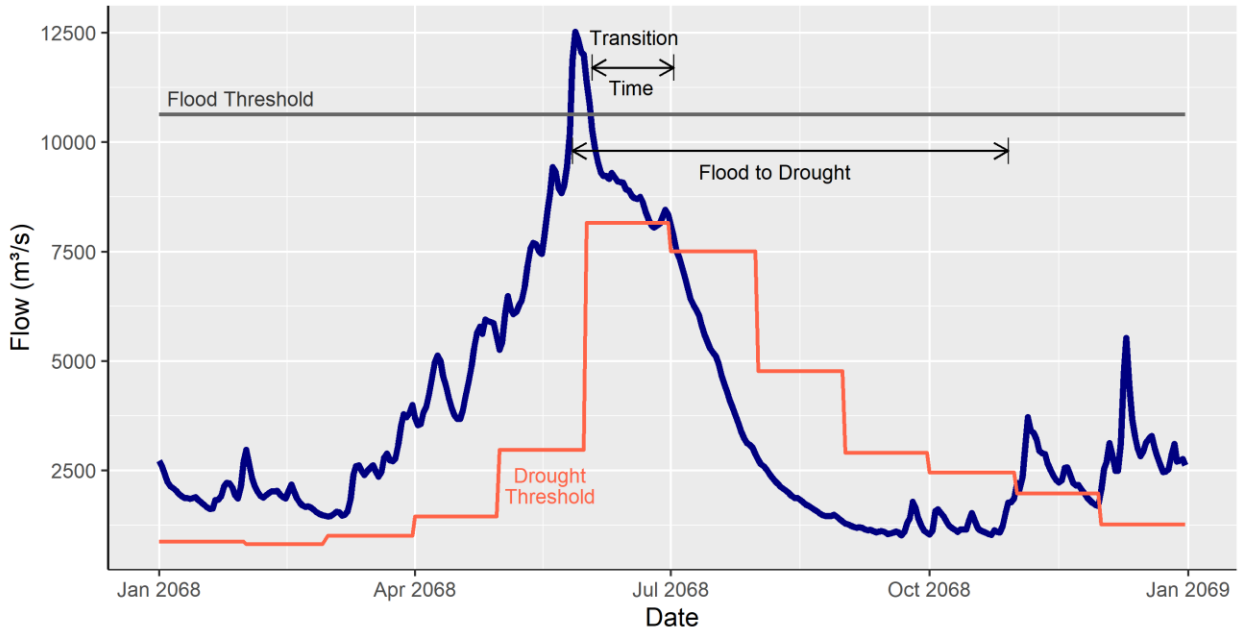

Figure 6 - Example of compound hydrologic event (CHE, flood-to-drought). Floods and droughts are extracted based on partial duration series using monthly varying threshold for droughts (15th quantile) and a constant threshold for floods (95th quantile). The timespan between the start of the first hazard to the end of the second hazard is referred to as compound hydrologic event, while transition time refers to the time span between the end of first and start of the second hazard.

- 3.3.3.2. Characteristics of Compound Hydrologic Events

We characterize the compound hydrologic events (CHEs) based on several indices presented in Table 3. The choice of suitable flood and drought characteristics for a specific study depends on the purpose of the study, hydroclimatology, geophysical characteristics and the natural and societal vulnerability of the region (Fleig et al., 2006). Therefore, it is hoped that implementing the indices in Table 3 would characterise the CHEs from different aspects that are of interest of a wide range of sectors.

Table 3 - List of the indices proposed/used in this study to characterise the compound hydrologic events (CHEs)

Index	Description	Unit	Application
Frequency (F)	Count of events over the warming period (30 years)	unitless	Individually (I)/ Compound (C)
Duration (D)	The timespan between the onset and termination of the event (duration above/below threshold)	days	I
Transition time (Tr)	The timespan between the termination of the former event and the onset of the latter event in a CHE	days	C

Abrupt transition (AbTr)	Transition times shorter than a month	days	C
Flood magnitude (FM)	Difference between the peak flood magnitude and the flood threshold	m^3/s	I
Flood volume (FV)	Volume of flood excess water (the area between the hydrograph and the flood threshold)	Bm^3 (billion cubic meters)	I
Drought severity (DS)	Volume of drought deficit water (the area between the hydrograph and the drought threshold)	Bm^3	I
Drought intensity (DI)	also referred to as deficit or drought magnitude, is the ratio between drought severity and drought duration	m^3/s	I
Seasonality of CHEs (SEA)	The mean time of year (month) at which the flood and drought of the CHEs peak **(*)**	unitless	I/C

Strength of the seasonality (SS)	Indicates how reliable the calculated seasonality is **(*)**	unitless	I/C
Fraction of CHEs having AbTr (FAbTr)	The ratio between the count of CHEs with AbTr and all CHEs	unitless	C
Fraction of CHEs having Tr less than 3 months (FTr3)	The ratio between the count of CHEs with Tr less than three month and all CHEs	unitless	C
Empirical compound severity index (ECSI)	A standardised index that compares the CHEs based on their FV and DS **(**)**	unitless	C
Empirical compound weighting angle (ECWA)	Describes which of the flood or drought in a CHE outweighs the other in terms of severity **(**)**	° (degrees)	C

***** Equations 3.5, 3.6.1, 3.6.2, 3.7, and 3.8

****** Equations 3.9 and 3.10

While some of the characteristics presented in Table 3 (such as duration, severity, magnitude, etc.) have been commonly applied on floods and droughts individually, we aim to characterise each CHE using the characteristics of its components (i.e., flood and drought). For instance, the

seasonality refers to the timing of events' peaks (flood or drought). However, we apply this index to both flood and drought of the CHE and show the seasonality of the flood and drought in CHEs. Therefore, our results show the timing of floods and droughts that are linked, which could help water resources managers to identify the time of year they should look for CHE's flood and drought occurrences. Moreover, identifying the seasonality of the CHEs provides a useful source of information about the properties of each compound flood and drought, as it could reflect the flood/drought generating mechanisms (e.g., winter low flow versus summer low flow).

In this study, seasonality (SEA) is shown with the help of circular statistics derived from the date information (Robson and Reed, 1999). To this end, a circle of unit radius is used, and the date is presented as the angle θ, measured anti-clockwise from the x-axis (one revolution of the circle corresponds to a whole year). θ is calculated from the Equation 3.5:

$$\theta = (day\ number - 0.5)\frac{2\pi}{Length\ of\ year} \quad \text{(Equation 3.5)}$$

where day number represents the number of the day in a calendar year (1 to 365 or 366 if in a leap year), length of year is 365 (or 366 in leap years), and the 0.5 term adjusts θ to represent the middle of the day.

Then, the centroid of these points (θ_s) is used to summarise the seasonal behaviour. The centroid provides information about (Figure 7):

a) The mean time of year at which flooding/drought occur, which is summarised by the angle $\bar{\theta}$ between the initial line and the radial line into centroid.
b) The concentration of the seasonal distribution is summarised by the $\bar{r}$, which is the distance from the origin to the centroid. $\bar{r}$ values close to 1 indicate floods/droughts

usually occur at the same time of year and seasonality is strong. On the other hand, smaller $\bar{r}$ suggests the timing of the event is more complex and seasonality is weak. Moreover, small $\bar{r}$ suggests that the direction of $\bar{\theta}$ is less meaningful.

The centroid can be found by either using polar coordinates ($\bar{\theta}\ and\ \bar{r}$) or by the Cartesian coordinates using XEVENT and YEVENT (Equations 3.6.1 and 3.6.2).

$$XEVENT = \bar{x} = \frac{1}{n}\sum_{i=1}^{n}\cos\theta_i \qquad \text{(Equation 3.6.1)}$$

$$YEVENT = \bar{y} = \frac{1}{n}\sum_{i=1}^{n}\sin\theta_i \qquad \text{(Equation 3.6.2)}$$

The polar coordinates can then be calculated from Equations 3.7 and 3.8 as:

$$\begin{cases} \bar{\theta} = \tan^{-1}\left(\frac{\bar{x}}{\bar{y}}\right)\ if\ \bar{x} \geq\ 0,\ \bar{y}\ \geq 0 \\ \bar{\theta} = \tan^{-1}\left(\frac{\bar{x}}{\bar{y}}\right) + \ \pi\ if\ \bar{x} < 0 \\ \bar{\theta} = \tan^{-1}\left(\frac{\bar{x}}{\bar{y}}\right) + 2\pi\ if\ \bar{x} \geq\ 0,\ \bar{y} < 0 \end{cases} \qquad \text{(Equation 3.7)}$$

$$\bar{r} = \sqrt{\bar{x}^2 + \bar{y}^2} \qquad \text{(Equation 3.8)}$$

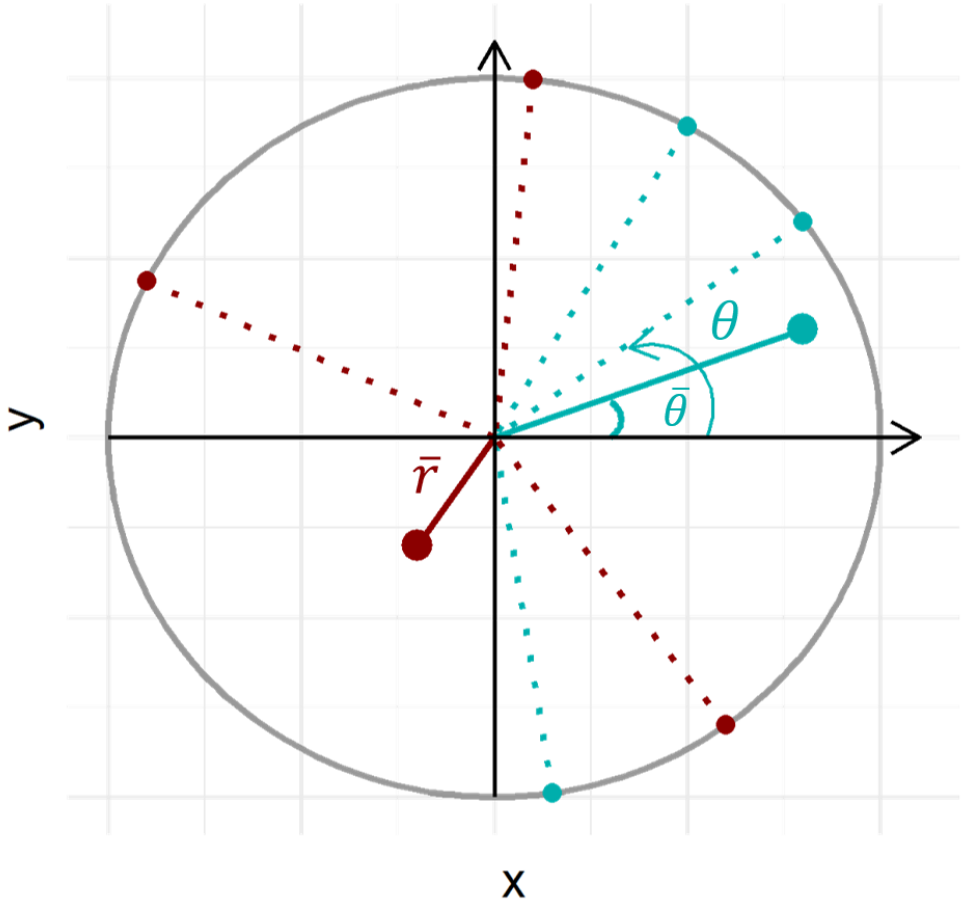

Figure 7 - Using circular statistics to identify the seasonality of compound hydrologic events. The point connected to the center with dashed lines show the timing of each event (blue and red represent flood and drought, respectively), while the points connected to the center with solid lines show the centroids.

The event fractions (FAbTr, FTr3) show the distribution of the CHEs' transition times, indicating the portion of the CHEs with the specified transition times (30 for abrupt and 90 days for 3 months) in different warming periods. These indices vary from 0 to 1, with 1 indicating all CHEs in a specific location occur within the given transition time, while the value of zero shows none of the CHEs have the given transition time.

To account for the severity of CHEs, the Empirical Compound Severity Index (ECSI) is proposed to compare the how problematic different CHEs could be. This index is designed in a way that considers the climate change induced non-stationarity in extremes. The ECSI is a standardized value, which is calculated based on the flood volume (FV) and drought severity (DS) of a CHE (both represent volume). For each of the CHE's components (i.e., flood and drought), the exceedance probability (EPr) of the flood/drought is retrieved from the empirical cumulative distribution function (ECDF) of the flood volume/drought severity in the base period (Figure 8). The extracted non exceedance probability (EPr(FV) and EPr(DS)) is an indicator of event's severity compared to all other floods/droughts occurring individually in the same location. This is inferred since higher EPr values would indicate the lower probability of the event occurrence compared to all other instances. Moreover, mapping the flood volumes and drought severities on the base period ECDF of events allows comparing different events at various warming levels with the ones in the base period. Therefore, ECSI can represent the possible non-stationarity induced by climate change in the time series.

When mapping each CHE based on its EPr(FV) and EPr(DS) on a cartesian coordinate system as (EPr(DS), EPr(FV)), the ECSI is calculated as the Euclidean distance between the mapped point and the origin (0, 0) point (Figure 9a) from Equation 3.9 . The F1-D1 and F4-D4 compounds in Figure 8 would lead to the least/most severe compound event as their flood and drought are less/more severe than any flood and drought (individual events) occurring in the base period of that location. ECSI values range between 0 and 1.41 (considering the (0, 0) and (1, 1) points, respectively), whereby 0 value indicates that both flood volume and drought severity of the CHE were smaller than the lowest ranked flood and drought of the historical events. On the other hand, value of 1.41 is obtained when the flood volume and drought severity is larger than the that

of the highest ranked flood drought in the base period (the most severe events), therefore such event would be problematic for water resources managers (Figure 9b).

$$Empirical\ Compound\ Severity\ Index\ (ECSI) = \sqrt{EPr(FV)^2 + EPr(DS)^2} \qquad \text{(Equation 3.9)}$$

The Empirical Compound Weighting Angle (ECWA) is proposed for each CHE to compare the relative severity of flood and drought components with each other and is presented in degrees (°) unit. The direction of the ECWA values (negative/positive) indicate which of the drought/flood is less/more severe compared to the other. The ECWA is calculated to be the angle that the ECSI vector makes with the line of equality (y = x line; dashed line in Figure 9a) based on Equation 3.10. The ECWA helps to locate the compound flood – drought event in the ECSI reference values (Figure 9b). Moreover, the larger ECWA values indicate that the ranks of flood and drought in the CHE are distant with regards to flood volume and drought severity (e.g., one is ranked to be at the first quartile while the other one is at fourth quartile). However, lower values of ECWA indicate that the flood and drought have similar ranks and the angle is close to 0.

$$Empirical\ Compound\ Weighting\ Angle\ (ECWA) = \tan^{-1}\left(\frac{EPr(FV)}{EPr(DS)}\right) - \frac{\pi}{4} \qquad \text{(Equation 3.10)}$$

Where the $\frac{\pi}{4}$ term is deducted to find the angle created with the line of equality (y = x line).

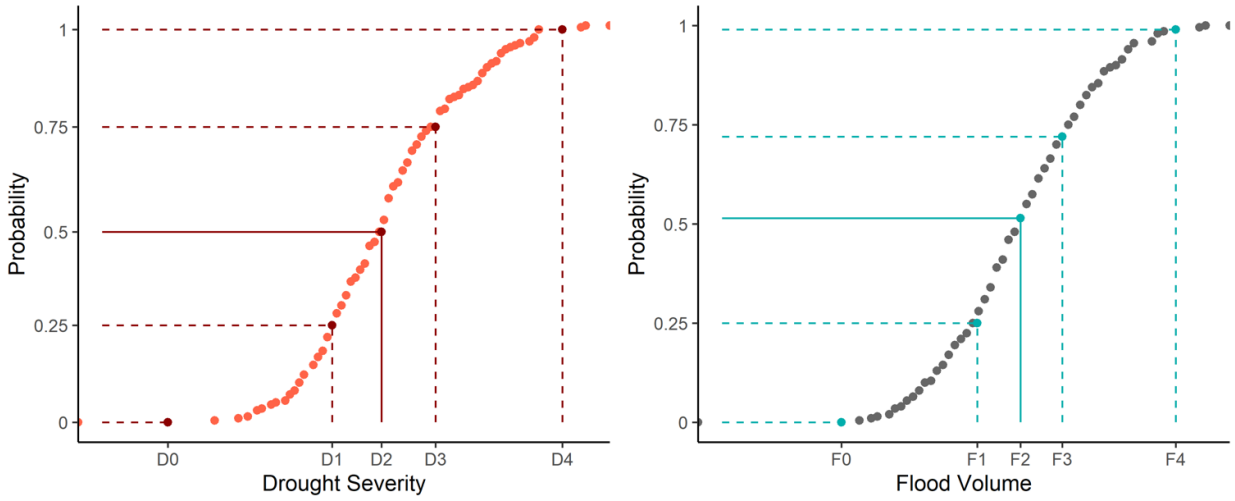

Figure 8 - The ECSI and ECWA calculation procedure. The non-exceedance probability of flood and drought of a CHE compared to all flood and drought occurrences in that location are extracted by mapping the flood volume (FV) and the drought severity (DS) of the CHE on the ECDF of the base period. The points shown with line segments are flood and droughts in compound events (in base or any warming period) while the points of the ECDF represent all floods and droughts (compound or individual instances) in the base period. The non exceedance probability of FV and DS extracted here are then paired for each event and fed into the Equations 3.9 and 3.10 to calculate the ECSI and ECWA values. The F1 (D1), F2 (D2), F3 (D3), and F4 (D4) represent events with the non exceedance probability of 0.25, 0.5, 0.75, and 1, respectively.

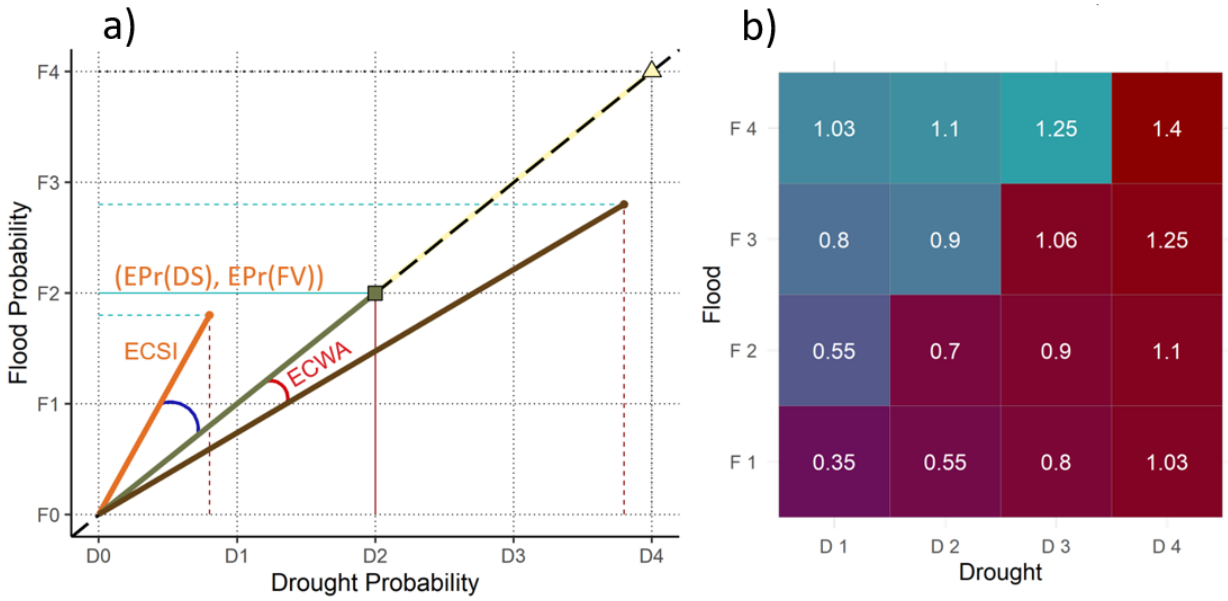

Figure 9 - Illustration of ECSI and ECWA calculation. Each CHE is shown by a point (here four events are shown by four points colored in orange, green, brown, and light yellow) in Figure 9(a). Each CHE is mapped as a point on the Cartesian coordinate system based on the non exceedance probabilities (EPr) extracted from Figure 8 and mapped as (EPr(DS), EPr(FV)). The ECSI is calculated as the Eculadian distance of each point to the origin point (0,0). The ECWA of each event is represented by the angle that ECSI vector of the event makes with the line of equality (dashed black line). The ECWA shown in blue has a positive value which indicates that the flood is more severe than the drought (had a higher non exceedance probability) when comparing the flood and drought of compound event to all other floods and droughts. Figure 9b shows the possible values of ECSI. The values shown on Figure 9(b) show the length of ECSI vector originating from the origin point and ending on the right upper corner of the shown rectangles. Blue squares show the ECSI values for CHEs with positive ECWA while the ECWA in red squares are negative (shown with red arc in Figure 9(a)).

Chapter 4: Results and Discussion

4.1. Results

4.1.1. Compound Climatic Events

- 4.1.1.1 Frequency of Compound Climatic Events

The climatology of the frequency of compound climatic events (CCEs) for the three accumulation periods of 1-, 3-, and 6-months are presented in Figure 10 and Figure 11 based on SPI and SPEI, respectively. The frequency of CCEs was calculated at every grid of each ensemble member over the given warming period. Then the gridded ensemble mean was created by taking the mean of the frequency for each grid between all ensemble members. The bars in figure 9 show the spatial mean (across all three basins) of the multi-model ensemble mean at different warming levels. The error bars represent the 95% confidence interval of the frequency spatially.

The two drought indices consistently indicate that the frequency of CCEs with different transition times is projected to increase under climate change in all accumulation periods. However, the increase of frequency is not even for different transition times. Overall, the region is more prone to dry-to-wet compound climatic events compared to wet-to-dry CCE at each accumulation period (Figures 10 and 11). Moreover, the dry-to-wet CCEs could be more problematic since such CCEs are projected to occur more abruptly. This is inferred from the more frequent CCEs with abrupt transition or transition time of less than 3 months compared to the wet-to-dry CCEs. A comparison between the accumulation periods indicates that the CCEs occur more frequently at short time scales (1-month) while increasing the accumulation period

tends to decrease the CCE occurrences. This results in more variability of transitions of short duration contrasting climatic hazards. In all accumulation periods, most of the dry-to-wet CCEs occur within 3 months based on SPI and SPEI (Figures 10 and 11). A comparison between SPI and SPEI reveals that SPEI captures more CCEs in all accumulation periods (both wet-to-dry and dry-to-wet).

Figure 10 - Spatial mean of the climatology of the CCEs at different warming levels for multiple accumulation periods based on SPI. The bars show the frequency over the 30-year warming period and the error bars represent the 95% confidence interval of spatial results. The bars are colored based on the transition time (yellow: all CCEs (transition within 6 months); blue: transition within 3 months; and orange: abrupt transition).

Figure 11 - Spatial mean of the climatology of the CCEs at different warming levels for multiple accumulation periods based on SPEI. The bars show the frequency over the 30-year warming period and the error bars represent the 95% confidence interval of spatial result. The bars are colored based on the transition time (yellow: all CCEs (transition within 6 months); blue: transition within 3 months; and orange: abrupt transition).

The climatology of frequency of dry-to-wet CCEs having the 1-, 3-, and 6-months accumulation periods based on SPI are spatially presented in Figures 12, 13, and 14, respectively. The climatology of frequency of dry-to-wet CCEs having the 1-, 3-, and 6-months accumulation periods based on SPEI are spatially presented in Figures 15, 16, and 17, respectively. The

frequency of CCEs was calculated at every grid of each ensemble member over the given warming period. Then the gridded ensemble mean was created by taking the mean of the frequency for each grid between all ensemble members at a given global warming level and presented in Figures 12 to 17. Results for frequency of wet-to-dry CCEs are presented in Appendix 1 to 6 due to similarities of the results.

There are similarities in the identified hotspots for the dry-to-wet CCEs frequency over different accumulation periods (compare Figures 12 to14). The frequency of dry-to-wet CCEs over all accumulation periods are projected to increase if the global warming is not limited (based on SPI). However, there are some exceptions such as the eastern portion of the Peace basin and northwest of the Fraser basin, whereby the frequency of CCEs is projected to decrease if warming continues. An inter-basin comparison of the results based on SPI indicates that the Columbia basin is most susceptible to CCEs inferred from the more frequent projected CCEs.

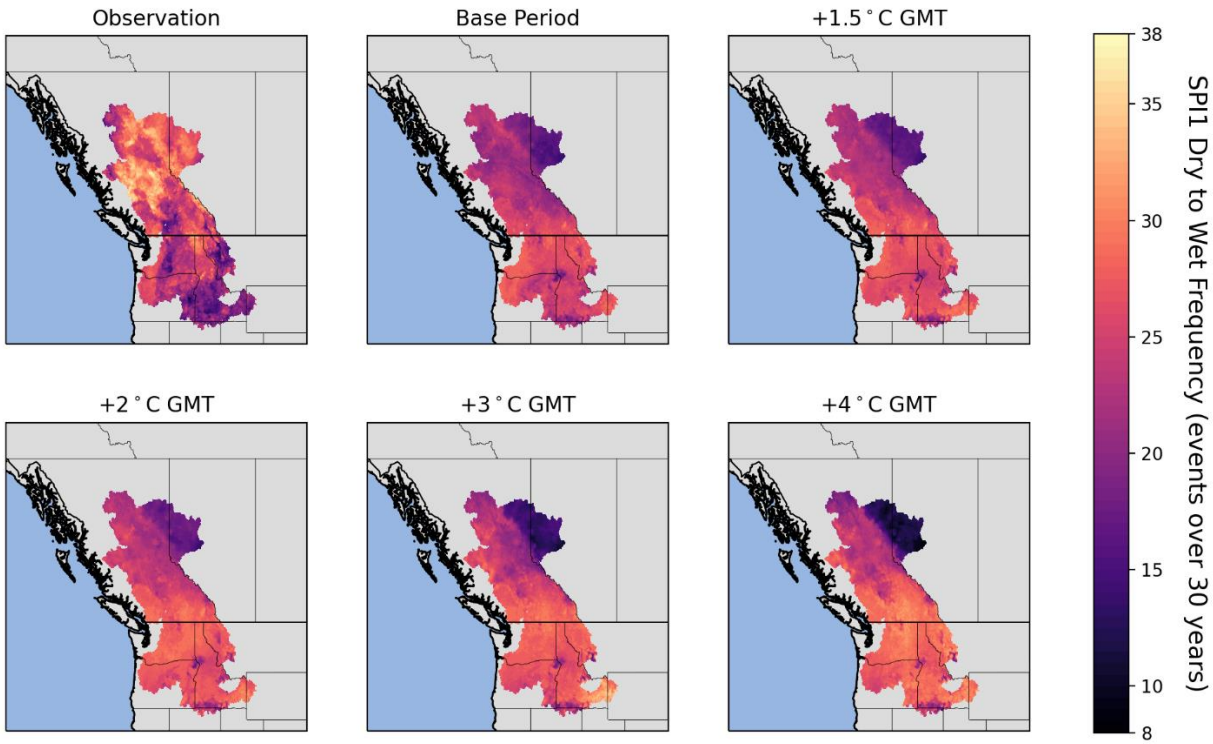

Figure 12 - Climatology of frequency of dry-to-wet CCEs (SPI1). Maps show the frequency of CCEs over each warming period (30 years).

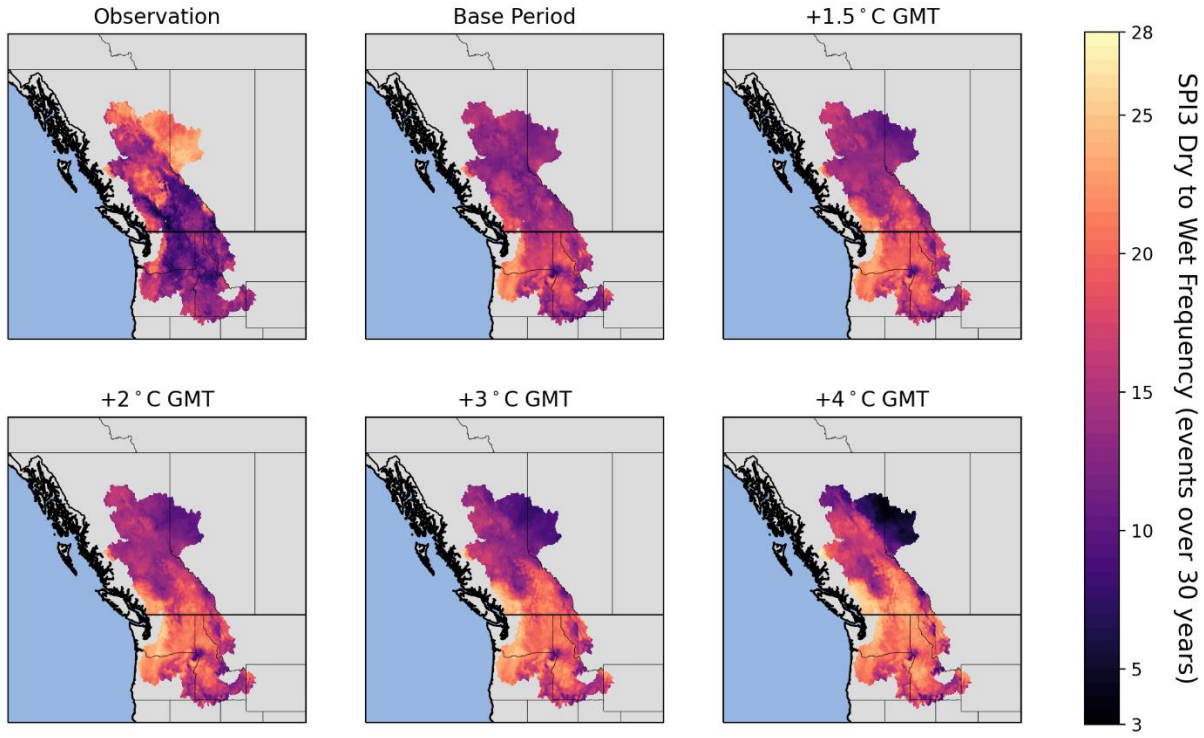

Figure 13 - Climatology of frequency of dry-to-wet CCEs (SPI3). Maps show the frequency of CCEs over each warming period (30 years).

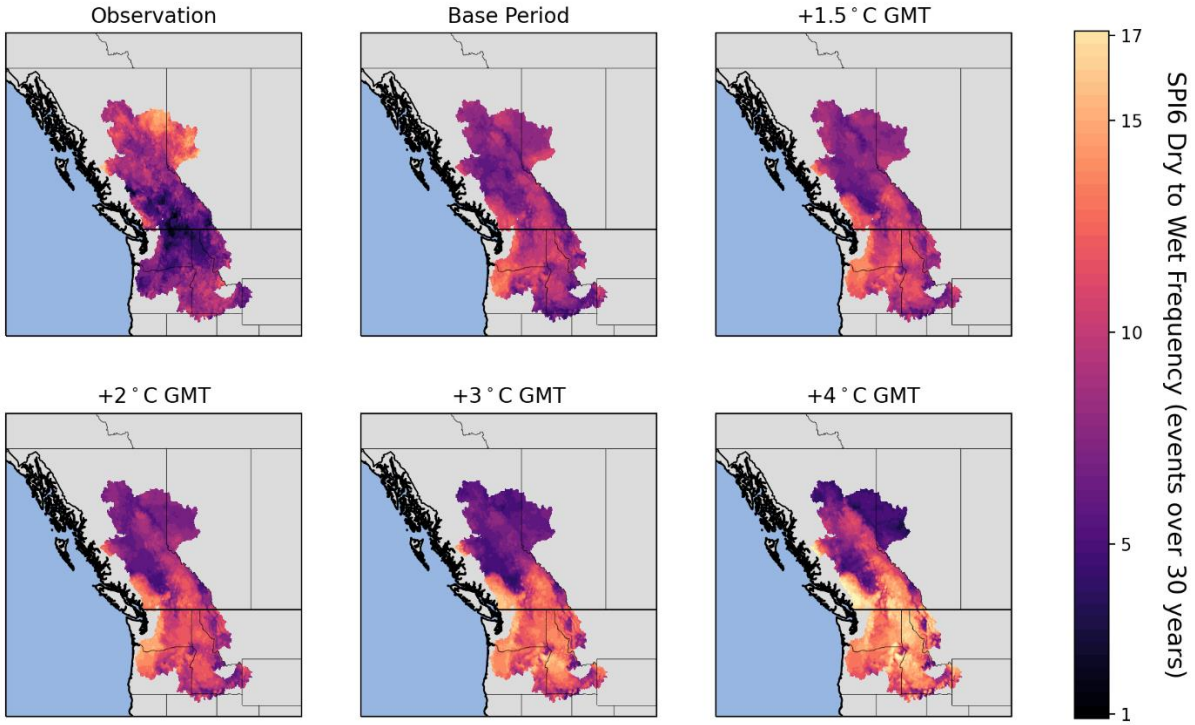

Figure 14 - Climatology of frequency of dry-to-wet CCEs (SPI6). Maps show the frequency of CCEs over each warming period (30 years).

In line with SPI, the frequency of dry-to-wet CCEs is projected to increase under climate change. However, there are some discrepancies between the identified hotspots by SPI and SPEI. Unlike SPI, the ensemble mean projects that the entire northwest North America is prone to CCEs, with more frequent CCEs projected at higher global warming levels (except in southwest of Columbia basin at the 4°C warming level). However, SPI overlooks some hotspots in the Canadian portion of the study area.

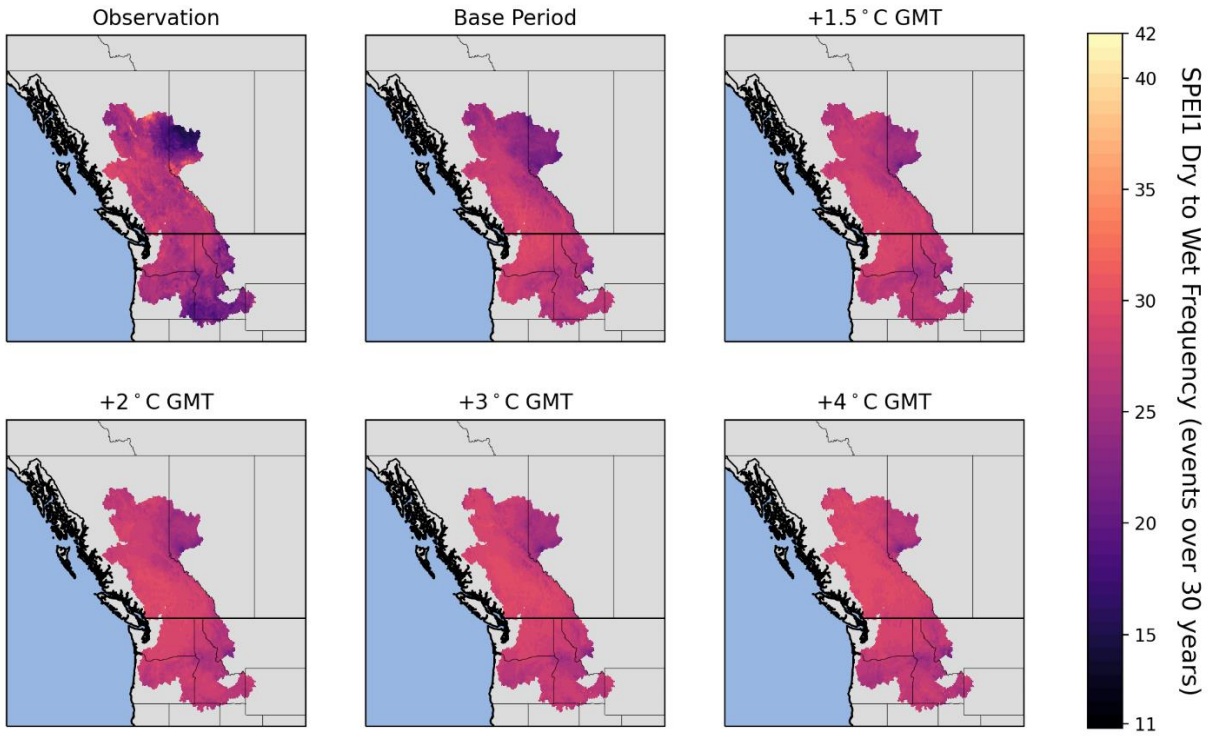

Figure 15 - Climatology of frequency of dry-to-wet CCEs (SPEI1). Maps show the frequency of CCEs over each warming period (30 years).

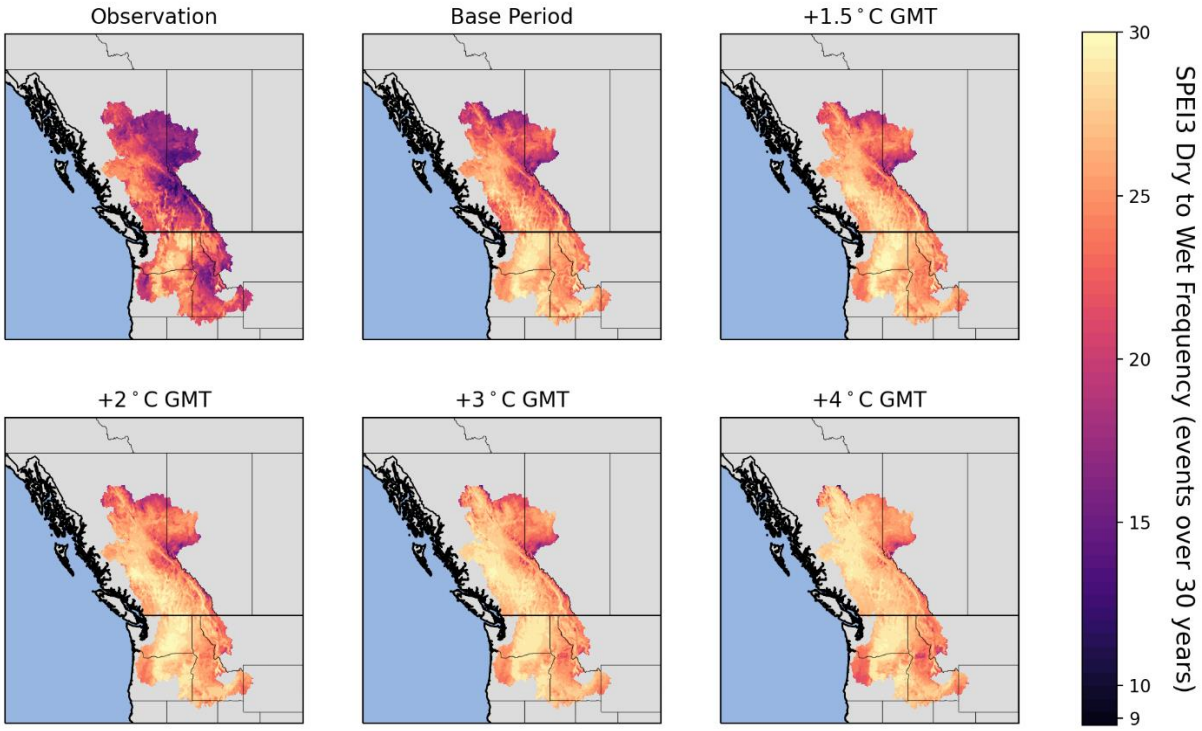

Figure 16 - Climatology of frequency of dry-to-wet CCEs (SPEI3). Maps show the frequency of CCEs over each warming period (30 years).

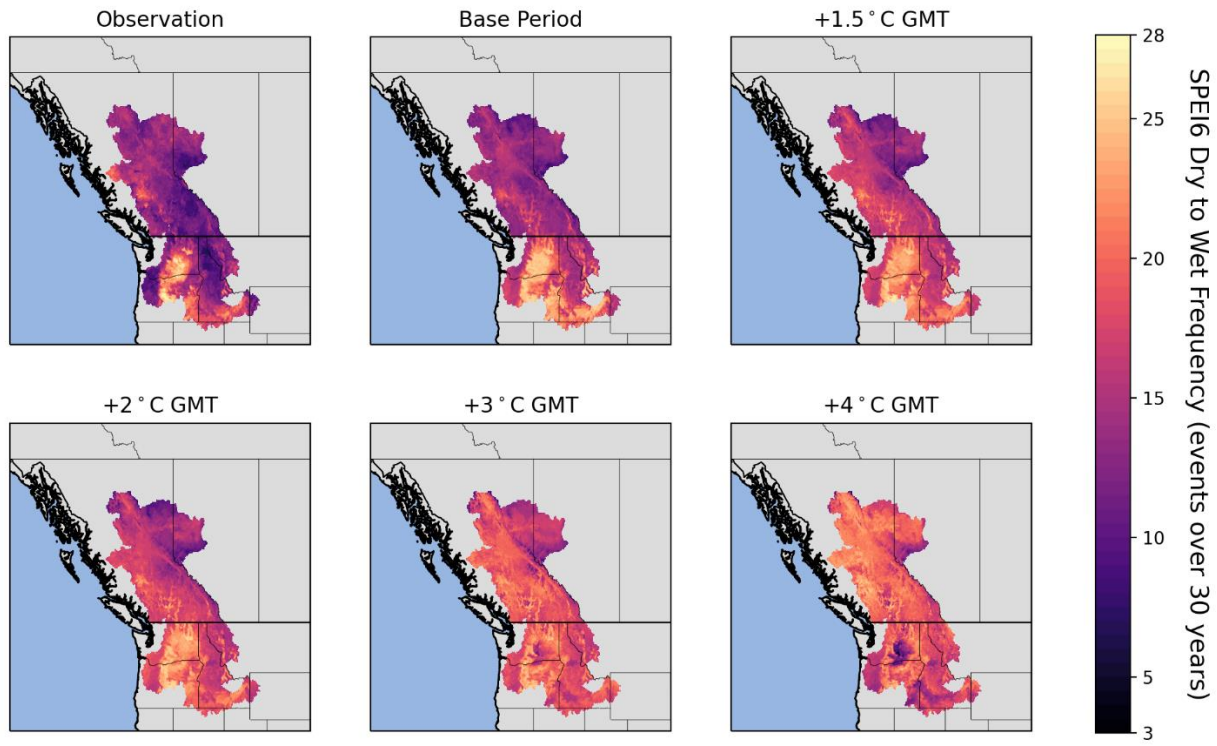

Figure 17 - Climatology of frequency of dry-to-wet CCEs (SPEI6). Maps show the frequency of CCEs over each warming period (30 years).

- 4.1.1.2. Duration of Wet and Dry Spells and Transition Time of Compound Climatic Events

The duration of wet and dry spells and the transition time of CCEs at different warming levels is presented in Figures 18 and 19 respectively based on SPI and SPEI. The durations and transition times were calculated at every grid of each ensemble member over the given warming period. Then the gridded ensemble mean was created by taking the mean of the durations and transition times for each grid between all ensemble members at a given global warming level and presented as ensemble mean. Figures 18 and 19 show the spatial variation of the ensemble mean.

When comparing dry-to-wet and wet-to-dry CCEs, the duration of wet and dry spells in both types of CCEs are almost identical at each warming level and accumulation period (based on

both SPI and SPEI in Figures 18 and 19). However, the SPI suggests that the duration of wet spells in CCEs are projected to increase if global warming continues. Generally, dry-to-wet CCEs based on SPI have shorter transition times compared to the wet-to-dry events. In addition, the transition time is projected to decrease at higher level of global warming (SPI, Figure 18)

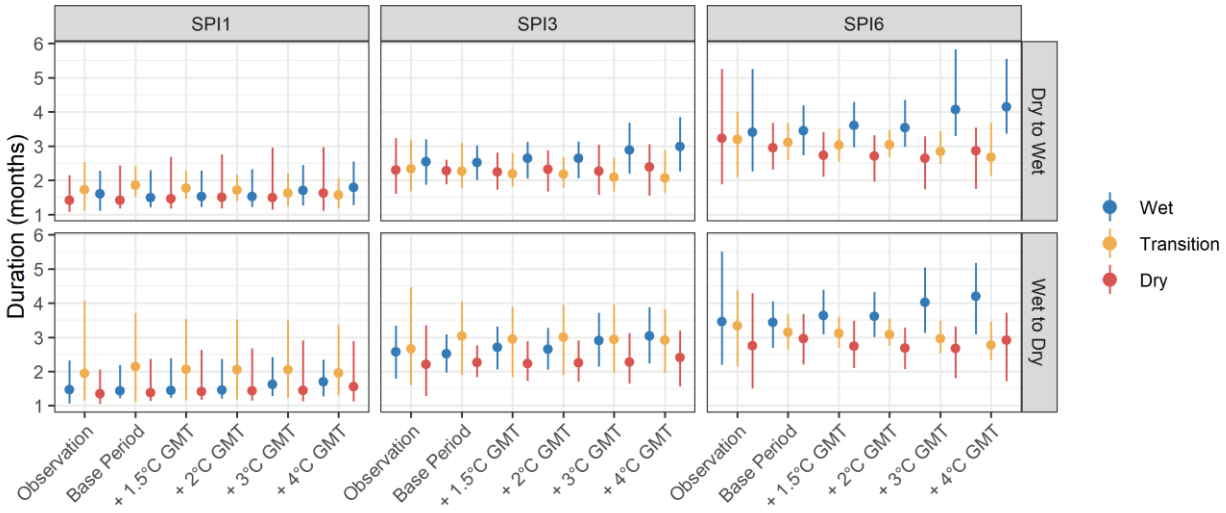

Figure 18 - Duration of wet and dry spells and transition time of CCEs (based on SPI). The bars show the 95% confidence interval of the durations spatially and the points represent the median.

When considering CCEs based on SPEI, the duration of dry spells is projected to increase at higher global warming levels. A comparison between the different types of CCEs reveal that generally, the transition time of dry-to-wet CCEs is shorter than wet-to-dry events. Furthermore, both types of CCEs are projected to occur more swiftly under global warming, which is inferred from the projected decreasing transition times if warming continues.

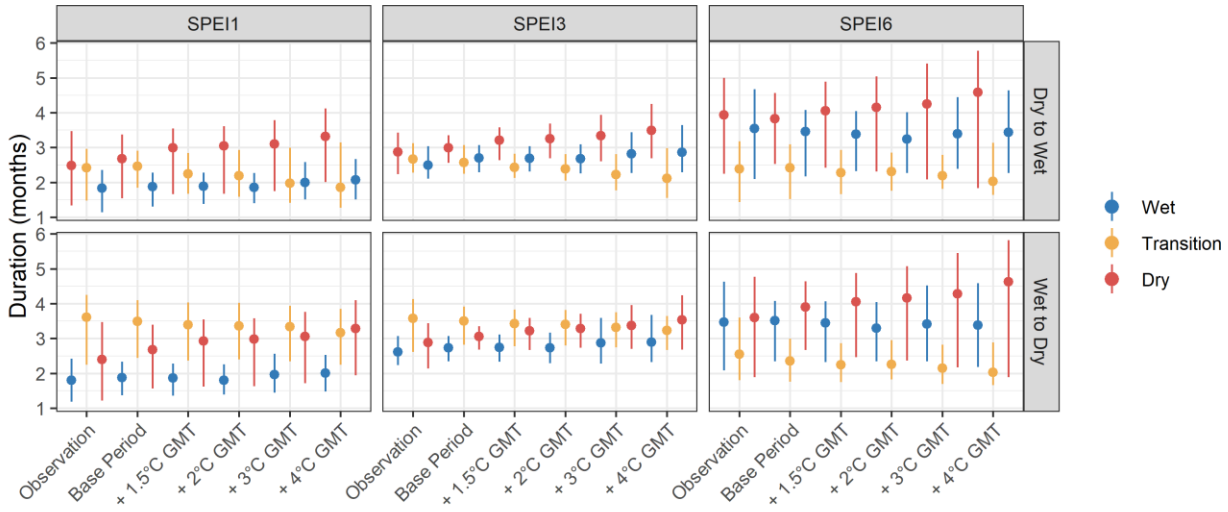

Figure 19 - Duration of wet and dry spells and transition time of CCEs (based on SPEI). The bars show the 95% confidence interval of the durations spatially and the points represent the median.

Given that shorter transition times decreases the chance of the water resources managers and emergency responders to adequately prepare for the successive events, it is important to know how often it takes for the two climatic extremes to swing. Since the drought indices used in this study (SPI and SPEI) are calculated monthly, the transition time of the CCEs would vary in the range of 0 to 6 months (transition time of 0 indicates that wet and dry spells occur successively with no lag between them). The climatology of transition time for dry-to-wet CCEs for the 1-, 3-, and 6-months accumulation periods based on SPI are presented in Figures 20, 21, and 22, respectively. Results for the transition times of dry-to-wet CCEs are presented in Figures 23, 24, and 25 for SPEI1, SPEI3, and SPEI6, respectively. Results for transition time of wet-to-dry CCEs are presented in Appendix 7 to 12. The transition times were calculated at every grid of each ensemble member over the given warming period. Then the gridded ensemble mean was

created by taking the mean of the durations and transition times for each grid between all ensemble members at a given global warming level and presented as ensemble mean. Maps in Figures 20 to 25 show the ensemble mean.

Figures 20 to 22 indicate that the transition time of the dry-to-wet CCEs based on SPI do not spatially vary considerably at each warming level. However, the transition times are projected to decrease under climate change and the number of hotspots for abrupt transitions increase at higher global warming levels. On a monthly basis (SPI1), abrupt transitions are projected in eastern and central Peace, east and west of Fraser, as well as north of Columbia at the highest warming level (Figure 20).

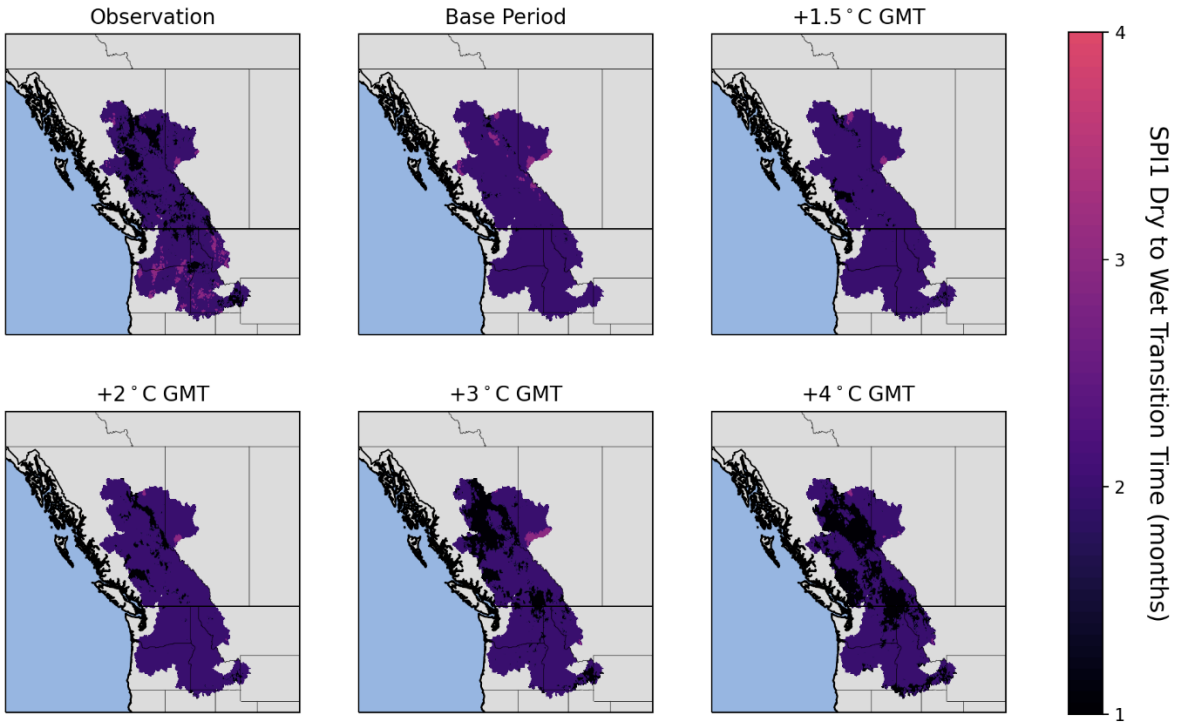

Figure 20 - Climatology of the transition time of dry-to-wet CCEs (SPI1). The maps report the transition time of CCEs in months.

Like the SPI1, SPI3 results indicate that the timespan over which dry and wet spells swing shorten and occur within two months over most of the study area under global warming (Figure 21). However, eastern Peace basin is an exception and the ensemble mean projects increases in the transition time for some parts of this area.

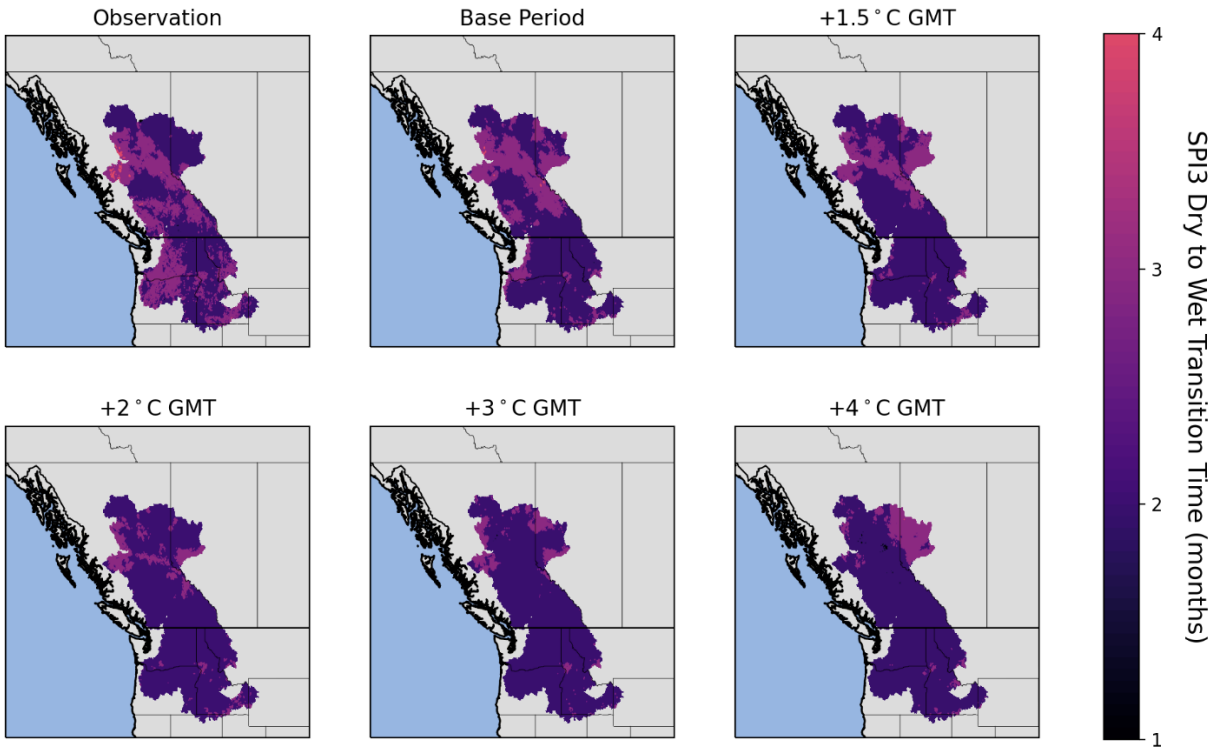

Figure 21 - Climatology of the transition time of dry-to-wet CCEs (SPI3). The maps report the transition time of CCEs in months.

Compared to SPI1 and SPI3, the projected transition time for dry-to-wet CCEs is longer when considering SPI6 (Figure 22). Like the shorter timescales, the transition time of dry-to-wet CCEs based on SPI6 are projected to decrease if warming continues. However, this decrease is more evident in southern Peace basin, eastern Fraser basin, and southwest of Columbia basin at 4°C global warming level (Figure 22). On the other the transition time is projected to increase in northern parts of the Peace basin at 4°C global warming level (Figure 22).

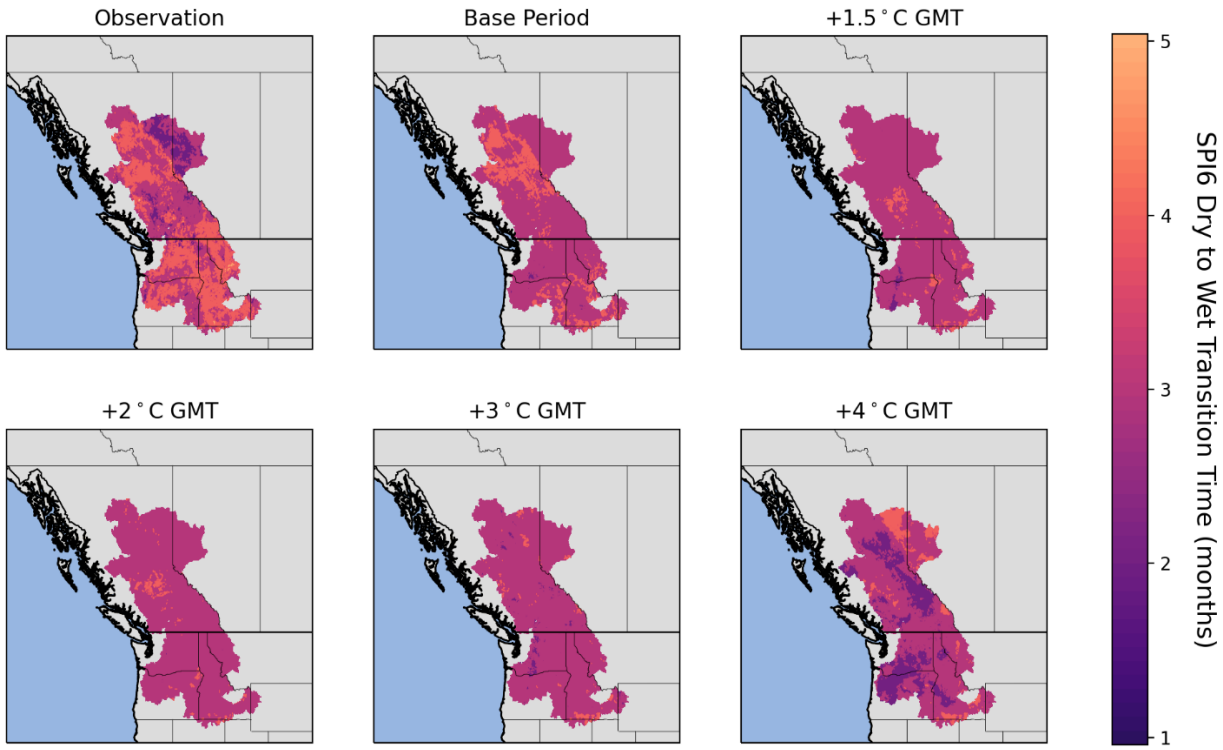

Figure 22 - Climatology of the transition time of dry-to-wet CCEs (SPI6). The maps report the transition time of CCEs in months.

Although there as several similarities between the projected transition time of dry-to-wet CCEs based on SPEI1 and SPEI3 (Figures 23 and 24), more hotspots for abrupt transitions are identified based on SPEI1 (Figure 23). The transition time of CCEs across the Canadian portion of the study area is projected to decrease if the warming continues. However, the results based on both SPEI1 and SPEI3 indicate that the transition time is projected to increase in some parts of the Columbia basin if warming continues (Figures 23 and 24). Moreover, the transition time is projected to be a month longer across the Columbia compared to the rest of the study area at higher levels of global warming (Figures 23 and 24).

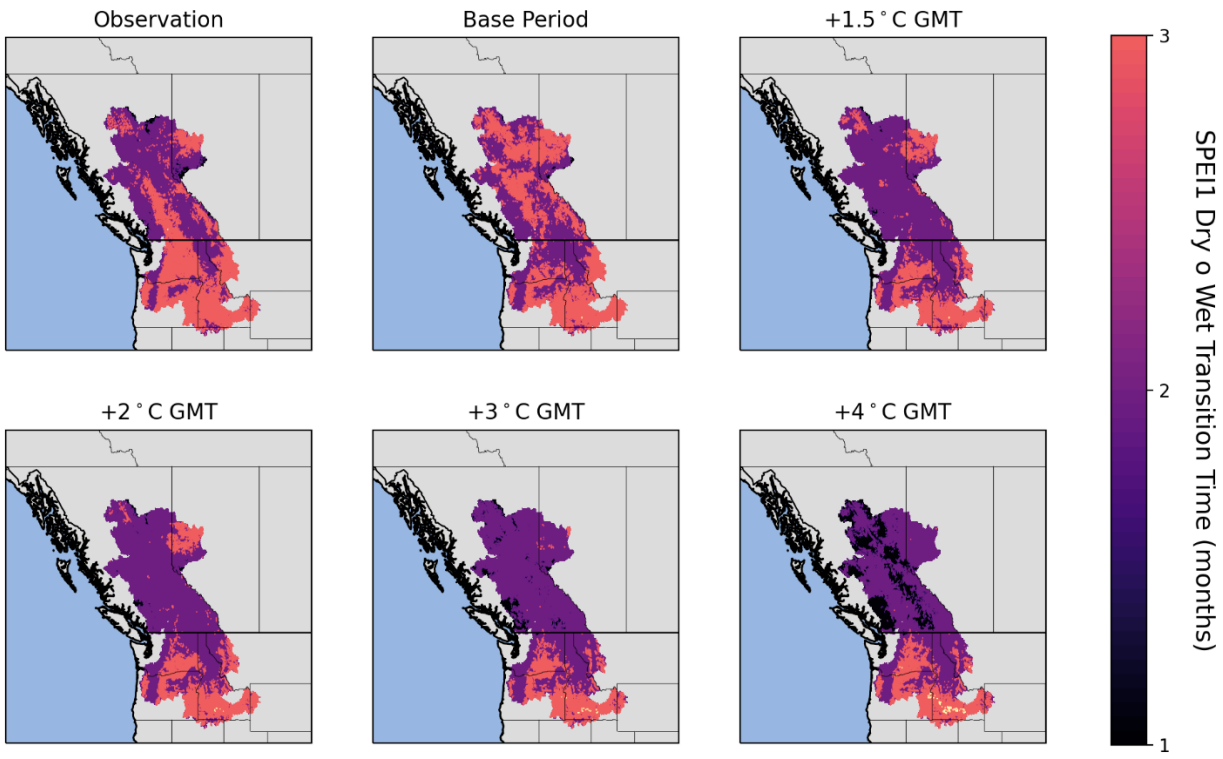

Figure 23 - Climatology of the transition time of dry-to-wet CCEs (SPEI1). The maps report the transition time of CCEs in months.

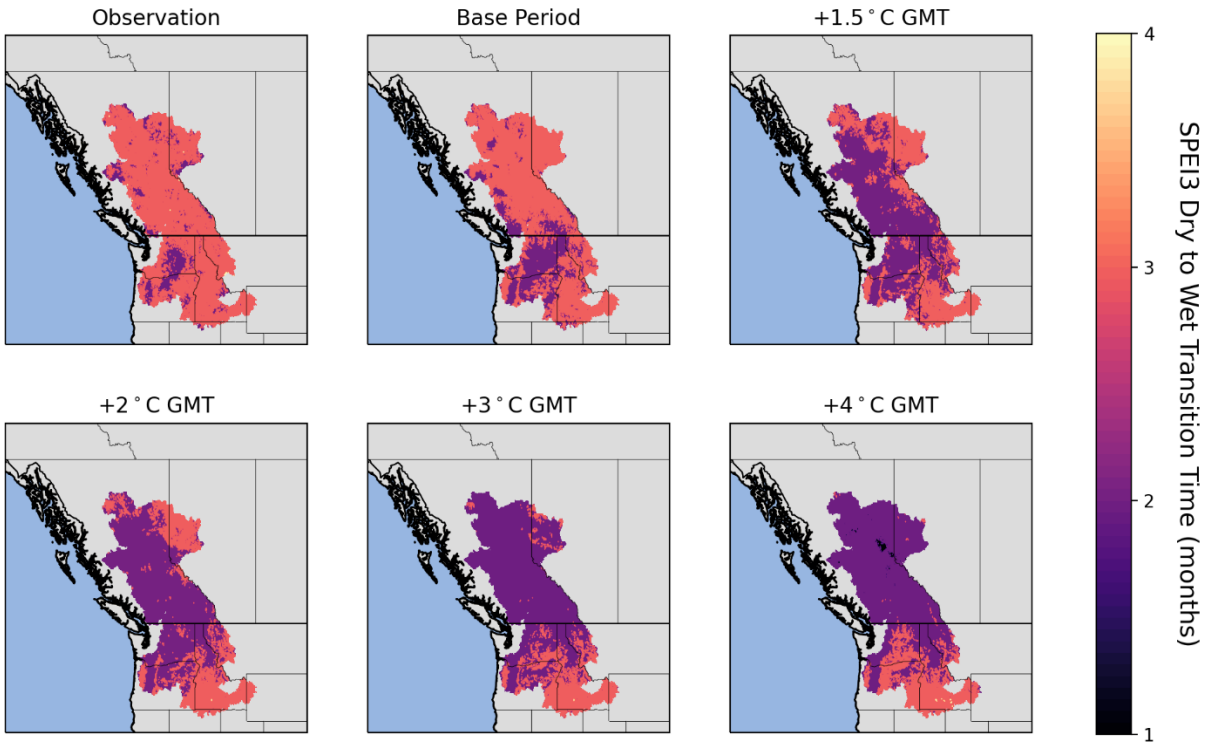

Figure 24 - Climatology of the transition time of dry-to-wet CCEs (SPEI3). The maps report the transition time of CCEs in months.

Considering the SPEI6, the ensemble mean projects decreasing transition time with increasing global warming levels with the exception of southwest of Columbia basin (Figure 25).

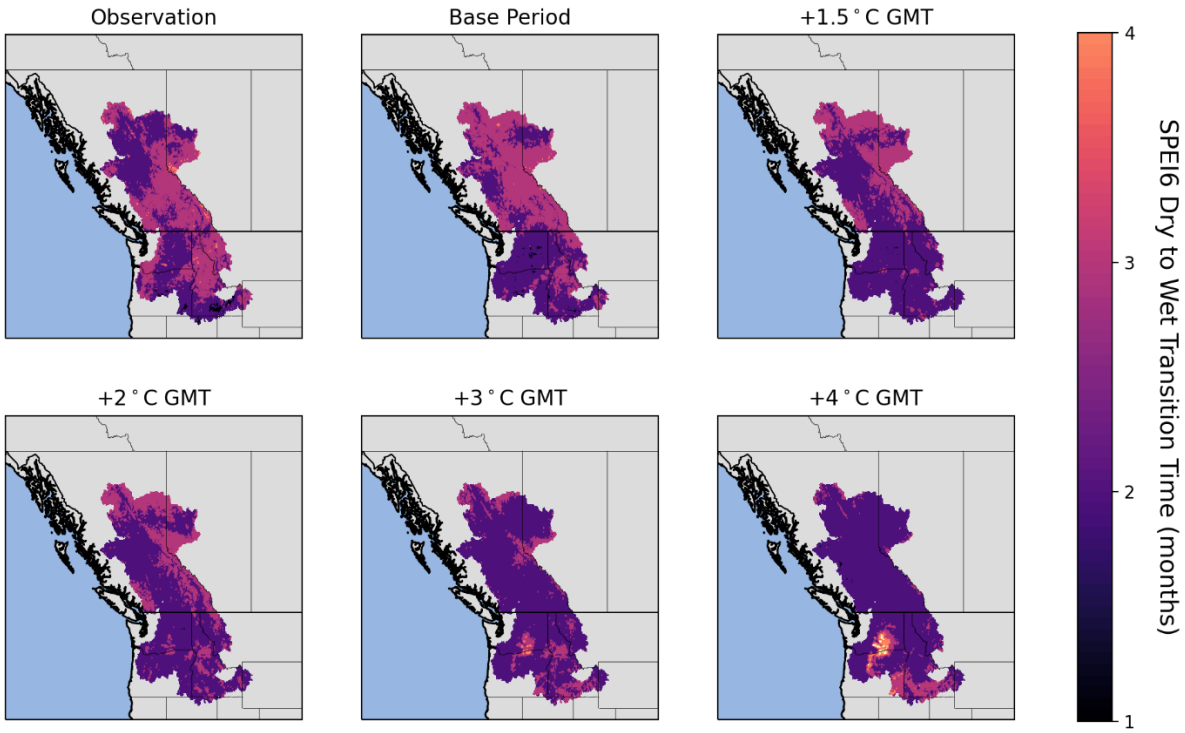

Figure 25 - Climatology of the transition time of dry-to-wet CCEs (SPEI6). The maps report the transition time of CCEs in months.

- 4.1.1.3.1 Seasonality of Wet, Dry, and Concurrent Wet-Dry Spells

The average area experiencing wet, dry, and concurrent wet-dry conditions in every month is illustrated in Figures 26 and 27 respectively for SPI and SPEI (see Appendix 13 to 18 for the 95% confidence interval (CI) of the ensemble). The area experiencing wet, dry, and concurrent wet-dry spells is first calculated for every month of every year at different warming levels in each model-RCP. Then the areas for each month are averaged between the 30 years of the warming period. The points in Figures 26 and 27 show the ensemble mean of the monthly areas.

The seasonality of the wet and dry periods as well as their concurrency is projected to change under climate change. Since larger accumulation periods (3- and 6-months) tend to vary less than

the monthly timescale (1-month), the SPI3 and SPI6, and SPEI3 and SPEI6 better represent the long-term patterns of the changes in seasonality.

There are differences between the seasonality of wet and dry periods captured by SPI and SPEI. While SPI projects that the study area is prone to year-round wet and dry conditions (Figure 26), SPEI shows that the wet and dry spells mostly occur during the first (January – June) and second half (July – December) of year, respectively (Figure 27). In addition, SPEI indicates that more locations in the study area are projected to experience wet and dry spells if warming is not limited (Figure 27). Similarly, SPI projections suggest increases in the area experiencing wet spells under global warming (Figure 26). However, the SPI projects shift in the seasonality of dry spells at higher levels of global warming. SPI projects the timing of dry spells would shift from January – July occurrences to August – November.

Given that the SPEI suggest wet and dry spells would occur in the first and second half of year, respectively, the concurrency of wet-dry spells could affect almost half of the study area in January and July (Figure 27). On the other hand, SPI projections indicate that concurrent wet-dry spells could occur during August – November and expand over almost 50% of the study area during October – December (Figure 26).

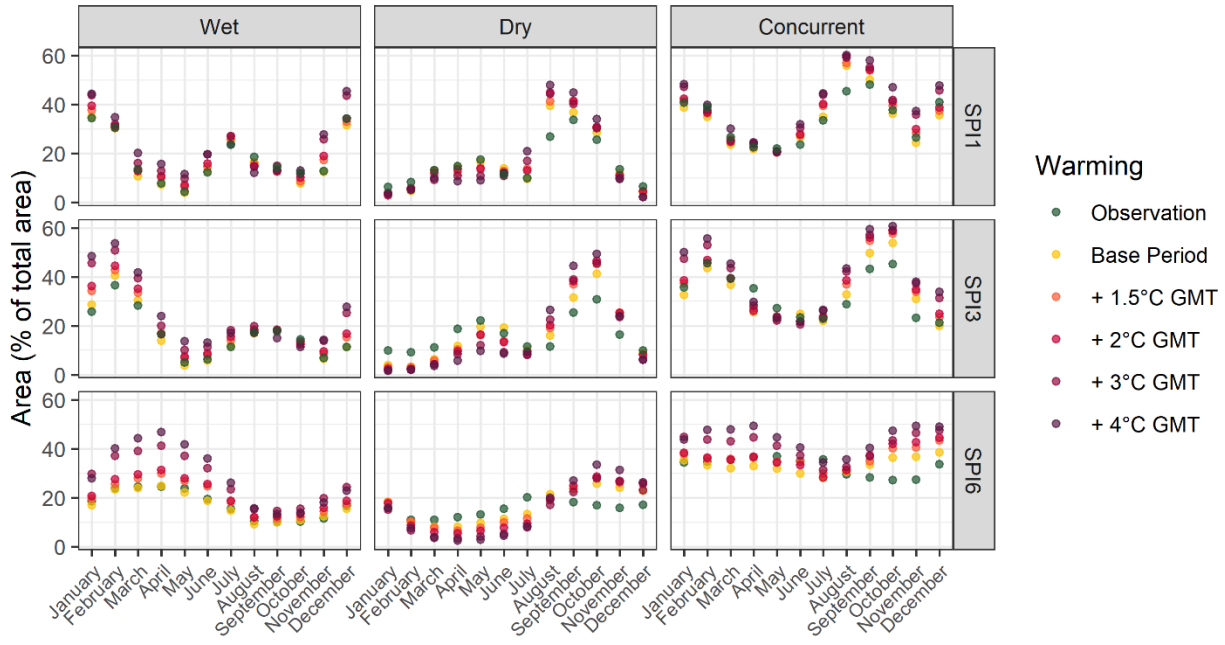

Figure 26 - Average monthly area experiencing dry, wet, and concurrent dry-wet spells based on SPI. The points show the ensemble mean.

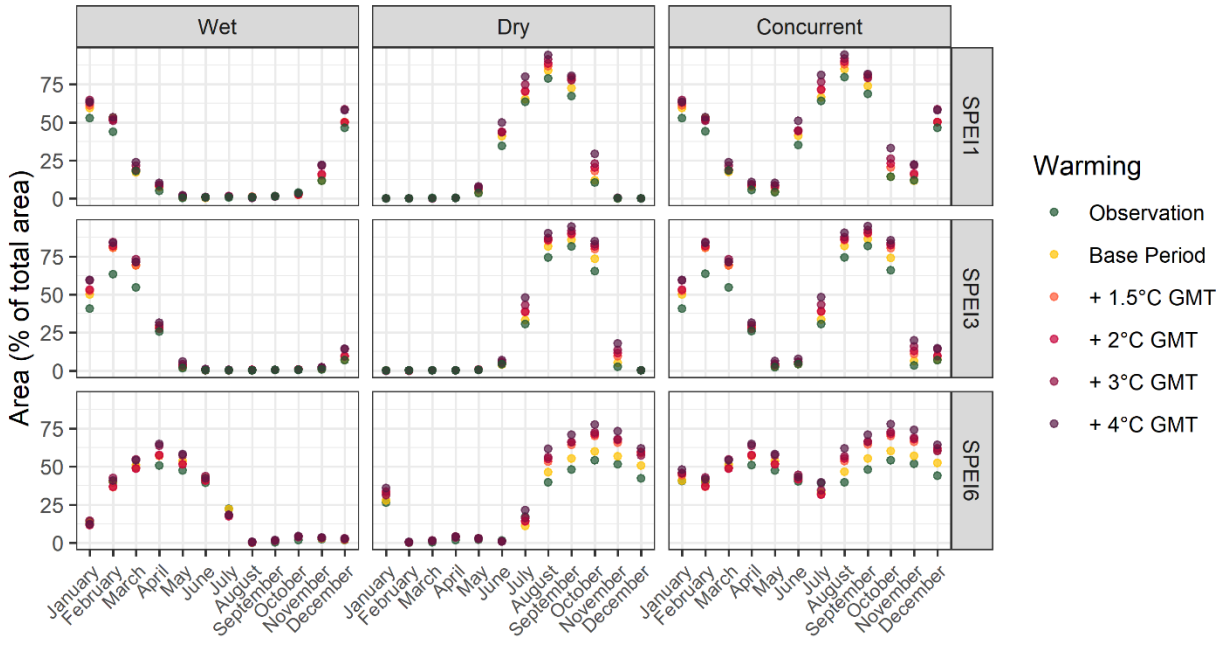

Figure 27 - Average monthly area experiencing dry, wet, and concurrent dry-wet spells based on SPEI. The points show the ensemble mean.

- 4.1.1.3.2 Annual Area Experiencing Wet, Dry, and Concurrent Wet-Dry Spells

Figures 28 and 29 shows the average annual area under wet, dry, and concurrent wet-dry spells. For each ensemble member, the area experiencing wet, dry, and concurrent wet-dry spells in every year have been calculated as the number of total grids experiencing these meteorological conditions. The area experiencing wet, dry, concurrent wet-dry spells is first calculated for every month of every year. Then, the areas for every year in the warming period is averaged (30 values for 30 years in warming period) and reported as the annual area simulated by each ensemble member. The annual areas are reported as the fraction of the study area (by dividing the calculated area to the total number of grids in the study area). The boxplots in Figures 28 and 29 depict the ensemble range of the annual areas at each warming level. Concurrency was calculated as the sum of grids experiencing wet and dry conditions in every timestep.

Based on SPI, the study area is more prone to wet spells than dry spells on an annual basis (Figure 28). Moreover, the annual area experiencing wet spells is projected to increase if global warming continues (Figure 28). On the contrary, the ensemble median projects the study area to be less vulnerable to dry spells as inferred from the decreasing annual area experiencing dry spells (Figure 29). On the other hand, SPEI indicates the study area is more prone to dry spells annually. Moreover, future projections based on SPEI suggest more locations in the study area would be exposed to both wet and dry spells under climate change (Figure 29). However, the increase in the area experiencing dry spells is more pronounced compared to wet spells.

Although both indices project increases in the exposure to concurrent wet-dry spells under climate change, this increase is mostly associated with growing area experiencing wet spells considering SPI (Figure 28). On the contrary, the projected increases in the annual area affected by dry spells contributes to the increasing exposure to concurrent wet-dry spells (Figure 29).

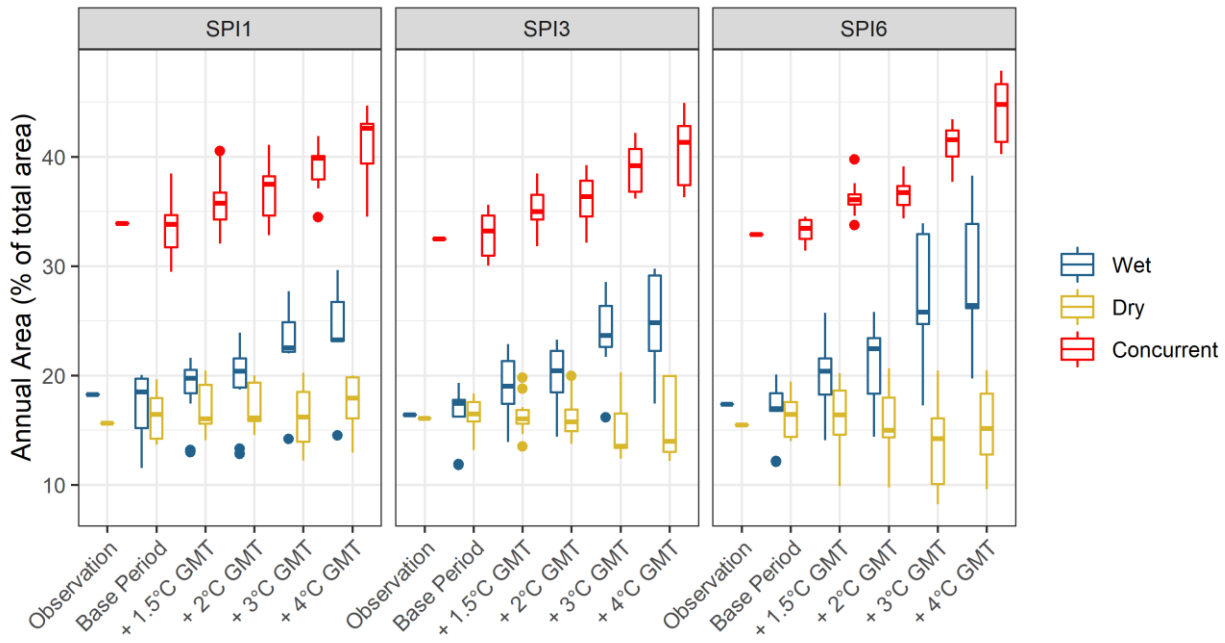

Figure 28 - Average annual area experiencing dry, wet, and concurrent dry-wet spells based on SPI. The boxplots show the range of the areas simulated by all the ensemble members.

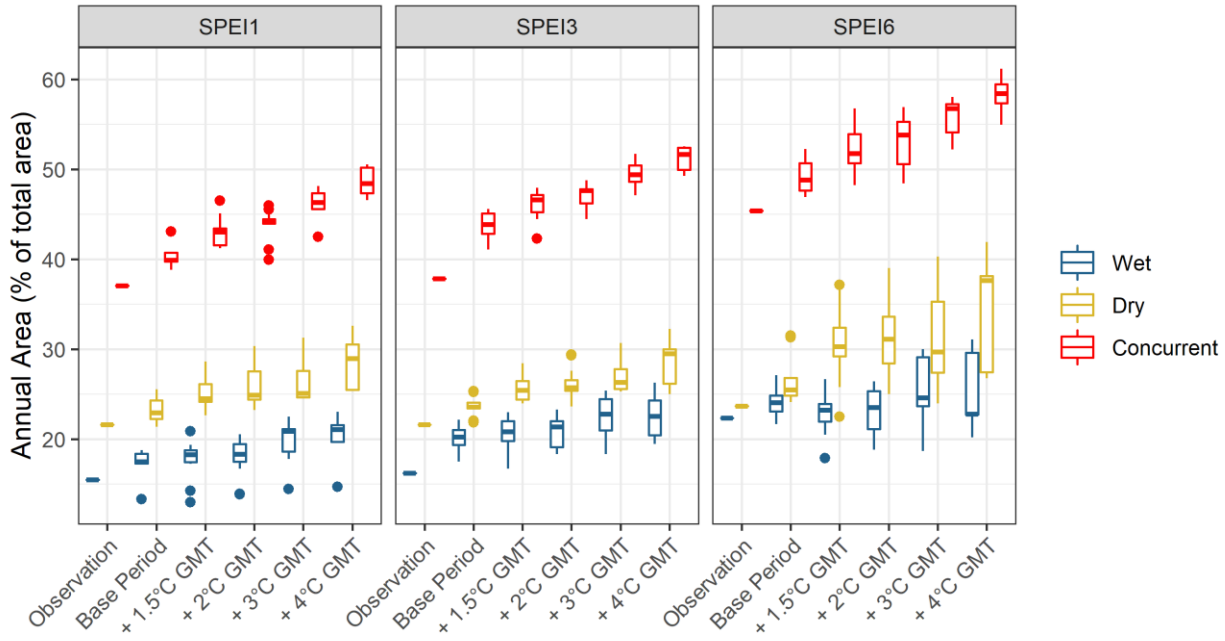

Figure 29 - Average annual area experiencing dry, wet, and concurrent dry-wet spells based on SPEI. The boxplots show the range of the areas simulated by all the ensemble members.

- 4.1.1.4. Magnitude and Intensity of Compound Climatic Events

The 2D Kernel Density plots for the magnitude and intensity of dry-to-wet CCEs based on SPI for 1-, 3-, and 6-months timescales are shown in Figures 30-31, 32-33, and 34-35, respectively. The results for dry-to-wet CCEs based on SPEI are presented in Figures 36-37, 38-39, and 40-41 for 1-, 3-, and 6-months timescales, respectively. In Figures 30-41, the climatology of the SPI/SPEI of wet and dry spells in CCEs are paired. Then the density plots for the pairs are generated spatially, based on the ensemble mean. Results for wet-to-dry events are presented in Appendix 19 to 30 due to similarities in the results.

Magnitude of both wet and dry spells in CCEs based on SPI are projected to increase under climate change (Figures 30, 32, and 34). Magnitude can be influence by the intensity and the duration of the spells. Therefore, the projected increase in the magnitude of wet spells can be

associated to the projected increases in the duration of wet spells (Figure 18). Moreover, the intensity of wet spells based on SPI are also projected to increase in a warmer world, as the ensemble mean indicates wet spells in CCEs are projected to be categorised as ‘very wet’ (except for CCEs shown by SPI6) based on classification system introduced in Figure 4 (Figures 31, 33, and 35). On the other hand, the projected increases of dry spells magnitude in CCEs can be attributed to the intensification of dry spells since the future projections of the ensemble mean based on SPI does not suggest considerable changes in the duration of the dry spells (Figures 18, 31, 33, and 35).

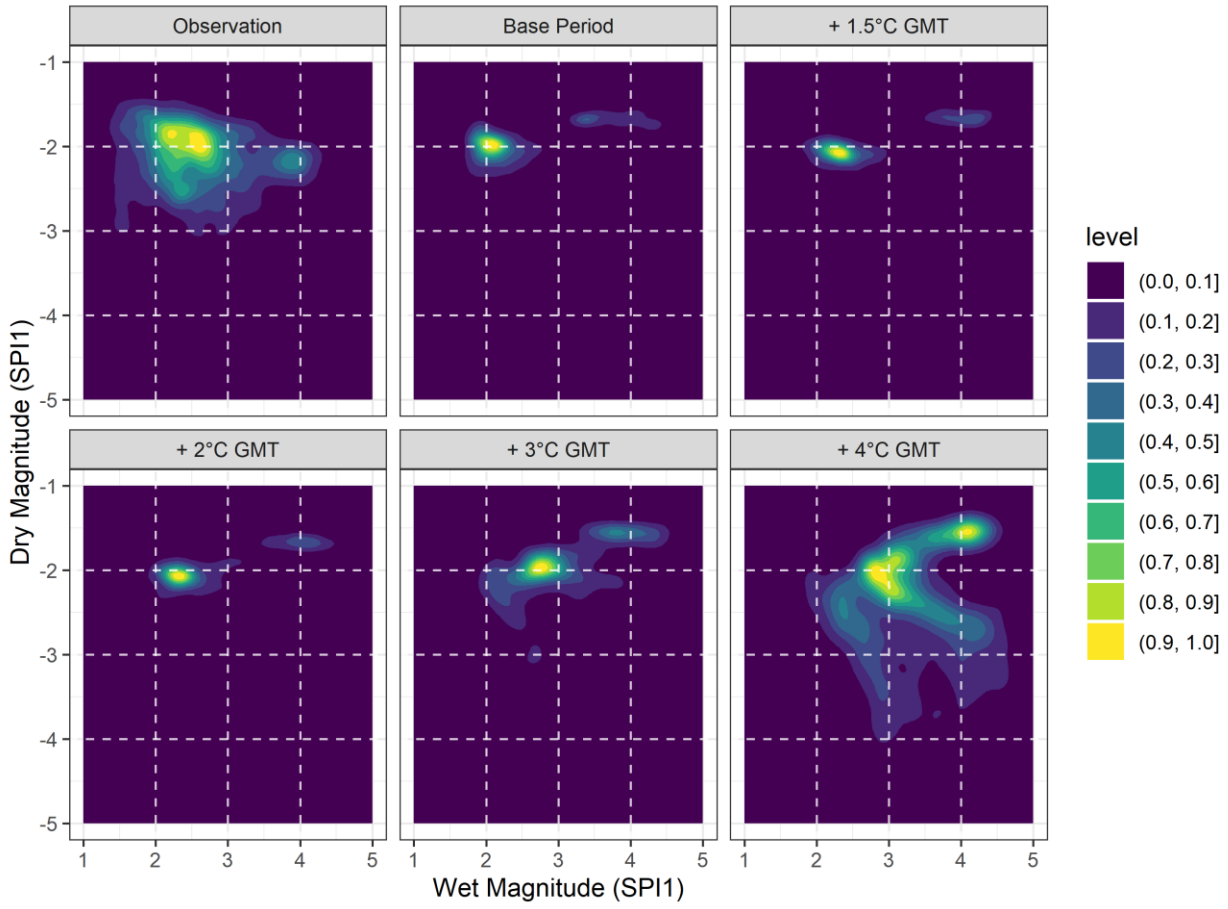

Figure 30 - 2D Kernel Density plots for the magnitude of wet and dry spells in dry-to-wet CCEs based on SPI1. The contours show the spatial density of the CCEs based on their dry and wet spells magnitudes.

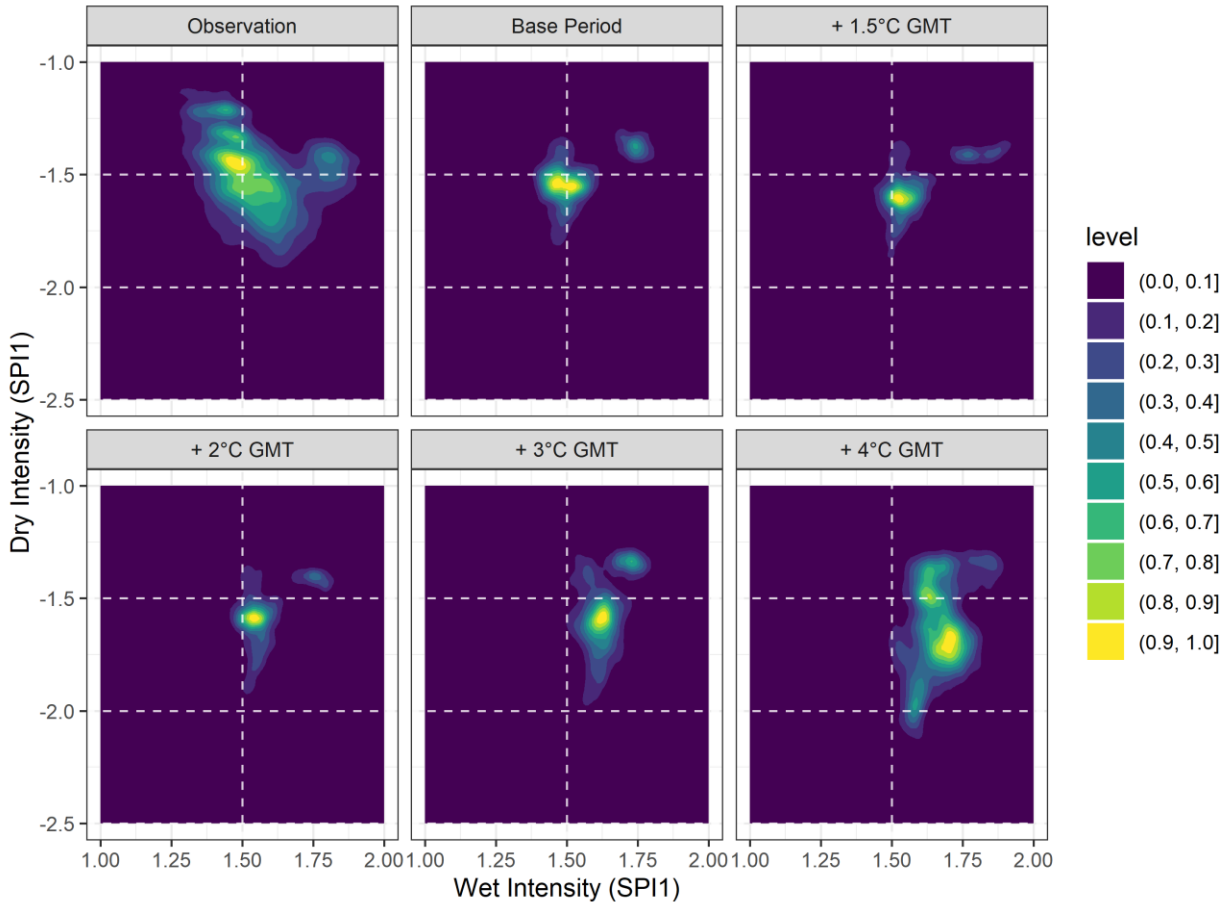

Figure 31- 2D Kernel Density plots for the intensity of wet and dry spells in dry-to-wet CCEs based on SPI1. The dashed lines show the SPI thresholds used to categorise wet and dry conditions (Figure 4). The contours show the spatial density of the CCEs based on their dry and wet spells intensities.

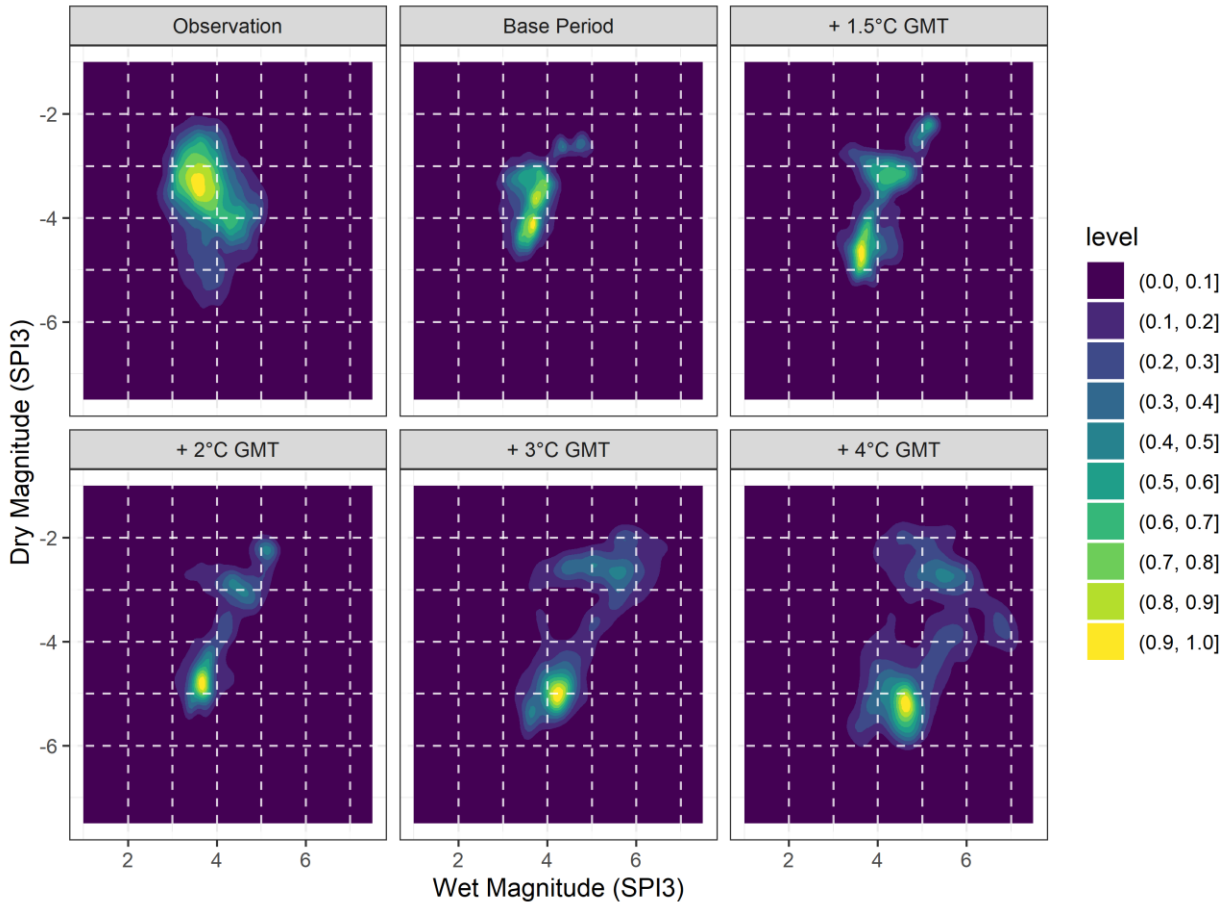

Figure 32 - 2D Kernel Density plots for the magnitude of wet and dry spells in dry-to-wet CCEs based on SPI3. The contours show the spatial density of the CCEs based on their dry and wet spells magnitudes.

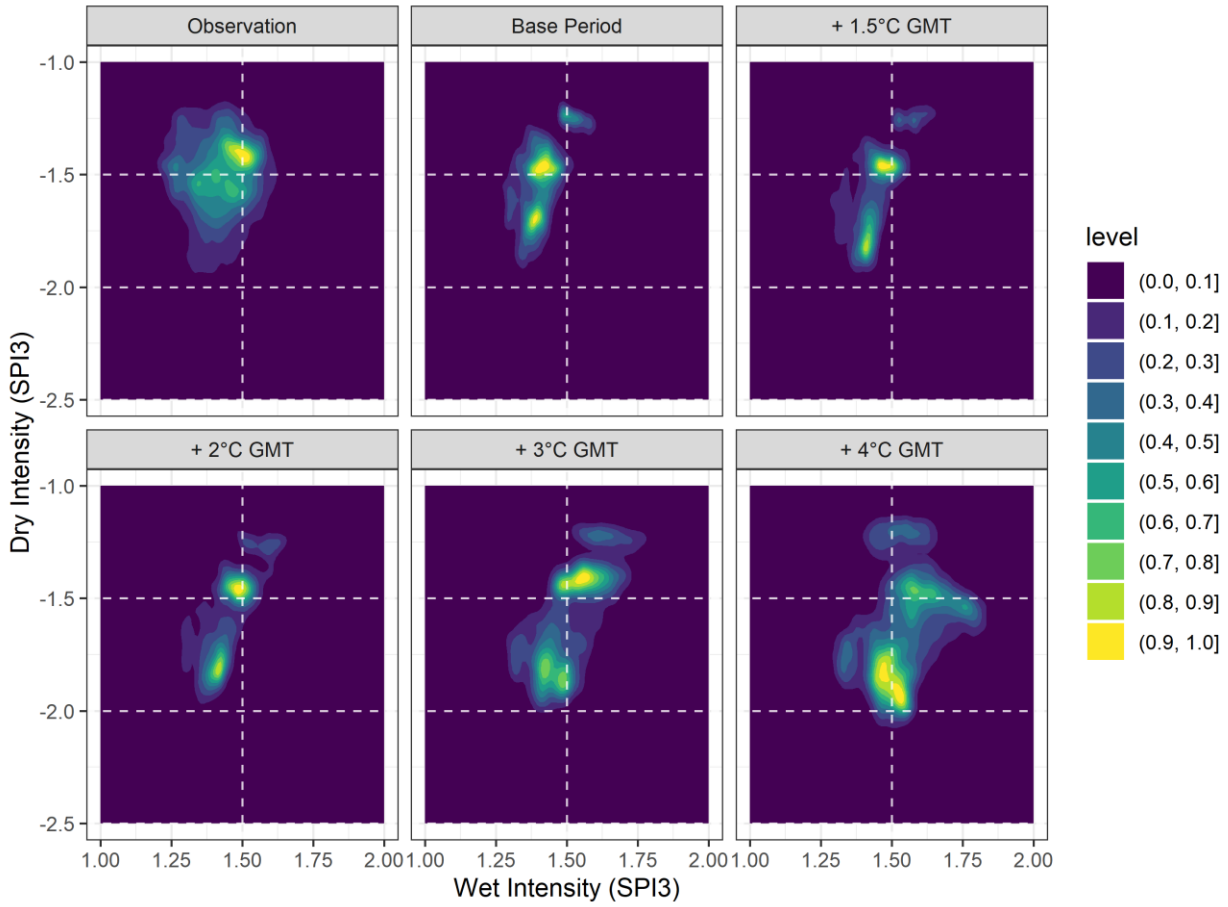

Figure 33 - 2D Kernel Density plots for the intensity of wet and dry spells in dry-to-wet CCEs based on SPI3. The dashed lines show the SPI thresholds used to categorise wet and dry conditions (Figure 4). The contours show the spatial density of the CCEs based on their dry and wet spells intensities.

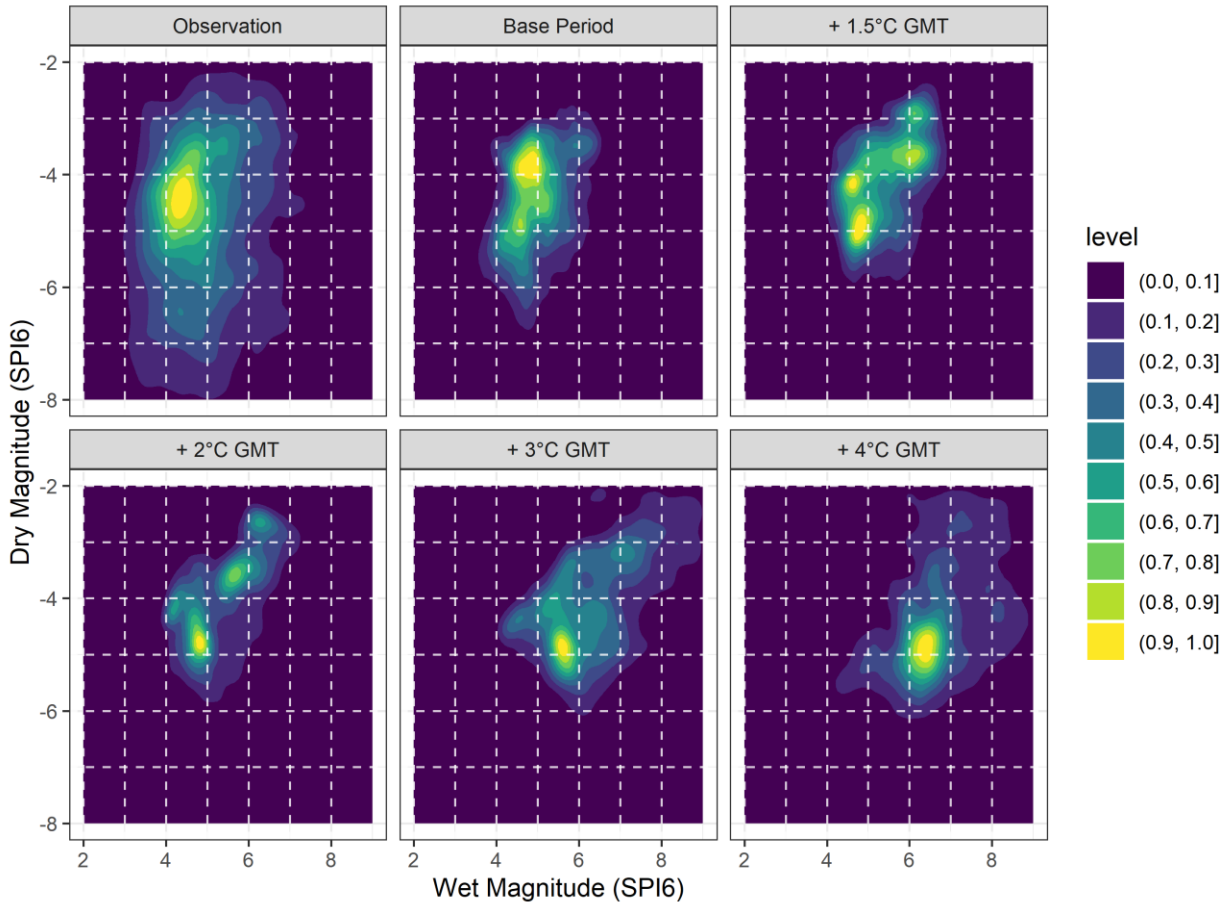

Figure 34 - 2D Kernel Density plots for the magnitude of wet and dry spells in dry-to-wet CCEs based on SPI6. The contours show the spatial density of the CCEs based on their dry and wet spells magnitudes.

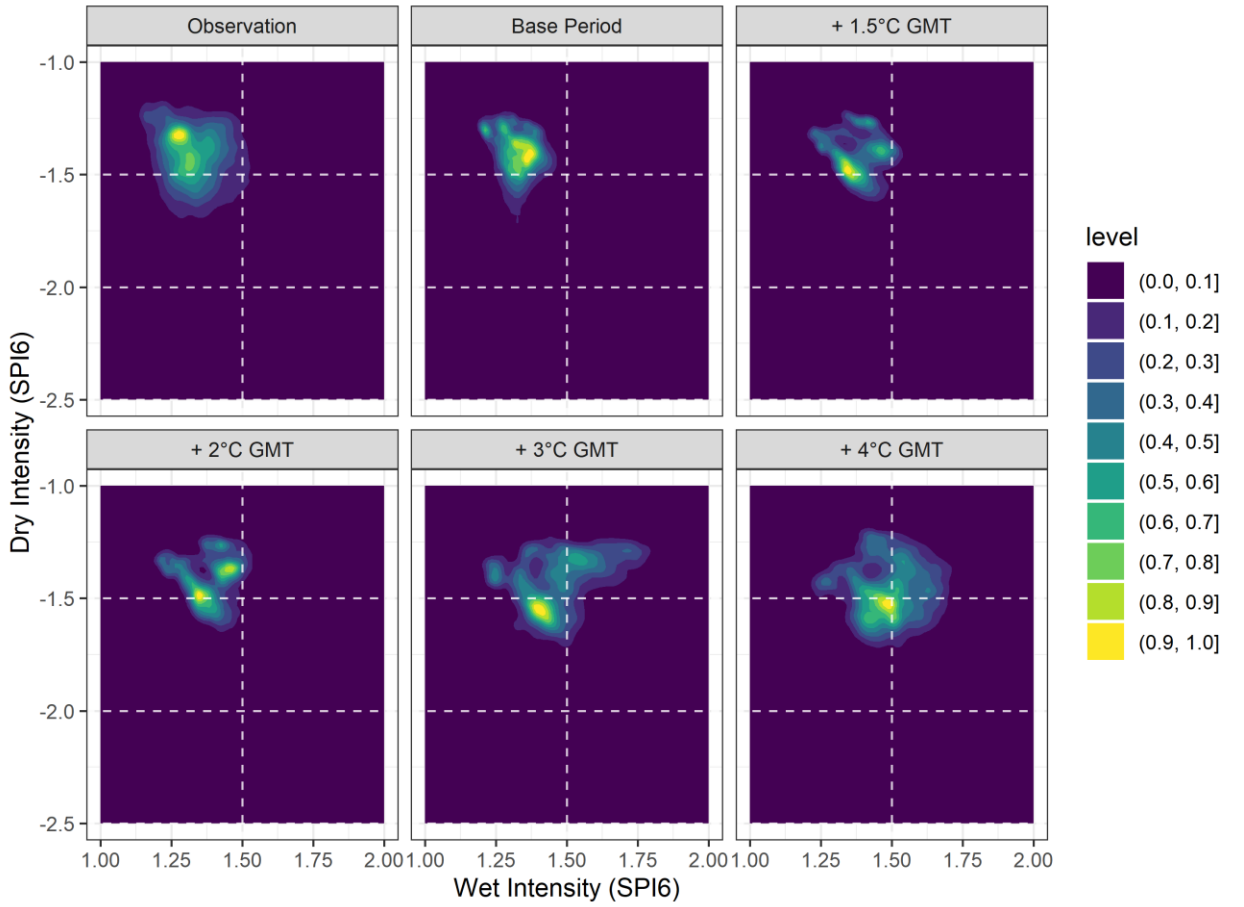

Figure 35 - 2D Kernel Density plots for the intensity of wet and dry spells in dry-to-wet CCEs based on SPI6. The dashed lines show the SPI thresholds used to categorise wet and dry conditions (Figure 4). The contours show the spatial density of the CCEs based on their dry and wet spells intensities.

In line with projections based on SPI, SPEI also indicates that the magnitude of both wet and dry spells in CCEs are projected to increase under climate change (Figures 36, 38, and 40). However, the increase is more noticeable in the magnitude of dry spells. Since the ensemble mean suggests increasing patterns in the duration of dry spells based on SPEI (Figure 19) in a warming world, some part of the grow in the magnitude of dry spells in CCEs could be attributed to the changes in duration. However, dry spells in CCEs are projected to also intensify in a warmer world

(Figures 37, 39, and 41). Therefore, increases in both the duration and intensity of dry spells could lead to the growth in the magnitude of dry spells in CCEs. Intensification of future wet spells in CCEs are also projected by the ensemble mean. Since the projected changes in the duration of wet spells is not considerable, the projected pattern of increasing wet spell magnitudes in CCEs could be due to the intensification of them in a warming world (Figures 19, 37, 39, and 41).

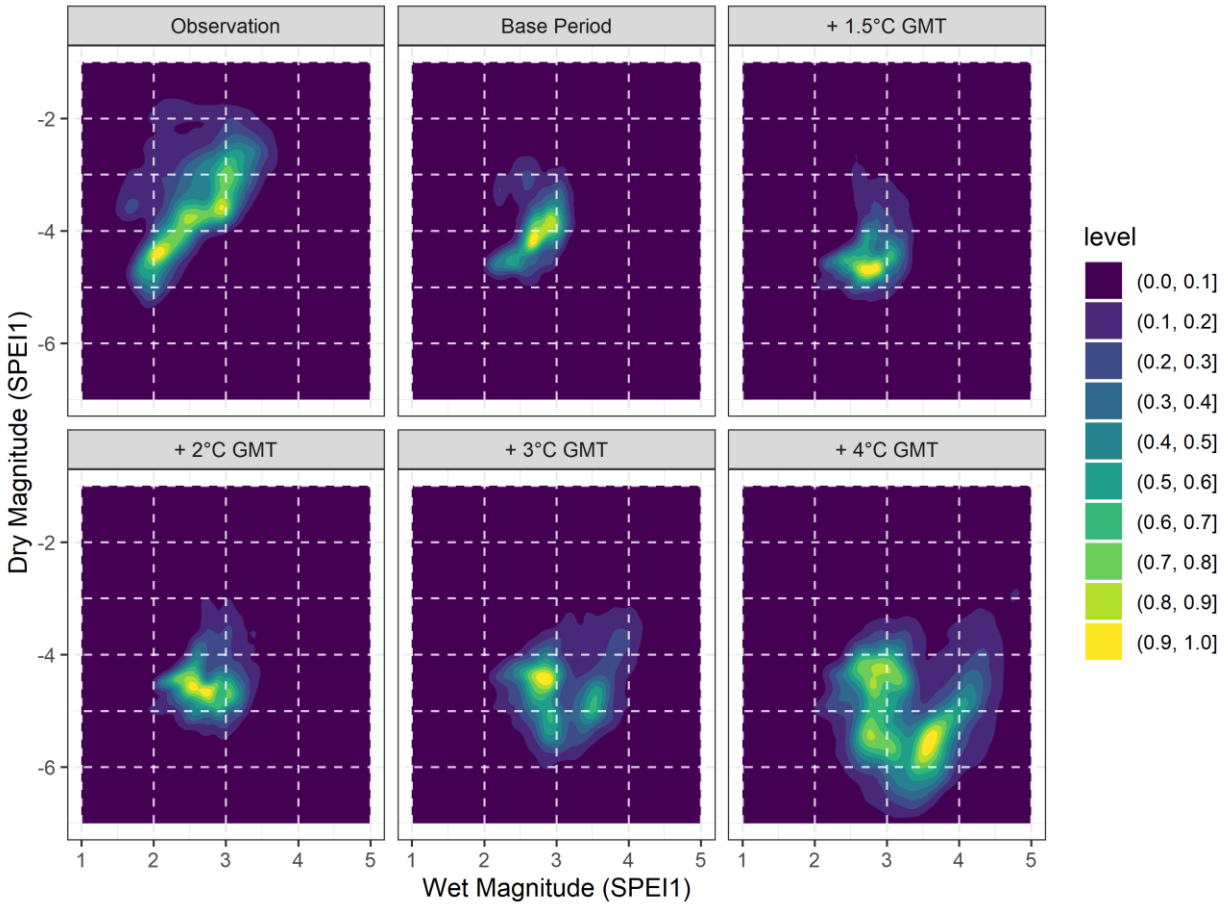

Figure 36 - 2D Kernel Density plots for the magnitude of wet and dry spells in dry-to-wet CCEs based on SPEI1. The contours show the spatial density of the CCEs based on their dry and wet spells magnitudes.

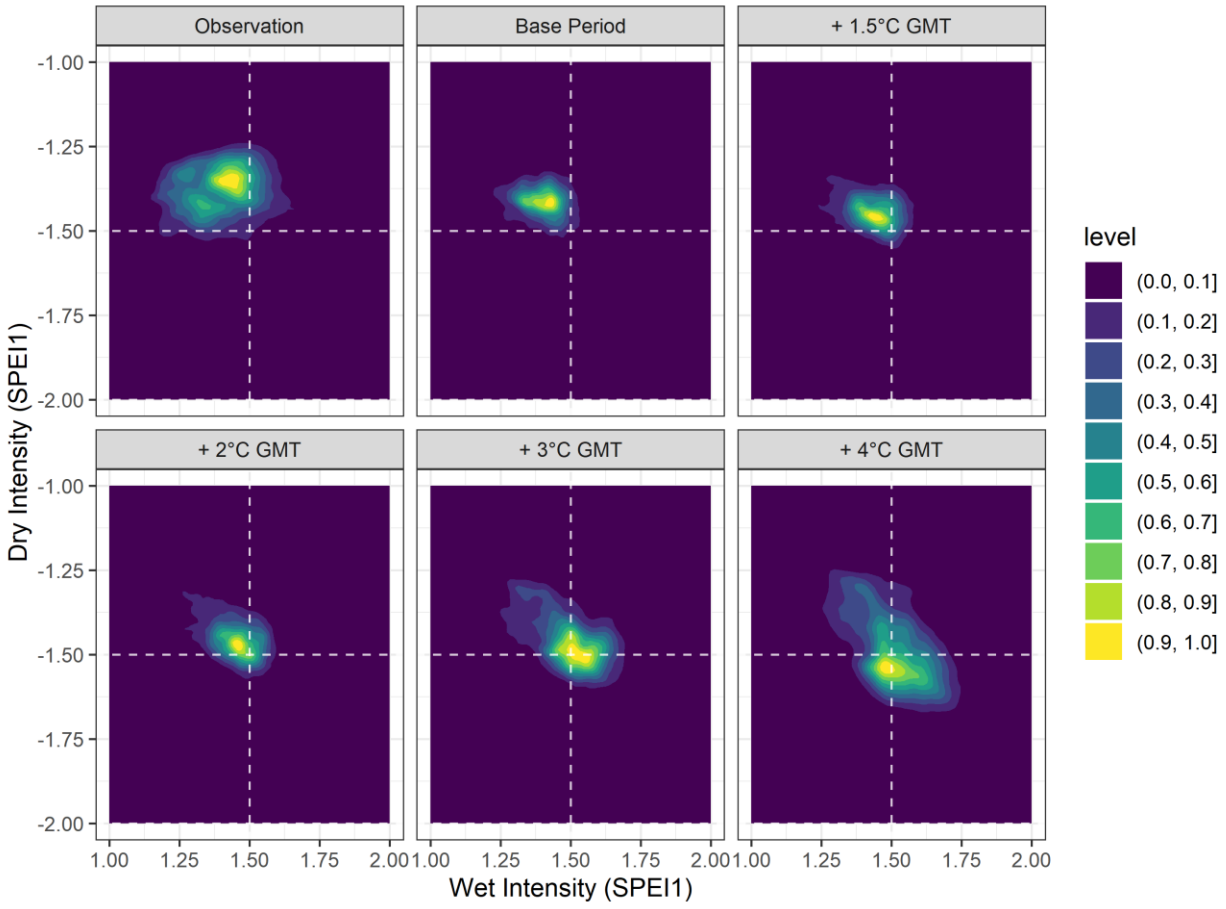

Figure 37 - 2D Kernel Density plots for the intensity of wet and dry spells in dry-to-wet CCEs based on SPEI1. The dashed lines show the SPEI thresholds used to categorise wet and dry conditions (Figure 4). The contours show the spatial density of the CCEs based on their dry and wet spells intensities.

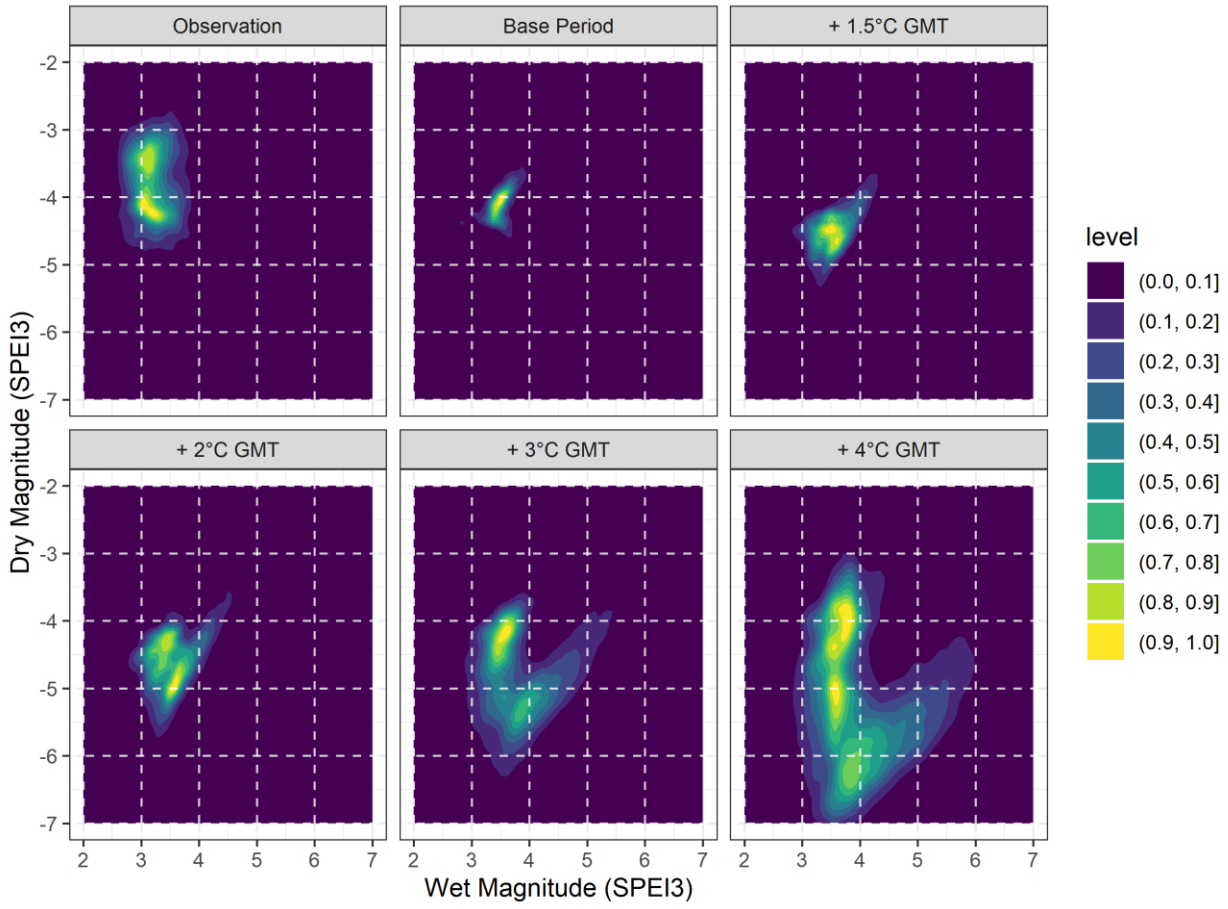

Figure 38 - 2D Kernel Density plots for the magnitude of wet and dry spells in dry-to-wet CCEs based on SPEI3. The contours show the spatial density of the CCEs based on their dry and wet spells magnitudes.

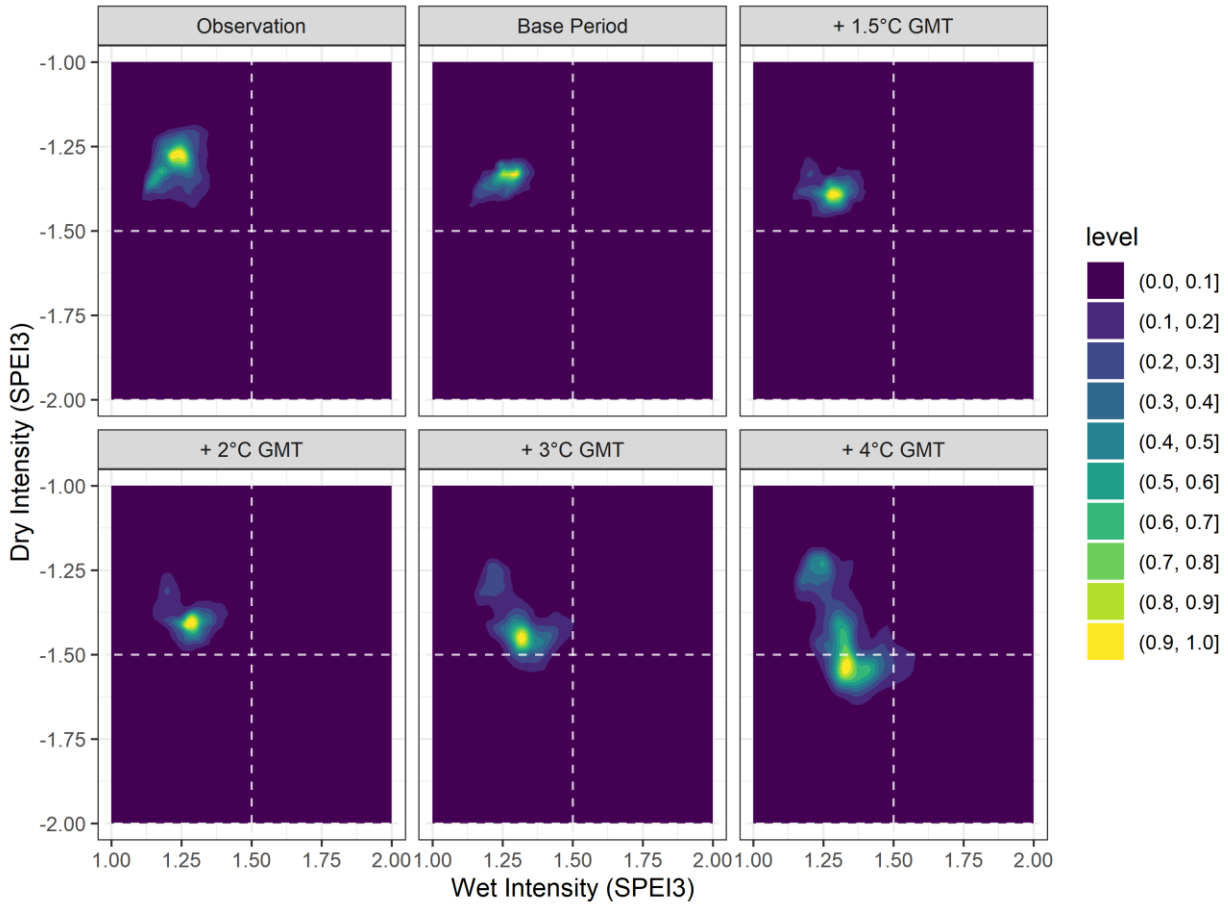

Figure 39 - 2D Kernel Density plots for the intensity of wet and dry spells in dry-to-wet CCEs based on SPEI3. The dashed lines show the SPEI thresholds used to categorise wet and dry conditions (Figure 4). The contours show the spatial density of the CCEs based on their dry and wet spells intensities.

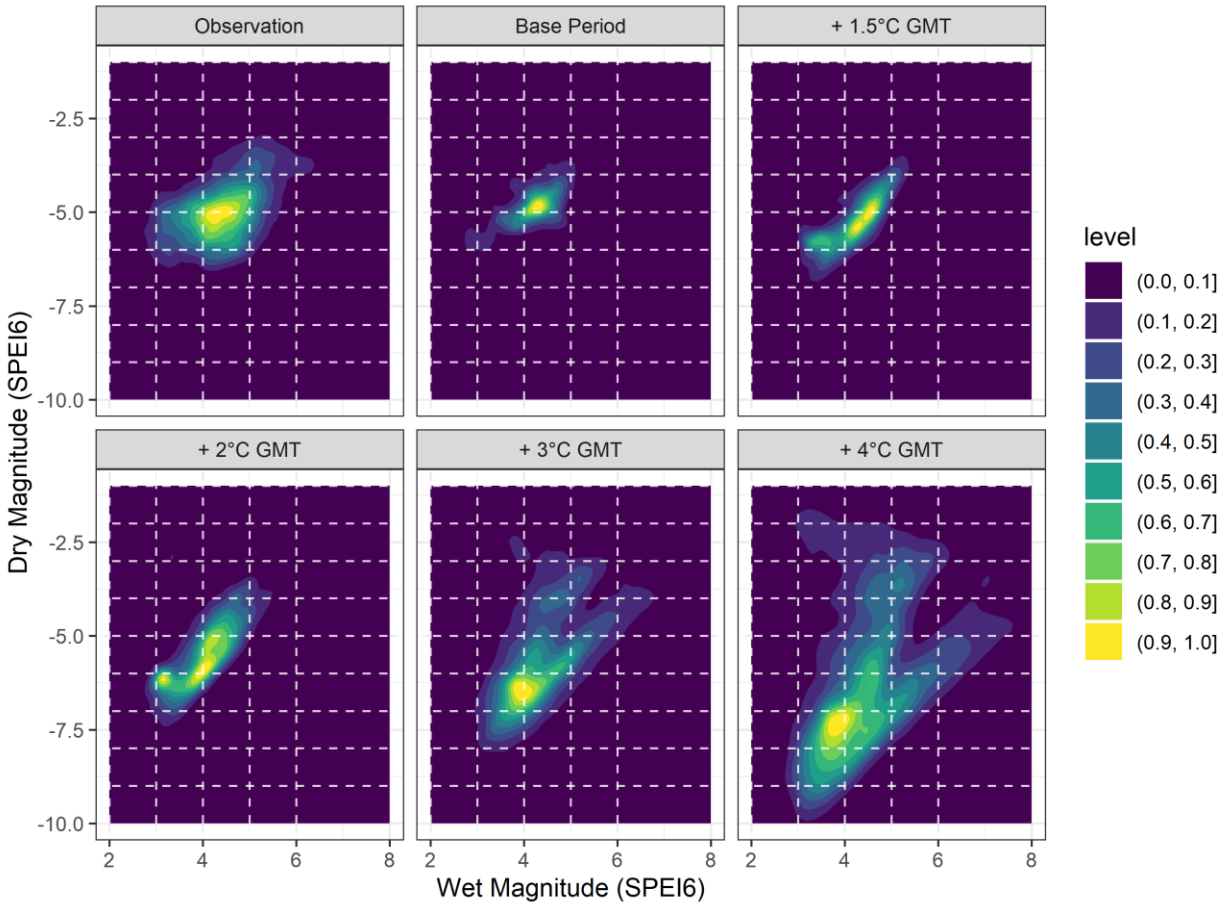

Figure 40 - 2D Kernel Density plots for the magnitude of wet and dry spells in dry-to-wet CCEs based on SPEI6. The contours show the spatial density of the CCEs based on their dry and wet spells magnitudes.

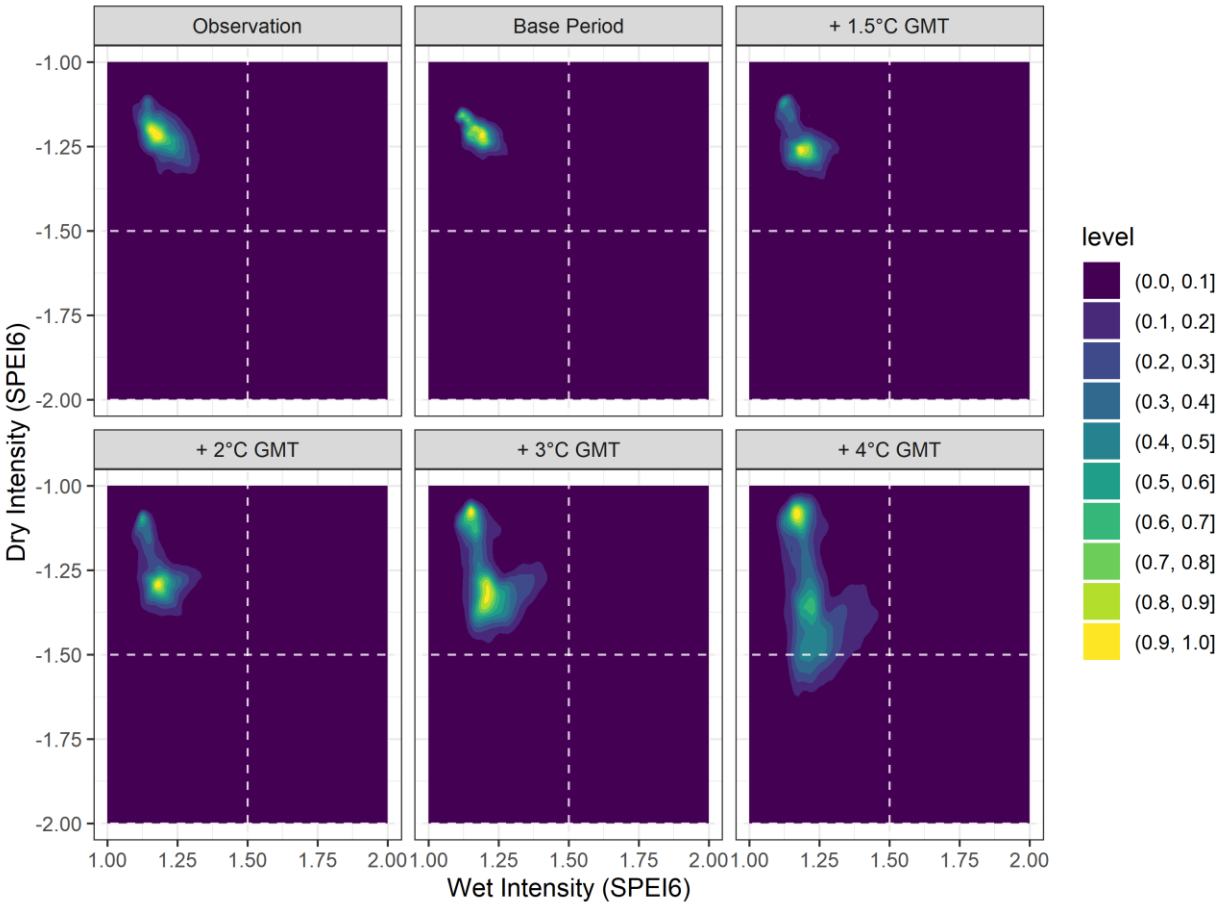

Figure 41 - 2D Kernel Density plots for the intensity of wet and dry spells in dry-to-wet CCEs based on SPEI6. The dashed lines show the SPEI thresholds used to categorise wet and dry conditions (Figure 4). The contours show the spatial density of the CCEs based on their dry and wet spells intensities.

The magnitude of the wet and dry spells in the dry-to-wet CCEs are spatially presented in the maps of Figures 42 and 43 for SPI1, 44 and 45 for SPI3, 46 and 47 for SPI6, 48 and 49 for SPEI1, 50 and 51 for SPEI3, and 52 and 53 for SPEI6. The maps (Figures 42 – 53) show the ensemble mean of the SPI/SPEI values of the wet and dry spells in dry-to-wet CCEs. Results for wet-to-dry CCEs are presented in Appendix 31 to 42.

The magnitude of both dry and wet spells in CCEs based on SPI is projected to intensify at higher levels of global warming (Figures 42 – 47). However, the projected changes in the magnitude vary spatially and some locations are hotspots. CCEs are projected to have more severe dry spells across the American portion of the study area (Figures 42, 44, and 46). On the other hand, the Canadian portion of the study area is prone to more severe wet spells with increasing magnitudes if warming is not limited. Specifically, eastern Peace and Fraser basins, as well as southwest of Fraser near Vancouver area are future hotspots for severe wet spells in CCEs (Figures 43, 45, and 47).

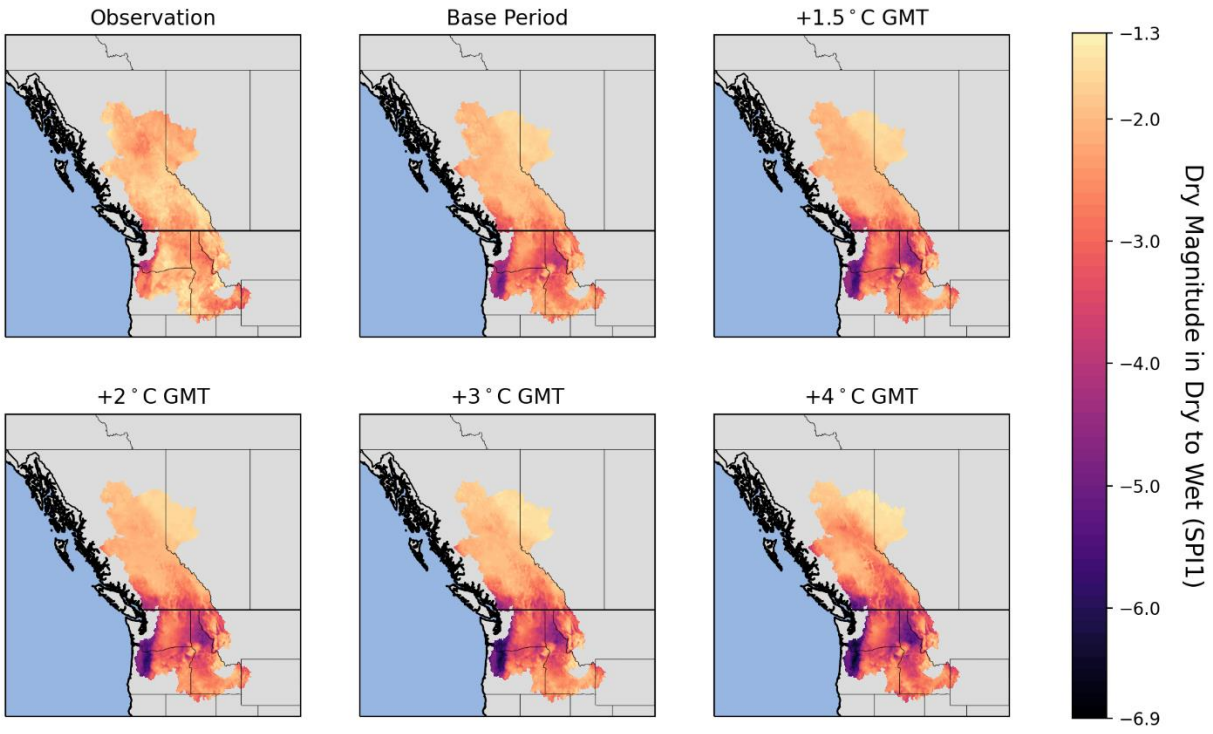

Figure 42 - Climatology of the dry spell magnitude in the dry-to-wet CCEs (SPI1). The map shows the magnitude based on the SPI values of dry spells in the CCEs.

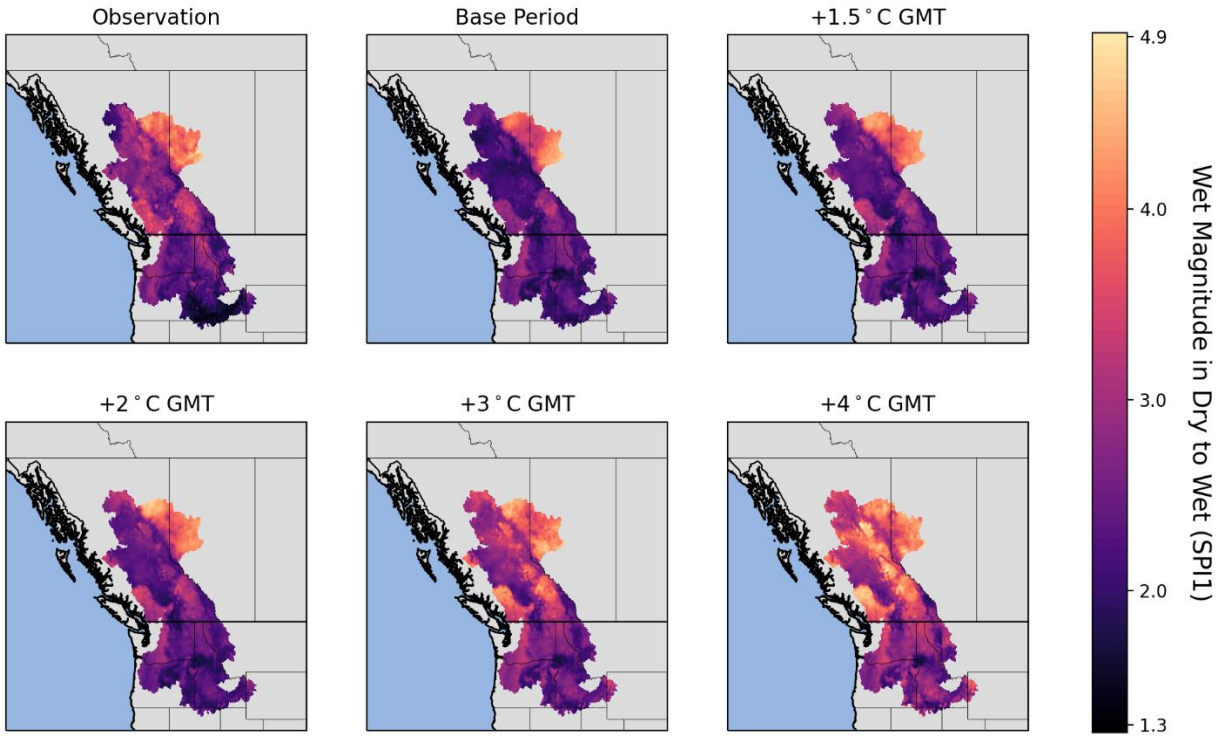

Figure 43 - Climatology of the wet spell magnitude in the dry-to-wet CCEs (SPI1). The map shows the magnitude based on the SPI values of wet spells in the CCEs.

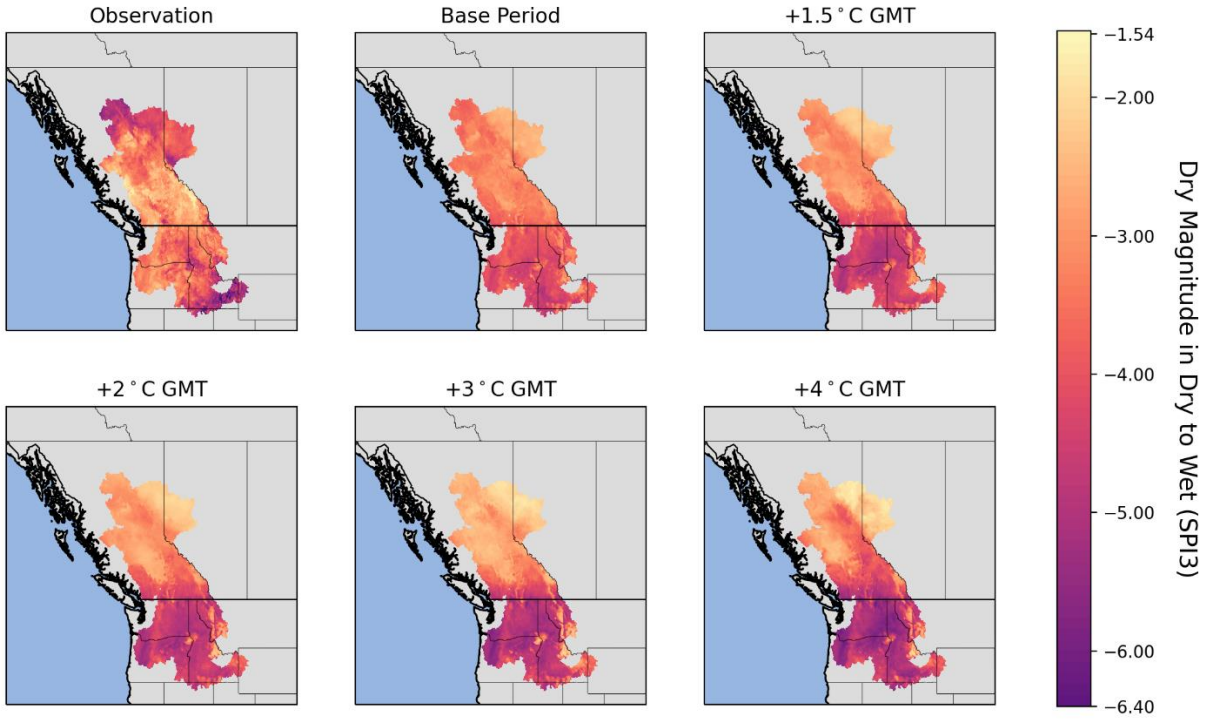

Figure 44 - Climatology of the dry spell magnitude in the dry-to-wet CCEs (SPI3). The map shows the magnitude based on the SPI values of dry spells in the CCEs.

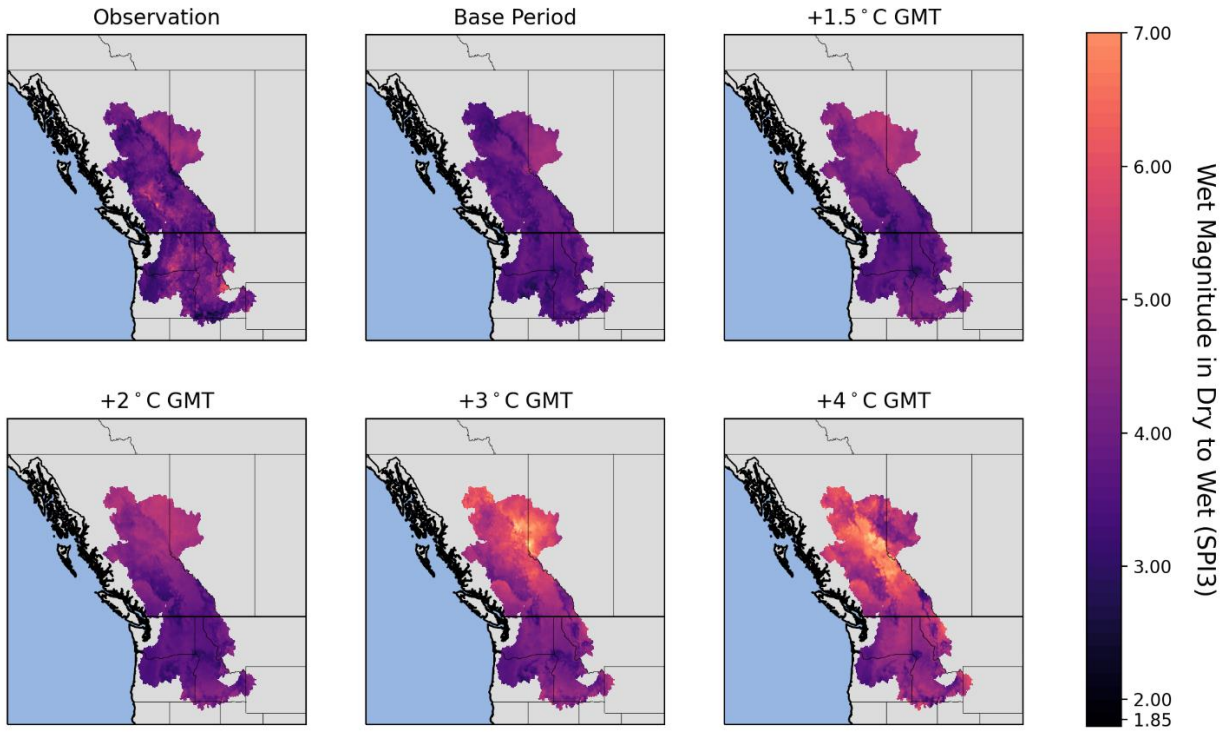

Figure 45 - Climatology of the wet spell magnitude in the dry-to-wet CCEs (SPI3). The map shows the magnitude based on the SPI values of wet spells in the CCEs.

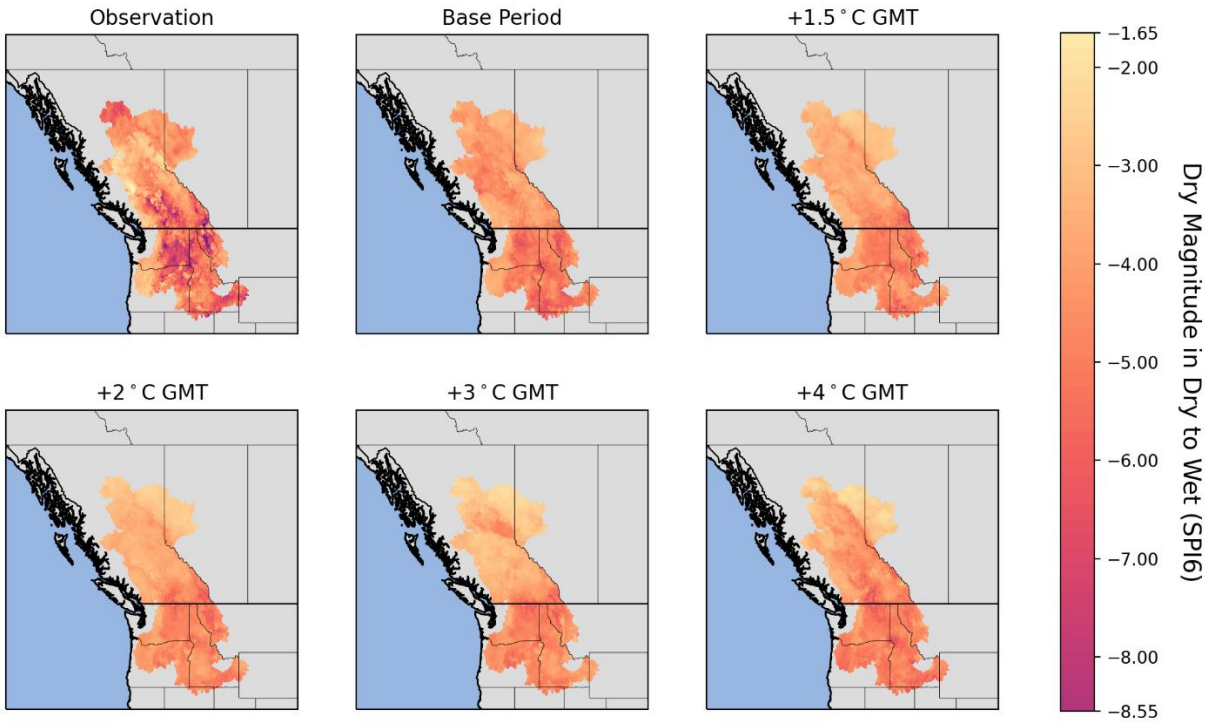

Figure 46 - Climatology of the dry spell magnitude in the dry-to-wet CCEs (SPI6). The map shows the magnitude based on the SPI values of dry spells in the CCEs.

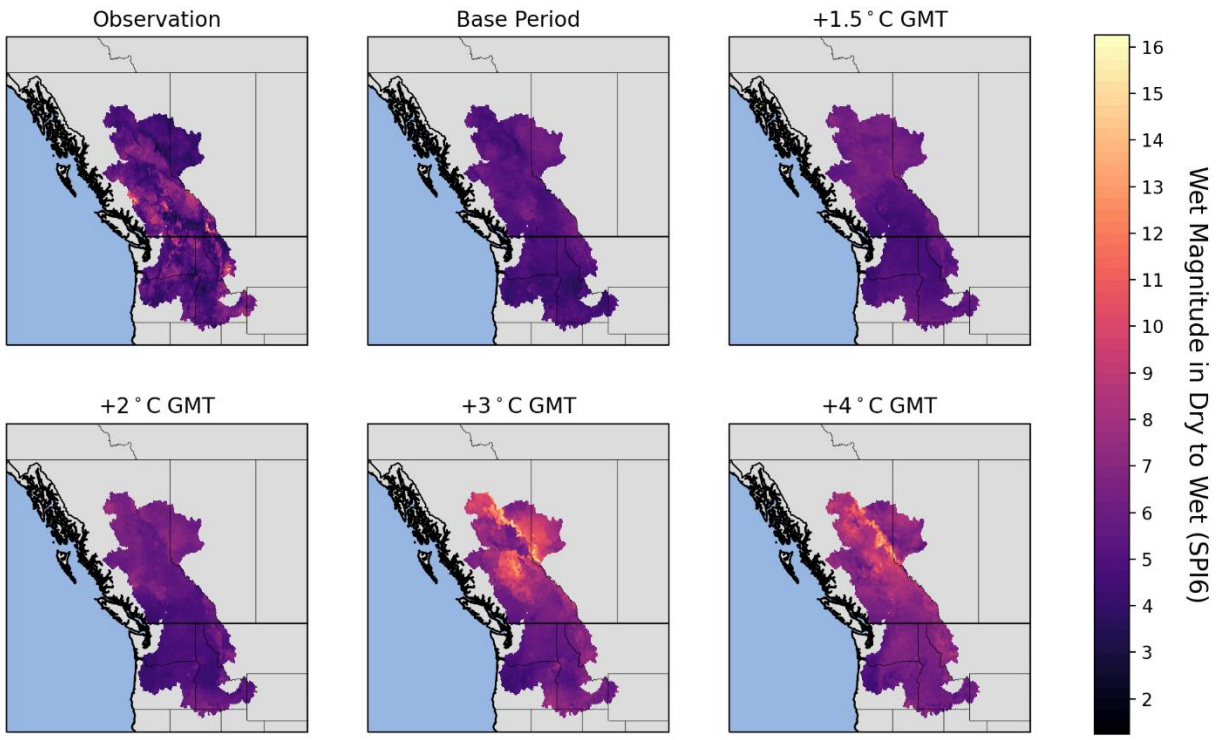

Figure 47 - Climatology of the wet spell magnitude in the dry-to-wet CCEs (SPI6). The map shows the magnitude based on the SPI values of wet spells in the CCEs.

Inline with SPI results, future projections of wet spells magnitudes based on SPEI indicate that the Canadian portion of the study area is prone to more severe wet spells (except in eastern Peace basin) (Figures 49, 51, and 53). On the other hand, the identified hotspots for the dry spell magnitudes based on SPEI are not similar to hotspots shown by SPI. Future projections of the ensemble mean indicate the more severe dry spells are across Peace and Fraser basins are projected under climate change (Figures 48, 50, and 52).

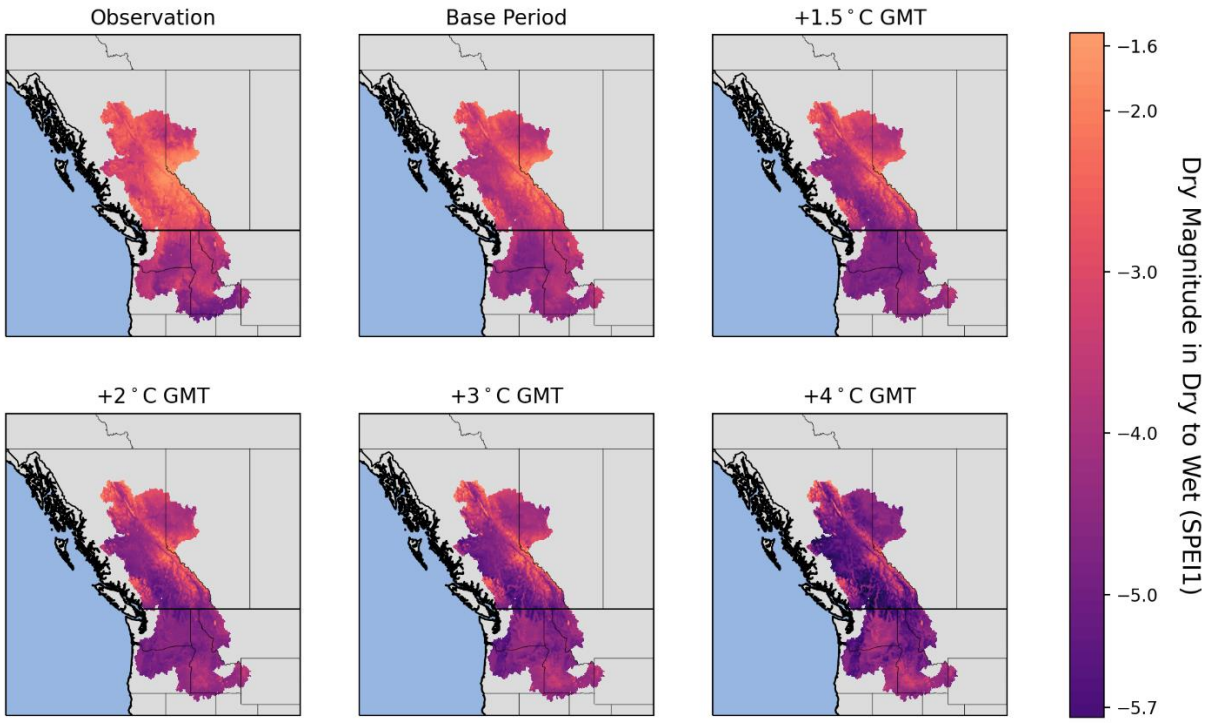

Figure 48 - Climatology of the dry spell magnitude in the dry-to-wet CCEs (SPEI1). The map shows the magnitude based on the SPEI values of dry spells in the CCEs.

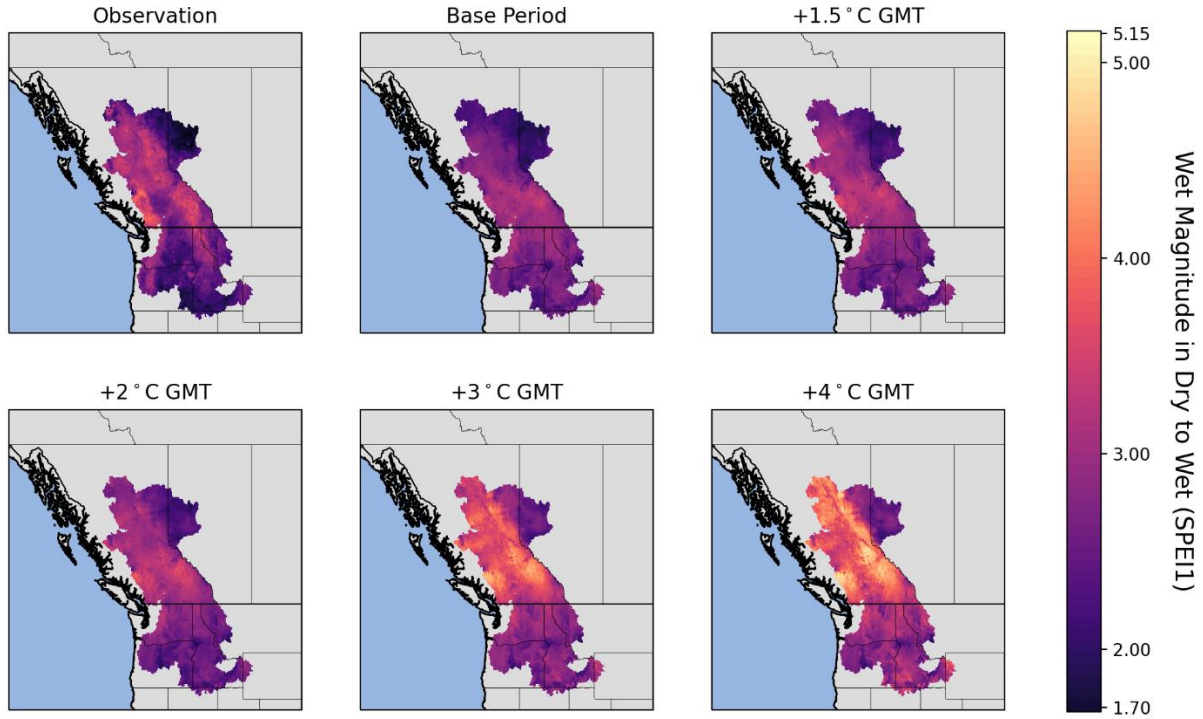

Figure 49 - Climatology of the wet spell magnitude in the dry-to-wet CCEs (SPEI1). The map shows the magnitude based on the SPEI values of wet spells in the CCEs.

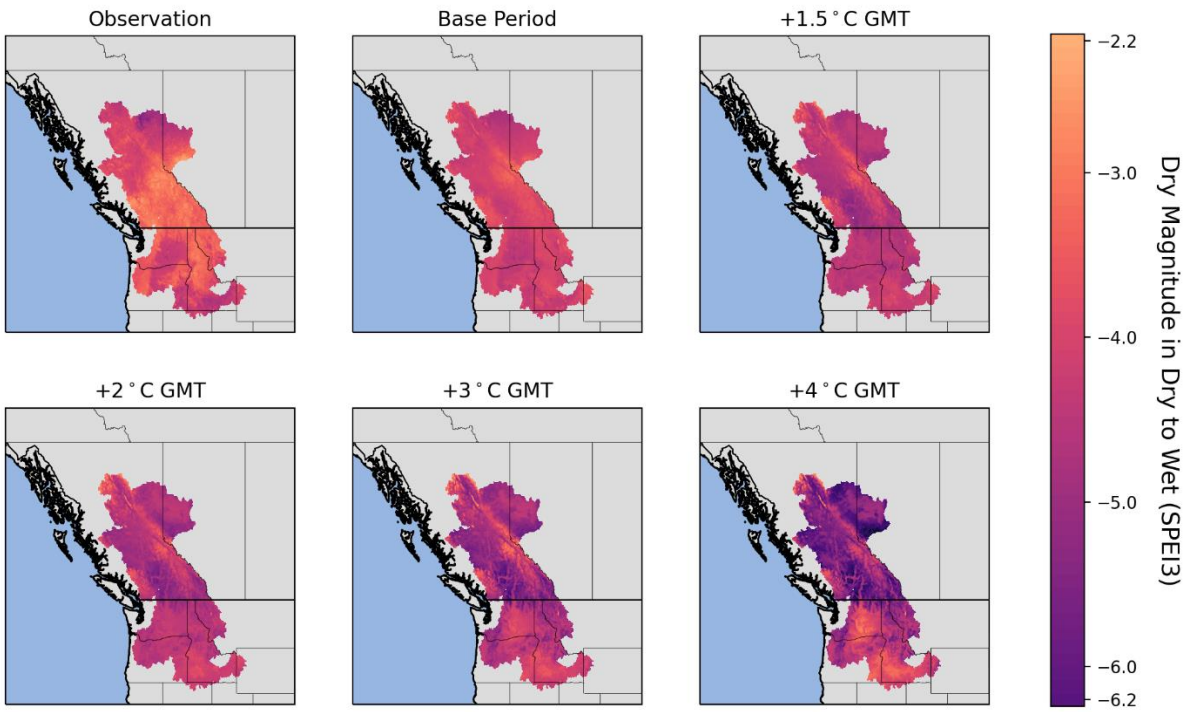

Figure 50 - Climatology of the dry spell magnitude in the dry-to-wet CCEs (SPEI3). The map shows the magnitude based on the SPEI values of dry spells in the CCEs.

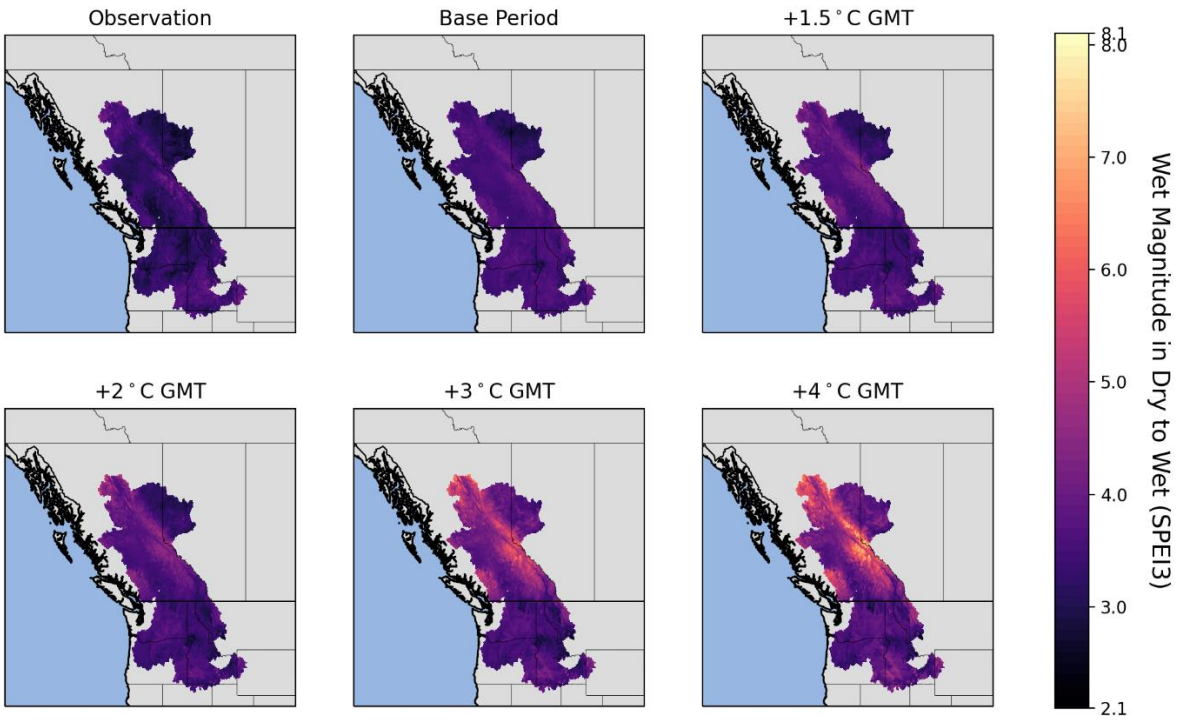

Figure 51 - Climatology of the wet spell magnitude in the dry-to-wet CCEs (SPEI3). The map shows the magnitude based on the SPEI values of wet spells in the CCEs.

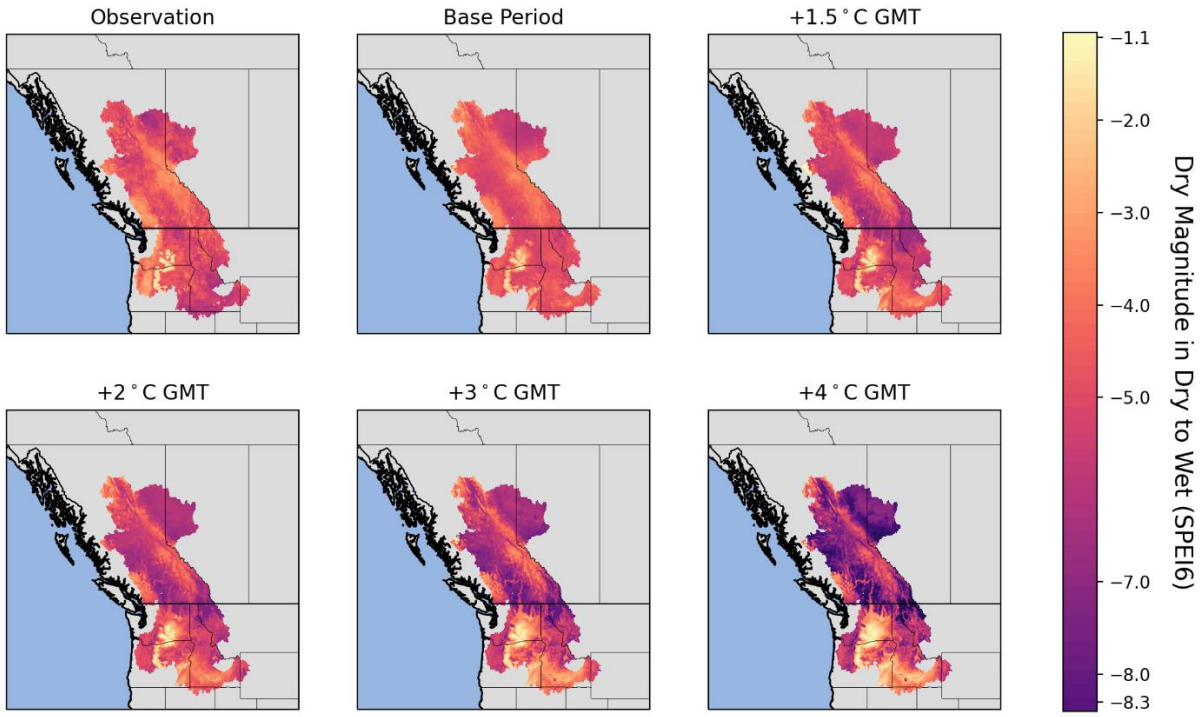

Figure 52 - Climatology of the dry spell magnitude in the dry-to-wet CCEs (SPEI6). The map shows the magnitude based on the SPEI values of dry spells in the CCEs.

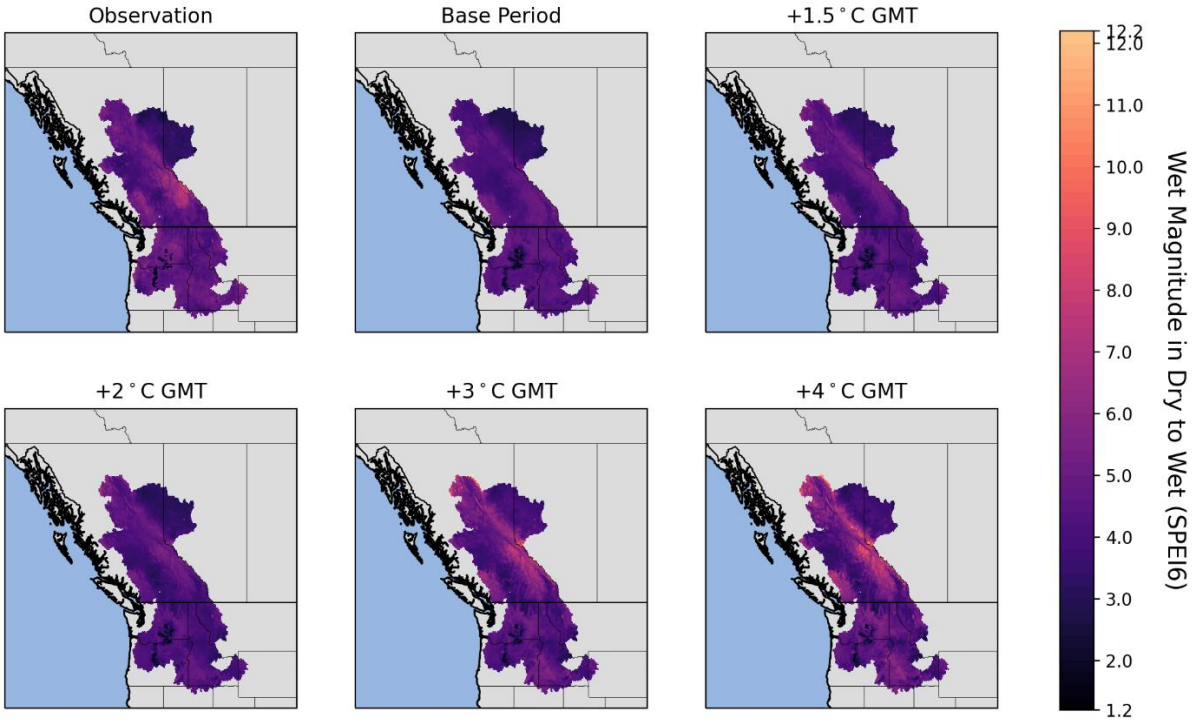

Figure 53 - Climatology of the wet spell magnitude in the dry-to-wet CCEs (SPEI6). The map shows the magnitude based on the SPEI values of wet spells in the CCEs.

4.1.2. Compound Hydrologic Events

- 4.1.2.1 Frequency of Compound Hydrologic Events

The spatial frequency of compound hydrologic events (CHEs) at the three river basins of the study area at different warming levels are presented in Figure 54. For each model-RCP pair in our multi-model ensemble, the frequency of flood-to-drought and drought-to-flood CHEs are calculated at every warming period. Then the ensemble climatology of frequency for each warming level is calculated by taking the mean of frequencies of all ensemble members at each warming period. The abrupt CHEs (CHEs having transition time of shorter than a month) are extracted in a similar manner. The spatial median and the 95% confidence interval (CI) of the

frequency of CHEs (abrupt and all events) are presented in Figure 54. All CHEs are presented with crossbars while the abrupt CHEs are illustrated using bars and points in Figure 54.

When comparing the two compound scenarios of flood-to-drought and drought-to-flood, the three watersheds are more prone to the CHEs of the former case. While the median frequency of drought-to-flood CHEs are projected to not change considerably in a warming climate, the flood-to-drought CHEs are projected to increase substantially under climate change, with the largest projected values at the 4°C global warming level (crossbars in Figure 54). Even though drought-to-flood CHEs occur more frequently than flood-to-drought CHEs in the base period, the projections indicate that the region is expected to become more susceptible to the latter if the global warming continues (crossbars in Figure 54). Amongst all basins, flood-to-drought CHEs occur more frequently in Fraser Basin at all warming levels (crossbars in Figure 54).

The future projections indicate that none of the basins in the study area are prone to abrupt drought-to-flood CHEs (bars and points in Figure 54). However, an emergence of abrupt flood-to-drought CHEs is projected under climate change, with an increasing pattern in the frequency if the global warming is not limited (bars and points in Figure 54). Amongst all, Fraser basin is the most susceptible to abrupt flood-to-drought CHEs under all warming scenarios (bars and points in Figure 54). A comparison between the uncertainty of the presented results indicates that the frequency of abrupt flood-to-drought CHEs is increasing in the entire study area which also suggests increasing exposure to such compound events under climate change.

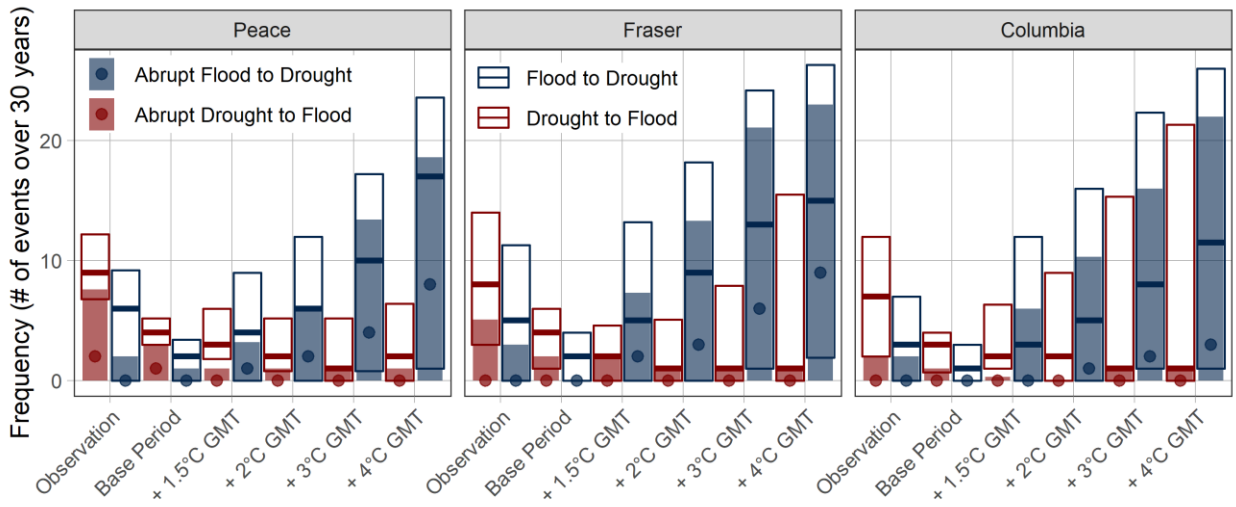

Figure 54 - Climatology of frequency of compound hydrological events (CHEs) in the watersheds of the study area at different warming levels. The cross bars represent the spatial median and 95% confidence interval (CI) (q2.5-q97.5) of frequency of all CHEs in the ensemble mean. The bars and points illustrate the spatial median and the CI of frequency of abrupt CHEs. Bars and cross bars are colored based on the CHE type (blue: flood to drought; red: drought-to-flood).

The frequency of drought-to-flood CHEs at each hydrometric gauge is spatially presented in the maps of Figure 55. The maps show the ensemble mean at each station over different warming levels. In the base period, the frequency of drought-to-flood CHEs is almost evenly distributed across the study area with less than 5 CHE occurrences over 30 years (Figure 55). However, the global warming is projected to decrease the frequency of drought-to-flood CHEs over most of the study area, with some exceptions. Although future drought-to-flood CHEs are rare in many locations of the study area, it is projected that some locations in middle of the Peace Basin as well as some areas in the southwest of the Columbia Basin experience CHEs more often (Figure 55). In addition, the gauge located in the southwest of Columbia are the hotspots for drought-to-

flood CHEs with average frequency of more than 20 events over 30 years if the global warming reaches the 4°C level (Figure 55).

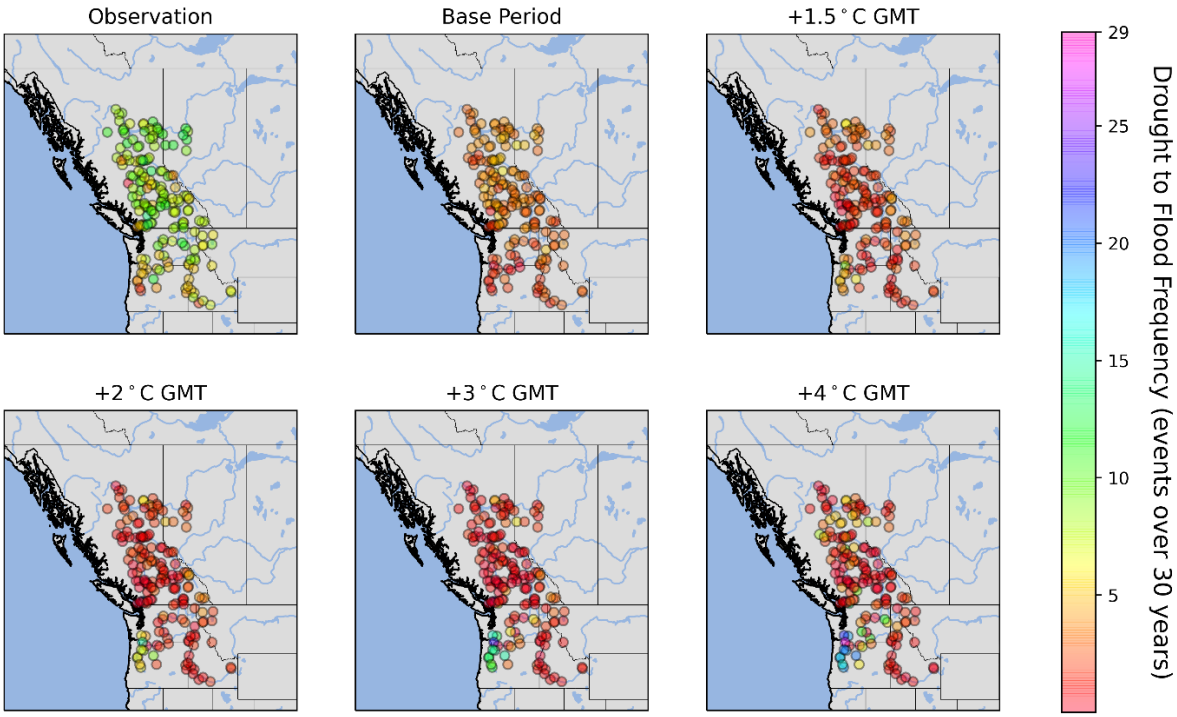

Figure 55 - Climatology of the frequency of drought-to-flood CHEs. The maps show the ensemble mean at each hydrometric gauge.

The climatology of frequency of flood-to-drought CHEs at each hydrometric gauge is presented in the maps of Figure 56. The frequencies have been calculated like Figure 55. Flood-to-drought CHEs are rare over the entire study area (not exceeding 5 instances at any location) in the base period. However, such compound extremes become more frequent and occur almost 15 times over 30 years at the 1.5°C global warming level and continue to increase if global warming is not limited (Figure 56). Except for some locations in southeast of the Columbia, flood-to-droughts CHEs are projected to become commonplace under climate change, with more prevalent occurrences in central and eastern Fraser basin and southwest of Columbia (Figure 56). A

comparison of Figures 55 and 56 reveals that the gauges located in southeast of the Columbia are not prone to either of flood-to-drought and drought-to-flood CHEs and this pattern is not projected to change under climate change. On the other hand, some areas in the southwest of Columbia are susceptible to both flood-to-drought and drought-to-flood CHEs, which could cause hardship for water management and disaster response and recovery at these sites.

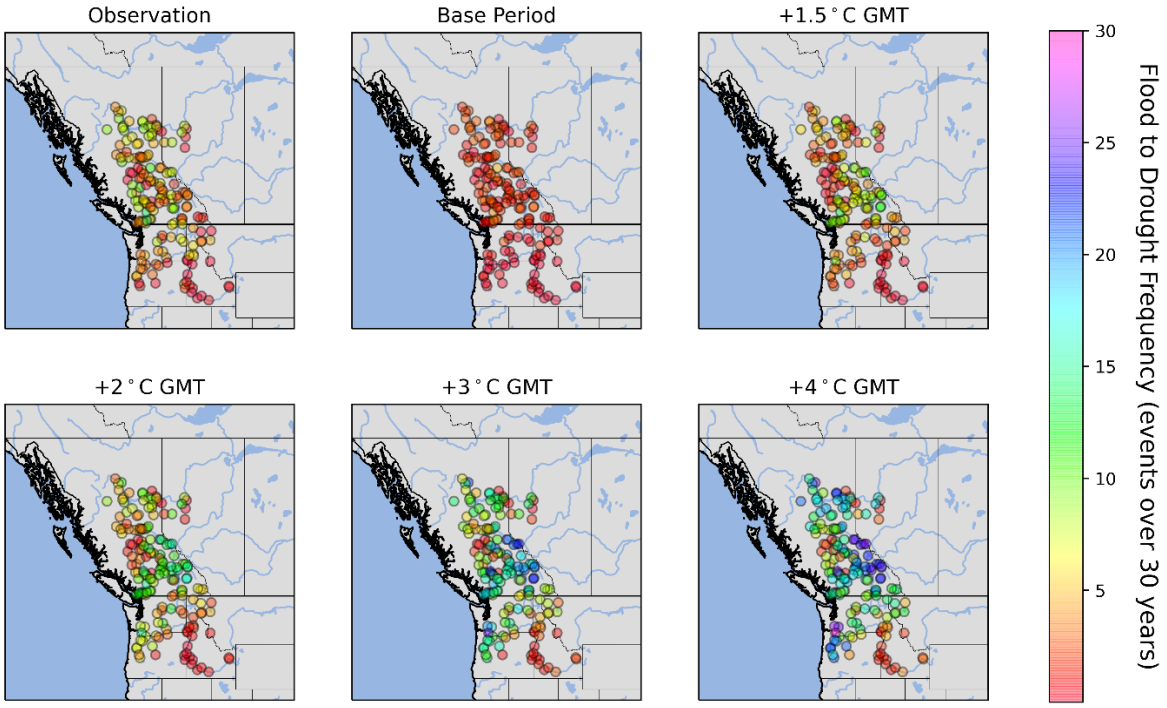

Figure 56 - Climatology of the frequency of the flood-to-drought CHEs. The maps show the ensemble mean at each hydrometric gauge.

- 4.1.2.2 Duration and Transition Time of Compound Hydrologic Events

The climatology of the durations of floods and droughts of the two CHE cases (flood-to-drought and drought-to-flood) as well as their transition times are illustrated in Figure 57. For each model-RCP pair in our multi-model ensemble, the duration of the flood and drought as well as transition time of CHEs are calculated at every warming period. Then the ensemble climatology

for each warming level is calculated by taking the mean of these durations across every member at a given warming period. The multi-model ensemble mean suggests that in the Columbia basin, the duration of drought in both flood-to-drought and drought-to-flood CHEs are projected the increase as the global warming level increases (Figure 57). On the hand, some changes to the durations of floods and droughts in CHEs are projected when comparing warming levels and the base period. However, these changes have contrasting directions when comparing the CHE types (flood-to-drought and drought-to-flood) (Figure 57). For instance, future projections of the multi-model ensemble mean suggest the duration of flood in drought-to-flood events are decreasing, which could potentially increase the risk of flash flooding after droughts. On the other hand, the floods of flood-to-drought CHEs are projected to have longer durations than the base period at higher levels of the global warming (Figure 57).

The transition time of CHEs of different types, also shows contrasting patterns of changes for future projections when comparing the drought-to-flood and flood-to-drought CHEs at different warming levels. Overall, the transition time of drought-to-flood/flood-to-drought events are projected to increase/decrease at all three basins of the study area when comparing future projections to that of the base period. Across the basins, the drought-to-flood CHEs occur more swiftly in Peace basin at almost all warming levels. These CHEs have the average transition time of two months in the base period and almost over three months at the highest warming level. On the other hand, flood-to-drought CHEs are expected to occur more swiftly. This is inferred from the decreasing pattern of the transition times of such CHEs, as the global warming level increases.

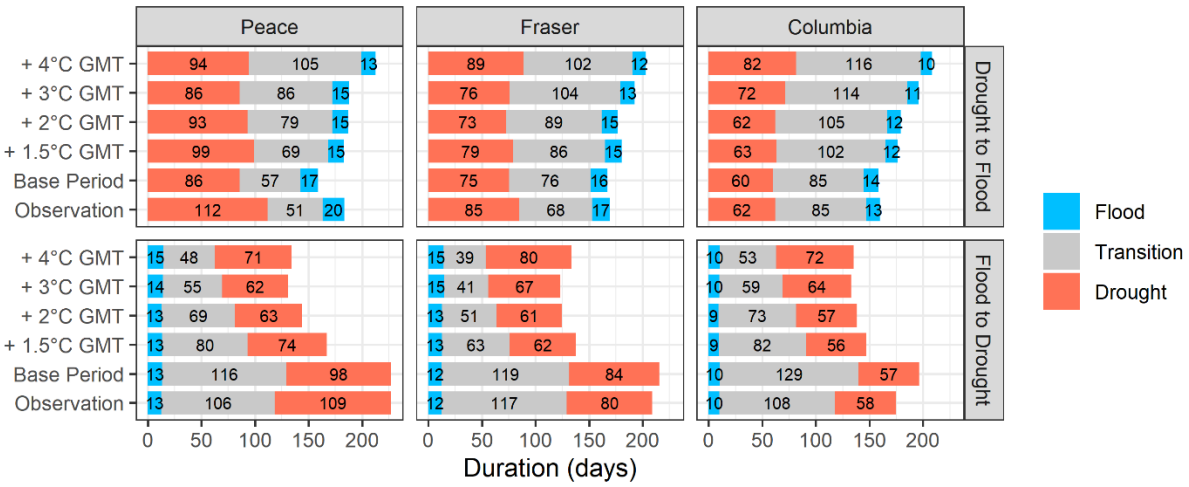

Figure 57 - Climatology of flood and drought durations, and transition time of CHEs. The bars represent the ensemble mean of durations. The numbers report the length of flood and drought durations, and transition time of the CHEs.

The transition times of the drought-to-flood CHEs at different warming levels for each hydrometric gauge are presented at in the maps of Figure 58. The maps in Figure 58 represent the multi-model ensemble mean. Although the transition time of drought-to-flood CHEs are almost 3 months on average in the base period, many gauges over Peace and northern Fraser basins are prone to abrupt transitions (transition time shorter than a month). However, this pattern is expected to change under climate change. Future projections indicate that transition time of drought-to-flood CHEs at these locations as well as in other parts of the study area are expected to increase (Figure 58), with the exception of a few locations north of the Vancouver area. When comparing the global warming levels to the base period, the transition time of the CHEs is projected to increase over southeast of the Columbia basin and southeast of the Fraser basin (Figure 58).

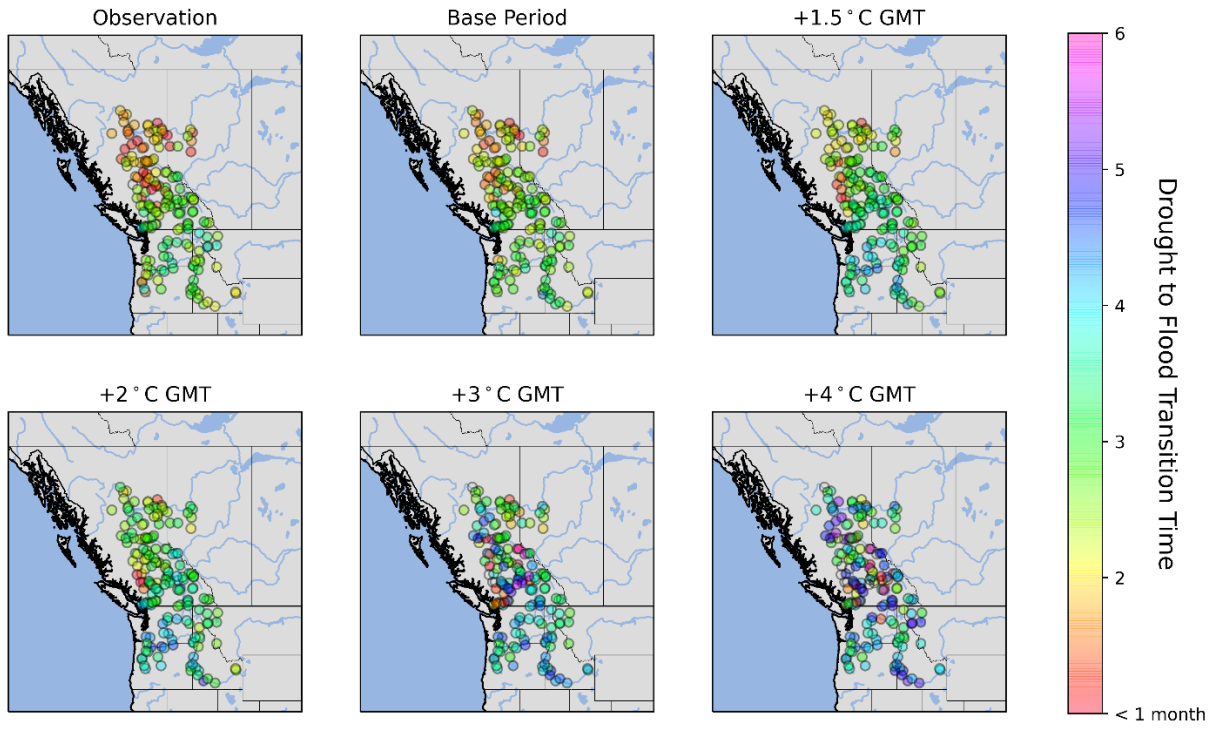

Figure 58 - Climatology of transition times of drought-to-flood CHEs. The maps represent the multi-model ensemble mean of transition time of CHEs (reported in months) at each hydrometric gauge.

The transition times of the flood-to-drought CHEs at each hydrometric gauge at different warming levels are presented in the maps of Figure 59. While the results indicate that in base period, floods and droughts are temporally compounded with lags ranging from 3 to 6 months, the future projections suggest that failure to limit the global warming could lead to more rapid transitions of floods to droughts across the entire study area (Figure 59). Although at lower levels of global warming, gauges in the Fraser basin are projected to experience abrupt flood to drought events more often, this pattern is expected to expand in Peace basin as well if the global warming reaches the +4°C GMT level (Figure 59). On the other hand, except for the gauges in southeastern Columbia basin, other areas in this basin experience flood to drought events that

successively occur within two to three months (Figure 59). A comparison between Figures 58 and 59 reveals that although infrequent, the flood-to-drought CHEs for the gauges in southeastern Columbia are projected to be abrupt at high warming levels (+3 and +4°C GMT).

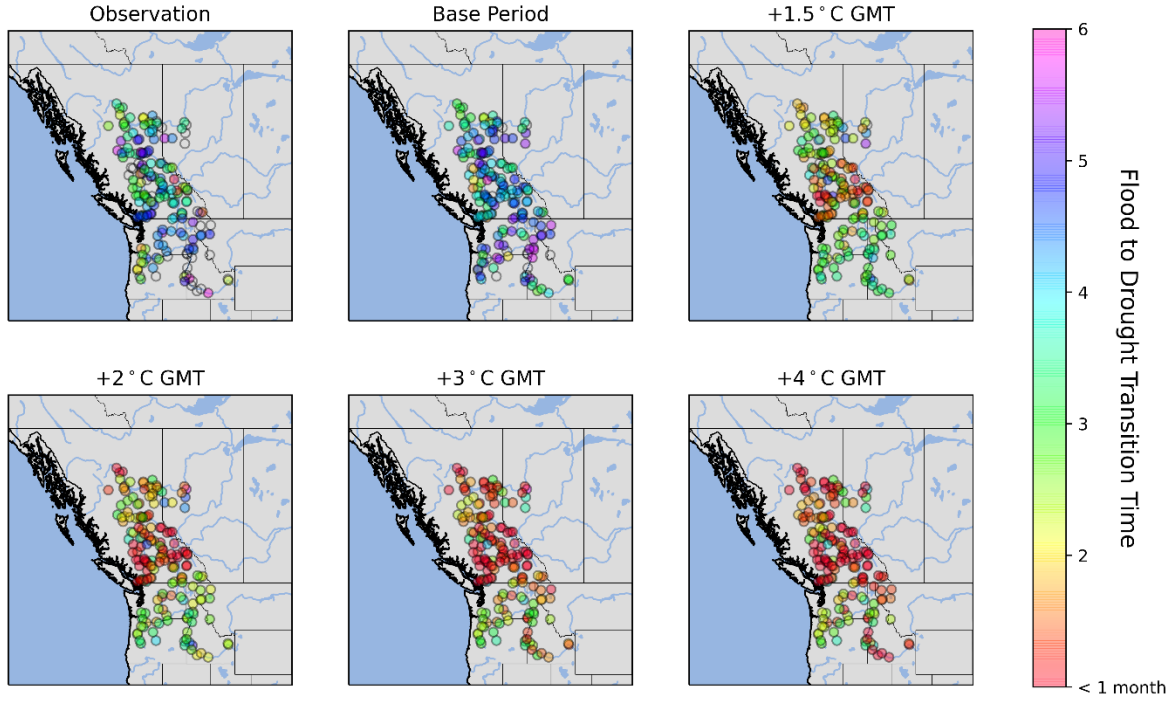

Figure 59 - Climatology of transition time of flood-to-drought CHEs. The maps represent the multi-model ensemble mean of transition time of CHEs (reported in months) at each hydrometric gauge.

- 4.1.2.3. Fraction of Compound Hydrologic Events with Different Transition Times

To illustrate how often CHEs with different transition times occur, the results of the fraction of CHEs having transition time of less than 3 months (FTr3), and fraction of CHEs having abrupt transition (FAbTr) are represented in Figure 60. On average, abrupt drought-to-flood CHEs are rare (also shown in Figure 60, frequency of abrupt hydrological compound events). Except in Columbia, such abrupt CHEs constitute less than 25% of the total drought-to-flood CHEs under

all warming scenarios (Figure 60). Amongst all, the Columbia basin shows the largest spatial variations at all warming levels (see the CI). Moreover, the upper limit of the CI (Figure 60) indicates that there are some locations in the Columbia basin where all the compound drought-to-flood events are projected to occur abruptly at the +4°C warming level. On the other hand, more of the drought-to-flood CHEs are projected to occur with longer transition times, as seen in the decreasing projected pattern of the mean FTr3 and its uncertainty range in all three basins under climate change (Figure 60). On the contrary, more of the flood-to-drought CHEs are projected to abruptly transition if the global warming is not limited (Figure 60).

An inter-basin comparison (Figure 60) reveals that except in the base period, more of the compound flood-to-drought CHEs in the Columbia basin occur abruptly compared to other two basins under all global warming scenarios. Even though the lower bound of the IC of the FAbTr of flood-to-drought CHEs indicates that there are some locations where abrupt transitions do not occur, the higher limit reveals that such abrupt transitions constitute all of the CHE occurrences in some other locations. When considering the FTr3 for flood-to-drought CHEs, more of the flood-to-drought CHEs are projected to occur within 3 months in the Columbia basin compared to the other two basins at all warming levels, except in the base period (Figure 60). Moreover, most of the flood-to-drought transitions tend to occur within 3months under climate change.

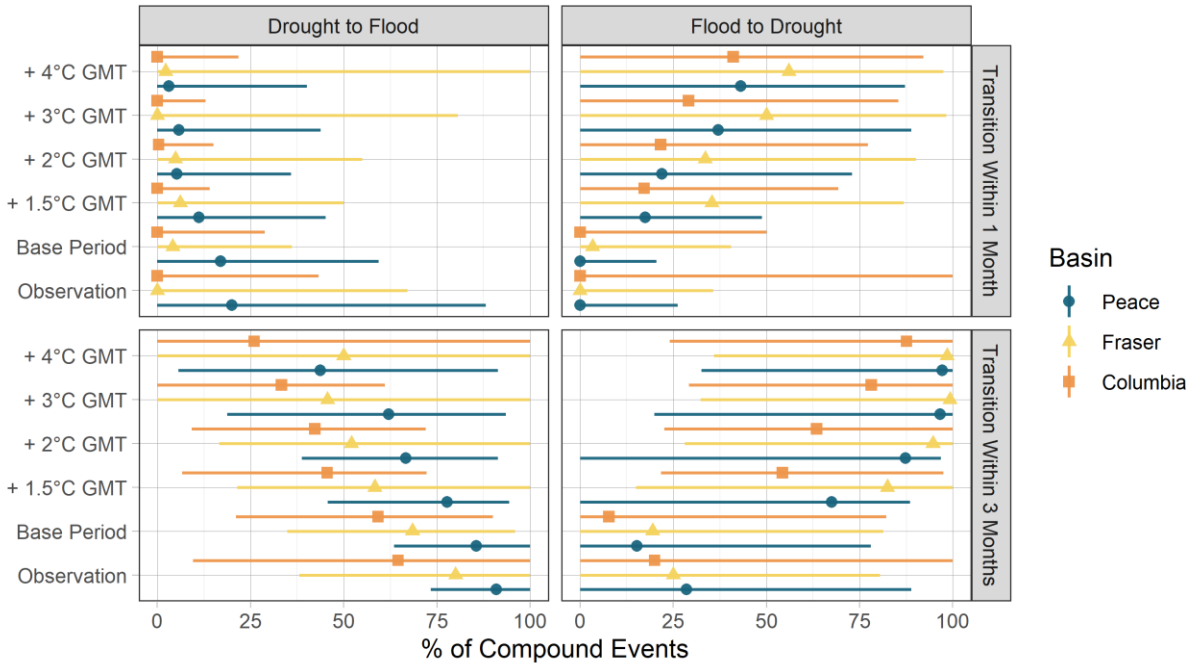

Figure 60 - The fraction of CHEs having transition time of less than 3 months (FTr3, the right panel), and fraction of CHEs having abrupt transition (FAbTr, the left panel). The colored bars show the spatial mean while the error bars represent the CI of the FTr3 and FAbTr.

- 4.1.2.4. Seasonality of Compound Hydrologic Events

The mean date of occurrence for the peak of drought and flood components of the two CHE types (flood-to-drought and drought-to-flood) at the Peace, Fraser, and Columbia basin are shown in Figures 61, 63, and 65, respectively. Results for the seasonality of abrupt CHEs for Peace, Fraser, and Columbia basins are presented in Figures 62, 64, and 66, respectively. The mean date of occurrence and the strength of seasonality have been calculated based on Equations 3.7 and 3.8, respectively.

Under climate change, the seasonality of the floods and droughts in CHEs (flood-to-drought and drought-to-flood) are projected to shift to earlier and later occurrences for floods and droughts,

respectively (Figures 61, 63, and 65). However, the timings of floods and droughts in flood-to-drought events are different than drought-to-flood events at lower levels of global warming (1.5 and 2°C) (Figures 61, 63, 65). In the base period, and 1.5 and 2°C warming periods, flood-to-drought events occur with spring freshets and summer droughts, whereas drought-to-floods are droughts in March and floods in April-May (Figures 61, 63, 65). However, if warming continues, the floods and droughts in CHEs would occur with floods in May-June and droughts in August-September (Figures 61, 63, 65).

On the contrary, the seasonality of abrupt flood-to-drought and drought-to-flood events are not expected to change in a warming world. Abrupt flood-to-droughts occur mostly between floods in April-June and droughts in August-September. On the other hand, abrupt drought-to-flood events occur with droughts in February-April and floods in April-June (Figures 62, 64, 66).

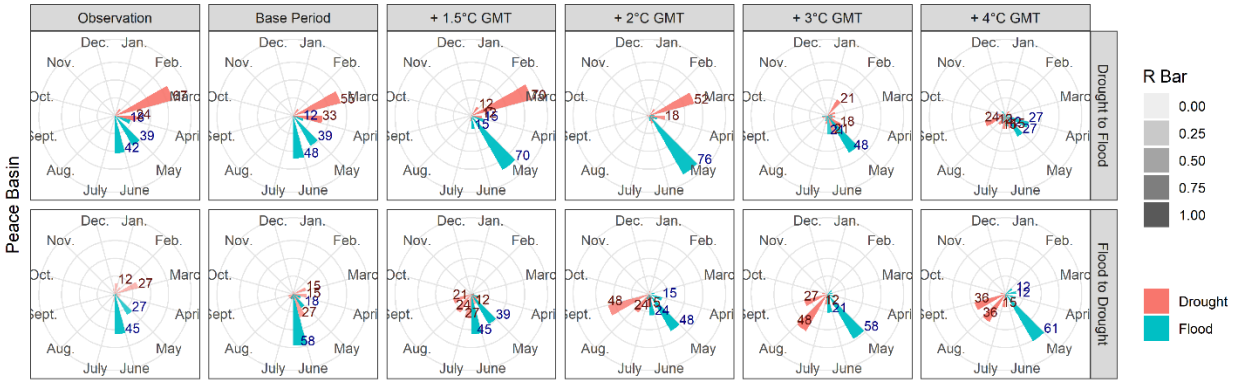

Figure 61 - Mean date of occurrence of the peak of the flood and drought of CHEs in the Peace basin. The numbers and the height of the bars show the percentage of stations at the basin with the same mean date of occurrence. The bars are colored based on being flood or drought in CHE and the transparency of bars indicates the strength of seasonality (r bar).

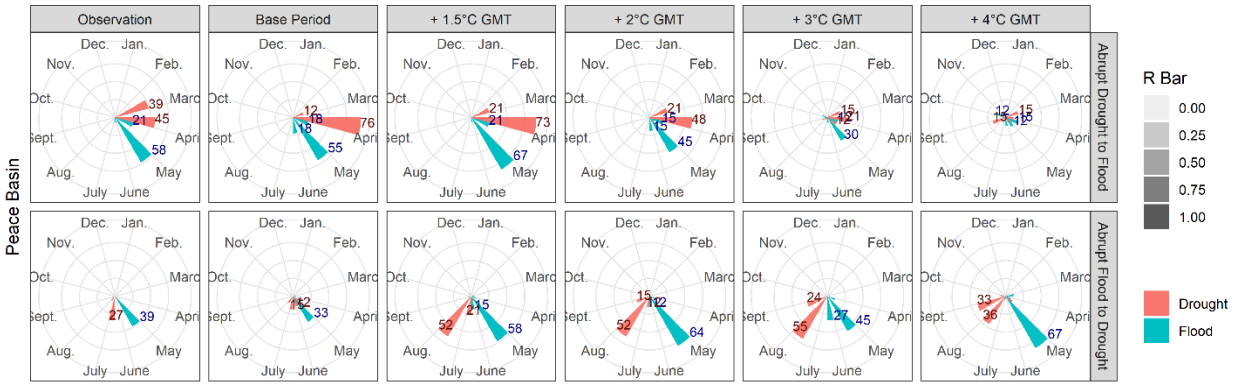

Figure 62 - Mean date of occurrence of the peak of the flood and drought of abrupt CHEs in the Peace basin. The numbers and the height of the bars show the percentage of stations at the basin with the same mean date of occurrence. The bars are colored based on being flood or drought in CHE and the transparency of bars indicates the strength of seasonality (r bar).

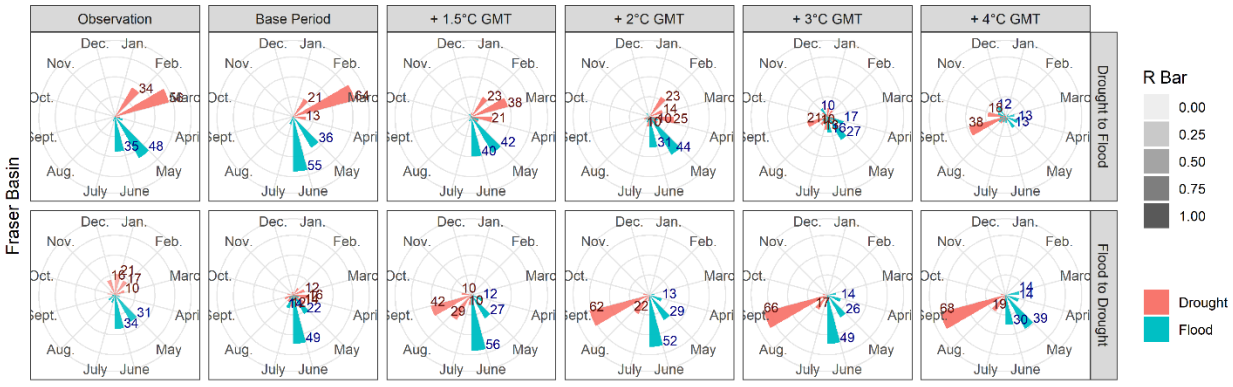

Figure 63 - Mean date of occurrence of the peak of the flood and drought of CHEs in the Fraser basin. The numbers and the height of the bars show the percentage of stations at the basin with the same mean date of occurrence. The bars are colored based on being flood or drought in CHE and the transparency of bars indicates the strength of seasonality (r bar).

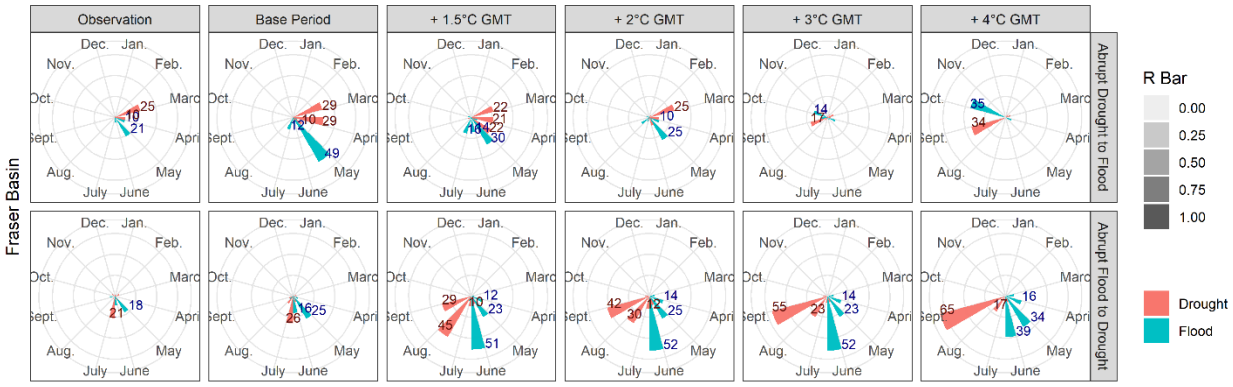

Figure 64 - Mean date of occurrence of the peak of the flood and drought of abrupt CHEs in the Fraser basin. The numbers and the height of the bars show the percentage of stations at the basin with the same mean date of occurrence. The bars are colored based on being flood or drought in CHE and the transparency of bars indicates the strength of seasonality (r bar).

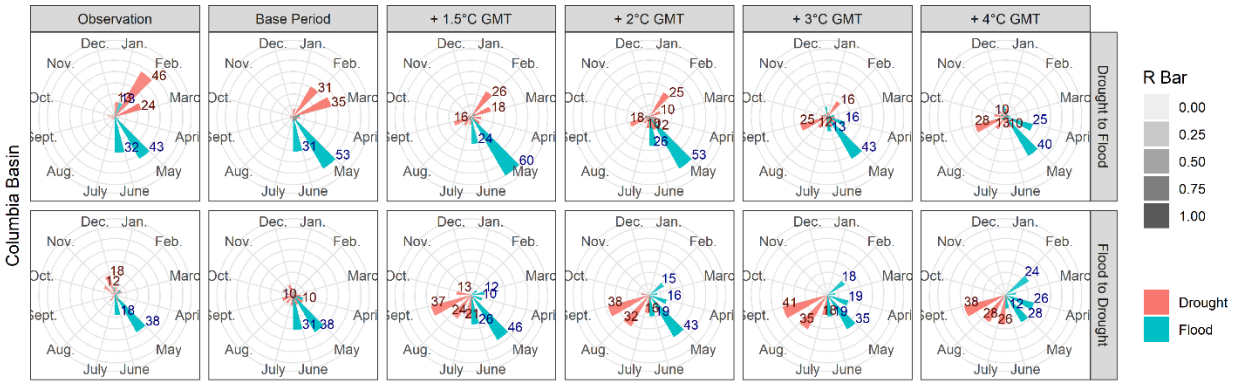

Figure 65 - Mean date of occurrence of the peak of the flood and drought of CHEs in the Columbia basin. The numbers and the height of the bars show the percentage of stations at the basin with the same mean date of occurrence. The bars are colored based on being flood or drought in CHE and the transparency of bars indicates the strength of seasonality (r bar).

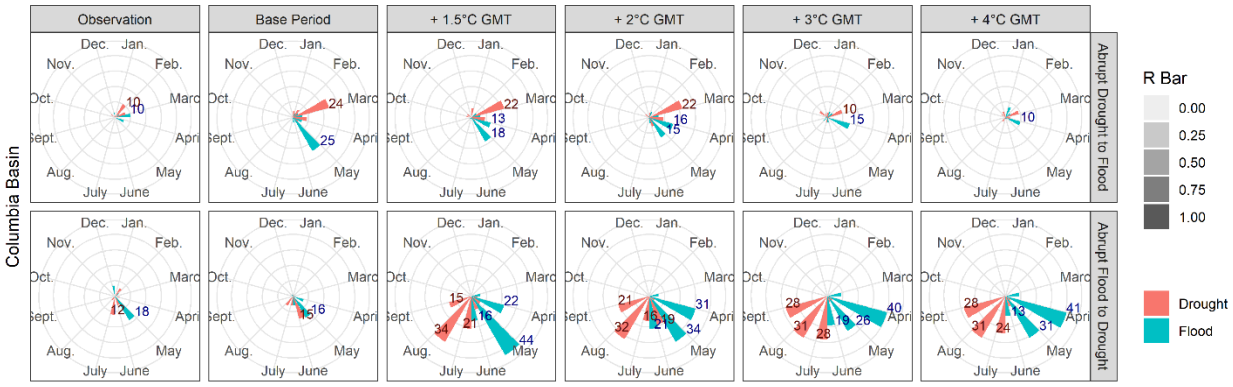

Figure 66 - Mean date of occurrence of the peak of the flood and drought of abrupt CHEs in the Columbia basin. The numbers and the height of the bars show the percentage of stations at the basin with the same mean date of occurrence. The bars are colored based on being flood or drought in CHE and the transparency of bars indicates the strength of seasonality (r bar).

- 4.1.2.5. Severity of Compound Hydrologic Events

The spatial variation of the empirical compound severity index (ECSI) based on the multi-model ensemble mean is presented in Figure 67 for the three basins of the study area at different warming levels (calculated based on Equation 3.9). The ECSI compares the CHEs based on the non exceedance probabilities of their flood volume and drought severity on their historical ECDF. Therefore, increasing values indicate that the probabilities of the flood and drought were lower in the base period (Figure 67), depending on the angle they make with the equality line (Figure 9 in the methods section).

When comparing the drought-to-flood and flood-to-drought CHEs, the ECSI values indicate that the flood-to-drought CHEs are more severe compared to drought-to-flood events. Moreover, it is projected that both types of CHEs will intensify under climate change, as illustrated by the shifts

in the spatial distribution of the ECSI values as well as increasing pattern of the ECSI boxplots (Figure 67). However, the climatology of ECSI indicates that there are some locations that experience the lowest severity of drought-to-flood CHEs (both flood and drought ranked in the first quartile) under climate change in the Peace basin. Likewise, some parts of the Fraser basin also experience transitions of less severe droughts to floods compared to other floods and droughts in the same location. In the base period, the ECSI values suggest that the drought-to-flood CHEs occur amongst the floods and droughts ranked to be in the third quartile (based on the ECWA range, Figure 68). However, the overall projected pattern of the drought-to-flood ECSI climatology indicate than in more than 75% of the locations, the drought-to-flood CHEs occur with their floods and drought ranked lower than the second quartile of all floods and droughts in that location. This is inferred from the ECSI values above 0.7 and the large value of the ECWA (Figures 67 and 68). Larger values of ECWA indicates that there is a bigger difference in the ranks of the flood and drought of drought-to-flood CHEs. Therefore, the future projections of ECSI for drought-to-flood indicates that while the droughts in these CHEs are becoming more severe when compared to other droughts in those locations, the floods that follow them are less severe than at least half of the local floods. On the other hand, the ECSI for the flood-to-drought CHEs suggest that the transitions occur between the events that are ranked higher than the flood and drought of the base period. Therefore, transitions from more severe floods to droughts compared to base period is projected in all three basins under climate change.

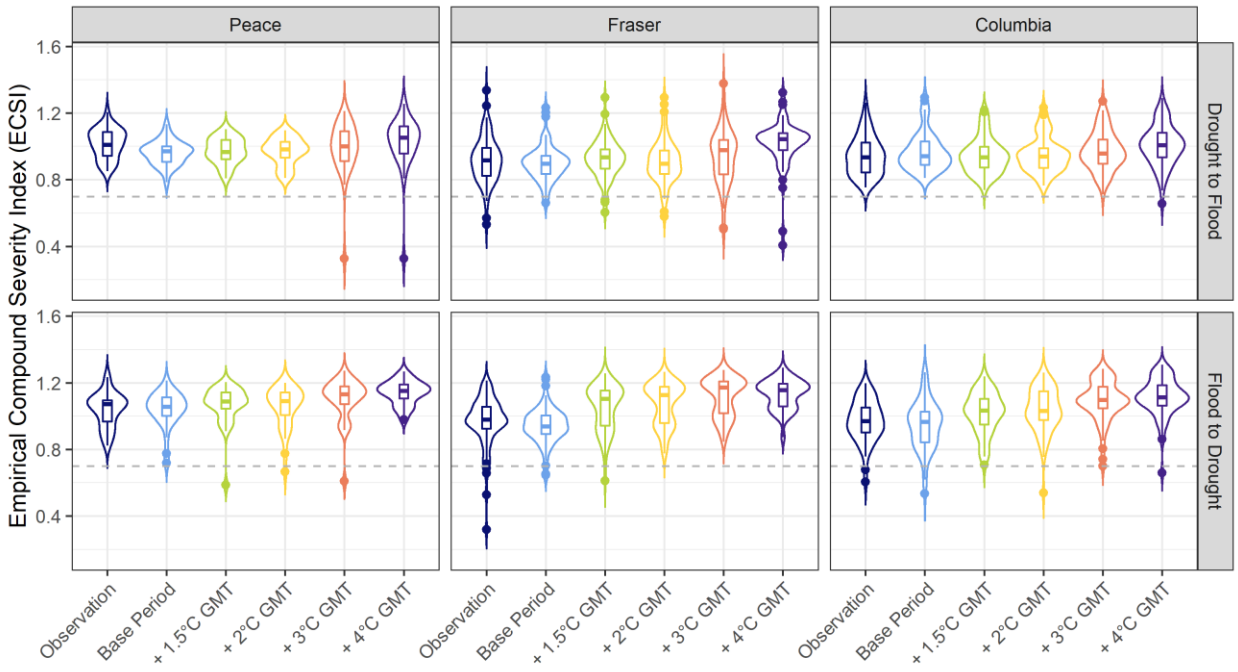

Figure 67 - Empirical Compound Severity Index (ECSI). The box and violin plots show the spatial distribution of the ECSI of each CHE type at different basins and various global warming level based on the multi-model ensemble mean.

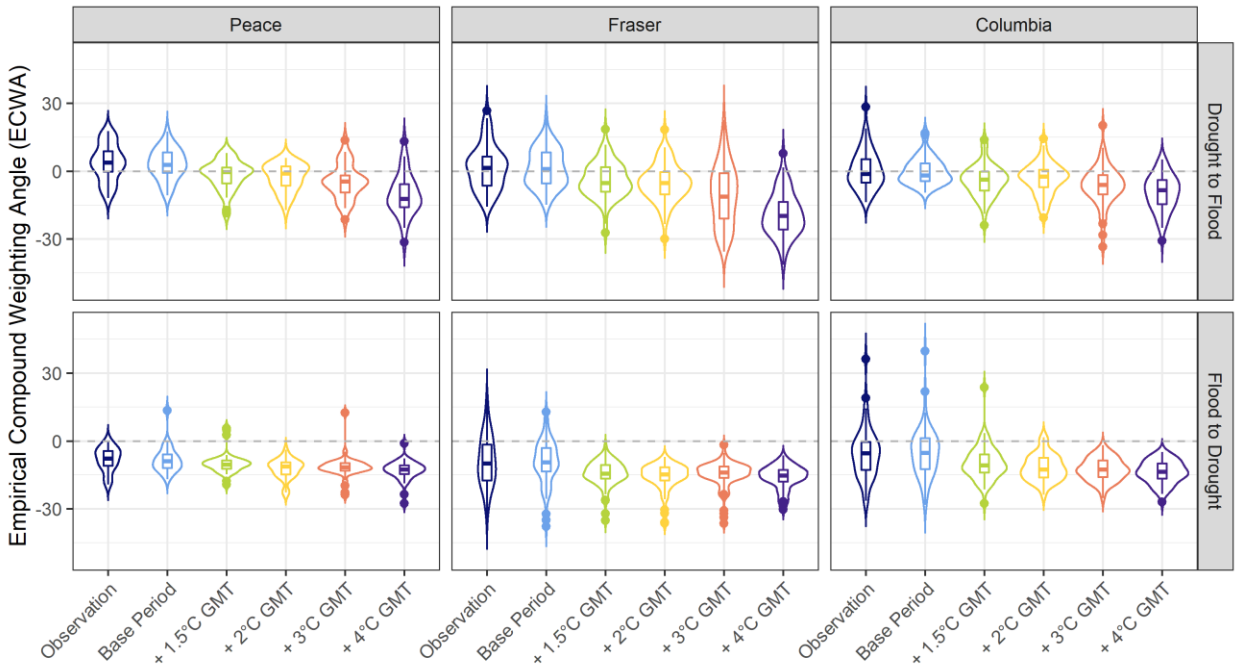

Figure 68 - Empirical Compound Weighting Angle (ECWA). The box and violin plots show the spatial distribution of the ECWA of each CHE type at different basins and various global warming level based on the multi-model ensemble mean.

4.2. Discussion

4.2.1. Compound Climatic Events

As shown in Figures 10 and 11, the frequency of CCEs at different timescales is projected to increase under climate change. The SPI1 and SPEI1 could represent how climatic conditions could propagate to affect short-term soil moisture conditions. Therefore, less than normal monthly precipitation or negative climatic water balance represented as dry spells can cause crop stress due to reduced short-term water availability. On the other hand, the higher-than-normal precipitation and positive climatic water balance can lead to increased soil moisture, and therefore potentially increase the flood risk due to reduced infiltration capacity. When

considering seasonal timescales (SPI3/SPEI3), the hydrologic impact of the CCEs would vary depending on the timing of the wet and dry spells. Dry spells in the cold season results in less than usual snowfall and reduced snowpack, which exerts stress to water resources in the subsequent seasons due to reduced streamflow and reservoir storage. On the other hand, warm season dry spells affect the long-term soil moisture conditions, that could reduce the crop yields (Rossato et al., 2017). Season-long wet spells in warm seasons could lead to increased water supply and boosts the chances of flooding. In addition, wetter than normal cold seasons lead to increased snowpack which could exacerbate the spring freshet due to more than normal snow accumulation. Furthermore, increasing frequency of long-term (SPI6/SPEI6) wet and dry spells could enhance the chances of hydrologic floods and droughts, respectively.

While the aforementioned consequences of wetter and drier than normal meteorological conditions are problematic and could exert serious economic and environmental costs, the transitions of these contrasting conditions (CCEs) can pose challenges for water-resources management. For instance, the flood of Brisbane in January 2011, the Australia's most expensive natural disaster to date which led to the evacuation of almost a million people, was caused not only by several days of intense rainfall, but also by the flood operation decisions at the Wivenhoe and Somerset Dams (Garcia et al., 2022). This flood event occurred at the end of the decade-long Millennium drought, during which the dam operators struggled to meet water supply objectives and flood control was back of mind. Garcia et al. (2022) suggest that this experience led to a cognitive bias which affected the decision-making of the operators during the 2011 flood. In this case, the operators' recent experience with drought may have prompted them to underweight the risk of extreme flooding and over-weight the risk of water supply deficit. When faced with complexity and uncertainty, decision-makers across all levels, from reservoir

operators to flood plain residents turn to heuristics to simplify decisions, which results in cognitive biases and errors in decision-making (Garcia et al. 2022).

Moreover, climate change can exacerbate the impacts of such biases. While cognitive biases are based on experience with historical conditions, the non-stationarity caused by climate change brings about unprecedented climatic situations. In addition, failure to detect, acknowledge, and manage such cognitive biases could create fragilities that can lead to catastrophic failures when extreme events occur. For instance, our multi-model ensemble projects change in the duration of the wet and dry spells of CCEs (presented in Figure 18 and 19). Considering and incorporating such insights about the changing future characteristics of extreme events in reservoir operations and strategic planning for disaster risk reduction could limit the cognitive biases brought about by heuristics. Moreover, our spatial projections (Figures 12 – 17 and Appendix 1 – 6) are of great value for reservoir operation in the identified hotspots such as Columbia basin (Figures 12 – 14) and the northwest North America (Figures 15 – 17).

Figures 18 – 25 and Appendix 7 – 12 indicate that the transition time of the CCEs at 1-, 3-, and 6-months timescales are projected to decrease under climate change. Coupled with the projected increase of the frequency of CCEs (Figures 10 – 17), the variability of contrasting extreme precipitation alterations is projected to increase under climate change. The increased variability of the monthly (SPI1/SPEI1) CCEs (Figures 12, and 15, and Appendix 1 and 4), reduces the predictability of these transitions that could challenge decision making for water-resources managers. Moreover, increased variability of transitions between wet and dry spells accumulated over 3-months (Figures 13 and 16, and Appendix 2 and 5) can put pressure on reservoir operations, decreasing the reliability of water supply, flood control and other reservoir benefits (Garcia et al., 2022). Due to the persistence of wet and dry spells on longer timescale

(SPI6/SPEI6), such abnormal (wet or dry) conditions can alter long-term patterns of water-resources such as groundwater levels or streamflow (Figures 14 and 17 and Appendix 3 and 6).

Moreover, CHEs are projected to occur more swiftly under climate change due to decreases in their transition time. Therefore, this decrease in the timespan over which actions to prepare for and cope with hazards must be taken reduces the recovery time and increase the failure probability of infrastructure and water demands (Figures18 – 25 and Appendix 7 – 12). Furthermore, projections indicate that the transition time of CCEs decrease by a month over the entire study under climate change (Figure 18 and 19).

When considering Disaster Risk Reduction strategies, it is important to note that the risk of meteorological hazards as well as their concurrent occurrences is projected to increase under climate change, as inferred from the projected growing area experiencing such hazards on an annual basis (Figure 28 and 29). Although projections based on SPI indicate that the study area is more prone to wet spells every year (Figure 28), SPEI suggests that the area is more prone to dry spells (Figure 29). Furthermore, the annual area experiencing wet and dry spells as well as their concurrent occurrence is projected to increase in a warming world (Figures 28 and 29). Several other studies have previously reported this increasing wetness of the atmosphere based on the observations and future projections under climate change in western North America. For instance, the historical observations have shown increasing trends of the area alleviated from drought by extreme precipitation (Maxwell et al., 2013). Moreover, projections of the large ensemble used by Hagos et al. (2016) indicates more frequent and intensified precipitation events in the future over western North America, with more atmospheric rivers projected to hit the area. The attribution study of Hagos et al. (2016) reveals only 8% of the increase in the landfalling

atmospheric rivers and extreme precipitation days could be due to internal climate variability, which highlights the role of anthropogenic factors.

Our future projections show increasing risk of concurrent dry-wet conditions in the study area under climate change. This increase is mostly due to the wetting pattern of the atmospheric conditions projected by SPI (Figure 28), whereas increases of the concurrent wet-dry spells based on SPEI is due to the projected grow in the area affected by dry spells in a warmer world (Figure 29). Therefore, climate change adaptation strategies must pay special attention to mitigation measures targeting both floods and droughts.

Furthermore, our projections show the seasonality of dry and wet conditions as well as their concurrency would change under climate change (Figures 26 and 27), which have implications for a multitude of water-resources dependant sectors. The wet and dry spells captured by SPEI occur during the first (January – June) and second half (July – December) of year, respectively (Figure 27). Moreover, SPEI indicates that the concurrency of wet-dry spells could affect almost half of the study area in January and July (Figure 27). On the other hand, an overall shift in the seasonality of the wet and dry conditions are projected under climate change (SPI6), with more area projected to undergo wetter and drier conditions in the cold and warm seasons, respectively (Figure 26). While our ensemble indicates increasing area affected by monthly wet spells (SPI1) in April, May, June (Figure 26), the precipitation type in this period is mostly rain and if fell on the snow-covered ground, the chance of rain-on-snow (ROS) increases like the 2013 ROS flood in the Canadian Rockies. Likewise, the seasonal precipitation accumulations are projected to affect a larger area in the three months ending in April (Figure 26) which calls for preparing for ROS occurrence. The projected increasing area affected by dry spells in August, and September (on 3- and 6-months timescales) could put plants under stress during the growing season (May,

June, July and June, July, August) (Figure 26), and could bring about rivalry between the urban, agricultural, and industrial consumers. The maximum monthly area under concurrent wet-dry spells is projected for August (Figure 25). On the other hand, the transition seasons (spring and fall) are the most prone for wet and dry concurrency (SPI3) (Figure 25). Therefore, it is vital for water resources managers to be prepared for both hydrologic hazards (i.e., floods and droughts) during these periods to minimize the financial costs of such natural hazards.

The future CCEs are projected have larger magnitudes and intensify under climate change (Figures 30 – 41). However, our findings suggest that the magnitude of change in the intensity is not similar for all accumulation periods. For instance, while the largest variability is projected for shorter accumulation periods (Figure 31, and 37) (also projected by Hartmann et al., 2013), the most intense transitions are also projected to occur for this time scale as seen in the increase of the area experiencing severely dry and extremely wet CCEs. Such increasing precipitation variabilities in sub seasonal timescales have important implications for the predictability of weather and climate extreme (Dong et al., 2018). In addition, larger areas in the study area are projected to experience season-long wet-dry transitions with less variability (lower uncertainty) compared to monthly accumulations under climate change (Figures 33, and 38). Our findings of transitions between more intense wet and dry conditions are inline with the with projections of Dong et al. (2018) that shows intensified swing between wet and dry extremes in the sub seasonal timescales. The increased dryness has been previously reported by the projections of Wartenburger et al. (2017) for many regions globally. Furthermore, the intensification of precipitation under climate change has been shown by Hartmann et al., 2013. Moreover, this intensification of precipitation has been attributed to the anthropogenic factors by Bindoff et al. (2013).

We show that under climate change, CCEs on monthly timescales have the highest magnitude compared to other areas in western Columbia and eastern Fraser basins (Figures 42 and 43). Our future spatial projections suggest that transitions between more severe wet and dry precipitation accumulated over 3 months would occur in northern Fraser and southern Peace and entire Columbia basins under climate change (Figures 44 and 45). Moreover, more severe 6-months of wet and dry conditions are expected to swing over south-central B.C. (northern Vancouver area) if warming is not limited (Figures 46 and 47).

4.2.2. Compound Hydrologic Events

Hydrologic floods and droughts are propagation of extreme meteorological events with significant environmental, agricultural, economic, and social consequences such as water restrictions for irrigation, agricultural crop failures, power generation reductions, and recreation activity limitations (Li et al., 2017). It is evident that the frequency and number of hydrologic hazards (i.e., floods and droughts) has been on a rise (Li et al., 2017; Adikari and Yoshitani, 2009). Moreover, climate change is projected to alter the frequency and magnitude of runoff, thereby threatening the global water resources as well as the health of ecosystem and humans (Omer et al., 2016). Previously, He and Sheffield (2020) conducted a global study on the historical drought and flood swings (referred to as pluvial-drought seesaw) and identified western North America as a hotspot for lagged compound flood-drought events as inferred by increases in the frequency of such compound event occurrences over the past seven decades.

Our findings assert the increasing frequency of hydrologic flood-to-drought CHEs in the study area under climate change (Figures 54 and 56). The projected increases in the frequency of flood-to-drought CHEs are inline with the future projections of the compound climatic events

(Figures 10 and 11). However, the future projections of the flood-to-drought and drought-to-flood CHEs show contrasting results (Figures 54, 55, and 56). While the former is expected to occur more frequently (Figure 56), the latter instances are is expected to decrease in a warming world (Figure 55). Moreover, more frequent abrupt flood to drought swings (transition time less than 30 days) are projected over the study area if the global warming is not limited (Figure 54). Such abrupt swings between contrasting hydrological extremes could cause huge economic losses and serious damage to agriculture and the environment (Li et al, 2017). Explaining these projected patterns of transitions from a physical standpoint is difficult. The mechanisms causing individual hydrological extreme are complex, let alone their compounded occurrences. Therefore, understanding lagged compound flood-drought events are difficult and likely case dependant, and potentially can be influenced by not only climate variability, but also climate change (He and Sheffield, 2020). An explanation for the projected increase in the frequency of the flood-to-drought events could be due to the projected increases in the frequency of droughts and floods. Previous studies have shown that the increased evapotranspiration induced by rising global temperature could lead to more frequent drought occurrences. At the same time, flood risk is projected to increase as more extreme rainfall events are projected due to the increased water holding capacity of the atmosphere under global warming. On top of both, warming can also change the global climate variability such as El Nino/La Nina (Yu et al., 2017), or Arctic sea ice (Francis et al., 2017), which can bring more year-to-year variability or persistence to weather patterns and influence regional precipitation and temperature anomalies (He, 2019). Human interventions can also further exacerbate the drought risk (e.g., due to increased consumption for irrigation and groundwater pumping) (Het et al., 2017) and flood risk (e.g., due to land use

changes like urbanization or agricultural practices) (Yang et al., 2013; Villarini and Strong, 2014).

In addition to projected more frequent occurrences of flood-to-drought CHEs, our findings indicate their transition time is projected to decrease under climate change, leading to increased variability of transitions between hydrologic extremes in the future (Figures 57, 58, and 59). In addition, more of the compound flood-to-drought swings are projected to occur abruptly (within 1 month, almost 50% of the events on average under the worst-case warming scenario across our three basins) or within 3 months (more than 75% of the events on average under the worst-case warming scenario in our study area) (Figure 60), which reduces the recovery time for water resources and preparation time for decision makers and emergency response teams (Parry, 2019).

As mentioned, detailed analysis on individual flood-to-drought or drought-to-flood CHE occurrences are required to identify the favourable synoptic conditions for such lagged compound events to occur. However, previously Maxwell et al. (2013) have investigated the role of the tropical cyclones on the abrupt drought-flood alterations in the southern United States. Their findings indicate that historically, tropical cyclones have frequently caused abrupt drought-to-flood occurrences over the past 117 years. In another study, Maxwell et al. (2017) have investigated how three different storm types of "Frontal, Tropical, and Air mass" can cause drought-flood abrupt alterations in the southern U.S. during the 1979–2013 warm season (April–November). Their findings indicate that "Frontal storms" have caused rapid alterations more frequently. However, the occurrences of "Frontal storms" significantly decreased and were negatively correlated to increases in Northern Hemisphere air temperatures, with continuing declines their projected frequency and relative contributions to drought-flood abrupt swings. Therefore, future transitions between hydrological extremes may be caused by other storm types

such as air mass atmospheric rivers, which historically have occasionally caused abrupt transitions in the southern U.S. (Maxwell et al., 2017). Furthermore, 60-74% of drought-flood transitions in the Pacific Northwest U.S. (a part of our study area) have been caused by atmospheric rives (He, 2019; Dettinger, 2013). Our study area is prone to atmospheric rivers (AR). Thus, investigating whether AR could lead to compound flood-drought events in the NWNA would be of particular value.

Although droughts, floods, and their transitions (CHEs) are inevitable, fatalities, infrastructure failures and economic losses are not (He and Sheffield, 2020). Moreover, reliable streamflow is of particular importance for water users and aquatic ecosystems, which makes adequate water supplies at certain times of the year necessary. Therefore, streamflow timing is an important indicator for freshwater availability (Bonsal et al., 2019). Thus, understanding when to look for CHEs is invaluable for policymakers and local stakeholders prone to risk, which in turn can lead to development of more effective water and agricultural management policies and implementation of more robust mitigation measures and plans. Since the timing of streamflow events is significantly influenced by climate (Bonsal et al., 2019), in this study we use a multi-model ensemble of high-resolution hydrologic projections to present the seasonality and timing of the flood and droughts that temporally swing at different global warming levels (Figures 61 – 66). Our findings indicate that the timing of floods and droughts is CHEs are projected to shift to earlier and later occurrences under climate change, respectively. In line with previous studies on the timing of the peak streamflow, our projections assert a shift in the seasonality of the flood and drought of CHEs. A shift into earlier flood occurrence in spring has been attributed to the observed trend of smaller mountain snowpacks and earlier melt onset in British Columbia (Kang et al., 2016; DeBeer et al., 2016). Moreover, the trends in the observations of annual winter and

summer low-flows indicate a tendency to shift the timing towards later dates as shown by Khaliq et al. (2008).

For the first time, we have tried to quantify the intensity of the CHEs. To this end, we have used streamflow as an indicator and quantified the severity of both floods and droughts by the water volume (common characteristic in both flood and drought). This has The ECSI is designed to compare magnitude of the CHEs to the individual event occurrences at the same location. To this end, the ECDF of floods and droughts are used to consistently compare the CHEs with individual occurrences. Since streamflow is the input for calculating this index, the location specific nature of ECSI allows us to take into account the physical characteristics of the location such topography, soil type, vegetation coverage, and land use, that can directly influence how the terrain hydrologically translates the precipitation to streamflow. Moreover, to account for the non-stationarity of the streamflow timeseries induced by climate change, we use the base period ECDF of floods and droughts volume to show how the future CHEs would rank compared to the historical events. However, the two faceted design of ECSI allows the users to compare the severity of CHEs with other floods and droughts in the same warming period. Since the timeseries is assumed to be stationary over each of 30-years warming periods, one can simply use the ECDF of the floods and droughts of the desired warming period and simply compare the magnitude of floods and droughts that temporally swing with other hydrological extremes in the same period. To show this feature of the ECSI, we have shown the severity of flood-to-drought and drought-to-flood CHEs at each warming period by mapping the events' volumes to the ECDF of floods and droughts at each warming level (Appendix 43, 44).

Chapter 5: Conclusions and Future Recommendations

In the present study, we characterise lagged compound hydroclimatic dry and wet spells and investigate how these compound extremes alter spatiotemporally in a changing climate. We first assess how hydroclimatic wet and dry periods, as the climatological drivers of hydrological floods and droughts, transition (accumulated at 1, 3, and 6-months timescales) at the global warming levels of 1.5°C – 4°C. To this end, we use the Standardized Precipitation Index (SPI) and Standardised Precipitation Evapotranspiration Index (SPEI) calculated by an ensemble of high-resolution precipitation simulations of 6 downscaled and statistically bias corrected (via Bias Correction/Constructed Analogues with de-trended Quantile mapping reordering downscaling technique, BCCAQv2) Global Climate Models (GCMs), each coupled with the medium and high emission scenarios (RCP4.5 and 8.5). Gamma and Log-logistic distributions are used to calculate the SPI and SPEI, respectively. To classify wet and dry conditions, +1 and -1 thresholds are used, respectively. A compound climatic event (CCE) is defined as a wet/dry period of any length (at least a month) that is followed by a dry/wet period of any length (at least a month) in a timespan less than 6 months. The transition time is defined as the time span from the end of first event (dry/wet) to the start of the second event (wet/dry). Our findings indicate the CCEs are projected to occur more frequently under global warming. Moreover, CCEs are expected to occur more swiftly if the global warming is not limited. CCEs are also projected to intensify in a changing climate.

Since the hydrological floods and droughts are the propagation of wet and dry hydroclimatic conditions, and the impacts of such hydrological extreme events are felt on a locale scale, we further assess how hydrological floods and droughts swing in the rivers of the Northwest North America (NWNA). Given that the hydrologic response of the land depends on a multitude of

factors including the topography and land use amongst others, we use high resolution streamflow simulations of the Variable Infiltration Capacity (VIC) hydrologic model forced with our ensemble of downscaled and bias corrected GCMs. To characterize and assess the compound hydrologic floods and droughts, we first extract floods and droughts in a consistent manner using the theory of runs. The 15^{th} and 95^{th} quantiles of the daily streamflow data are used to find droughts and floods, respectively. The compound hydrologic events (CHEs) are defined as floods and droughts that temporally follow each other within 6 months. The transition time is defined as the timespan between the finish of the former extreme event and the onset of the latter extreme event. For the first time, we propose an empirical index, Empirical Compound Severity Index (ECSI), to quantify the changes of severity of the CHEs. Our findings indicate that the study area is more prone to flood-to-drought CHEs, with increasing frequency under climate change. Moreover, the transition time of flood-to-drought CHEs are projected to decrease in a changing climate. We also show when to expect the CHE occurrences at different warming levels, as well as the changes of their seasonality. Our proposed index suggests that flood-to-drought CHEs are more severe than drought-to-flood CHEs. Furthermore, the projected future ECSI values indicate that the severity of both CHE types will increase in a warming world.

Although our projections of the future characteristics of the compound hydroclimatic events (CHCEs) as well the identified hotspots provide invaluable insights for a wide range of decision makers including the dam reservoir operators and water resources managers, there remains several unanswered questions. Therefore, future studies are required to extend the analyses and address some of the limitations in this work:

- The climatic and hydrologic simulations that we use are based on the 5^{th} phase of the Coupled Model Intercomparison Project (CMIP5). Using climatic and hydrologic

simulations of the CMIP6 is recommended to assess the future projections of the CHCEs with the newer generation of climate models.

- Explaining the processes leading to CHCE occurrences from a physical standpoint is difficult. We recommend conducting a detailed analysis on a range of recorded instances of such compound extremes to identify the favourable synoptic conditions for these events.
- Since the global atmospheric circulation controls the average pattern of rainfall, temperature, and associated evapotranspiration in different climate zones, investigating possible teleconnections of the CHCEs with the large-scale modes of climate variability that impact the study area could improve the predictability of these compound extreme events.
- Finally, understanding to what extent the anthropogenic climate change is contributing to the projected changes of CHCEs and the role of internal climate variability in the projected patterns can proved invaluable insights for policy makers. Therefore, conducting an attribution study using a variety of indicators is recommended.

It is hoped that the insights of this study and the recommendations provided here pave the way for better understanding the unprecedented conditions of the future climate and to better adapt to the new climatic norms projected for a changing climate.

Appendix

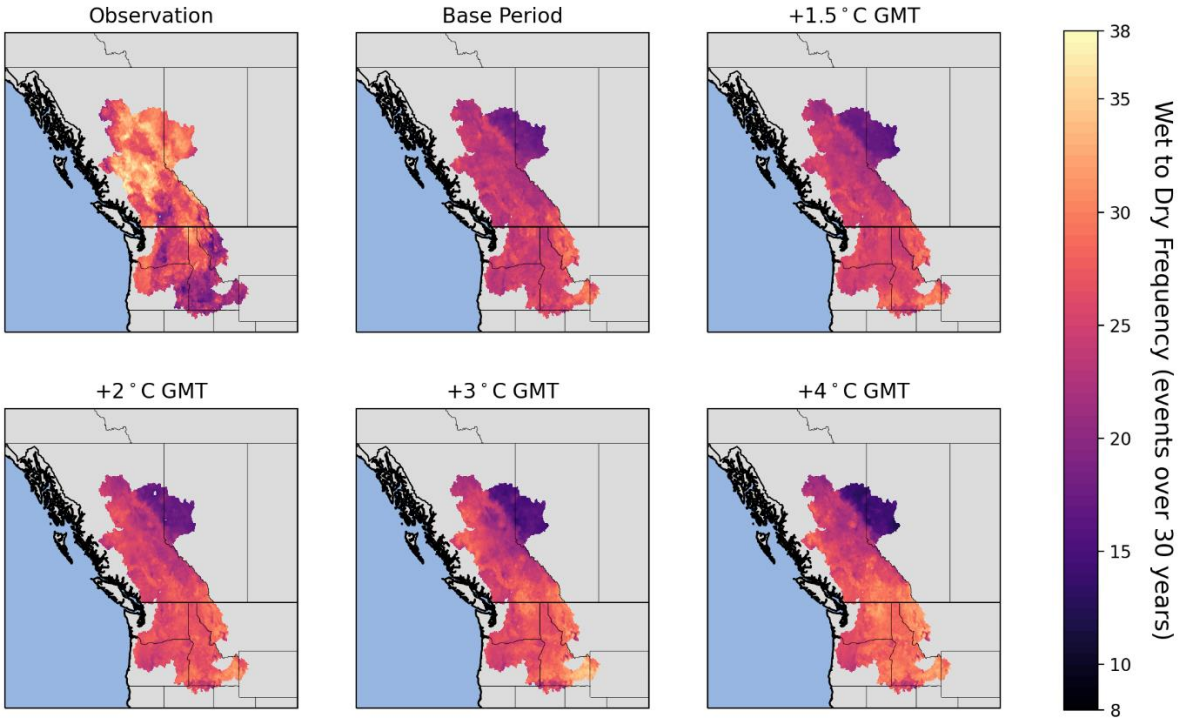

Appendix 1 - Climatology of frequency of wet-to-dry CCEs (SPI1). Maps show the frequency of CCEs over each warming period (30 years).

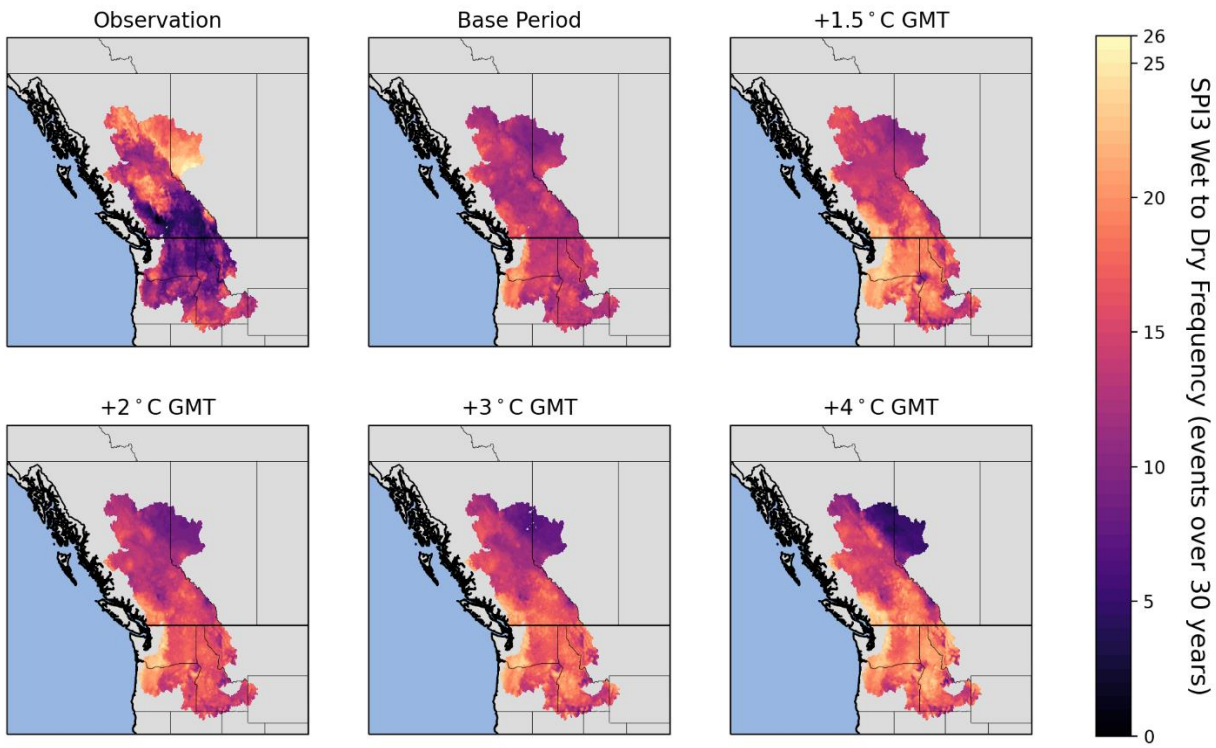

Appendix 2 - Climatology of frequency of wet-to-dry CCEs (SPI3). Maps show the frequency of CCEs over each warming period (30 years).

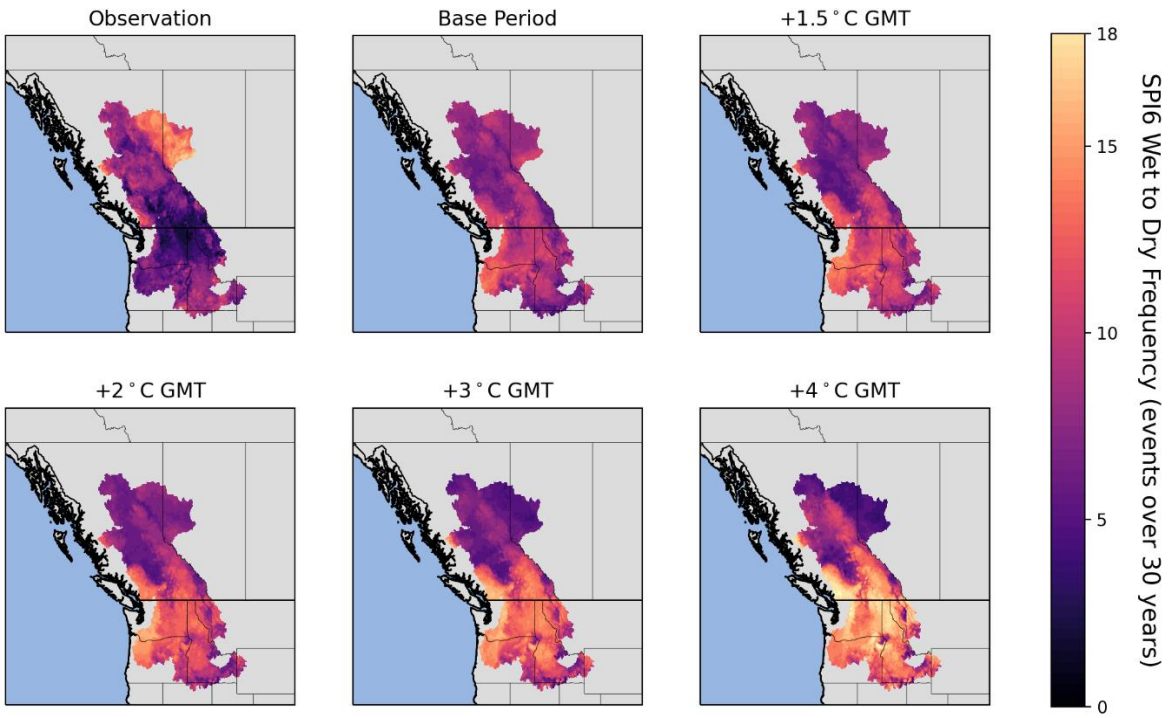

Appendix 3 - Climatology of frequency of wet-to-dry CCEs (SPI6). Maps show the frequency of CCEs over each warming period (30 years).

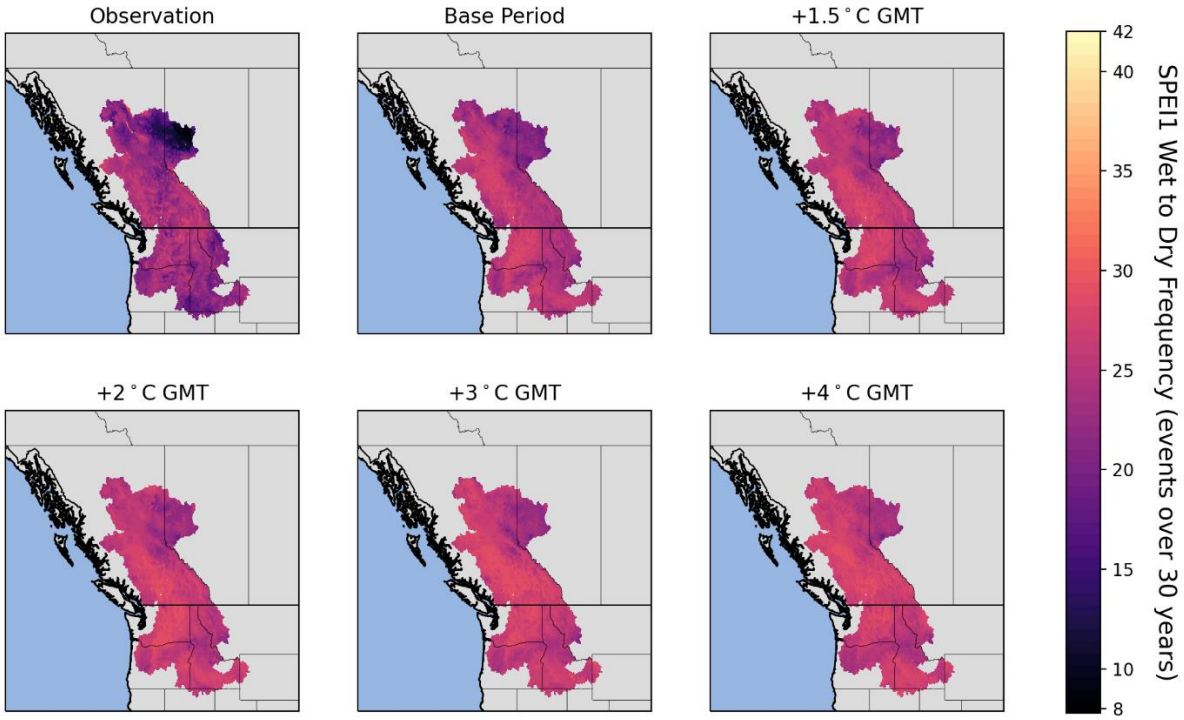

Appendix 4 - Climatology of frequency of wet-to-dry CCEs (SPEI1). Maps show the frequency of CCEs over each warming period (30 years).

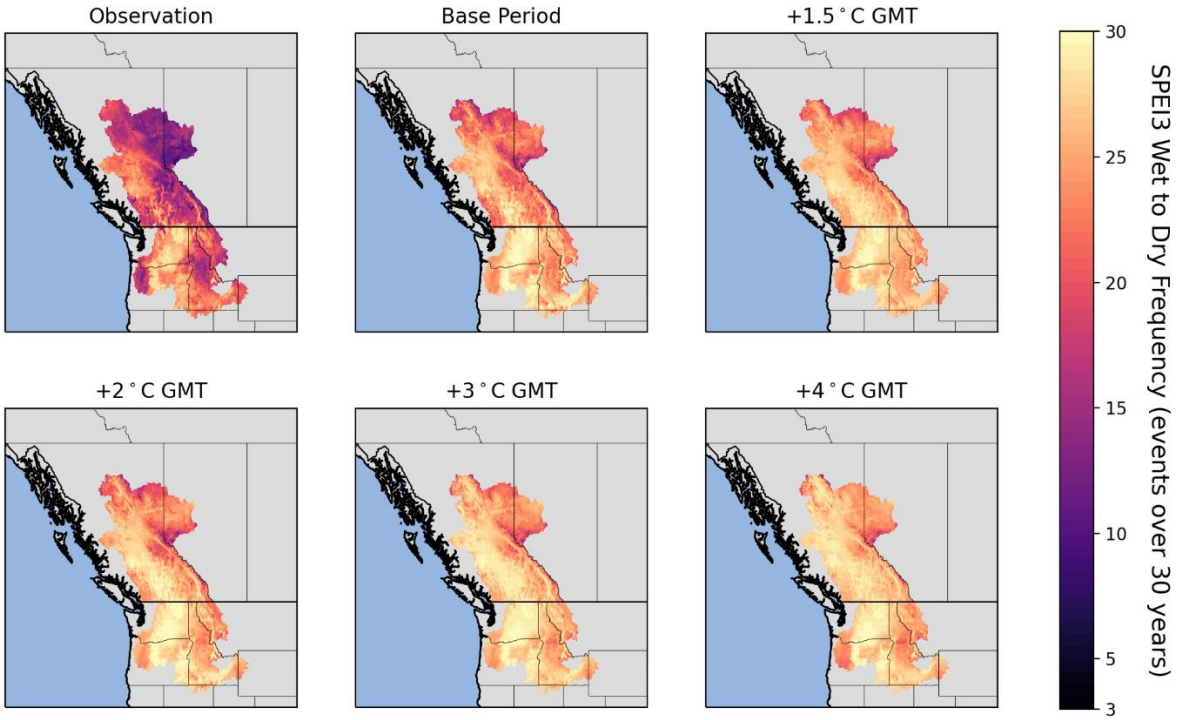

Appendix 5 - Climatology of frequency of wet-to-dry CCEs (SPEI3). Maps show the frequency of CCEs over each warming period (30 years).

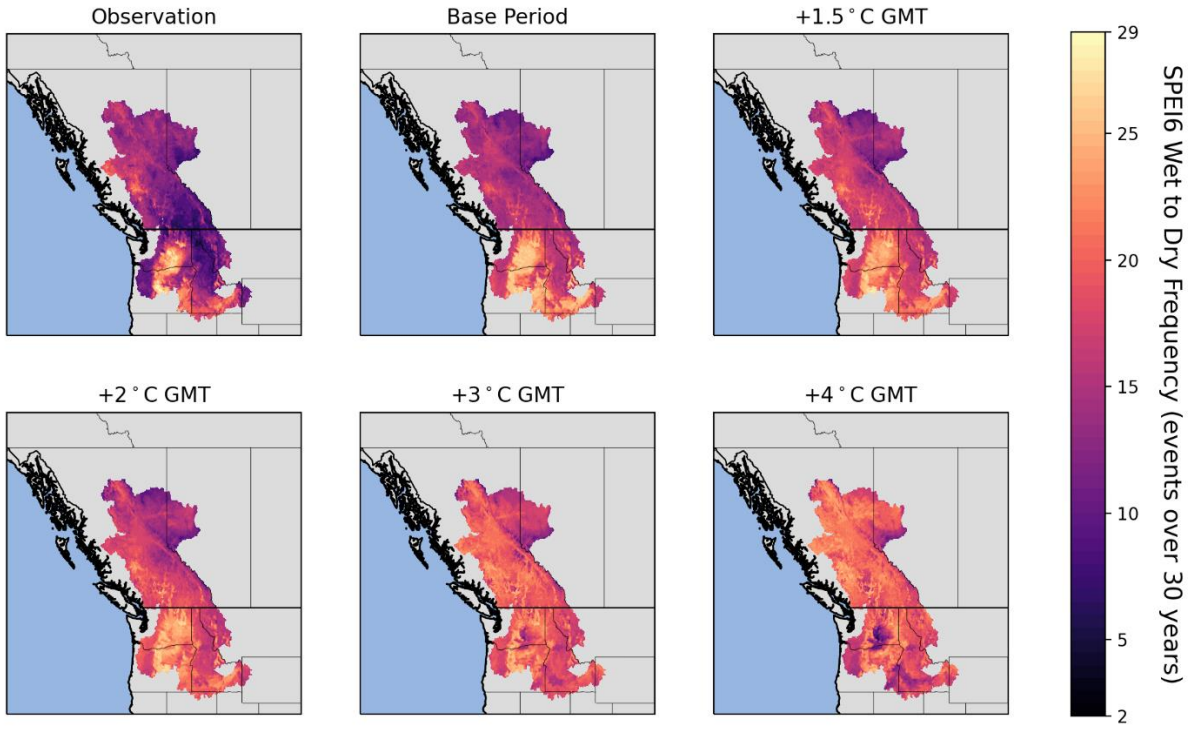

Appendix 6 - Climatology of frequency of wet-to-dry CCEs (SPEI6). Maps show the frequency of CCEs over each warming period (30 years).

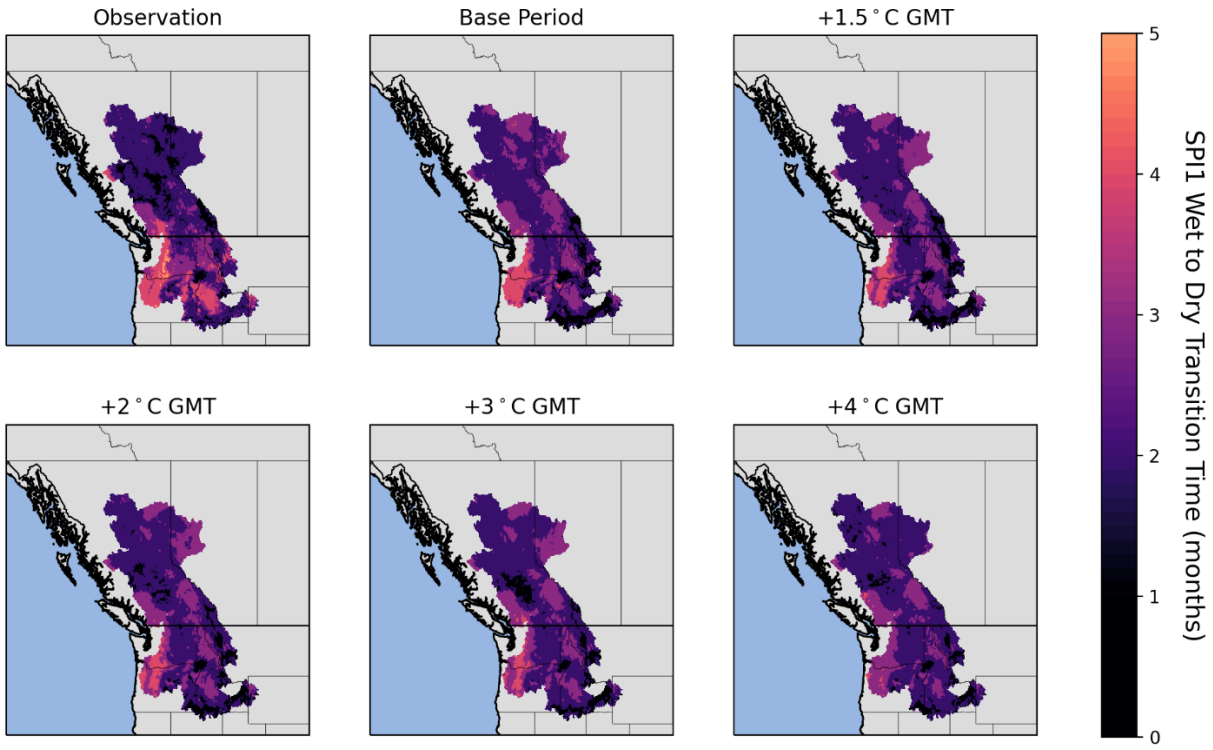

Appendix 7 - Climatology of the transition time of wet-to-dry CCEs (SPI1). The maps report the transition time of CCEs in months.

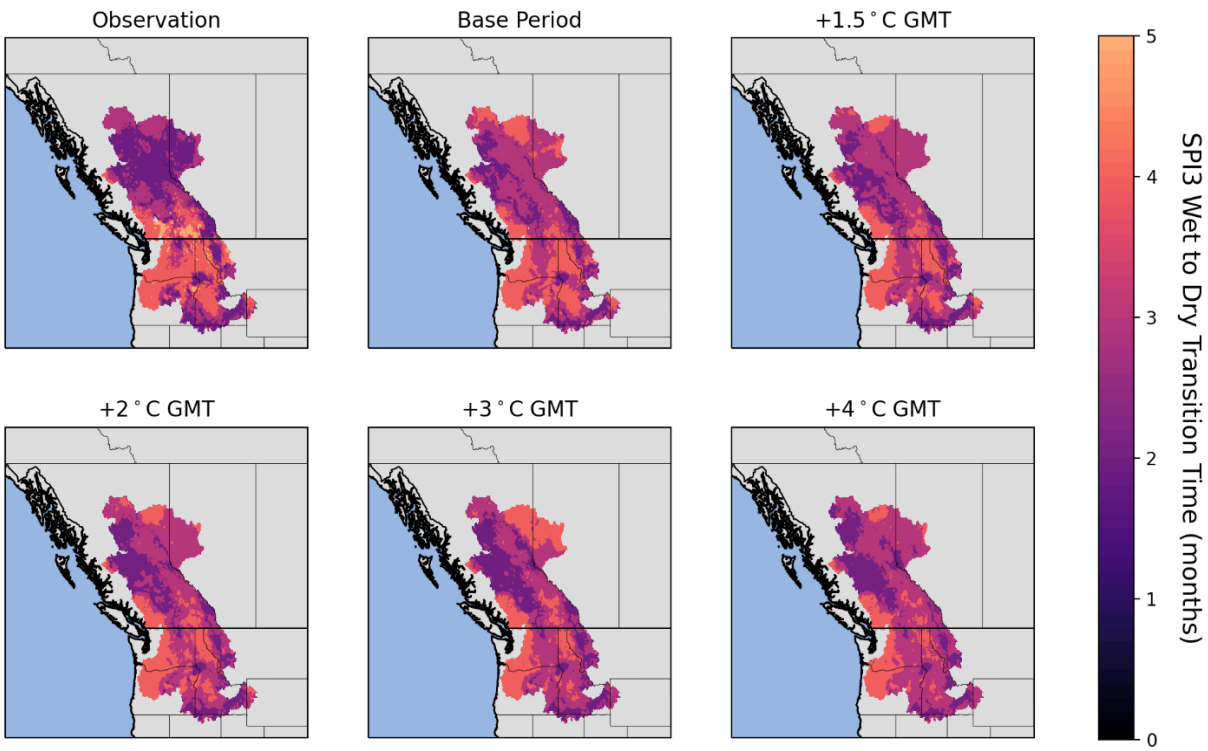

Appendix 8 - Climatology of the transition time of wet-to-dry CCEs (SPI3). The maps report the transition time of CCEs in months.

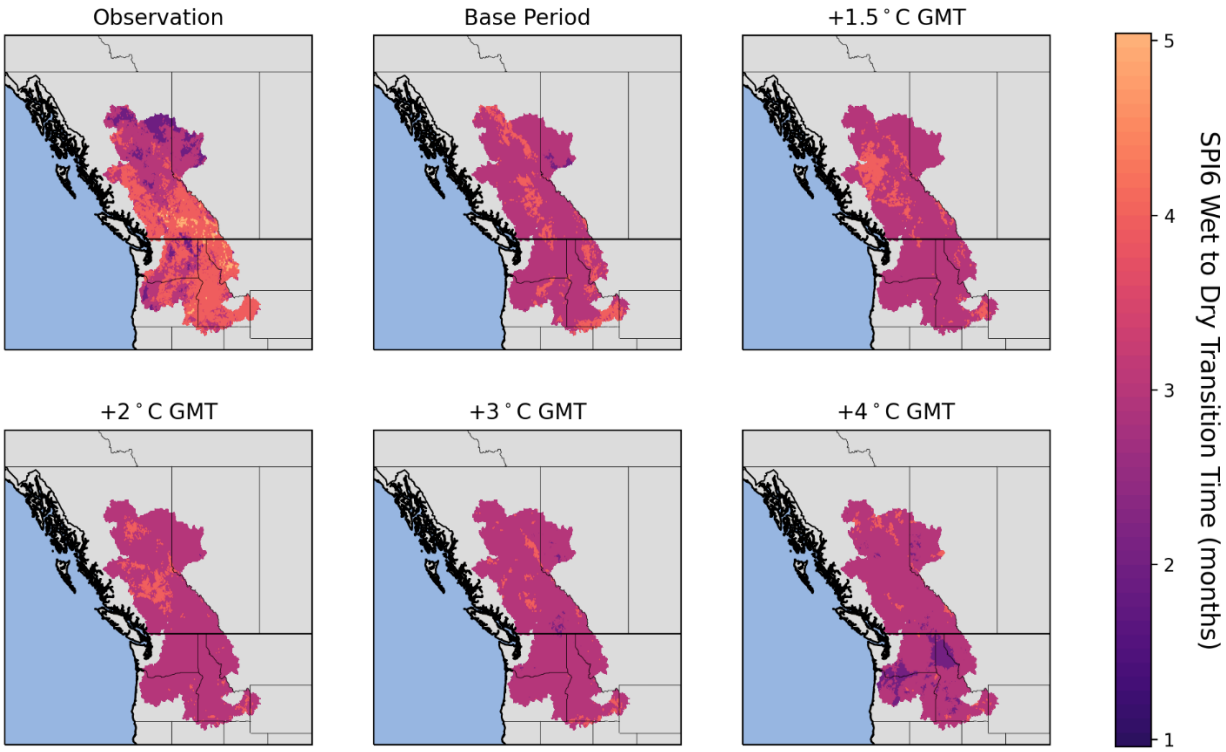

Appendix 9 - Climatology of the transition time of wet-to-dry CCEs (SPI6). The maps report the transition time of CCEs in months.

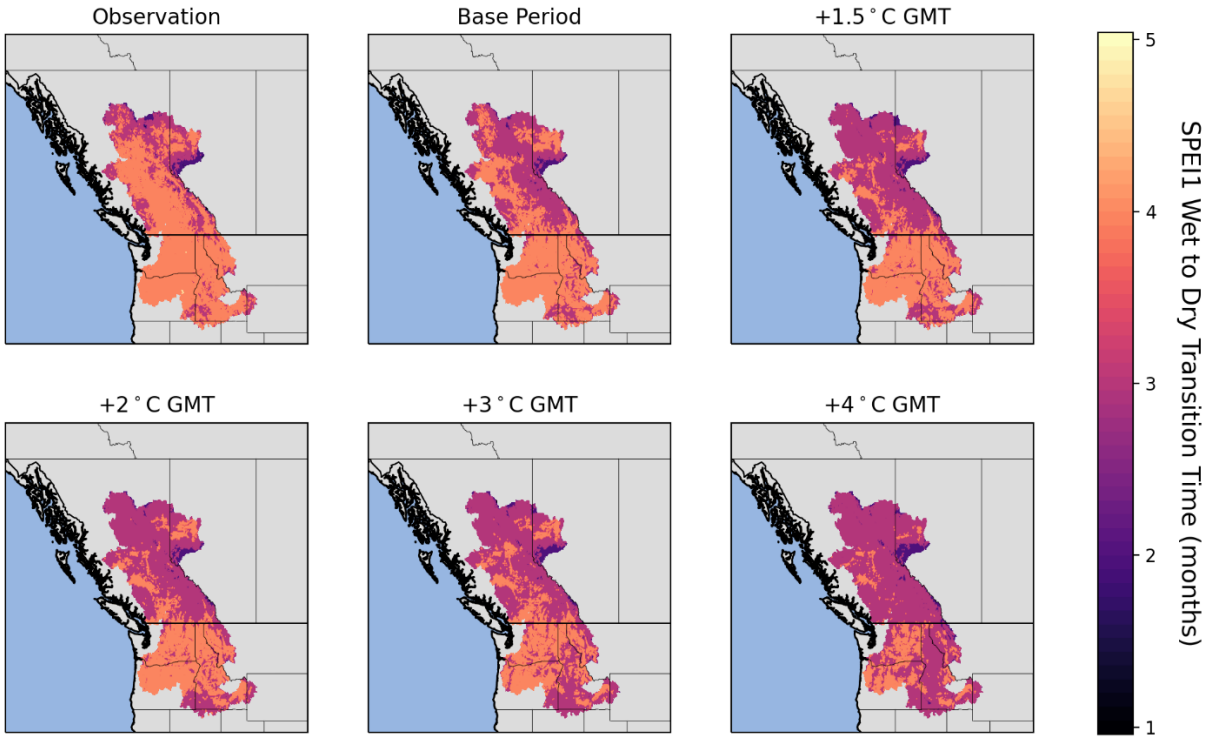

Appendix 10 - Climatology of the transition time of wet-to-dry CCEs (SPEI1). The maps report the transition time of CCEs in months.

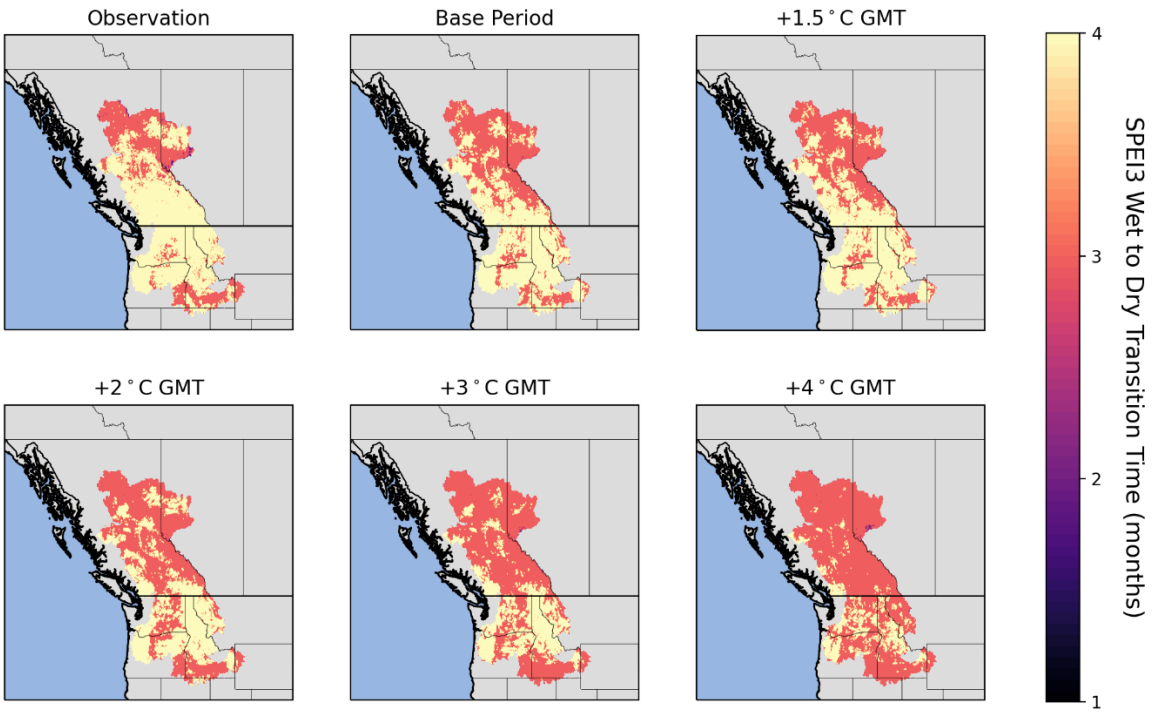

Appendix 11 - Climatology of the transition time of wet-to-dry CCEs (SPEI3). The maps report the transition time of CCEs in months.

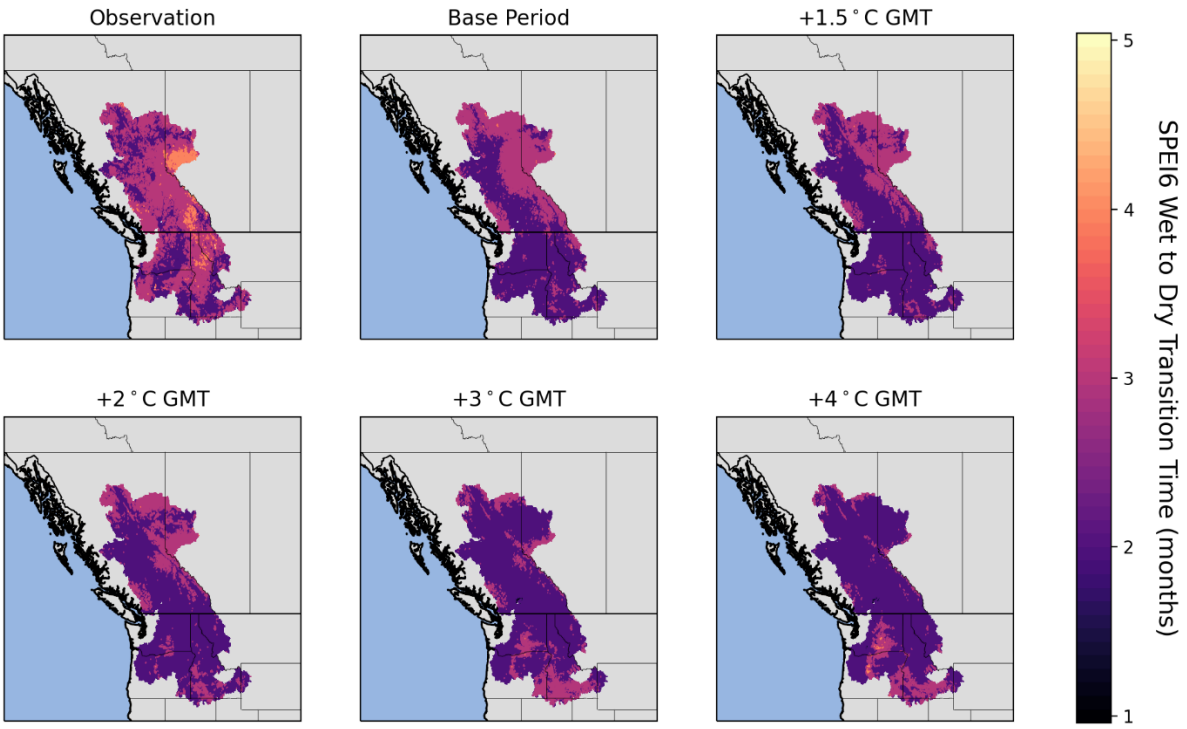

Appendix 12 - Climatology of the transition time of wet-to-dry CCEs (SPEI6). The maps report the transition time of CCEs in months.

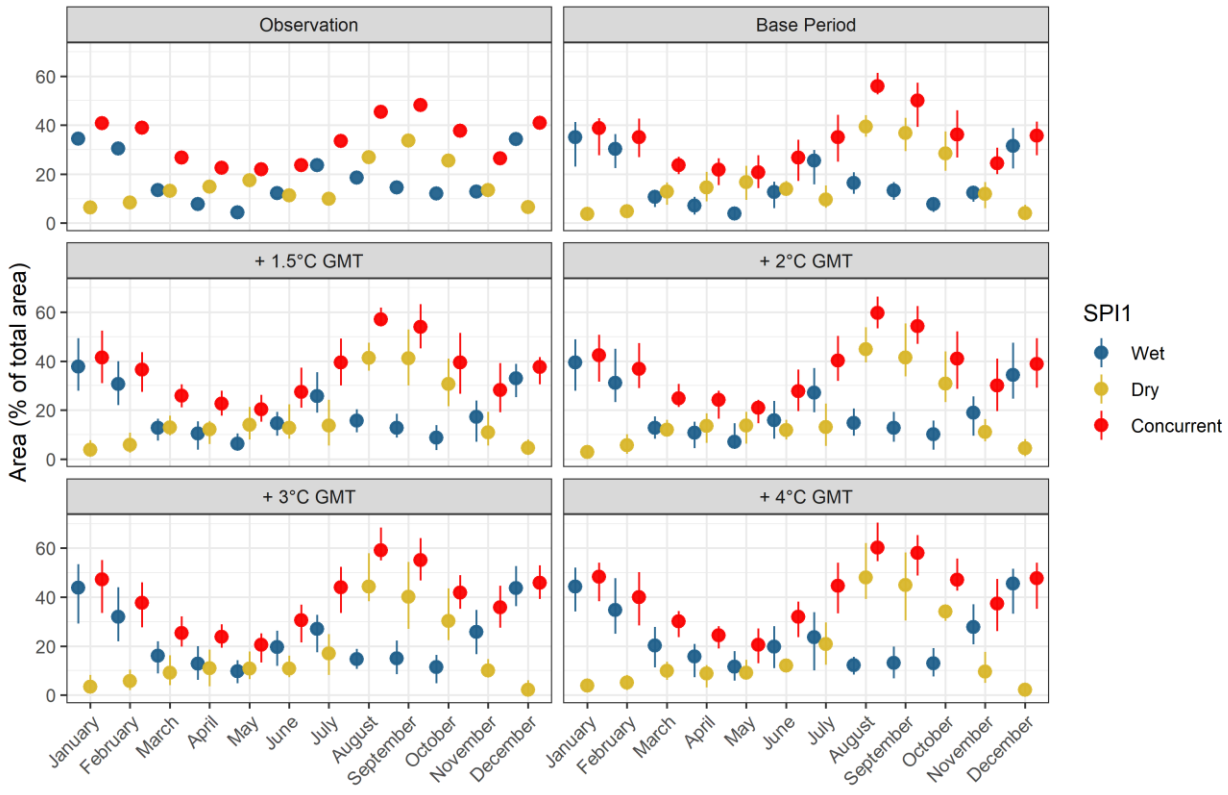

Appendix 13 - Average monthly area experiencing dry, wet, and concurrent dry-wet conditions (SPI1). The dots show the ensemble median, while the bars represent the 95% (CI, q2.5 – q97.5) of the ensemble.

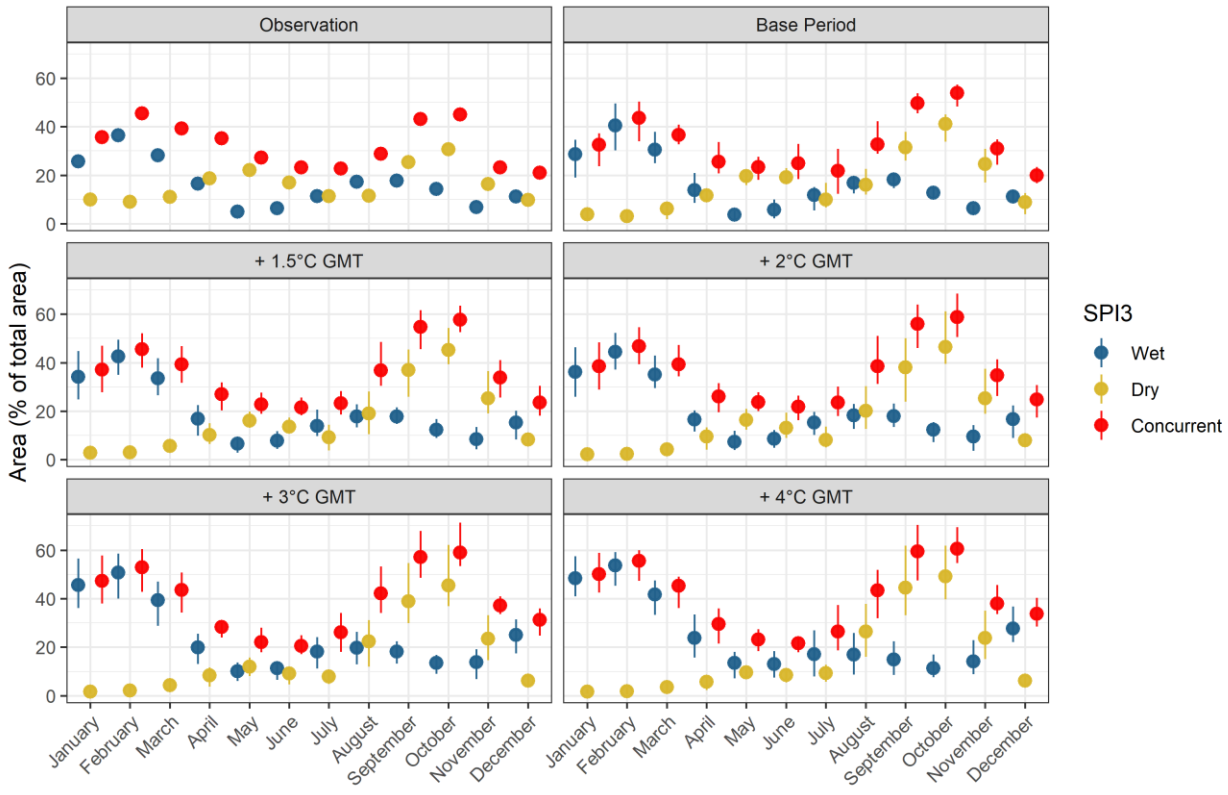

Appendix 14 - Average monthly area experiencing dry, wet, and concurrent dry-wet conditions (SPI3). The dots show the ensemble median, while the bars represent the 95% (CI, q2.5 – q97.5) of the ensemble.

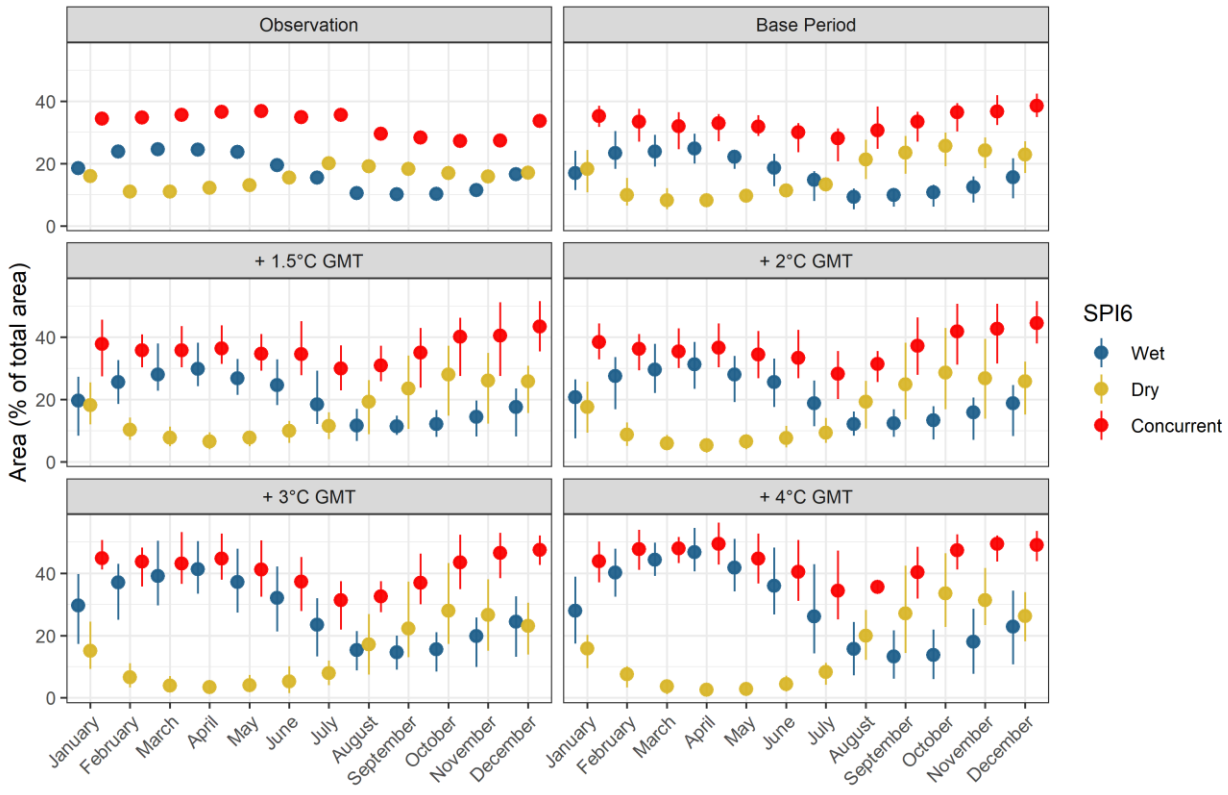

Appendix 15 - Average monthly area experiencing dry, wet, and concurrent dry-wet conditions (SPI6). The dots show the ensemble median, while the bars represent the 95% (CI, q2.5 – q97.5) of the ensemble.

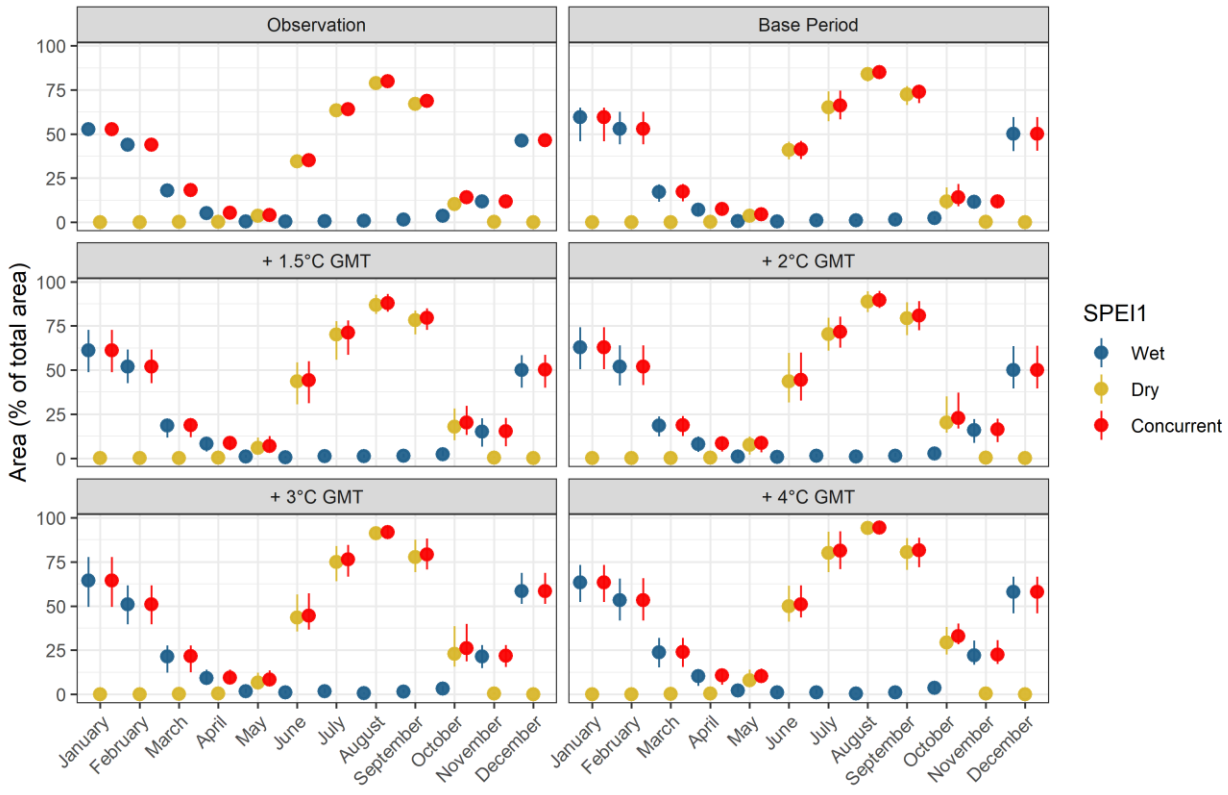

Appendix 16 - Average monthly area experiencing dry, wet, and concurrent dry-wet conditions (SPEI1). The dots show the ensemble median, while the bars represent the 95% (CI, q2.5 – q97.5) of the ensemble.

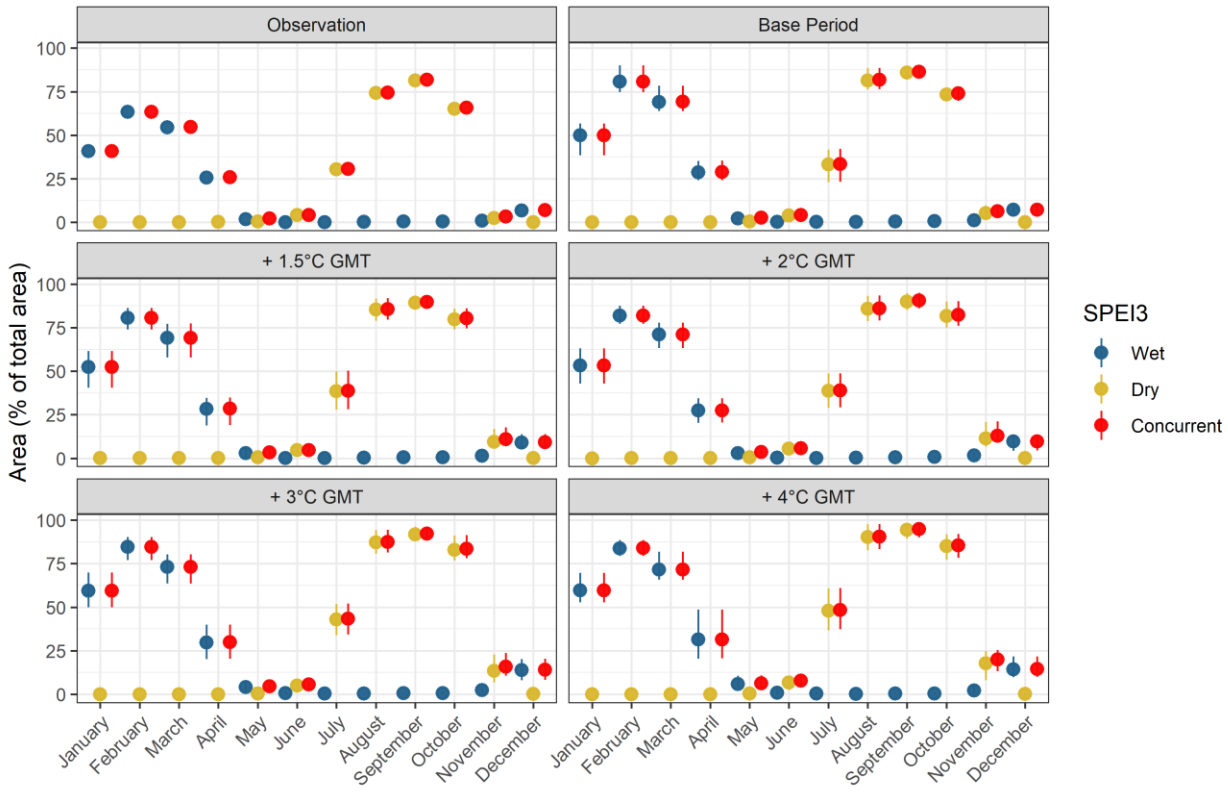

Appendix 17 - Average monthly area experiencing dry, wet, and concurrent dry-wet conditions (SPEI3). The dots show the ensemble median, while the bars represent the 95% (CI, q2.5 – q97.5) of the ensemble.

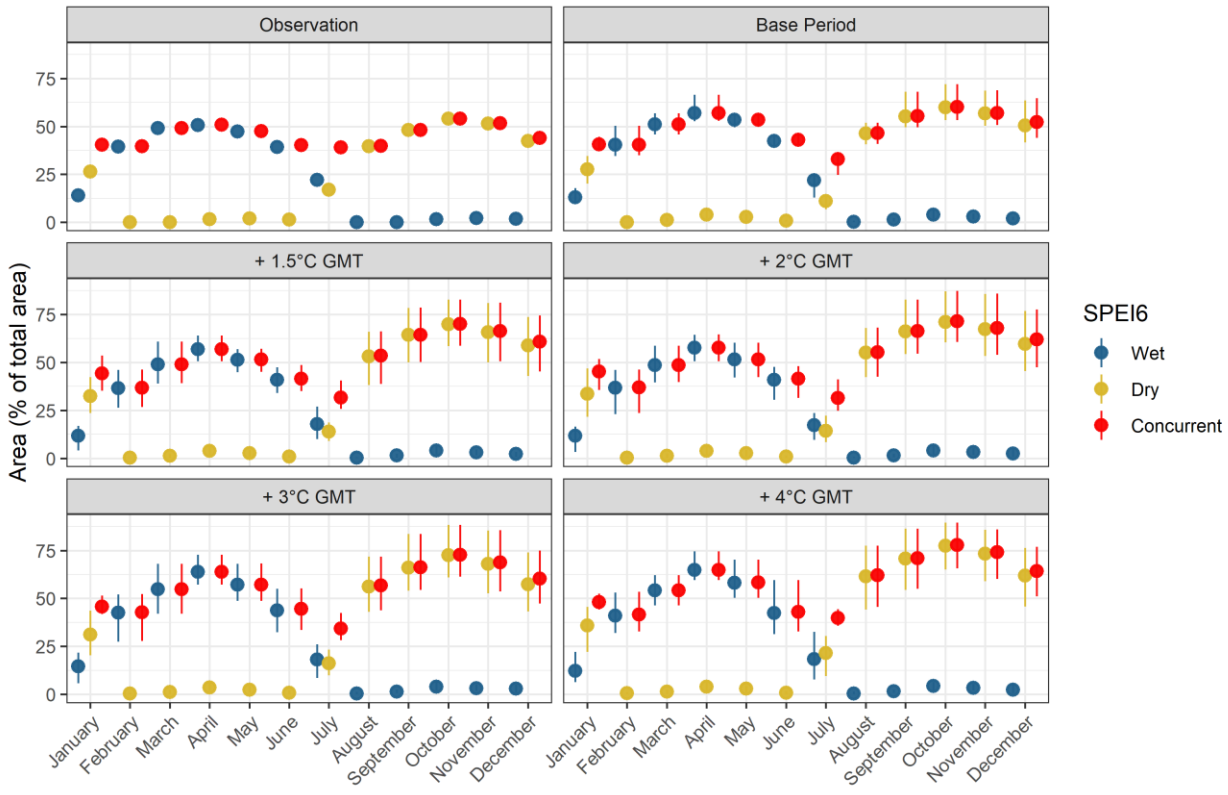

Appendix 18 - Average monthly area experiencing dry, wet, and concurrent dry-wet conditions (SPEI6). The dots show the ensemble median, while the bars represent the 95% (CI, q2.5 – q97.5) of the ensemble.

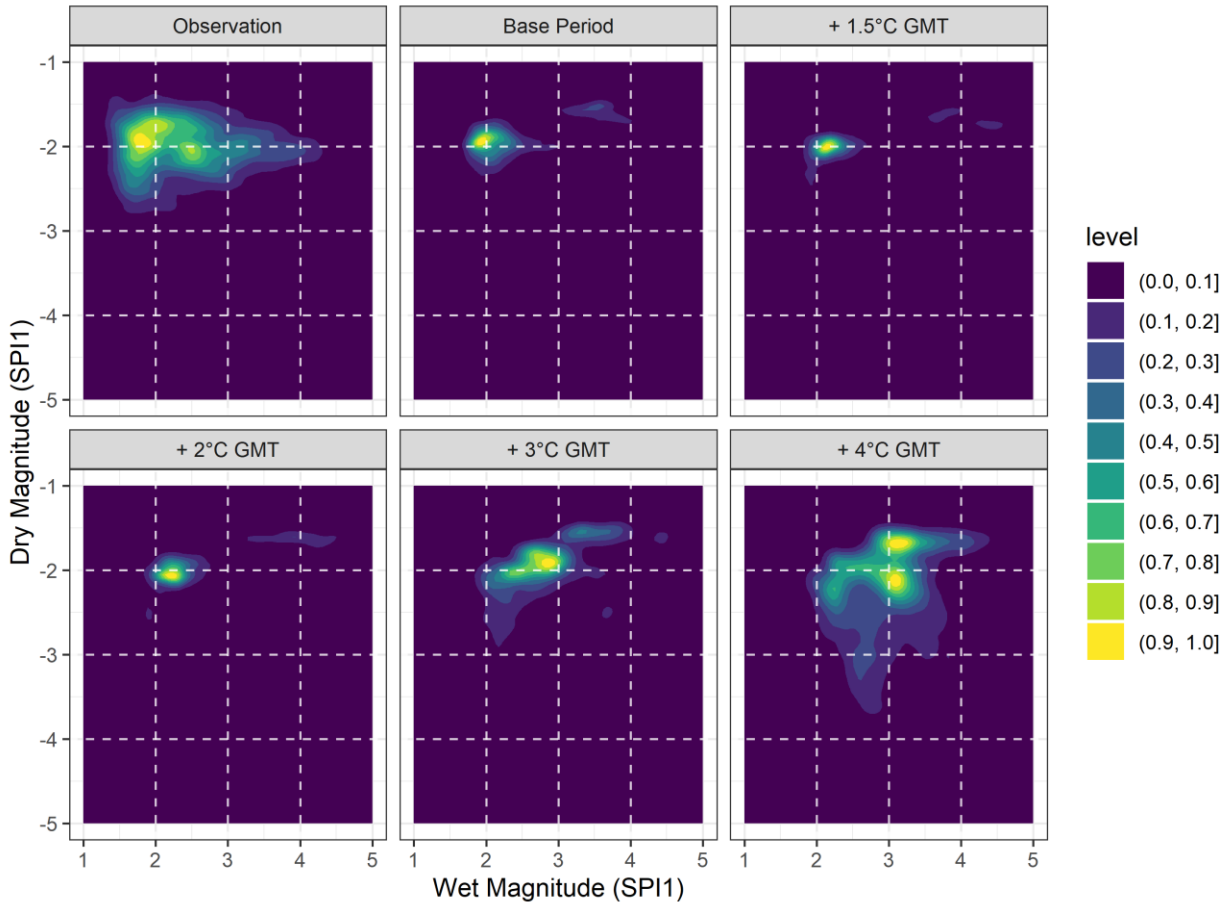

Appendix 19 - 2D Kernel Density plots for the magnitude of wet and dry spells in wet-to-dry CCEs based on SPI1. The contours show the spatial density of the CCEs based on their dry and wet spells magnitudes.

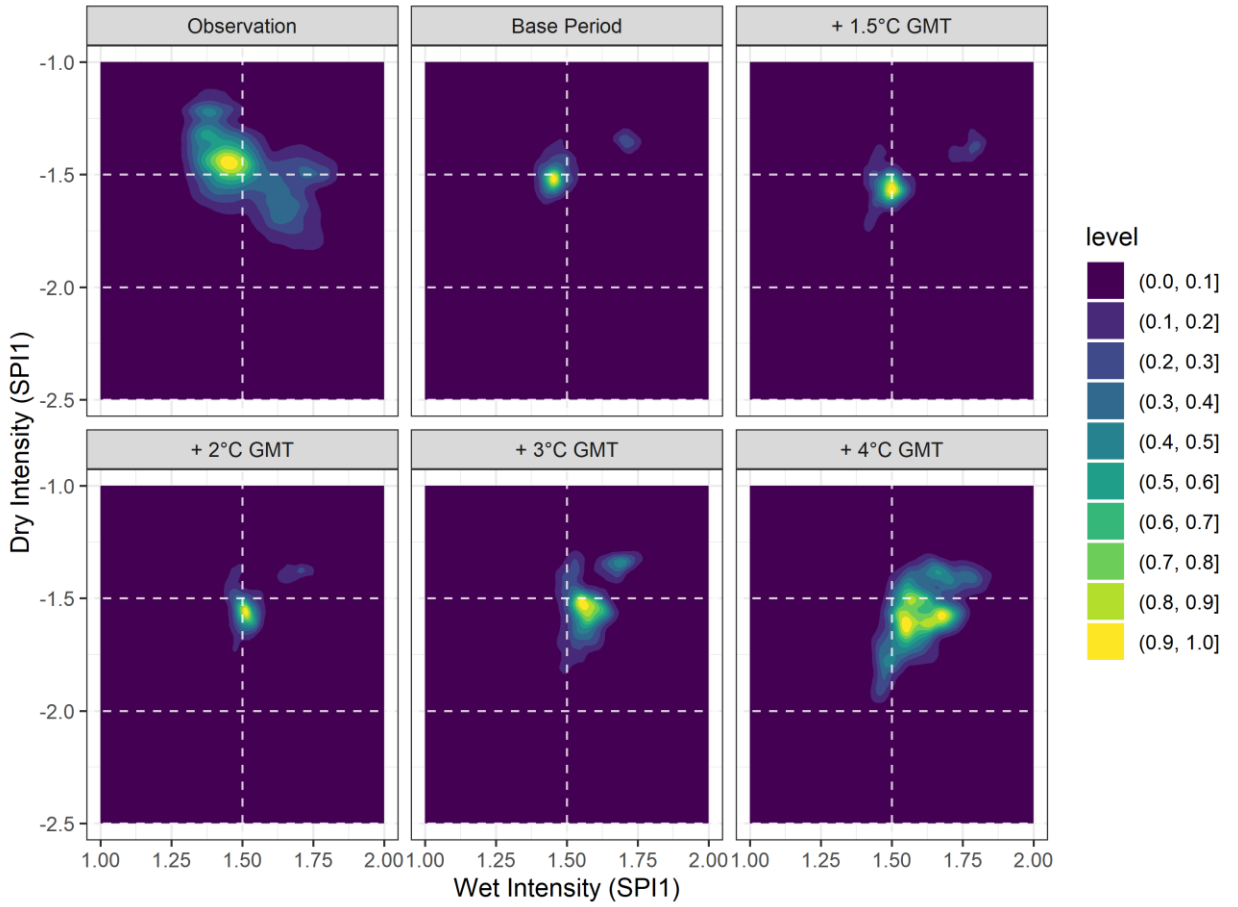

Appendix 20 - 2D Kernel Density plots for the intensity of wet and dry spells in wet-to-dry CCEs based on SPI1. The dashed lines show the SPI thresholds used to categorise wet and dry conditions (Figure 4). The contours show the spatial density of the CCEs based on their dry and wet spells intensities.

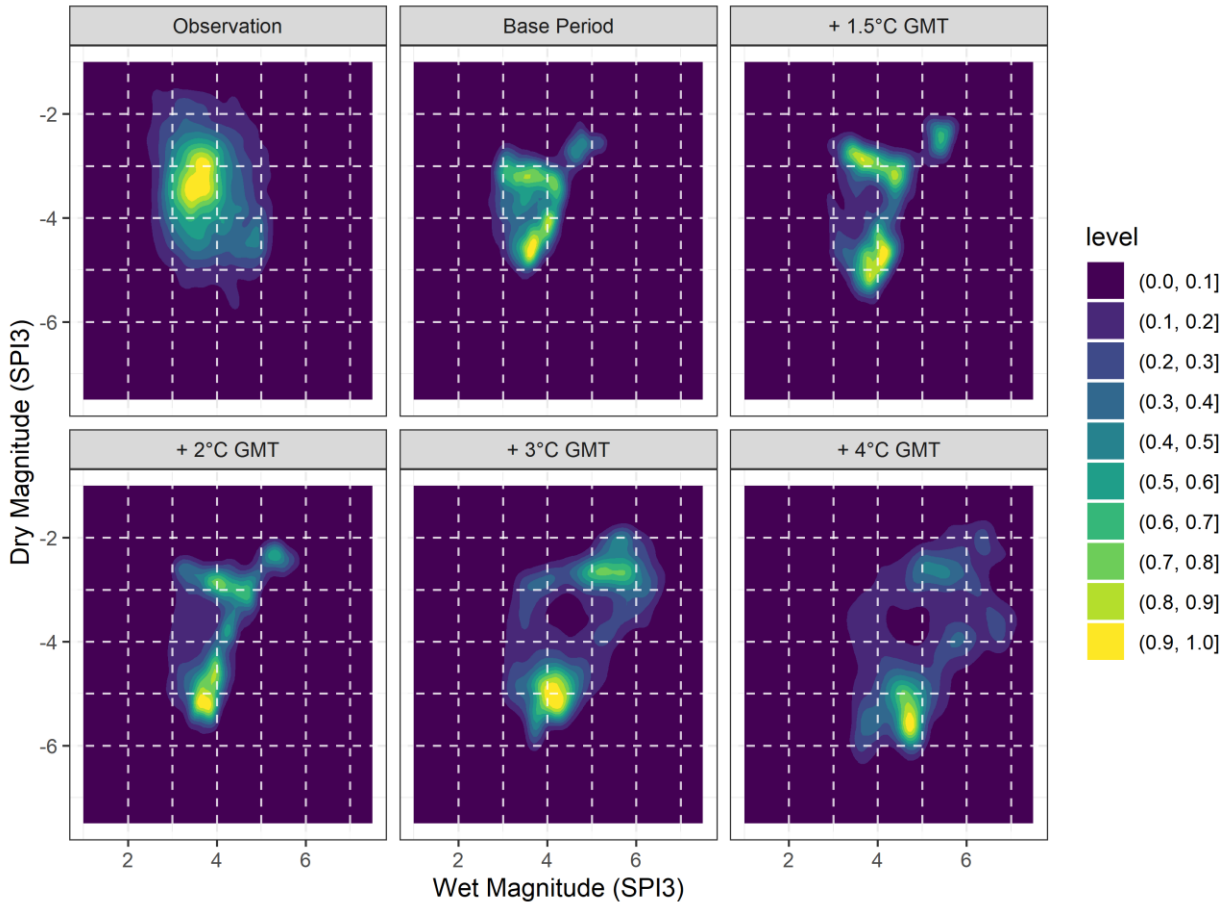

Appendix 21 - 2D Kernel Density plots for the magnitude of wet and dry spells in wet-to-dry CCEs based on SPI3. The contours show the spatial density of the CCEs based on their dry and wet spells magnitudes.

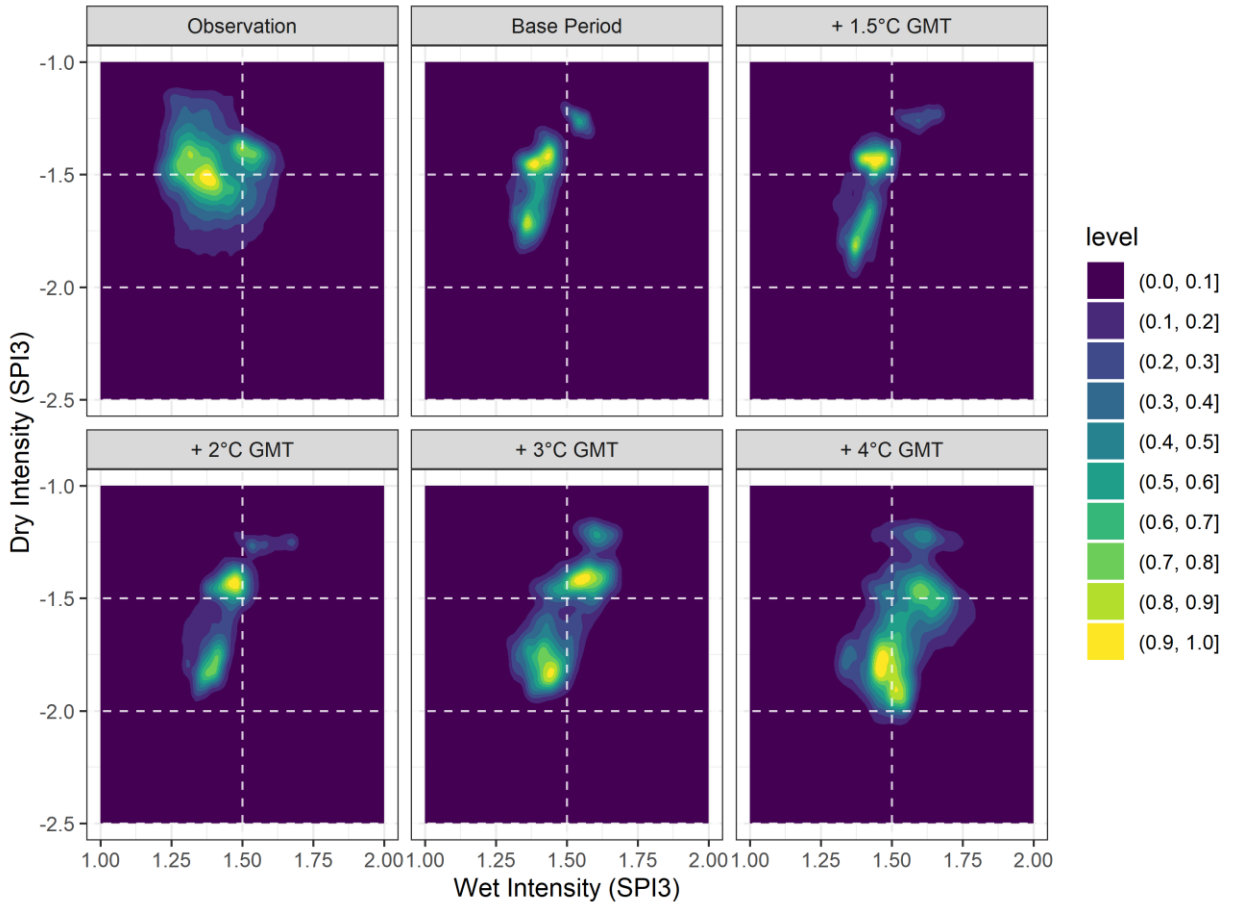

Appendix 22 - 2D Kernel Density plots for the intensity of wet and dry spells in wet-to-dry CCEs based on SPI3. The dashed lines show the SPI thresholds used to categorise wet and dry conditions (Figure 4). The contours show the spatial density of the CCEs based on their dry and wet spells intensities.

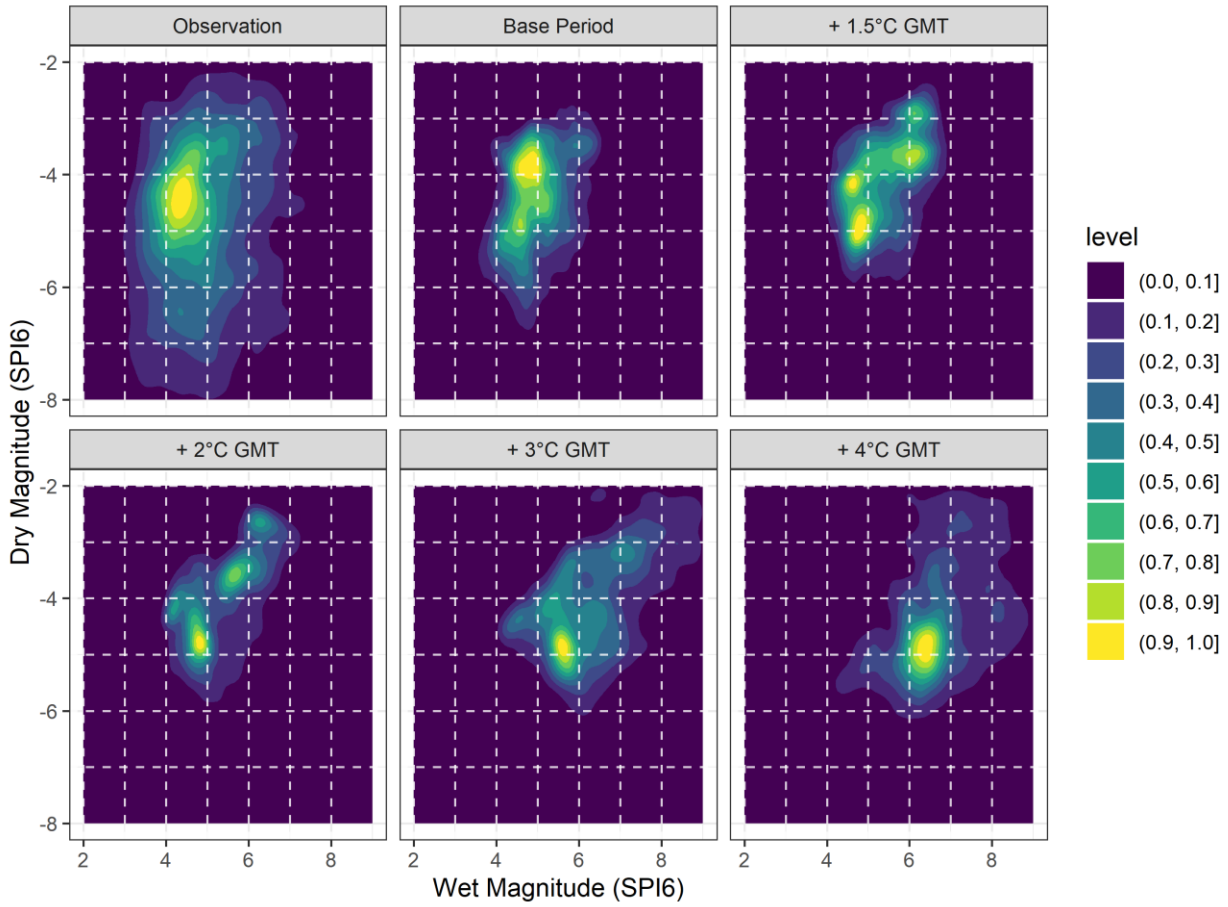

Appendix 23 - 2D Kernel Density plots for the magnitude of wet and dry spells in wet-to-dry CCEs based on SPI6. The contours show the spatial density of the CCEs based on their dry and wet spells magnitudes.

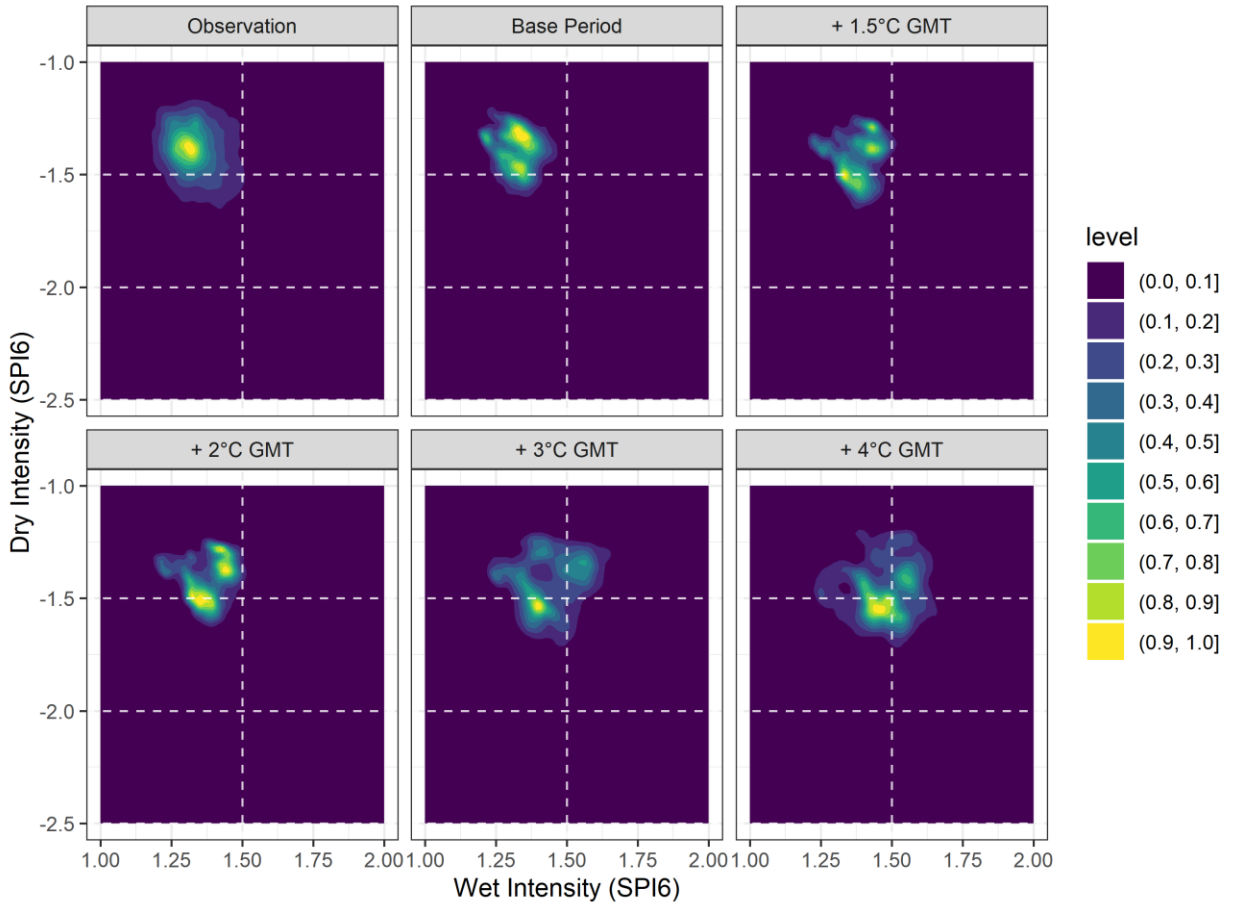

Appendix 24 - 2D Kernel Density plots for the intensity of wet and dry spells in wet-to-dry CCEs based on SPI6. The dashed lines show the SPI thresholds used to categorise wet and dry conditions (Figure 4). The contours show the spatial density of the CCEs based on their dry and wet spells intensities.

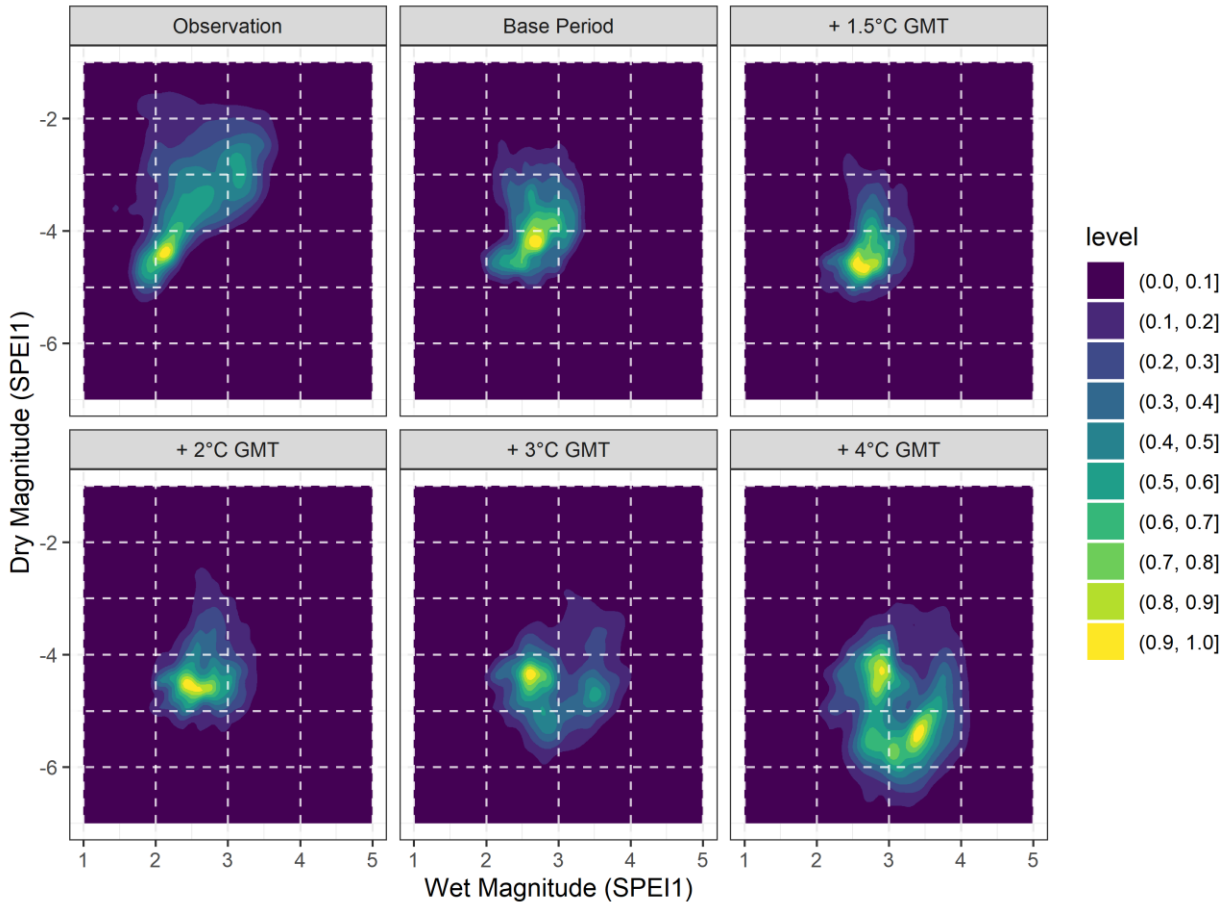

Appendix 25 - 2D Kernel Density plots for the magnitude of wet and dry spells in wet-to-dry CCEs based on SPEI1. The contours show the spatial density of the CCEs based on their dry and wet spells magnitudes.

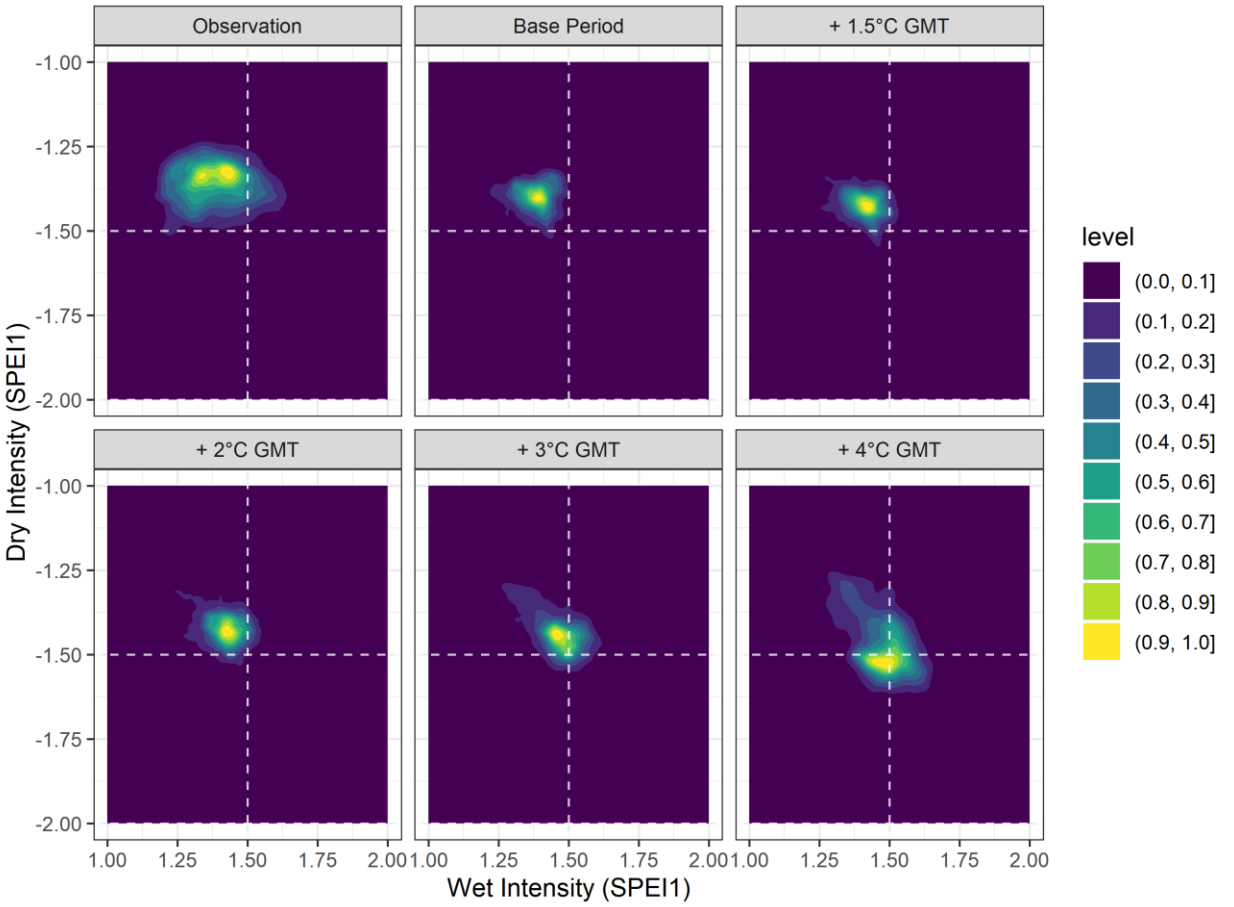

Appendix 26 - 2D Kernel Density plots for the intensity of wet and dry spells in wet-to-dry CCEs based on SPEI1. The dashed lines show the SPEI thresholds used to categorise wet and dry conditions (Figure 4). The contours show the spatial density of the CCEs based on their dry and wet spells intensities.

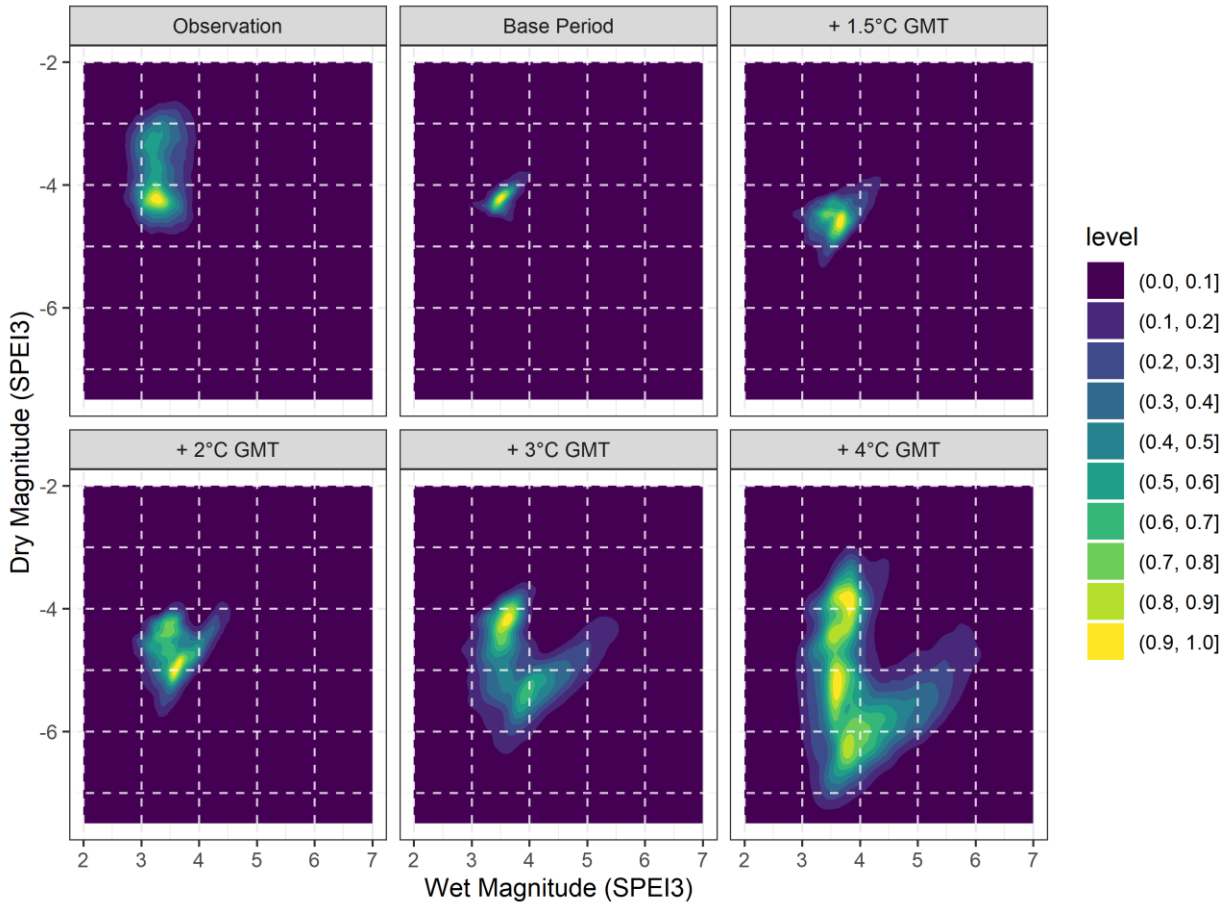

Appendix 27 - 2D Kernel Density plots for the magnitude of wet and dry spells in wet-to-dry CCEs based on SPIE3. The contours show the spatial density of the CCEs based on their dry and wet spells magnitudes.

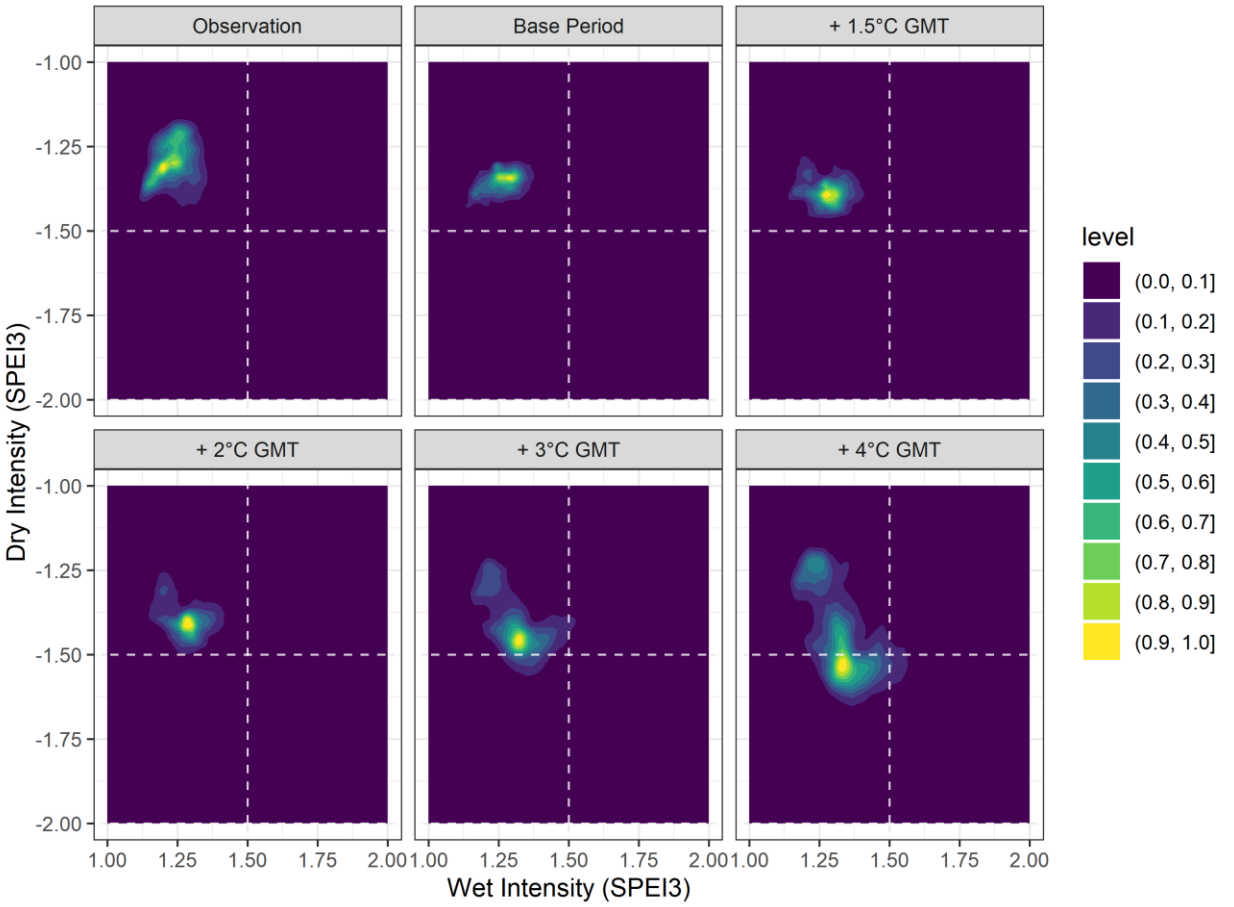

Appendix 28 - 2D Kernel Density plots for the intensity of wet and dry spells in wet-to-dry CCEs based on SPEI3. The dashed lines show the SPEI thresholds used to categorise wet and dry conditions (Figure 4). The contours show the spatial density of the CCEs based on their dry and wet spells intensities.

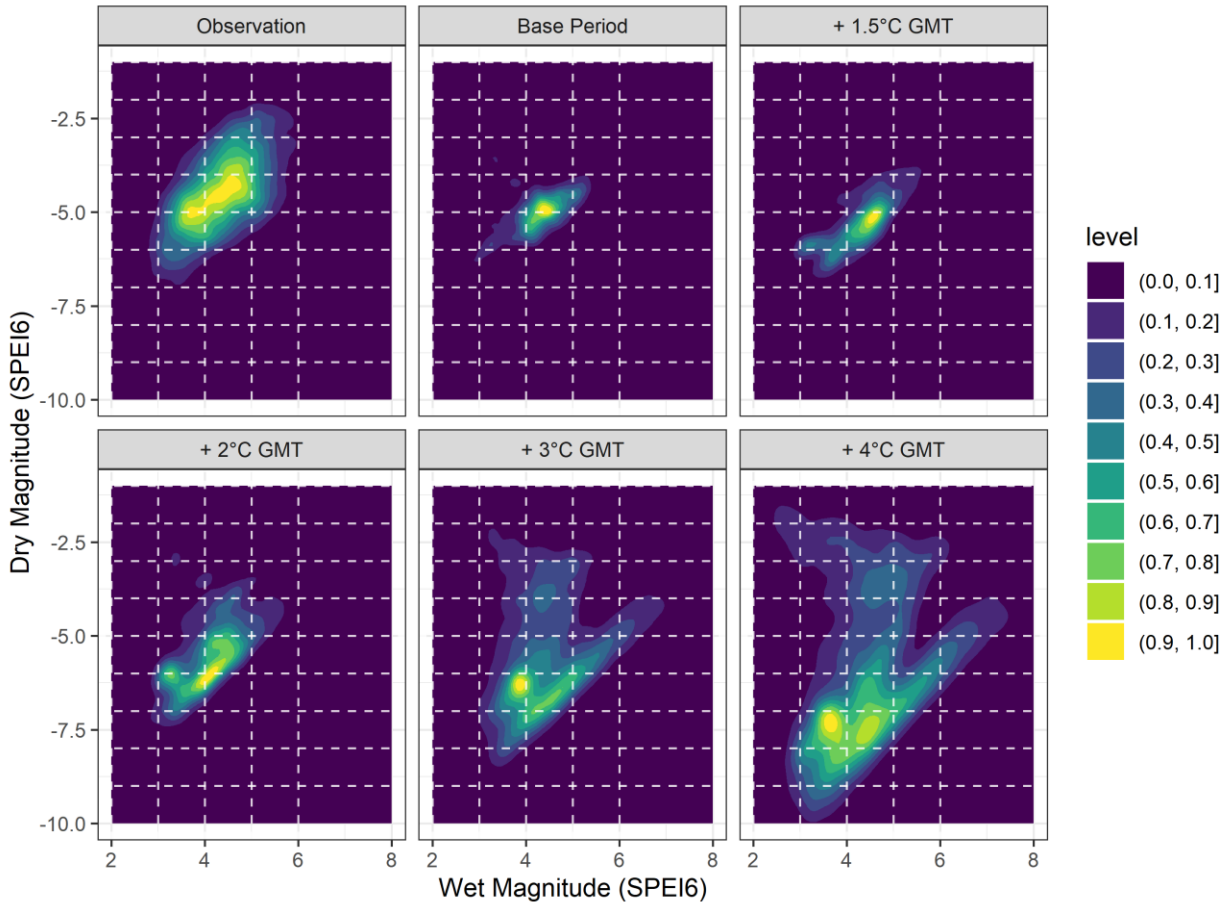

Appendix 29 - 2D Kernel Density plots for the magnitude of wet and dry spells in wet-to-dry CCEs based on SPEI6. The contours show the spatial density of the CCEs based on their dry and wet spells magnitudes.

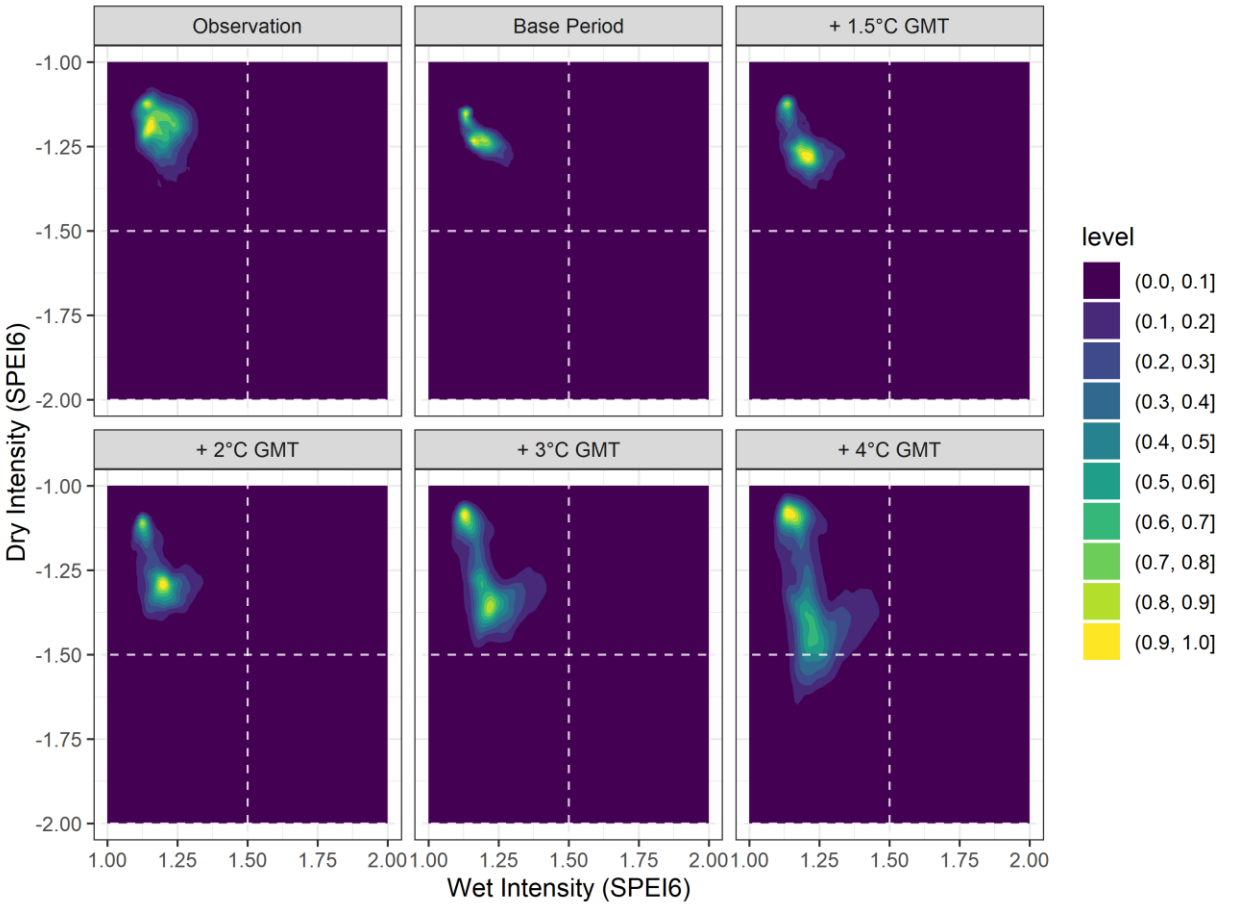

Appendix 30 - 2D Kernel Density plots for the intensity of wet and dry spells in wet-to-dry CCEs based on SPEI6. The dashed lines show the SPEI thresholds used to categorise wet and dry conditions (Figure 4). The contours show the spatial density of the CCEs based on their dry and wet spells intensities.

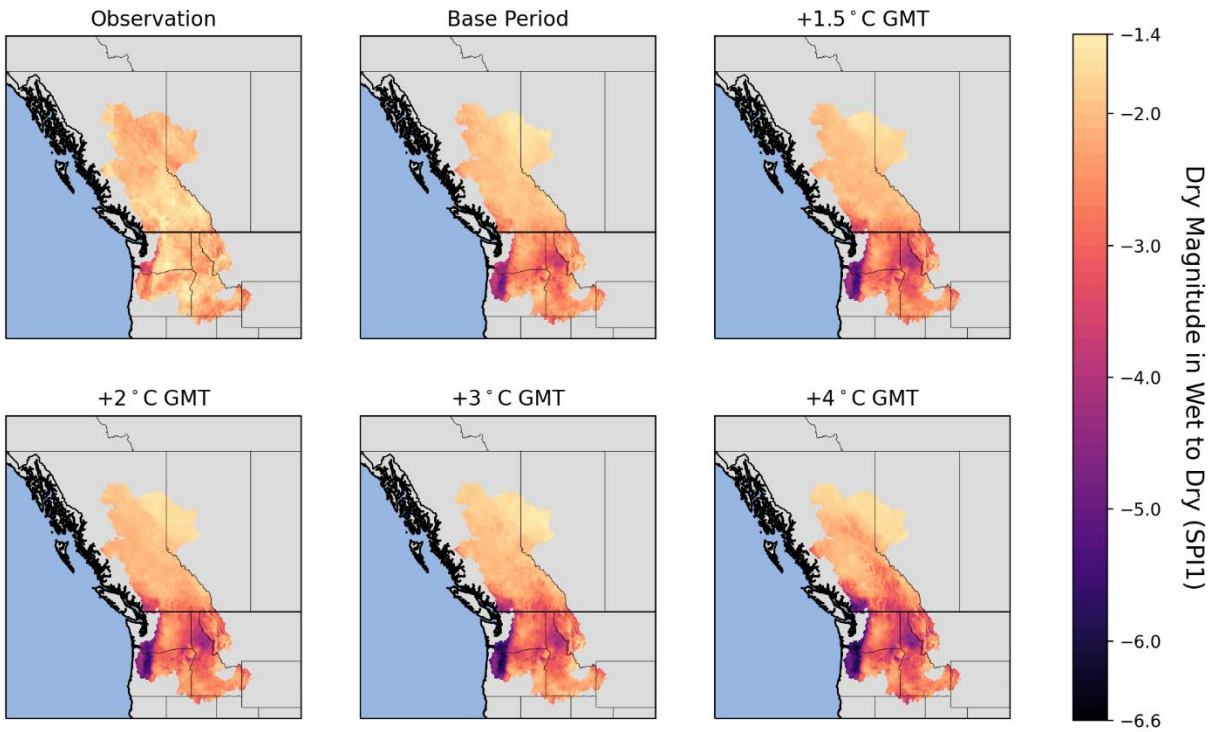

Appendix 31 - Climatology of the dry spell magnitude in the wet-to-dry CCEs (SPI1). The map shows the magnitude based on the SPI values of dry spells in the CCEs.

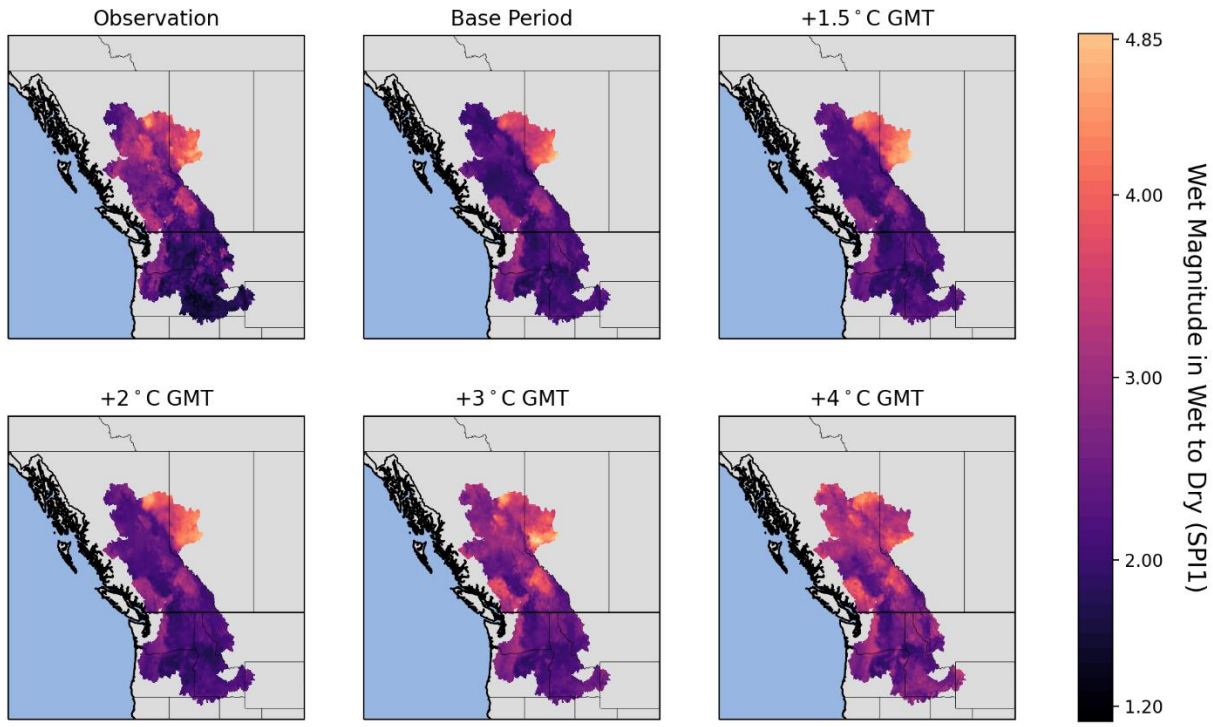

Appendix 32 - Climatology of the wet spell magnitude in the wet-to-dry CCEs (SPI1). The map shows the magnitude based on the SPI values of wet spells in the CCEs.

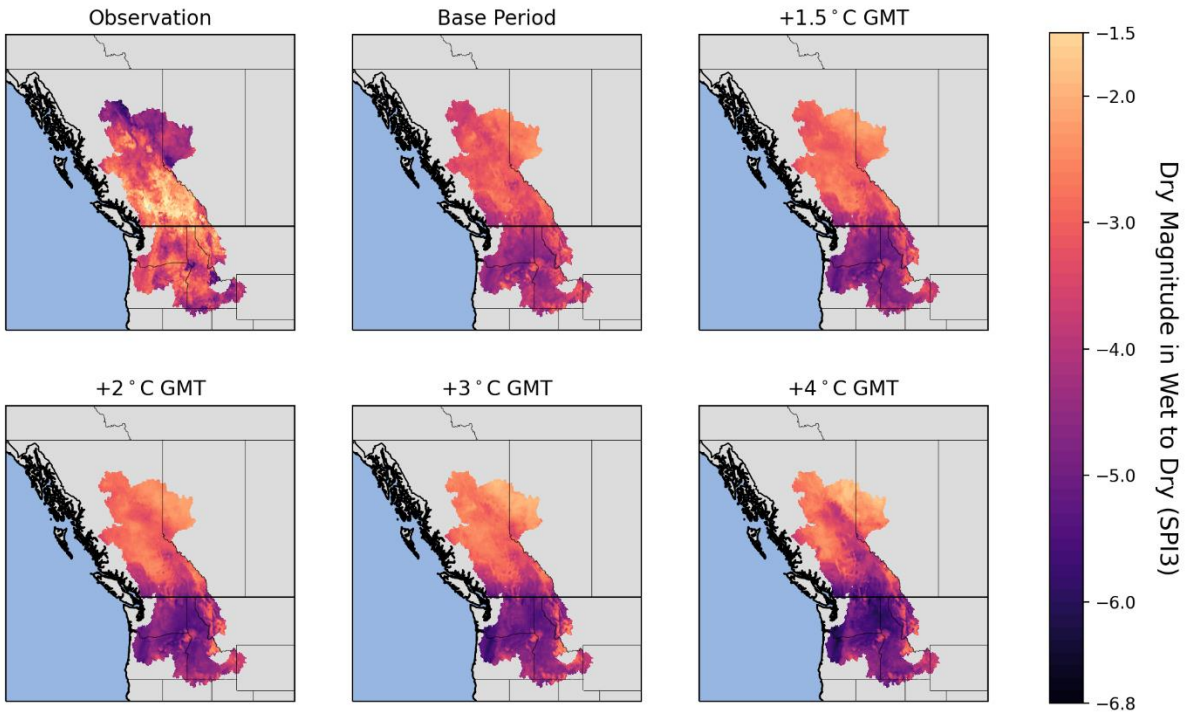

Appendix 33 - Climatology of the dry spell magnitude in the wet-to-dry CCEs (SPI3). The map shows the magnitude based on the SPI values of dry spells in the CCEs.

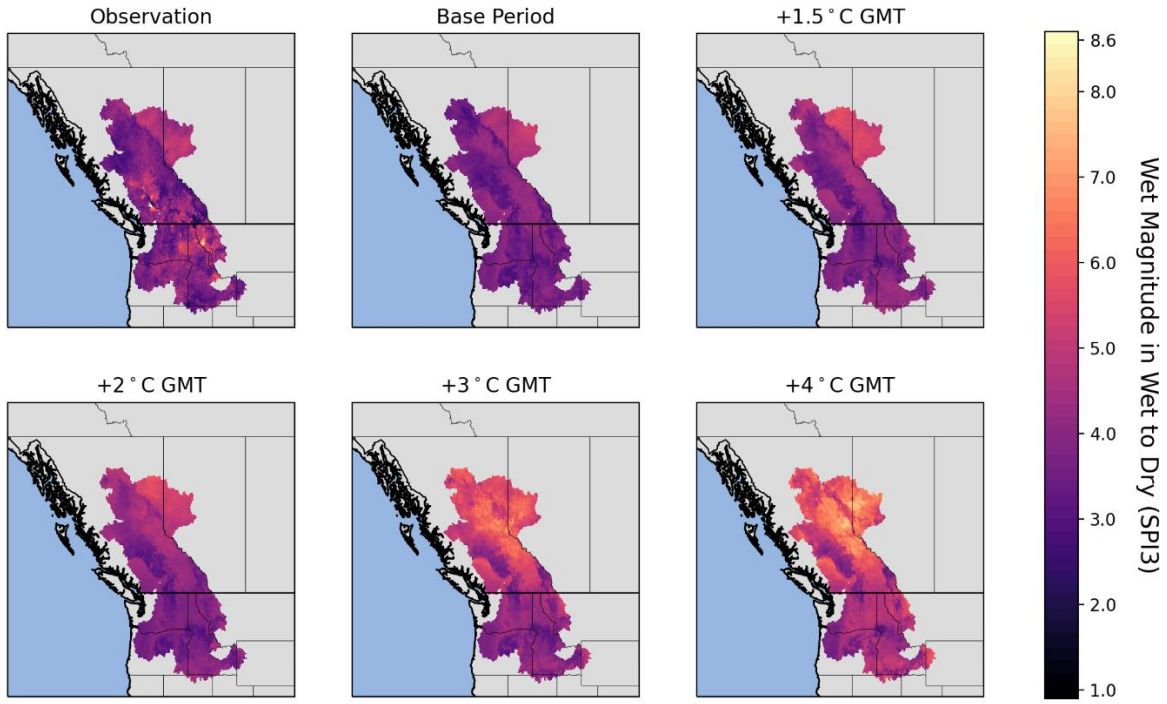

Appendix 34 - Climatology of the wet spell magnitude in the wet-to-dry CCEs (SPI3). The map shows the magnitude based on the SPI values of wet spells in the CCEs.

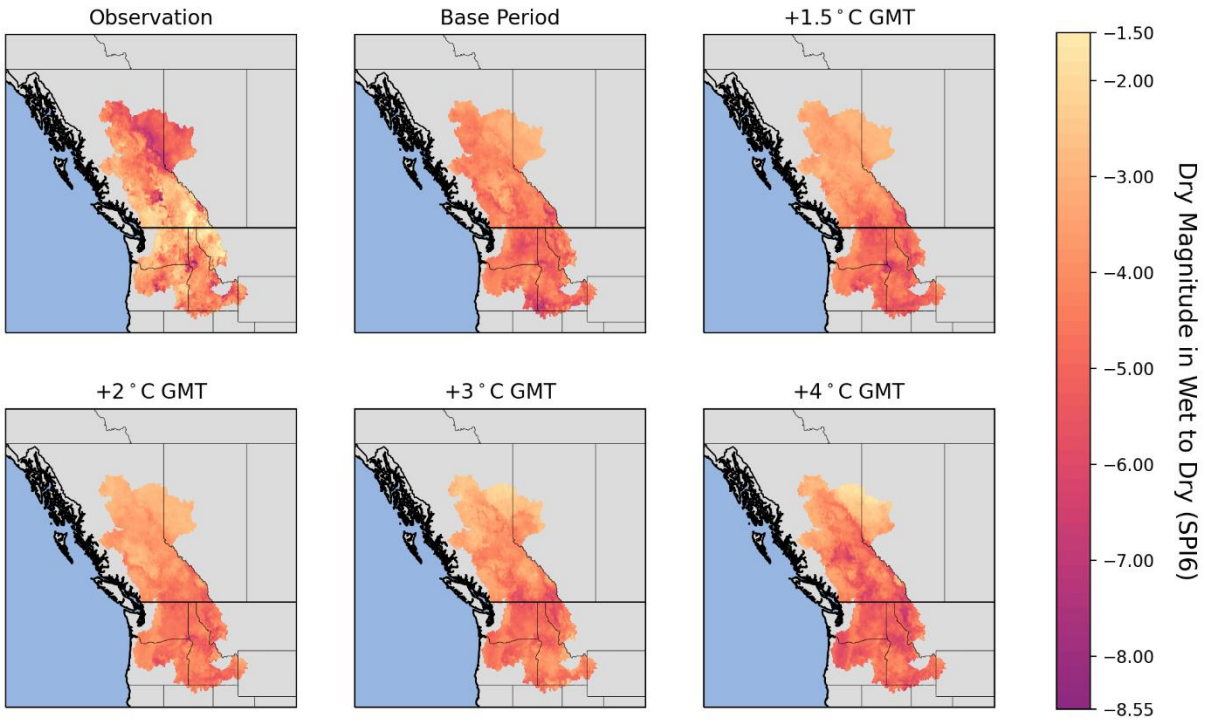

Appendix 35 - Climatology of the dry spell magnitude in the wet-to-dry CCEs (SPI6). The map shows the magnitude based on the SPI values of dry spells in the CCEs.

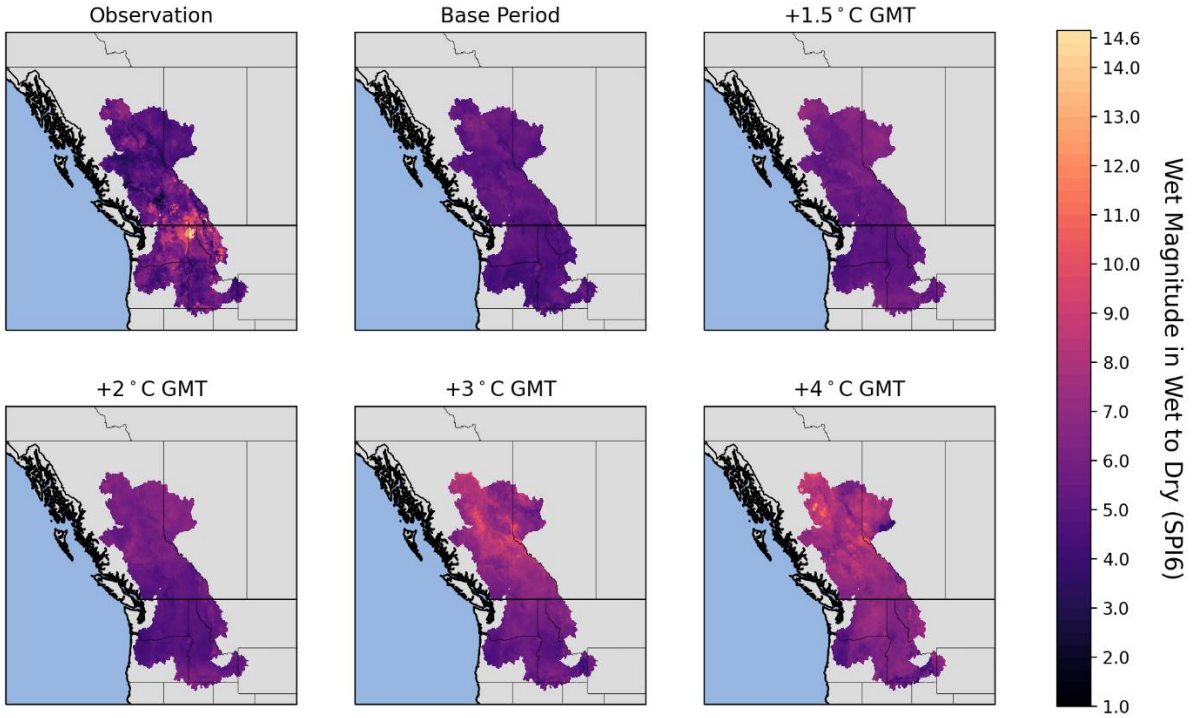

Appendix 36 - Climatology of the wet spell magnitude in the wet-to-dry CCEs (SPI6). The map shows the magnitude based on the SPI values of wet spells in the CCEs.

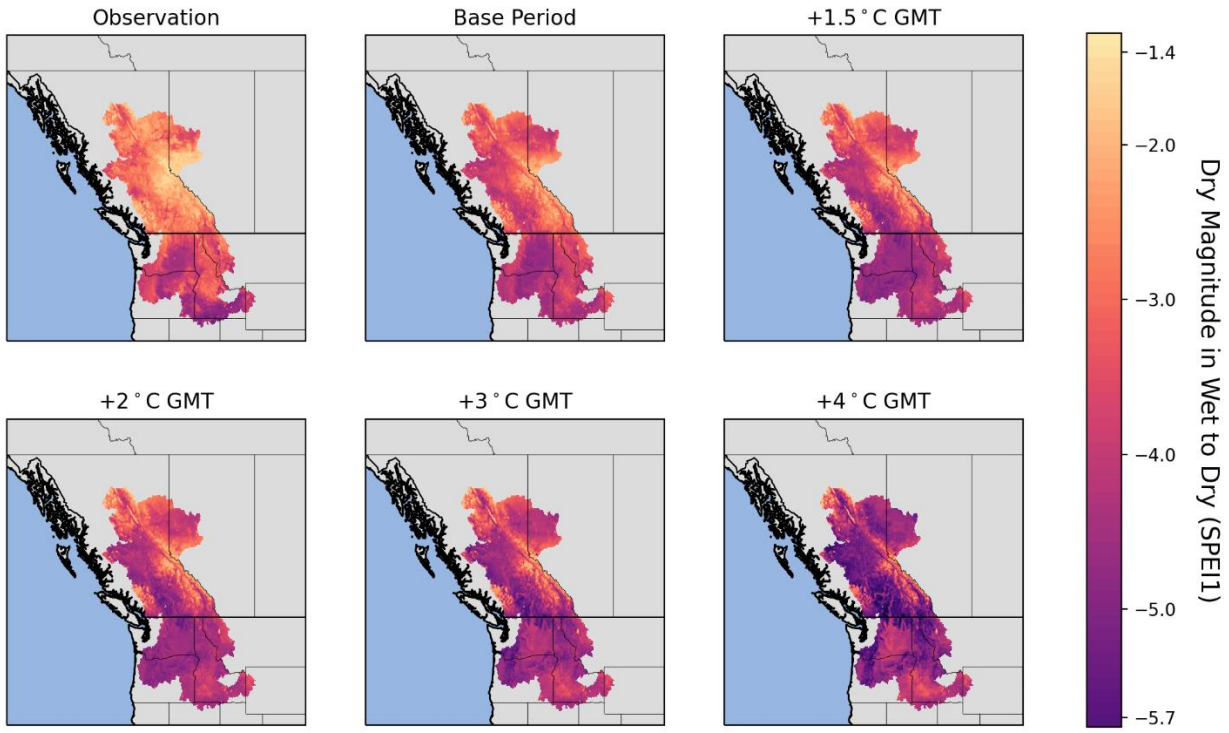

Appendix 37 - Climatology of the dry spell magnitude in the wet-to-dry CCEs (SPEI1). The map shows the magnitude based on the SPEI values of dry spells in the CCEs.

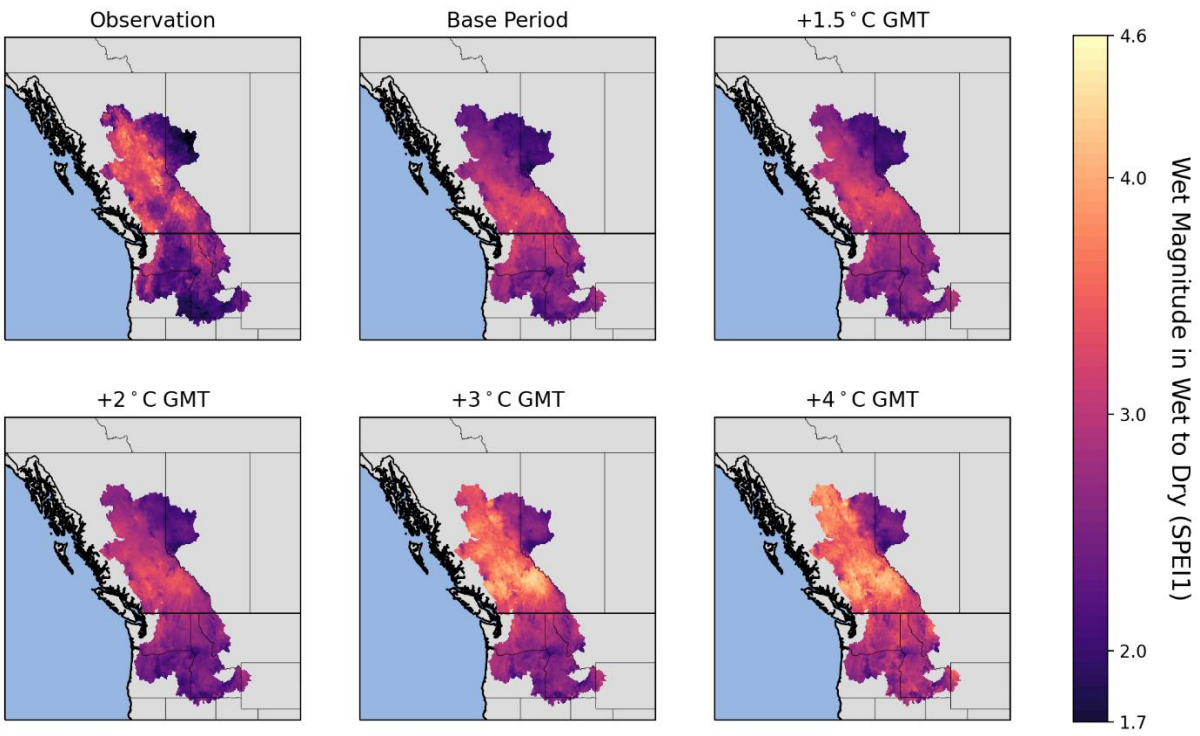

Appendix 38 - Climatology of the wet spell magnitude in the wet-to-dry CCEs (SPEI1). The map shows the magnitude based on the SPEI values of wet spells in the CCEs.

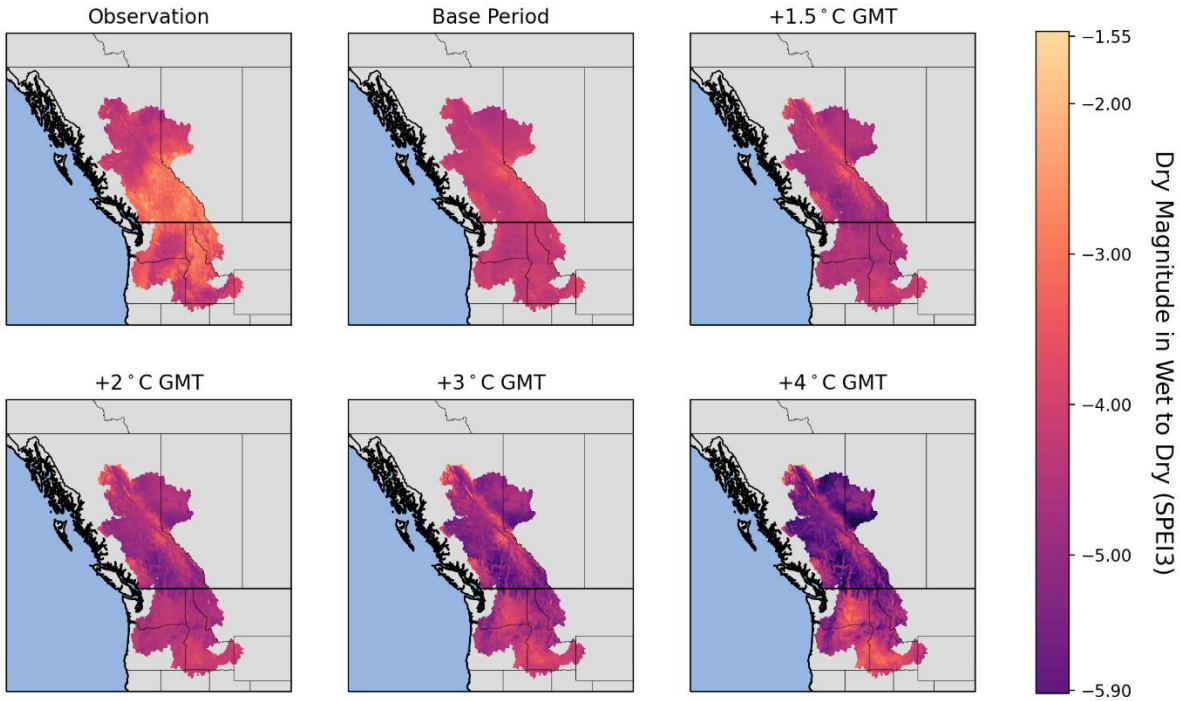

Appendix 39 - Climatology of the dry spell magnitude in the wet-to-dry CCEs (SPEI3). The map shows the magnitude based on the SPEI values of dry spells in the CCEs.

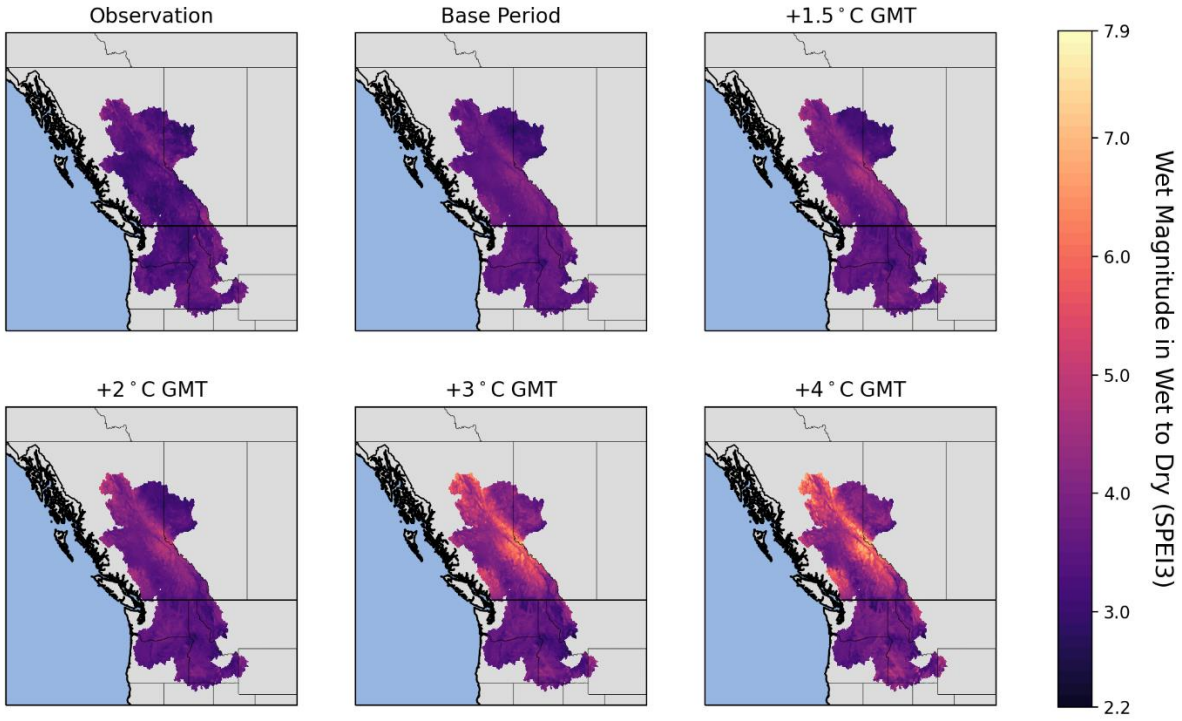

Appendix 40 - Climatology of the wet spell magnitude in the wet-to-dry CCEs (SPEI3). The map shows the magnitude based on the SPEI values of wet spells in the CCEs.

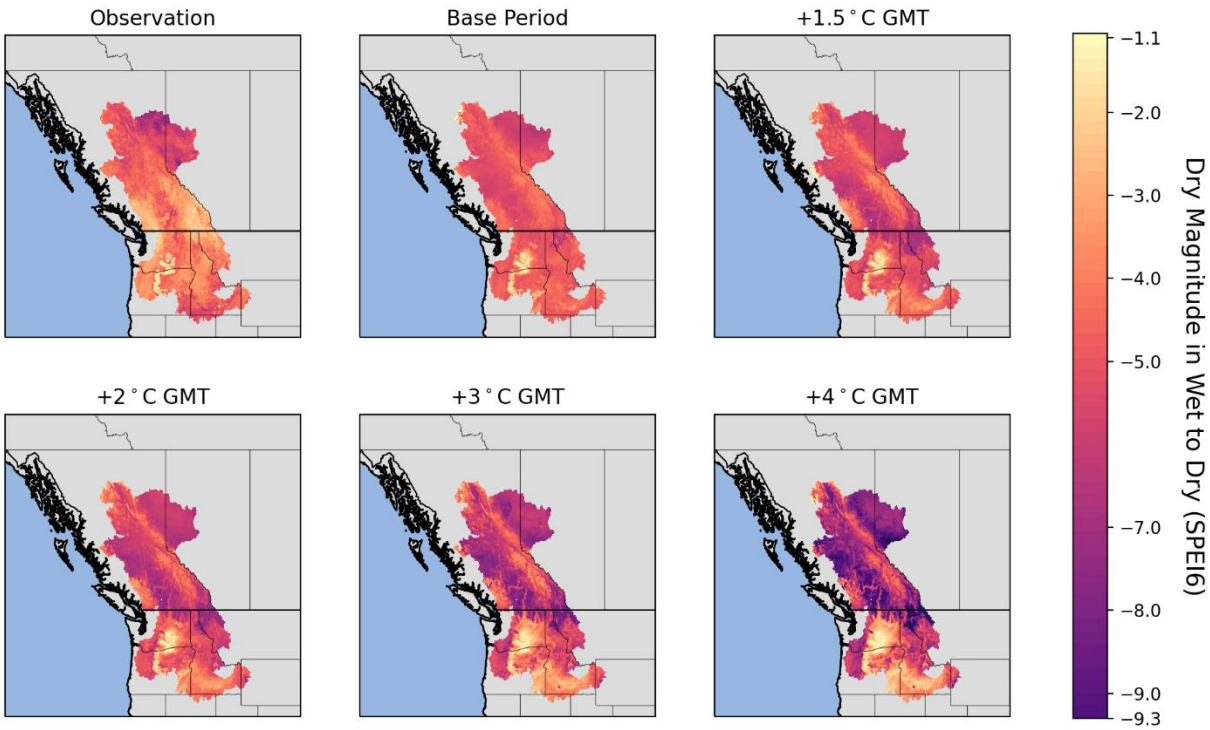

Appendix 41 - Climatology of the dry spell magnitude in the wet-to-dry CCEs (SPEI6). The map shows the magnitude based on the SPEI values of dry spells in the CCEs.

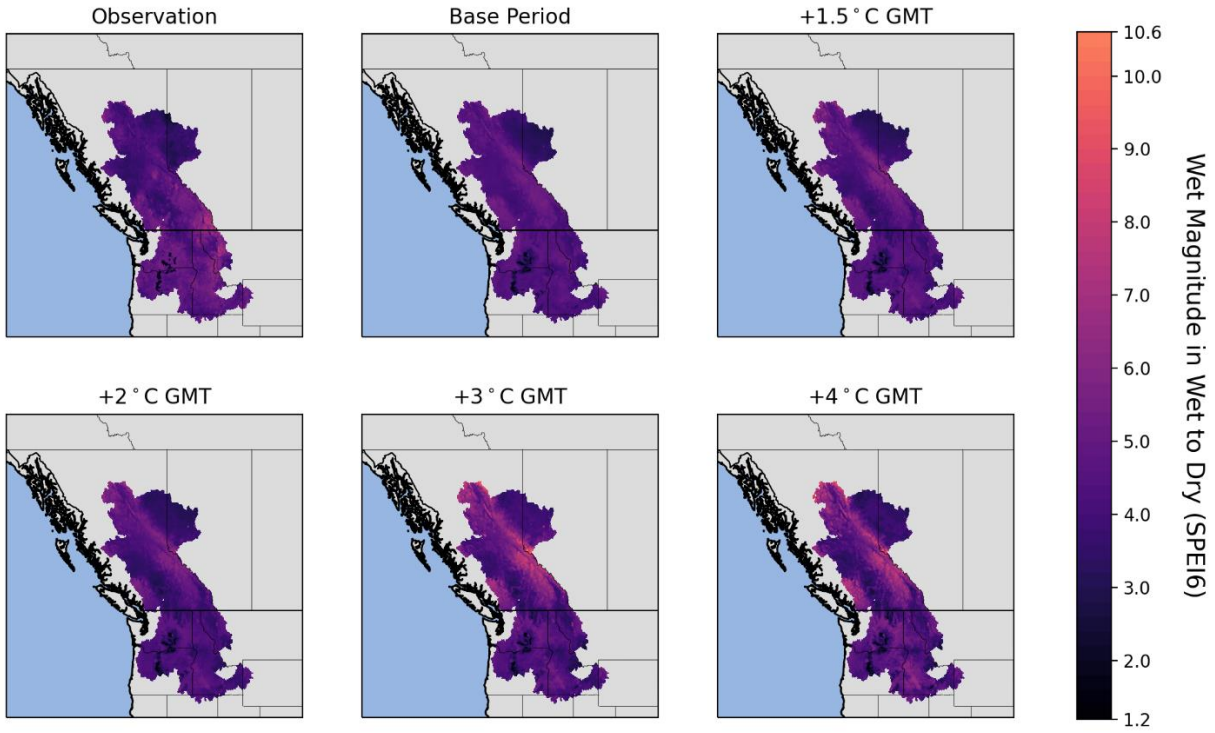

Appendix 42 - Climatology of the wet spell magnitude in the wet-to-dry CCEs (SPEI6). The map shows the magnitude based on the SPEI values of wet spells in the CCEs.

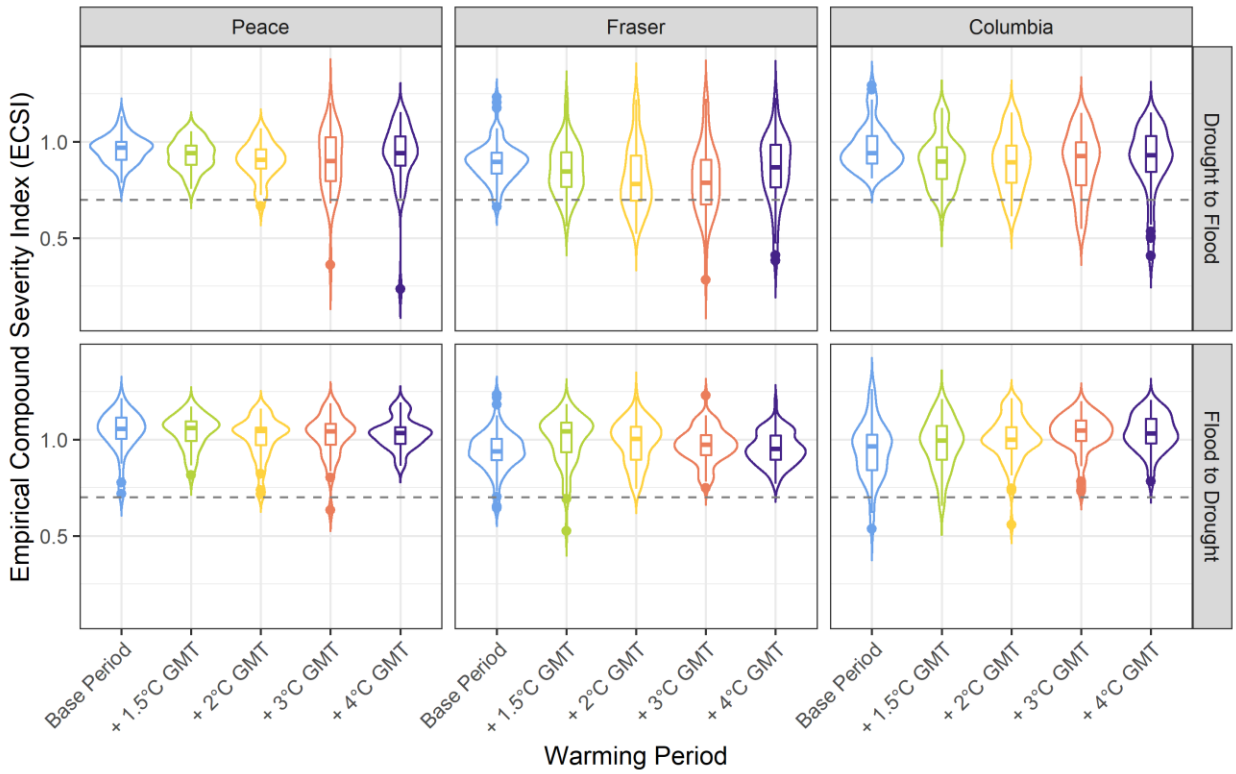

Appendix 43 - Empirical Compound Severity Index (ECSI). The box and violin plots show the spatial distribution of the ECSI in the ensemble mean for different basins at each global warming level.

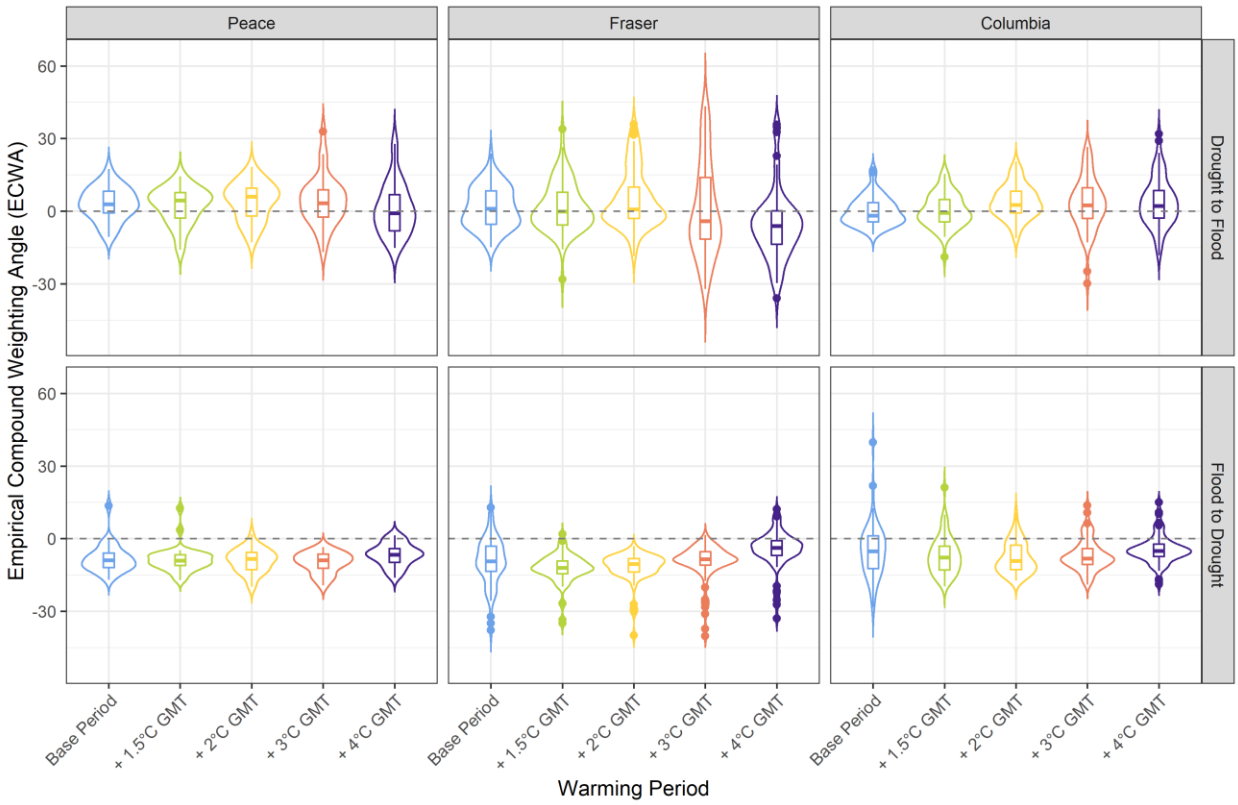

Appendix 44 - Empirical Compound Weighting Angle (ECWA). The box and violin plots show the spatial distribution of the ECWA in the ensemble mean for different basins at each global warming level.

Bibliography

Abbasian, M. S., Abrishamchi, A., Najafi, M. R., & Moghim, S. (2020). Multi-site statistical downscaling of precipitation using generalized hierarchical linear models: a case study of the imperilled Lake Urmia basin. Hydrological Sciences Journal, 65(14), 2466-2481.

Abbasian, M. S., Najafi, M. R., & Abrishamchi, A. (2021). Increasing risk of meteorological drought in the Lake Urmia basin under climate change: Introducing the precipitation–temperature deciles index. Journal of Hydrology, 592, 125586.

Adikari, Y., & Yoshitani, J. (n.d.). Global Trends in Water-Related Disasters: An insight for policymakers. 28.

AghaKouchak, A., Mirchi, A., Madani, K., Di Baldassarre, G., Nazemi, A., Alborzi, A., Anjileli, H., Azarderakhsh, M., Chiang, F., Hassanzadeh, E., Huning, L. S., Mallakpour, I., Martinez, A., Mazdiyasni, O., Moftakhari, H., Norouzi, H., Sadegh, M., Sadeqi, D., Van Loon, A. F., & Wanders, N. (2021). Anthropogenic drought: Definition, challenges, and opportunities. Reviews of Geophysics, 59(2). https://doi.org/10.1029/2019rg000683

Agriculture and Agri-Food Canada (2016). Synthesis report: Lessons Learned from the Canadian Drought Years 2001 and 2002. Government of Canada. https://agriculture.canada.ca/en/agriculture-and-environment/drought-watch-and-agroclimate/managing-agroclimate-risk/lessons-learned-canadian-drought-years-2001-and-2002

Ansari, R., & Grossi, G. (2022). Spatio-temporal evolution of wet–dry event features and their transition across the Upper Jhelum Basin (UJB) in South Asia. Natural Hazards and Earth System Sciences, 22(2), 287–302. https://doi.org/10.5194/nhess-22-287-2022

Bevacqua, E., De Michele, C., Manning, C., Couasnon, A., Ribeiro, A. F. S., Ramos, A. M., Vignotto, E., Bastos, A., Blesić, S., Durante, F., Hillier, J., Oliveira, S. C., Pinto, J. G., Ragno, E., Rivoire, P., Saunders, K., Wiel, K., Wu, W., Zhang, T., & Zscheischler, J. (2021). Guidelines for Studying Diverse Types of Compound Weather and Climate Events. Earth's Future, 9(11). https://doi.org/10.1029/2021EF002340

Bindoff, N.L., P.A. Stott, K.M. AchutaRao, M.R. Allen, N. Gillett, D. Gutzler, K. Hansingo, G. Hegerl, Y. Hu, S. Jain, I.I. Mokhov, J. Overland, J. Perlwitz, R. Sebbari and X. Zhang, 2013: Detection and Attribution of Climate Change: from Global to Regional. In: Climate Change 2013: The Physical Science Basis. Contribution of Working Group I to the Fifth Assessment Report of the Intergovernmental Panel on Climate Change [Stocker, T.F., D. Qin, G.-K. Plattner, M. Tignor, S.K. Allen, J. Boschung, A. Nauels, Y. Xia, V. Bex and P.M. Midgley (eds.)]. Cambridge University Press, Cambridge, United Kingdom and New York, NY, USA.

Blain, G. C., De Avila, A. M. H., & Pereira, V. R. (2018). Using the normality assumption to calculate probability-based standardized drought indices: selection criteria with emphases on typical events. International journal of climatology, 38(1), 418–436. DOI: 10.1002/joc.5381.

Bonsal, B.R., Peters, D.L., Seglenieks, F., Rivera, A., and Berg, A. (2019). Changes in freshwater availability across Canada; Chapter 6 in Canada's Changing Climate Report, (ed.) E. Bush and D.S. Lemmen; Government of Canada, Ottawa, Ontario, p. 261–342.

Bonsal, B. R., Wheaton, E. E., Chipanshi, A. C., Lin, C., Sauchyn, D. J., & Wen, L. (2011). Drought Research in Canada: A Review. Atmosphere-Ocean, 49(4), 303–319. https://doi.org/10.1080/07055900.2011.555103

Bubeck, P., Aerts, J. C. J. H., de Moel, H., & Kreibich, H. (2016). Preface: Flood-risk analysis and integrated management. Natural Hazards and Earth System Sciences, 16(4), 1005–1010. https://doi.org/10.5194/nhess-16-1005-2016

Burke, E. J., Brown, S. J., & Christidis, N. (2006). Modeling the Recent Evolution of Global Drought and Projections for the Twenty-First Century with the Hadley Centre Climate Model. Journal of Hydrometeorology, 7(5), 1113–1125. https://doi.org/10.1175/JHM544.1

Burn, D. H., & Whitfield, P. H. (2016). Changes in floods and flood regimes in Canada. Canadian Water Resources Journal / Revue Canadienne Des Ressources Hydriques, 41(1–2), 139–150. https://doi.org/10.1080/07011784.2015.1026844

Bush, E., & Lemmen, D. S. (2019). Canada's changing climate report. https://doi.org/10.4095/314614

Byrne, P., Hudson-Edwards, K. A., Bird, G., Macklin, M. G., Brewer, P. A., Williams, R. D., & Jamieson, H. E. (2018). Water quality impacts and river system recovery following the 2014 Mount Polley mine tailings dam spill, British Columbia, Canada. Applied Geochemistry, 91, 64–74. https://doi.org/10.1016/j.apgeochem.2018.01.012

Canada's changing climate report. (2019). Environment and Climate Change Canada = Environnement et changement climatique Canada.

Cannon, A. J. (2015). Selecting GCM Scenarios that Span the Range of Changes in a Multimodel Ensemble: Application to CMIP5 Climate Extremes Indices*. Journal of Climate, 28(3), 1260–1267. https://doi.org/10.1175/JCLI-D-14-00636.1

Cannon, A. J., Piani, C., & Sippel, S. (2020). Bias correction of climate model output for impact models. In Climate Extremes and Their Implications for Impact and Risk Assessment (pp. 77–104). Elsevier. https://doi.org/10.1016/B978-0-12-814895-2.00005-7

Cannon, A. J., Sobie, S. R., & Murdock, T. Q. (2015). Bias Correction of GCM Precipitation by Quantile Mapping: How Well Do Methods Preserve Changes in Quantiles and Extremes? Journal of Climate, 28(17), 6938–6959. https://doi.org/10.1175/JCLI-D-14-00754.1

Chegwidden, O. S., Nijssen, B., Rupp, D. E., Arnold, J. R., Clark, M. P., Hamman, J. J., Kao, S., Mao, Y., Mizukami, N., Mote, P. W., Pan, M., Pytlak, E., & Xiao, M. (2019). How Do Modeling Decisions Affect the Spread Among Hydrologic Climate Change Projections? Exploring a Large Ensemble of Simulations Across a Diversity of Hydroclimates. Earth's Future, 7(6), 623–637. https://doi.org/10.1029/2018EF001047

Coulthard, B., Smith, D. J., & Meko, D. M. (2016). Is worst-case scenario streamflow drought underestimated in British Columbia? A multi-century perspective for the south coast, derived from tree-rings. Journal of Hydrology, 534, 205–218. https://doi.org/10.1016/j.jhydrol.2015.12.030

Cunderlik, J. M., & Ouarda, T. B. M. J. (2009). Trends in the timing and magnitude of floods in Canada. Journal of Hydrology, 375(3–4), 471–480. https://doi.org/10.1016/j.jhydrol.2009.06.050

Curry, C. L., Islam, S. U., Zwiers, F. W., & Déry, S. J. (2019). Atmospheric Rivers Increase Future Flood Risk in Western Canada's Largest Pacific River. Geophysical Research Letters, 46(3), 1651–1661. https://doi.org/10.1029/2018GL080720

Dai, A. (2011). Drought under global warming: A review. WIREs Climate Change, 2(1), 45–65. https://doi.org/10.1002/wcc.81

Dai, A. (2013). Increasing drought under global warming in observations and models. Nature Climate Change, 3(1), 52–58. https://doi.org/10.1038/nclimate1633

Day, J. W. (2014). The Peace-Athabasca Delta: Portrait of a Dynamic Ecosystem. By Kevin Timony: Edmonton: University of Alberta Press, 2013. 595 pp., $90.00 (softcover). ISBN: 978-0-88864-730-6. Arctic, Antarctic, and Alpine Research, 46(3), 699–701. https://doi.org/10.1657/1938-4246-46.3.699

DeBeer, C. M., Wheater, H. S., Carey, S. K., & Chun, K. P. (2016). Recent climatic, cryospheric, and hydrological changes over the interior of western Canada: A review and synthesis. Hydrology and Earth System Sciences, 20(4), 1573–1598. https://doi.org/10.5194/hess-20-1573-2016

Dettinger, M. D. (2013). Atmospheric Rivers as Drought Busters on the U.S. West Coast. Journal of Hydrometeorology, 14(6), 1721–1732. https://doi.org/10.1175/JHM-D-13-02.1

Dibike, Y. B., Shrestha, R. R., Johnson, C., Bonsal, B., & Coulibaly, P. (2021). Assessing Climatic Drivers of Spring Mean and Annual Maximum Flows in Western Canadian River Basins. Water, 13(12), 1617. https://doi.org/10.3390/w13121617

Dibike, Y., Prowse, T., Bonsal, B., & O'Neil, H. (2017). Implications of future climate on water availability in the western Canadian river basins: IMPLICATIONS OF FUTURE CLIMATE ON WATER AVAILABILITY IN WESTERN CANADA. International Journal of Climatology, 37(7), 3247–3263. https://doi.org/10.1002/joc.4912

Dong, L., Leung, L. R., & Song, F. (2018). Future Changes of Subseasonal Precipitation Variability in North America During Winter Under Global Warming. Geophysical Research Letters, 45(22). https://doi.org/10.1029/2018GL079900

Elshorbagy, A., Bharath, R., Lakhanpal, A., Ceola, S., Montanari, A., & Lindenschmidt, K.-E. (2017). Topography- and nightlight-based national flood risk assessment in Canada. Hydrology and Earth System Sciences, 21(4), 2219–2232. https://doi.org/10.5194/hess-21-2219-2017

EURO-CORDEX Guidelines (2017). Guidance for EURO-CORDEX climate projections data use. CORDEX, version 1.

Fleig, A. K., Tallaksen, L. M., Hisdal, H., & Demuth, S. (2006). A global evaluation of streamflow drought characteristics. Hydrol. Earth Syst. Sci., 18.

Ford, T. W., Chen, L., & Schoof, J. T. (2021). Variability and Transitions in Precipitation Extremes in the Midwest United States. Journal of Hydrometeorology, 22(3), 533–545. https://doi.org/10.1175/JHM-D-20-0216.1

Francis, J. A., Vavrus, S. J., & Cohen, J. (2017). Amplified Arctic warming and mid-latitude weather: new perspectives on emerging connections. Wiley's climate change, 8, 1 – 11.

Garcia, M., Yu, D., Park, S., Yousefi Bahambari, P., Mohajer Iravanloo, B., & Sivapalan, M. (2022). Weathering water extremes and cognitive biases in a changing climate. Water Security, 15, 100110. https://doi.org/10.1016/j.wasec.2022.100110

Gillett, N. P., Cannon, A. J., Malinina, E., Schnorbus, M., Anslow, F., Sun, Q., Kirchmeier-Young, M., Zwiers, F., Seiler, C., Zhang, X., Flato, G., Wan, H., Li, G., & Castellan, A. (2022). Human influence on the 2021 British Columbia floods. Weather and Climate Extremes, 36, 100441. https://doi.org/10.1016/j.wace.2022.100441

Gimbel, K. F., Puhlmann, H., & Weiler, M. (2016). Does drought alter hydrological functions in forest soils? Hydrology and Earth System Sciences, 20(3), 1301–1317. https://doi.org/10.5194/hess-20-1301-2016

Gudmundsson, L., Bremnes, J. B., Haugen, J. E., & Engen-Skaugen, T. (2012). Technical Note: Downscaling RCM precipitation to the station scale using statistical transformations – a comparison of methods. Hydrology and Earth System Sciences, 16(9), 3383–3390. https://doi.org/10.5194/hess-16-3383-2012

Guidelines on ensemble prediction systems and forecasting. (2012). World Meteorological Organization.

Guttman, N. B. (1999). ACCEPTING THE STANDARDIZED PRECIPITATION INDEX: A CALCULATION ALGORITHM 1. JAWRA Journal of the American Water Resources Association, 35(2), 311–322. https://doi.org/10.1111/j.1752-1688.1999.tb03592.x

Hagos, S. M., Leung, L. R., Yoon, J., Lu, J., & Gao, Y. (2016). A projection of changes in landfalling atmospheric river frequency and extreme precipitation over western North America from the Large Ensemble CESM simulations. Geophysical Research Letters, 43(3), 1357–1363. https://doi.org/10.1002/2015GL067392

Haile, G. G., Tang, Q., Li, W., Liu, X., & Zhang, X. (2020). Drought: Progress in broadening its understanding. WIREs Water, 7(2). https://doi.org/10.1002/wat2.1407

Hamman, J. J., Nijssen, B., Bohn, T. J., Gergel, D. R., & Mao, Y. (2018). The Variable Infiltration Capacity Model, Version 5 (VIC-5): Infrastructure improvements for new applications and reproducibility [Preprint]. Hydrology. https://doi.org/10.5194/gmd-2018-36

Hartmann, D.L., A.M.G. Klein Tank, M. Rusticucci, L.V. Alexander, S. Brönnimann, Y. Charabi, F.J. Dentener, E.J. Dlugokencky, D.R. Easterling, A. Kaplan, B.J. Soden, P.W. Thorne, M. Wild and P.M. Zhai, 2013: Observations: Atmosphere and Surface. In: Climate Change 2013: The Physical Science Basis. Contribution of Working Group I to the Fifth Assessment Report of the Intergovernmental Panel on Climate Change [Stocker, T.F., D. Qin, G.-K. Plattner, M. Tignor, S.K. Allen, J. Boschung, A. Nauels, Y. Xia, V. Bex and P.M. Midgley (eds.)]. Cambridge University Press, Cambridge, United Kingdom and New York, NY, USA.

He, X. (n.d.). Droughts and Floods in a Changing Environment Natural Influences, Human Interventions, and Policy Implications. 228.

He, X., & Sheffield, J. (2020). Lagged Compound Occurrence of Droughts and Pluvials Globally Over the Past Seven Decades. Geophysical Research Letters, 47(14). https://doi.org/10.1029/2020GL087924

He, X., Wada, Y., Wanders, N., & Sheffield, J. (2017). Intensification of hydrological drought in California by human water management. Geophysical Research Letters, 44(4), 1777–1785. https://doi.org/10.1002/2016GL071665

Herring, S. C., Hoerling, M. P., Kossin, J. P., Peterson, T. C., & Stott, P. A. (n.d.). EXPLAINING EXTREME EVENTS OF 2014 FROM A CLIMATE PERSPECTIVE. 180.

Hirabayashi, Y., Mahendran, R., Koirala, S., Konoshima, L., Yamazaki, D., Watanabe, S., Kim, H., & Kanae, S. (2013). Global flood risk under climate change. Nature Climate Change, 3(9), 816–821. https://doi.org/10.1038/nclimate1911

Hoegh-Guldberg, O., Jacob, D., Taylor, M., Bindi, M., Brown, S., Camilloni, I., Diedhiou, A., Djalante, R., Ebi, K. L., Engelbrecht, F., Hijioka, Y., Mehrotra, S., Payne, A., Seneviratne, S. I., Thomas, A., Warren, R., Zhou, G., Halim, S. A., Achlatis, M., … Sherstyukov, B. (n.d.). Impacts of 1.5°C of Global Warming on Natural and Human Systems. 138.

Hoover, D. L., Hajek, O. L., Smith, M. D., Wilkins, K., Slette, I. J., & Knapp, A. K. (2022). Compound hydroclimatic extremes in a semi-arid grassland: Drought, deluge, and the carbon cycle. Global Change Biology, 28(8), 2611–2621. https://doi.org/10.1111/gcb.16081

Insurance Bureau of Canada, 2021. British Columbia floods cause $450 million in insured

damage. http://www.ibc.ca/bc/resources/media-centre/media-releases/british-columbia-floods-cause-450-million-in-insured-damage.

Jalili Pirani, F., & Najafi, M. R. (2020). Recent trends in individual and multivariate compound flood drivers in Canada's coasts. Water Resources Research, 56(8), e2020WR027785.

Jalili Pirani, F., & Najafi, M. R. (2022). Multivariate Analysis of Compound Flood Hazard Across Canada's Atlantic, Pacific and Great Lakes Coastal Areas. Earth's Future, 10(8), e2022EF002655.

Jiang, D., Sui, Y., & Lang, X. (2016). Timing and associated climate change of a 2 °C global warming: TIMING AND ASSOCIATED CLIMATE CHANGE OF A 2 °C GLOBAL WARMING. International Journal of Climatology, 36(14), 4512–4522. https://doi.org/10.1002/joc.4647

Kang, D. H., Gao, H., Shi, X., Islam, S. ul, & Déry, S. J. (2016). Impacts of a Rapidly Declining Mountain Snowpack on Streamflow Timing in Canada’s Fraser River Basin. Scientific Reports, 6(1), 19299. https://doi.org/10.1038/srep19299

Keyantash, J., & Dracup, J. A. (2002). The Quantification of Drought: An Evaluation of Drought Indices. 14.

Khaliq, M. N., Ouarda, T. B. M. J., Gachon, P., & Sushama, L. (2008). Temporal evolution of low-flow regimes in Canadian rivers. Water resources research, 44, 1 – 19. doi:10.1029/2007WR006132.

Klaassen, J. M. (n.d.). A CLIMATOLOGICAL ASSESSMENT OF MAJOR 20TH CENTURY DROUGHT IN SOUTHERN ONTARIO, CANADA. 6.

Kundzewicz, Z. W., & Kaczmarek, Z. (2000). Coping with Hydrological Extremes. Water International, 25(1), 66–75. https://doi.org/10.1080/02508060008686798

Kundzewicz, Z. W., Kanae, S., Seneviratne, S. I., Handmer, J., Nicholls, N., Peduzzi, P., Mechler, R., Bouwer, L. M., Arnell, N., Mach, K., Muir-Wood, R., Brakenridge, G. R., Kron, W., Benito, G., Honda, Y., Takahashi, K., & Sherstyukov, B. (2014). Flood risk and climate change: Global and regional perspectives. Hydrological Sciences Journal, 59(1), 1–28. https://doi.org/10.1080/02626667.2013.857411

Lebre, D. M. (n.d.). Flood Risk Management in Canada: A Political Discourse Analysis. 144.

Leonard, M., Westra, S., Phatak, A., Lambert, M., van den Hurk, B., McInnes, K., Risbey, J., Schuster, S., Jakob, D., & Stafford-Smith, M. (2014). A compound event framework for understanding extreme impacts. WIREs Climate Change, 5(1), 113–128. https://doi.org/10.1002/wcc.252

Li, X., Zhang, Q., Zhang, D., & Ye, X. (2017). Investigation of the drought–flood abrupt alternation of streamflow in Poyang Lake catchment during the last 50 years. Hydrology Research, 48(5), 1402–1417. https://doi.org/10.2166/nh.2016.266

Liang, X., Lettenmaier, D. P., Wood, E. F., & Burges, S. J. (1994). A simple hydrologically based model of land surface water and energy fluxes for general circulation models. Journal of Geophysical Research, 99(D7), 14415. https://doi.org/10.1029/94JD00483

Liang, X., Wood, E. F., & Lettenmaier, D. P. (1996). Surface soil moisture parameterization of the VIC-2L model: Evaluation and modification. Global and Planetary Change, 13(1–4), 195–206. https://doi.org/10.1016/0921-8181(95)00046-1

Mahaffey, S. (2016). Adapting Urban Areas to Flooding. 5.

Mahmoudi, M. H., Najafi, M. R., Singh, H., & Schnorbus, M. (2021). Spatial and temporal changes in climate extremes over northwestern North America: The influence of internal climate variability and external forcing. Climatic Change, 165(1–2), 14. https://doi.org/10.1007/s10584-021-03037-9

Marston, M. L., & Ellis, A. W. (2018). Extreme reversals in successive winter season precipitation anomalies across the Western United States, 1895-2015: EXTREME PRECIPITATION REVERSALS ACROSS THE WESTERN UNITED STATES. International Journal of Climatology, 38(3), 1520–1532. https://doi.org/10.1002/joc.5263

Maurer, E. P., Hidalgo, H. G., Das, T., Dettinger, M. D., & Cayan, D. R. (2010). The utility of daily large-scale climate data in the assessment of climate change impacts on daily streamflow in California. Hydrology and Earth System Sciences, 14(6), 1125–1138. https://doi.org/10.5194/hess-14-1125-2010

Maxwell, J. T., Knapp, P. A., Ortegren, J. T., Ficklin, D. L., & Soulé, P. T. (2017). Changes in the Mechanisms Causing Rapid Drought Cessation in the Southeastern United States. Geophysical Research Letters, 44(24). https://doi.org/10.1002/2017GL076261

Maxwell, J. T., Ortegren, J. T., Knapp, P. A., & Soulé, P. T. (2013). Tropical Cyclones and Drought Amelioration in the Gulf and Southeastern Coastal United States. Journal of Climate, 26(21), 8440–8452. https://doi.org/10.1175/JCLI-D-12-00824.1

McKee, T. B., Doesken, N. J., & Kleist, J. (n.d.). THE RELATIONSHIP OF DROUGHT FREQUENCY AND DURATION TO TIME SCALES. 6.

Merrikhpour, M. H., Rahimzadegan, M., Najafi, M. R., & Mahjouri, N. (2021). Probable maximum precipitation estimation over western Iran based on remote sensing observations: comparing deterministic and probabilistic approaches. Hydrological Sciences Journal, 66(1), 165-178.

Meyer, L., Brinkman, S., van Kesteren, L., Leprince-Ringuet, N., & van Boxmeer, F. (n.d.). Technical Support Unit for the Synthesis Report. 169.

Mishra, A. K., & Singh, V. P. (2010). A review of drought concepts. Journal of Hydrology, 391(1–2), 202–216. https://doi.org/10.1016/j.jhydrol.2010.07.012

Moazami, S., & Najafi, M. R. (2021). A comprehensive evaluation of GPM-IMERG V06 and MRMS with hourly ground-based precipitation observations across Canada. Journal of Hydrology, 594, 125929.

Moazami, S., Na, W., Najafi, M. R., & de Souza, C. (2022). Spatiotemporal bias adjustment of IMERG satellite precipitation data across Canada. Advances in Water Resources, 104300.

Moss, R., & Intergovernmental Panel on Climate Change (Eds.). (2008). Towards new scenarios for analysis of emissions, climate change, impacts, and response strategies: IPCC Expert Meeting report: 19-21 September, 2007, Noordwijkerhout, The Netherlands. Intergovernmental Panel on Climate Change.

Mount, J., Gray, B., Chappelle, C., Gartrell, G., Grantham, T., Moyle, P., Seavy, N., & Szeptycki, L. (n.d.). Managing California's Freshwater Ecosystems: Lessons from the 2012-16 Drought. 54.

Mukherjee, S., & Mishra, A. K. (2021). Increase in Compound Drought and Heatwaves in a Warming World. Geophysical Research Letters, 48(1). https://doi.org/10.1029/2020GL090617

Mullan, B., Porteous, A., Wratt, D., & Hollis, M. (n.d.). Changes in drought risk with climate change. 6.

Najafi, M. R., Zwiers, F. W., & Gillett, N. P. (2017a). Attribution of observed streamflow changes in key British Columbia drainage basins. Geophysical Research Letters, 44(21), 11-012.

Najafi, M. R., Zwiers, F., & Gillett, N. (2017b). Attribution of the observed spring snowpack decline in British Columbia to anthropogenic climate change. Journal of Climate, 30(11), 4113-4130.

Nastev, M., & Todorov, N. (2013). Hazus: A standardized methodology for flood risk assessment in Canada. Canadian Water Resources Journal, 38(3), 223–231. https://doi.org/10.1080/07011784.2013.801599

Omer, A., Wang, W., Basheer, A. K., & Yong, B. (2017). Integrated assessment of the impacts of climate variability and anthropogenic activities on river runoff: A case study in the Hutuo River Basin, China. Hydrology Research, 48(2), 416–430. https://doi.org/10.2166/nh.2016.229

Parry, S. (n.d.). Characterising hydrological drought termination as a basis for improved forecasting. 277.

Parry, S., Marsh, T., & Kendon, M. (2013). 2012: From drought to floods in England and Wales. Weather, 68(10), 268–274. https://doi.org/10.1002/wea.2152

Pieper, P., Düsterhus, A., & Baehr, J. (2020). A universal Standardized Precipitation Index candidate distribution function for observations and simulations. Hydrology and Earth System Sciences, 24(9), 4541–4565. https://doi.org/10.5194/hess-24-4541-2020

Poitras, V., Sushama, L., Seglenieks, F., Khaliq, M. N., & Soulis, E. (2011). Projected Changes to Streamflow Characteristics over Western Canada as Simulated by the Canadian RCM. Journal of Hydrometeorology, 12(6), 1395–1413. https://doi.org/10.1175/JHM-D-10-05002.1

Pomeroy, J. W., Fang, X., & Marks, D. G. (2016). The cold rain-on-snow event of June 2013 in the Canadian Rockies — characteristics and diagnosis. Hydrological processes, 30, 2899–2914. DOI: 10.1002/hyp.10905.

Qian, B., Zhang, X., Chen, K., Feng, Y., & O'Brien, T. (2010). Observed Long-Term Trends for Agroclimatic Conditions in Canada. Journal of Applied Meteorology and Climatology, 49(4), 604–618. https://doi.org/10.1175/2009JAMC2275.1

Ribeiro, A. V., Shawcross, S. W. (2014). Flood damage assessment in Alberta: best practices principles and guidelines. IBI group and Golder associates limited, 1-120.

Robson. A, & Reed, D. (1999). Flood estimation handbook: 3 statistical procedures for flood frequency analysis. Centre for ecology and hydrology, 1 – 365.

Romolo, L., Prowse, T. D., Blair, D., Bonsal, B. R., & Martz, L. W. (2006). The synoptic climate controls on hydrology in the upper reaches of the Peace River Basin. Part I: Snow

accumulation. Hydrological Processes, 20(19), 4097–4111. https://doi.org/10.1002/hyp.6421

Rossato, L., Alvalá, R. C. dos S., Marengo, J. A., Zeri, M., Cunha, A. P. M. do A., Pires, L. B. M., & Barbosa, H. A. (2017). Impact of Soil Moisture on Crop Yields over Brazilian Semiarid. Frontiers in Environmental Science, 5, 73. https://doi.org/10.3389/fenvs.2017.00073

Schnorbus, M., 2018. VIC Glacier: Description of VIC model changes and updates (PCIC Internal Report). Pacific Climate Impacts Consortium, Victoria, BC.

Schnorbus, M., 2017. VICGL Model Calibration (PCIC Internal Report). Pacific Climate Impacts Consortium, Victoria, BC.

Schnorbus, M., Werner, A., & Bennett, K. (2010). Quantifying the water resource impacts of mountain pine beetle and associated salvage harvest operations across a range of watershed scales: Hydrologic modelling of the Fraser River Basin. Natural Resources Canada, Canadian Forest Service, Pacific Forestry Centre.

Schnorbus, M., Werner, A., & Bennett, K. (2014). Impacts of climate change in three hydrologic regimes in British Columbia, Canada: IMPACTS OF CLIMATE CHANGE IN BRITISH COLUMBIA. Hydrological Processes, 28(3), 1170–1189. https://doi.org/10.1002/hyp.9661

Schoeneberg, A. T., & Schnorbus, M. A. (n.d.). Exploring the Strength and Limitations of PCIC's CMIP5 Hydrologic Scenarios. 42.

Seneviratne, S. I., Donat, M. G., Pitman, A. J., Knutti, R., & Wilby, R. L. (2016). Allowable CO2 emissions based on regional and impact-related climate targets. Nature, 529(7587), 477–483. https://doi.org/10.1038/nature16542

Seneviratne, S. I., Rogelj, J., Séférian, R., Wartenburger, R., Allen, M. R., Cain, M., Millar, R. J., Ebi, K. L., Ellis, N., Hoegh-Guldberg, O., Payne, A. J., Schleussner, C.-F., Tschakert, P., & Warren, R. F. (2018). The many possible climates from the Paris Agreement's aim of 1.5 °C warming. Nature, 558(7708), 41–49. https://doi.org/10.1038/s41586-018-0181-4

Seneviratne, S. I., Wartenburger, R., Guillod, B. P., Hirsch, A. L., Vogel, M. M., Brovkin, V., van Vuuren, D. P., Schaller, N., Boysen, L., Calvin, K. V., Doelman, J., Greve, P., Havlik, P., Humpenöder, F., Krisztin, T., Mitchell, D., Popp, A., Riahi, K., Rogelj, J., … Stehfest, E. (2018). Climate extremes, land–climate feedbacks and land-use forcing at 1.5°C. Philosophical Transactions of the Royal Society A: Mathematical, Physical and Engineering Sciences, 376(2119), 20160450. https://doi.org/10.1098/rsta.2016.0450

Sheffield, J., Wood, E. F., & Roderick, M. L. (2012). Little change in global drought over the past 60 years. Nature, 491(7424), 435–438. https://doi.org/10.1038/nature11575

Shrestha, R. R., Cannon, A. J., Schnorbus, M. A., & Alford, H. (2019). Climatic Controls on Future Hydrologic Changes in a Subarctic River Basin in Canada. Journal of Hydrometeorology, 20(9), 1757–1778. https://doi.org/10.1175/JHM-D-18-0262.1

Shrestha, R. R., Schnorbus, M. A., & Peters, D. L. (2016). Assessment of a hydrologic model's reliability in simulating flow regime alterations in a changing climate: Hydrologic Model's Reliability in Simulating Flow Regime Alterations. Hydrological Processes, 30(15), 2628–2643. https://doi.org/10.1002/hyp.10812

Shukla, V. (2019). Top 10 Deadliest Floods In The Known History Of The World. Value Walk. https://www.valuewalk.com/2019/02/top-10-deadliest-floods-world-history/

Singh, H., Pirani, F. J., & Najafi, M. R. (2020). Characterizing the temperature and precipitation covariability over Canada. Theoretical and Applied Climatology, 139(3–4), 1543–1558. https://doi.org/10.1007/s00704-019-03062-w

Singh, H., & Najafi, M. R. (2020). Evaluation of gridded climate datasets over Canada using univariate and bivariate approaches: Implications for hydrological modelling. Journal of Hydrology, 584, 124673.

Singh, H., Najafi, M. R., & Cannon, A. J. (2021). Characterizing non-stationary compound extreme events in a changing climate based on large-ensemble climate simulations. Climate Dynamics, 56(5), 1389-1405.

Singh, H., Najafi, M. R., & Cannon, A. (2022). Evaluation and joint projection of temperature and precipitation extremes across Canada based on hierarchical Bayesian modelling and large ensembles of regional climate simulations. Weather and Climate Extremes, 36, 100443.

Sivakumar, M. V. K., Stefanski, R., Bazza, M., Zelaya, S., Wilhite, D., & Magalhaes, A. R. (2014). High Level Meeting on National Drought Policy: Summary and Major Outcomes. Weather and Climate Extremes, 3, 126–132. https://doi.org/10.1016/j.wace.2014.03.007

Skliris, N., Zika, J. D., Nurser, G., Josey, S. A., & Marsh, R. (2016). Global water cycle amplifying at less than the clausius-clapeyron rate. Scientific Reports, 6(1). https://doi.org/10.1038/srep38752

Stagge, J. H., Tallaksen, L. M., Gudmundsson, L., Van Loon, A. F., & Stahl, K. (2015). Candidate Distributions for Climatological Drought Indices (SPI and SPEI). International Journal of Climatology, 35(13), 4027–4040. https://doi.org/10.1002/joc.4267

Swain, D. L. (2015). A tale of two California droughts: Lessons amidst record warmth and dryness in a region of complex physical and human geography: A TALE OF TWO CALIFORNIA DROUGHTS. Geophysical Research Letters, 42(22), 9999-10,003. https://doi.org/10.1002/2015GL066628

Swain, D. L., Horton, D. E., Singh, D., & Diffenbaugh, N. S. (2016). Trends in atmospheric patterns conducive to seasonal precipitation and temperature extremes in California. Science Advances, 2(4), e1501344. https://doi.org/10.1126/sciadv.1501344

Swain, D. L., Langenbrunner, B., Neelin, J. D., & Hall, A. (2018). Increasing precipitation volatility in twenty-first-century California. Nature Climate Change, 8(5), 427–433. https://doi.org/10.1038/s41558-018-0140-y

Swiss RE (2021), Natural catastrophes in 2020: secondary perils in the spotlight,

but don’t forget primary-peril risks. Swiss RE institute. 1 – 34.

Szeto, K., Zhang, X., White, R. E., & Brimelow, J. (2016). The 2015 Extreme Drought in Western Canada. Bulletin of the American Meteorological Society, 97(12), S42–S46. https://doi.org/10.1175/BAMS-D-16-0147.1

Tallaksen, L. M., & Van Lanen (2004). Hydrological drought: Processes and Estimation Methods for Streamflow and Groundwater. Developments in water science, 1 – 35.

Teufel, B., Diro, G. T., Whan, K., Milrad, S. M., Jeong, D. I., Ganji, A., Huziy, O., Winger, K., Gyakum, J. R., de Elia, R., Zwiers, F. W., & Sushama, L. (2017). Investigation of the 2013 Alberta flood from weather and climate perspectives. Climate Dynamics, 48(9–10), 2881–2899. https://doi.org/10.1007/s00382-016-3239-8

Thorne, R. (2011). Uncertainty in the impacts of projected climate change on the hydrology of a subarctic environment: Liard River Basin. Hydrology and Earth System Sciences, 15(5), 1483–1492. https://doi.org/10.5194/hess-15-1483-2011

Todini, E. (1996). The ARNO rainfall—Runoff model. Journal of Hydrology, 175(1–4), 339–382. https://doi.org/10.1016/S0022-1694(96)80016-3

Touma, D., Ashfaq, M., Nayak, M. A., Kao, S.-C., & Diffenbaugh, N. S. (2015). A multi-model and multi-index evaluation of drought characteristics in the 21st century. Journal of Hydrology, 526, 196–207. https://doi.org/10.1016/j.jhydrol.2014.12.011

Touma, D., Stevenson, S., Swain, D. L., Singh, D., Kalashnikov, D. A., & Huang, X. (2022). Climate change increases risk of extreme rainfall following wildfire in the western United States. Science Advances, 8(13), eabm0320. https://doi.org/10.1126/sciadv.abm0320

Trenberth, K. E., Dai, A., van der Schrier, G., Jones, P. D., Barichivich, J., Briffa, K. R., & Sheffield, J. (2014). Global warming and changes in drought. Nature Climate Change, 4(1), 17–22. https://doi.org/10.1038/nclimate2067

USGS (n.d.). Water science for schools: Uses of Streamflow Information. USGS, 1 – 2.

Vahedifard, F., AghaKouchak, A., Ragno, E., Shahrokhabadi, S., & Mallakpour, I. (2017). Lessons from the Oroville dam. Science, 355(6330), 1139–1140. https://doi.org/10.1126/science.aan0171

Vahedifard, F., AghaKouchak, A., & Robinson, J. D. (2015). Drought threatens California's levees. Science, 349(6250), 799–799. https://doi.org/10.1126/science.349.6250.799-a

Van Loon, A. F. (2015). Hydrological drought explained. WIREs Water, 2(4), 359–392. https://doi.org/10.1002/wat2.1085

Van Loon, A. F. (2013). On the propagation of drought: How climate and catchment characteristics influence hydrological drought development and recovery. Wageningen University.

Villarini, G., & Strong, A. (2014). Roles of climate and agricultural practices in discharge changes in an agricultural watershed in Iowa. Agriculture, Ecosystems & Environment, 188, 204–211. https://doi.org/10.1016/j.agee.2014.02.036

Vincent, L. A., & Mekis, É. (2006). Changes in Daily and Extreme Temperature and Precipitation Indices for Canada over the Twentieth Century. Atmosphere-Ocean, 44(2), 177–193. https://doi.org/10.3137/ao.440205

Vore, M. E., Déry, S. J., Hou, Y., & Wei, X. (2020). Climatic influences on forest fire and mountain pine beetle outbreaks and resulting runoff effects in large watersheds in British Columbia, Canada. Hydrological Processes, 34(24), 4560–4575. https://doi.org/10.1002/hyp.13908

Wang, S.-Y. S., Yoon, J.-H., Becker, E., & Gillies, R. (2017). California from drought to deluge. Nature Climate Change, 7(7), 465–468. https://doi.org/10.1038/nclimate3330

Wang, S., Najafi, M. R., Cannon, A. J., & Khan, A. A. (2021). Uncertainties in Riverine and Coastal Flood Impacts under Climate Change. Water, 13(13), 1774.

Wernberg, T., Smale, D. A., Tuya, F., Thomsen, M. S., Langlois, T. J., de Bettignies, T., Bennett, S., & Rousseaux, C. S. (2013). An extreme climatic event alters marine ecosystem structure in a global biodiversity hotspot. Nature Climate Change, 3(1), 78–82. https://doi.org/10.1038/nclimate1627

Werner, A. T., & Cannon, A. J. (2015). Hydrologic extremes – an intercomparison of multiple gridded statistical downscaling methods [Preprint]. Hydrometeorology/Modelling approaches. https://doi.org/10.5194/hessd-12-6179-2015

Werner, A. T., Schnorbus, M. A., Shrestha, R. R., Cannon, A. J., Zwiers, F. W., Dayon, G., & Anslow, F. (2019). A long-term, temporally consistent, gridded daily meteorological dataset for northwestern North America. Scientific Data, 6(1), 180299. https://doi.org/10.1038/sdata.2018.299

Werner, A. T., Schnorbus, M. A., Shrestha, R. R., & Eckstrand, H. D. (2013). Spatial and Temporal Change in the Hydro-Climatology of the Canadian Portion of the Columbia River Basin under Multiple Emissions Scenarios. Atmosphere-Ocean, 51(4), 357–379. https://doi.org/10.1080/07055900.2013.821400

Westwood, C. G., England, J., Dunbar, M. J., Holmes, N. T. H., Leeming, D. J., & Hammond, D. (2017). An approach to setting ecological flow thresholds for southern English chalk

streams: Southern English chalk streams. Water and Environment Journal, 31(4), 528–536. https://doi.org/10.1111/wej.12275

Whitfield, P. H., Burn, D. H., Hannaford, J., Higgins, H., Hodgkins, G. A., Marsh, T., & Looser, U. (2012). Reference hydrologic networks I. The status and potential future directions of national reference hydrologic networks for detecting trends. Hydrological Sciences Journal, 57(8), 1562–1579. https://doi.org/10.1080/02626667.2012.728706

World economic forum (2019, 05, 27). 5 droughts that changed human history. https://www.weforum.org/agenda/2019/05/5-droughts-that-changed-human-history/

Yang, L., Smith, J. A., Wright, D. B., Baeck, M. L., Villarini, G., Tian, F., & Hu, H. (2013). Urbanization and Climate Change: An Examination of Nonstationarities in Urban Flooding. Journal of Hydrometeorology, 14(6), 1791–1809. https://doi.org/10.1175/JHM-D-12-095.1

Yang, Y., Gan, T. Y., & Tan, X. (2021). Recent changing characteristics of dry and wet spells in Canada. Climatic Change, 165(3–4), 42. https://doi.org/10.1007/s10584-021-03046-8

Yazdi, J., & Neyshabouri, S. A. A. S. (2012). Assessing flood vulnerability using a rule-based fuzzy system. Water Science and Technology, 66(8), 1766–1773. https://doi.org/10.2166/wst.2012.346

Yu, J.-Y., Wang, X., Yang, S., Paek, H., & Chen, M. (2017). The Changing El Niño-Southern Oscillation and Associated Climate Extremes. In S.-Y. S. Wang, J.-H. Yoon, C. C. Funk, & R. R. Gillies (Eds.), Geophysical Monograph Series (pp. 1–38). John Wiley & Sons, Inc. https://doi.org/10.1002/9781119068020.ch1

Zhang, Y., & Najafi, M. R. (2020). Probabilistic numerical modeling of compound flooding caused by Tropical Storm Matthew over a data-scarce coastal environment. Water Resources Research, 56(10), e2020WR028565.

Zhao, T., & Dai, A. (2015). The Magnitude and Causes of Global Drought Changes in the Twenty-First Century under a Low–Moderate Emissions Scenario. Journal of Climate, 28(11), 4490–4512. https://doi.org/10.1175/JCLI-D-14-00363.1

Zhao, T., & Dai, A. (2017). Uncertainties in historical changes and future projections of drought. Part II: Model-simulated historical and future drought changes. Climatic Change, 144(3), 535–548. https://doi.org/10.1007/s10584-016-1742-x

Zhou, S., Zhang, Y., Park Williams, A., & Gentine, P. (2019). Projected increases in intensity, frequency, and terrestrial carbon costs of compound drought and aridity events. Science Advances, 5(1), eaau5740. https://doi.org/10.1126/sciadv.aau5740

Zscheischler, J., Martius, O., Westra, S., Bevacqua, E., Raymond, C., Horton, R. M., van den Hurk, B., AghaKouchak, A., Jézéquel, A., Mahecha, M. D., Maraun, D., Ramos, A. M., Ridder, N. N., Thiery, W., & Vignotto, E. (2020). A typology of compound weather and climate events. Nature Reviews Earth & Environment, 1(7), 333–347. https://doi.org/10.1038/s43017-020-0060-z

Zscheischler, J., & Seneviratne, S. I. (2017). Dependence of drivers affects risks associated with compound events. Science Advances, 3(6), e1700263. https://doi.org/10.1126/sciadv.1700263

Zscheischler, J., Westra, S., van den Hurk, B. J. J. M., Seneviratne, S. I., Ward, P. J., Pitman, A., AghaKouchak, A., Bresch, D. N., Leonard, M., Wahl, T., & Zhang, X. (2018). Future

climate risk from compound events. Nature Climate Change, 8(6), 469–477. https://doi.org/10.1038/s41558-018-0156-3

Curriculum Vitae

Reza Rezvani

PROFILE SUMMARY

- Temporal and spatial data manipulation, analysis, management, and visualization
- Comfortable with big data (analyzed more than 5TB of various data types)
- Programming and geospatial data analysis using multiple programming languages and GIS products
- Strong written communication abilities gained through technical and scientific writing
- Effectively communicate orally with expert and nonexpert audiences
- Detail-oriented with strong work ethics and organizational skills

EDUCATIONAL BACKGROUND

Bachelor of Science, Civil Engineering — September/2013 – December/2018
Shahid Chamran University – Ahvaz, Khuzestan, Iran

PROFESSIONAL EXPERIENCE

Graduate Research Assistant, *Western University – London, Ontario* — May/2021 – October/2022

- Carried out multiple research projects under the supervision of Dr. Mohammad Reza Najafi

Graduate Teaching Assistant, *Western University – London, Ontario* — January/2022 – April/2022

- Assisted Dr. Mohammad Reza Najafi in teaching the "Watershed Modeling" course with running tutorial sessions as well as grading assignments
- Held software demo sessions on Arc Hydro, HEC-HMS, HEC-GeoHMS, HEC-RAS, HEC-GeoRAS and ArcGIS modules and troubleshot students' problems

Engineering Consultant (Undergraduate Internship), *Sabir Dam and Water Works Construction – Tehran, Iran* — May/2017 – August/2017

- Prepared construction drawings using the AutoCAD software for the construction of Helal-e-Ahmar subway station (line 7 of the Tehran subway project)

ACADEMIC PROJECTS

Spatiotemporal Changes of Lagged Compound Dry and Wet Spells in the Northwest North America Under Climate Change — May/2021 – October/2022

- Thesis written as a requirement for the degree of Master of Engineering Science

Projected Rain-on-Snow Events in a Sub-Arctic River Basin Under 1.5°C - 4°C Global Warming — September/2021 – April/2022

- Research article under review
- Coauthors: Harsimrenjit Singh, Dr. Mohammad Reza Najafi, Dr. Rajesh R. Shrestha

Engineering in a Changing Climate: A Transdisciplinary Workshop Series for Engineering and Climate Science Students — June/2021 – February/2022

- An online course developed by the University of Toronto Centre for Climate Science and Engineering in collaboration with the Western University targeted at senior undergraduate and graduate engineering and climate science students
- Helped with developing the Flood Risk module in a team of three research assistants

Towards a Comprehensive Assessment of Flood Risks in Canadian Urban Areas Based on the CanFlood Framework — January/2021 – April/2021

- Utilized the CanFlood tool in the QGIS to assess the monetary risk of different flood scenarios exerted to commercial and residential properties

Rainwater Tree Trenches: Application for Medway Parking Lot at Western University — January/2021 – March/2021

- Prepared for the “Rain it in” student competition by a team of 6 graduate students from Western University

ACADEMIC CONFERENCES

Oral Presentation, *Canadian Geophysical Union (CGU),* General Hydrology session — June/2022

- Spatiotemporal Changes of Hydrologic Drought and Flood Swings in Western North America Under Climate Change

Poster Presentation, *American Geophysical Union (AGU) Fall meeting 2021,* Natural Hazards session — December/2021

- Projected Rain-on-Snow Events in a sub-Arctic River Basin Under Climate Change

HONOURS AND AWARDS

Winner - the 3 Minute Thesis (3MT) competition — March/2022

- Held by the department of the Civil and Environmental Engineering at the Western University in the winter semester 2022 with 9 graduate students as competitors

Second place - the Rain it in student competition — April/2022

- Competition open to graduate students enrolled in Ontarian post-secondary schools

COMPUTER SKILLS

Operating system: Windows, Linux

Programming languages: Python, R

Geospatial analysis: ArcGIS Pro, ArcMap, QGIS

Modelling softwares: HEC-HMS, HEC-RAS

Organizational softwares: Microsoft Office suite, Google docs